EXPLORING THE POTENTIAL OF RED LIGHT THERAPY AS A TREATMENT FOR RETINAL GANGLION CELL DEGENERATION

Thesis submitted for the degree of Doctor of Philosophy

Cardiff University

September 2017

Kathy Beirne

School of Optometry and Vision Sciences

Cardiff University

Contents

Acknowledgements

I would like to thank my supervisors Prof. Marcela Votruba and Dr. Malgorzata Rozanowska for their continuous support and guidance throughout my PhD. Thank you to Sharon Seto for her help with Western blot analysis and maintenance of the colony. I would like to thank Nick White for his help with microscopy. Thank you to the people from 2.11 and 2.48 who have all helped to create an enjoyable working environment.

Abbreviations

Retinal ganglion cells (RGCs)

B6;C3-Opa1^{Q285STOP} (het)

Low level laser irradiation (LLLI)

Low level laser therapy (LLLT)

Reactive oxygen species (ROS)

Reactive nitrogen species (RNS)

Protein/nucleic acid deglycase (DJ1)

Nuclear factor kappa-light-chain-enhancer of activated B cells (NFκB)

Nuclear factor (erythroid-derived 2)-like 2 (Nrf2)

Protein kinase B (PKB/Akt)

3-nitrotyrosine (3-NT)

Ionized calcium binding adaptor molecule 1 (Iba1)

Autosomal dominant optic atrophy (ADOA)

Mitofusion (Mfn)

Electron transport chain (ETC)

Cytochrome c oxidase/ complex IV (COX)

Mitochondrial outer membrane permeabilization (MOMP)

Nerve growth factor (NGF)

Superoxide Dismutase (SOD)

Adenosine triphosphate (ATP)

Light emitting diode (LED)

Near infrared (NIR)

Intercellular Adhesion Molecule (ICAM)

Age-related macular degeneration (AMD)

Nitric oxide ($^{\bullet}NO$)

Nitric oxide synthase (NOS)

Superoxide radical anion ($O_2^{\bullet-}$)

Peroxynitrite ($ONOO^-$)

Leber's hereditary optic neuropathy (LHON)

Traumatic brain injury (TBI)

Parkinson's diseade (PD)

Alzheimer's disease (AD)

Lipopolysaccharide (LPS)

1,10-dioleyl-3,3,3,3 tetramethylindocarbocyanine methanesulphonate (DiO)

3,3'dihexadecyloxacarbocyanine perchlorate (DiI)

Ganglion cell layer (GCL)

Inner plexiform layer (IPL)

Inner nuclear layer (INL)

Outer nuclear layer (ONL)

Outer plexiform layer (OPL)

Optic nerve (ON)

Sodium dodecyl sulfate polyacrylamide gel electrophoresis (SDS-PAGE)

3-(4,5-Dimethylthiazol-2-yl)-2,5-Diphenyltetrazolium Bromide (MTT)

Carbonyl cyanide-p-trifluoromethoxyphenylhydrazone (FCCP)

Oxygen consumption rate (OCR)

Area under the curve (AUC)

Tyrosine hydroxylase (TH)

Continuous wave (CW)

List of figures

correspond. Three readings are taken for the oxygen consumption that results from basal respiration. Another three readings are taken after the addition of oligomycin to show the decrease in oxygen consumption following the inhibition of ATP synthase. The uncoupler FCCP is then added to uncouple oxidative phosphorylation from ATP synthesis, allowing the protons to flow through the mitochondrial inner membrane, from the intermembrane space back into the matrix, before they can be used to fuel ATP production by ATP synthase. Three readings are taken following FCCP addition to show the oxygen consumption at the maximal respiration ability of the mitochondria. The mitochondrial spare capacity is the difference in between the oxidative phosphorylation thar occurs under basal conditions for ATP production and that which occurs when oxidative phosphorylation is driven to maximum levels The addition of the complex III inhibitor Antimycin A and the complex I inhibitor Rotenone completely supresses oxidative phosphorylation. Three final readings are taken after the addition of Antimycin A and Rotenone to determine the oxygen consumption that occurs in the absence of mitochondrial respiration. The proton leak refers to the oxygen consumption that occurs from mitochondrial respiration under basal conditions that does not result from ATP production. 96

Figure 3.2: Optimisation of the MTT assay to detect reductions in mitochondrial reductive capacity in the retinal explant. The formazan crystal formation on the retinal explant after incubation with 0.5 mg/mL MTT for 2.5 hours immediately after explanting (n=1) (A), 1 hour after explanting (n=1) (B), 3 hours after explanting (n=1) (C) and 24 hours after explanting (n=1) (D). E: The formazan formation on a retina which was treated with TritonX100, to cause almost 100% cell death before incubation with

List of tables

below the concentration predicted to be suitable for a retinal section of 1.2 mm in area.

112

Summary

Mutations in OPA1 are the leading cause of autosomal dominant optic atrophy, a disease in which a progressive loss of retinal ganglion cells (RGCs) leads to blindness. In the B6;C3-Opa1^{Q285STOP} (het) mouse, an Opa1 mutation causes a decrease in ATP production and a progressive loss in visual acuity, which coincides with pruning of the predominantly ON-centre RGC dendrites. As 670 nm light can increase ATP production and provide neuroprotective effects, we hypothesise that protection from dendritic pruning will be observed in the ON-centre RGCs of the het mouse with 670 nm light.

By Sholl analysis, and other measures of dendritic complexity, we found that *ex vivo* delivery of 670 nm light to retinal explants provides partial protection against the *ex vivo* retinal ganglion cell dendropathy, triggered by axotomy, in young wild-type mice. By the same methods of analyses, *in vivo* delivery of 670 nm light to aged wild-type and het mice partial provided protection against *ex vivo* RGC dendropathy in RGCs from wild-type mice and partial protection in RGCs from het mice.

By immunohistochemistry, the transcription factor NFκB was found to be activated in RGCs from aged het mice treated with *in vivo* 670 nm light. The oxidative stress sensor, DJ1, was upregulated in RGCs from aged wild-type and het mice, by *in vivo* 670 nm light. The activation of the serine/threonine protein kinase, AKT, which plays a pivotal role in controlling cell survival and apoptosis, was decreased following *in vivo* 670 nm light treatment in aged wild-type RGCs.

Chapter 1. Introduction

1.1 Autosomal dominant optic atrophy

1.1.1 Clinical presentation and prevalence

Autosomal Dominant Optic Atrophy (ADOA) also known as Kjer's Optic Atrophy was first described in 19 Danish families in 1959 by the Danish ophthalmologist Dr. Poul Kjer (Kjer, 1959). The disease prevalence is estimated to be as high as 1 in 25,000 making it the most common cause of inherited blindness (Yu-Wai-Man et al., 2010). There is much clinical variation in ADOA ranging from a subclinical phenotype to those patients registered legally blind. ADOA patients predominantly experience visual defects however a small cohort develop additional extra-ocular symptoms giving rise to syndromic ADOA. The disease is characterized by a loss of retinal ganglion cells and subsequent atrophy of the optic nerve. The clinical presentation usually begins in childhood with a progressive bilateral loss of visual acuity (Kjer et al., 1983). The disease can be further characterized by colour vision defects, most commonly blue-yellow dyschromatopsia, centrocecal, central or paracentral visual field defects and temporal or diffuse optic nerve pallor with optic disc atrophy.

Figure 1.1: A left fundus photograph of a patient with ADOA, showing temporal pallor.

Approximately 20% of ADOA patients develop multi-system symptoms, most commonly sensorineural deafness. Other symptoms can also develop later in life including myopathy, peripheral neuropathy, paraplegia, cardiomyopathy and cataracts (Lenaers et al., 2012).

1.1.2 Disease pathology

The pathology of ADOA has not yet been fully clarified, however, much progress has been made to this end. Histological examination of the eyes of ADOA patients suggested that the loss of visual acuity was due to the loss of retinal ganglion cells. One patient showed a reduction in the number of ganglion cells in the retina with the remainder displaying classical features of degeneration such as cytoplasmic vacuolization. In addition there was a loss in myelin density, pallor, axonal swelling and demyelination in the temporal aspect of the optic nerve (Johnston et al., 1979). In another post-mortem examination by Kjer et al (1983) there was heavy fibrosis of the ganglion cell layer of the retina, a reduced number of ganglion cells in the posterior part of the retina as well as partial atrophy of the optic nerve, however, the other cell layers of the retina were unaffected. In the majority of cases the degree of optic disc pallor is representative of the loss of visual acuity (Votruba et al., 1998).

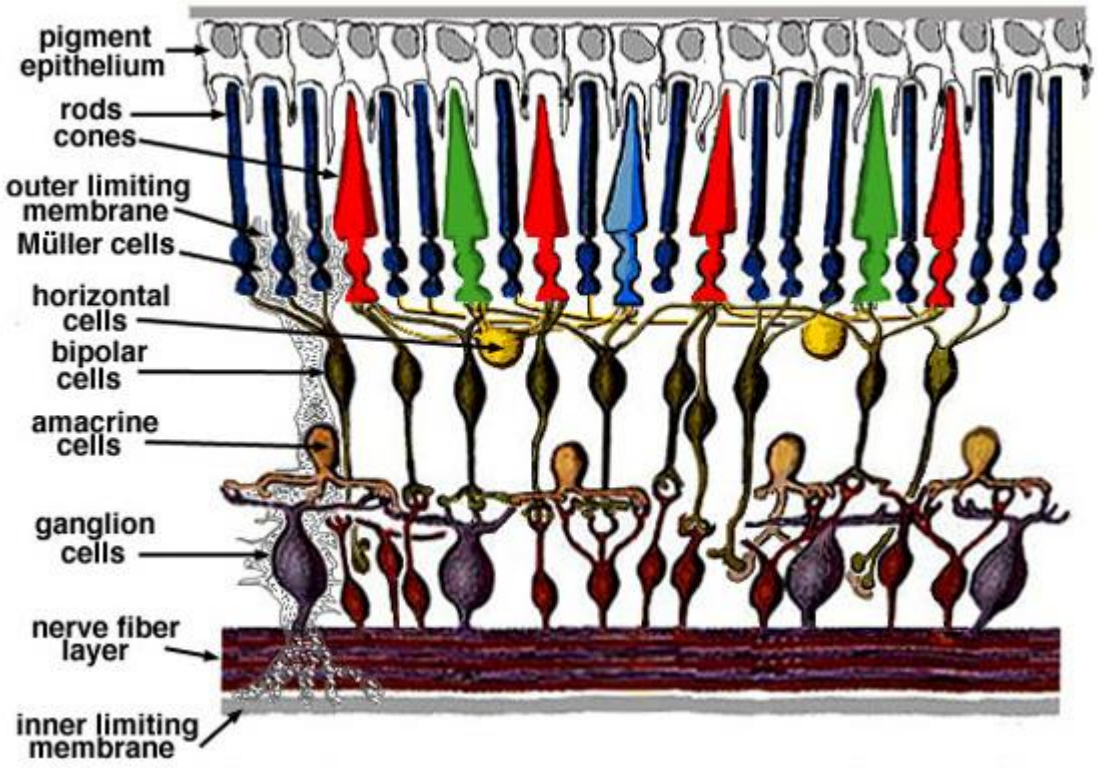

Figure 1.2: Cross section of the retina. Photons are absorbed by the visual pigment of the photoreceptors. The light signal is translated into an electrical signal which is passed from the photoreceptors to ganglion cells via bipolar cells. The axons of the retinal ganglion cells form the optic nerve which sends the light signal to the brain. Information can also be passed from photoreceptors to bipolar cells via horizontal cells. Amacrine cells function in integrating the signal from bipolar cells to the ganglion cells.

1.1.3 Genetic components

ADOA has a great degree of genetic heterogeneity as it has been associated with mutations in five different chromosomal loci, Optic atrophy 1, OPA3, OPA4, OPA5 and OPA7 found on chromosome 3q28, 19q13.2–q13.3, 18q12.2–q12.3, 22q12.1–q13.1 and 11q14.1-q21 respectively (Chen et al.). There are also other forms of optic atrophy associated with mutations in OPA4 and OPA6, which respectively follow X-linked and recessive modes of inheritance (Eiberg et al., 2006). Leber's Hereditary Optic Neuropathy is also a common cause of inherited optic atrophy displaying a similar phenotype to ADOA, however, it arises due to point mutations in mitochondrial DNA and therefore it is inherited maternally and predominantly affects males (Reynier et al., 2004). On the

other hand, ADOA follows an autosomal mode of inheritance and affects both males and females indiscriminately (Lenaers et al., 2012).

Mutations in the nuclear gene OPA1, which is located on the telomeric region of chromosome 3, has been found in 60-80% of patients and is thus the most common cause of ADOA. Mutations in OPA3, OPA5 and OPA7 have also been found in ADOA patients, albeit to a much lesser extent to OPA1, accounting for less than 1% of cases (Reynier et al., 2004), (Yu-Wai-Man et al., 2010). Numerous mutations in different regions of the OPA1 gene have been found in patients further extending the level of genetic heterogeneity of ADOA (Thiselton et al., 2002). To date, 230 pathogenic mutations have been found in OPA1 (Chen et al., 2013).

OPA1 spans approximately 100 kb and is comprised of 31 exons. Alternative splicing with exon 4b, 5b and 4 lead to the generation of eight transcripts and therefore eight different isoforms of the protein. Mutations found in patients with dominant optic atrophy have been found throughout the coding sequence of OPA1, the majority of which are located in exons 8-28. This region of the gene encodes for the GTPase domain (exon 8-15), the central dynamin domain (exon 16-24) and the C terminal region containing a coiled-coil domain (exon 25-28) (Delettre et al., 2002).

The mutations observed in OPA1 can be categorized into various types: nonsense, missense and splicing mutations (Delettre et al., 2002). Nonsense mutations, which can be found anywhere along the gene, arise due to the replacement of a nucleotide in the triplet code, which resultantly translates into a stop codon instead of an amino acid in the protein. Missense mutations which are predominantly located in the GTPase region

of the gene result from a change in a critical amino acid, giving rise to a malfunctioning protein. Splicing mutations are predominantly found in the GTPase region of the gene. They result from the replacement of a nucleotide in the splice site of the protein, leading to aberrant processing of the OPA1 transcript and possible skipping of an exon, which may contain amino acids critical for its function.

Approximately half of these mutations result in a truncated version of OPA1 (Delettre et al., 2002). Truncation of the C terminal means the protein cannot interact with itself and other proteins resulting in haploinsufficiency of OPA1 (Olichon et al., 2007). The dominant mode of inheritance may, in part, be explained by the abundance of OPA1 required in the retinal ganglion cells, meaning that the presence of one null allele could result in haploinsufficiency of OPA1, causing ADOA (Alexander et al., 2000). Non-truncating mutations allow the mutant protein to compete with the wild-type for interaction with OPA1, itself, and other proteins. As the mutant protein lacks the vital GTPase activity this causes a dominant negative effect in the cell (Olichon et al., 2006).

Although OPA1 expression is ubiquitous, it is most abundantly expressed in the brain and the retina, and to a lesser extent in the heart, liver, skeletal muscle and testis (Davies and Votruba, 2006). A wide range of tissues were examined by northern blot analysis and OPA1 transcripts were found in all tissues (Delettre et al., 2002). Predominant expression was noted in the ganglion cell layer of the retina above all other tissues in experiments carried out in rodents. The universal expression of OPA1 may explain the less common occurrence of extra ocular symptoms in syndromic ADOA.

1.2 OPA1

1.2.1 Protein structure

OPA1 is a ubiquitously expressed dynamin related GTPase attached to the inner mitochondrial membrane. The protein is comprised of a mitochondrial leader sequence with a highly basic amino terminal coiled-coil (CC) domain, a central dynamin domain, a highly conserved GTPase domain and a carboxy terminal domain of unknown function (Davies and Votruba, 2006). The leader sequence enables the protein to locate to the mitochondrion, the coiled coil enables interaction with other proteins, the central domain regulates the GTPase activity of the protein and the function of the C terminal domain has yet to be determined (Satoh et al., 2003). Opa1 is unique from other dynamin related GTPases (Figure 1.3) in that the carboxy terminus lacks a GTPase effector domain (GED), a pleckstrin homology (PH) domain and a proline rich domain (PRD) (Alexander et al., 2000).

Figure 1.3: A comparison between the structure of OPA1 and conventional Dynamins (Olichon et al., 2006). Opa1 is unique from other dynamin related GTPases in that the carboxy terminus lacks a pleckstrin homology domain and a proline rich domain.

The size of the OPA1 gene varies between isoforms, ranging from 924-1015 amino acids in length. The molecular weight also varies, and isoforms can either be 88 or 93 kDa

proteins. It has been shown that the 93 kDa isoforms have a stronger association to the mitochondrial membrane than the 88 kDa isoforms. It was also found that the 93 kDa isoforms were mainly associated with the inner membrane while the 88 kDa isoforms were exclusively associated with the outer membrane. Exon 5b encodes much of the N terminal coiled coil domain and this exon is skipped in the 88 kDa isoforms. This suggests a requirement for this region in the binding of OPA1 to the inner membrane (Satoh et al., 2003).

1.2.2 OPA1 and mitochondrial fusion dynamics

Opa1 has been found to play a vital role in mitochondrial fusion dynamics, a process by which mitochondria undergo continuous fusion and fission cycles maintaining equilibrium between interconnected networks or small individual units (Lee et al., 2004). Perturbing the balance between fusion and fission leads to an increase in ROS and a decrease in ATP production, events which favour cellular demise, most notably in highly energetic cells (Gray et al., 2013). In addition disruption to proteins involved in mitochondrial fusion dynamics have been implicated in neurodegenerative disorders, highlighting the importance of fusion dynamics for cell vitality (Twig and Shirihai, 2011).

OPA1 is a profusion protein with its optimal functioning being dependent on its GTPase domain and the coiled-coil region at the C terminal (Cipolat et al., 2004). As mentioned previously, most pathogenic mutations in ADOA affect these two regions of the protein. Mutations in the GTPase domain or the Carboxy terminus result in globular shaped mitochondria in transfected cells. The observed globular shape is indicative of unopposed fission arising from aberrant fusion.

It is thought that the coiled-coil domain is necessary for the protein interactions responsible for mitochondrial fusion (Cipolat et al., 2004). Fusion of mitochondria requires the synchronized fusion of both the inner and outer membrane, to allow the exchange of mitochondrial matrix contents and mitochondrial elongation. This process relies on the coordinated functioning of profusion dynamin GTPases on the inner and outer mitochondrial membrane, OPA1 and Mfn1/Mfn2 respectively (Figure 1.4) (Song et al., 2009).

Mitofusins; Mfn1 and Mfn2 are attached to the outer membrane with the GTPase domain and coiled-coil C terminal domain protruding into the cytosol. Fusion of the outer membrane of two adjacent mitochondria is facilitated by the interaction of the coiled-coil region of mitofusin proteins on one mitochondrion with those on an adjacent mitochondrion (Chen and Chan, 2005). OPA1 on the other hand is attached to the inner mitochondrial membrane with the GTPase domain and coiled-coil region protruding into the intermembrane space and is involved in the fusion of the inner membrane. The precise mechanism by which OPA1 mediates inner membrane fusion is unknown.

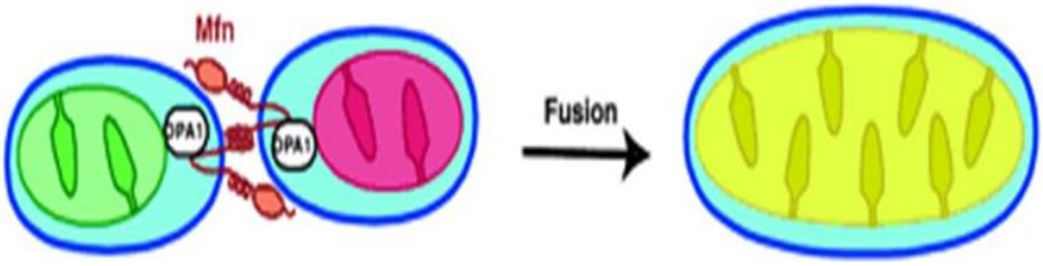

Figure 1.4: Opa1 is necessary for the fusion of fragmented mitochondria to create interconnected mitochondrial networks (Chen and Chan, 2005). OPA1 on the inner mitochondrial membrane works simultaneously with Mitofusins on the outer mitochondrial membrane to bring about mitochondrial fusion.

1.2.2.1 Mitochondrial membrane potential on the profusion function of OPA1

There are 8 different isoforms of the protein, all of which can be further processed to form either short (S) or long (L) isoforms (Song et al., 2009). The L isoform is bound to the innermembrane and is required for innermembrane fusion. Processing of the L isoform of Opa1 involves constitutive cleavage by the intermembrane space AAA (ATPase associated with diverse cellular activities) protease YME1L at the protease cleavage site-S1 of the protein at exon 5 (Head et al., 2009). The resulting S isoform is a soluble protein due to the removal of the amino terminal transmembrane domain (Alavi and Fuhrmann, 2013). The soluble form is required to protect cells against death by apoptosis, upon exposure to stress (Sanjuán Szklarz and Scorrano, 2012).

The ratio of L to S isoforms must be kept constant to maintain the balance between fusion and fission (An et al., 2013). A decrease in mitochondrial membrane potential leads to inducible cleavage of OPA1L via the zinc metalloprotease OMA1 (Alavi and Fuhrmann, 2013). This inducible cleavage of additional L isoforms of OPA1 upsets the balance between L and S isoforms and results in the loss of function of OPA1 as a profusion protein. Another innermembrane protein, Hypoxia inducible domain family, member 1a (Higd1a), an antiapoptotic protein, interacts with OPA1 and prevents cleavage of the L isoform. The N-terminal domain of Opa1 is thought to be essential for the interaction with Higd1a as only the L isoforms can interact successfully with Higd1a. Further, cleavage of Opa1 into its soluble form and subsequent mitochondrial fission and cell death occurs in the absence of Higd-1a.

1.2.2.1 Mitochondrial dynamics and mitophagy

Mitophagy is a quality control mechanism, whereby malfunctioning mitochondria are returned to the soma and eliminated from the cell by the autophagy system (Twig and Shirihai, 2011). Degradation of the mitochondria involves their engulfment into autophagosomes, which are subsequently fused with lysosomes to facilitate enzymatic demolition.

Mitophagy is essential for maintaining the quality of the mitochondria in the cell. Depolarized mitochondria undergo fission which is necessary to isolate damaged mitochondria from the mitochondrial population and facilitate their disposal by autophagy (Chen and Chan, 2009). The fate of the fragmented mitochondria is dependent on their cellular environment. They can be rescued by subsequent fusion with active mitochondria if unfavorable conditions are merely transitory. On the other hand, if the depolarized state is sustained OPA1 is cleaved and no longer able to carry out its profusion role.

Mitochondria incapable of fusion are retained in a preautophagic pool and are degraded. Also, if insufficient OPA1 is available then the incidence of fusion events will decline, allowing autophagy of the fragmented mitochondria to prevail leading to apoptosis (Twig and Shirihai, 2011). The role of OPA1 in mitophagy involves an interaction with the proapoptotic protein Bnip3 in response to cellular stress. Retinal ganglion cells (RGCs) can be exposed to various stress inducers such as hypoxia in several ocular diseases. Mitophagy aims to restore homeostasis, however if cellular stress reaches threshold levels, OPA1 complexes may be disassembled and cell death will ensue.

With respect to ADOA, mutations in OPA1 may render the RGCs more vulnerable to stressors, hence reducing their resistance to demise (Landes et al., 2010). In a mouse model of ADOA in which Opa1 is mutated, there was an increase in the number of autophagosomes, with the most in the RGCs and the surrounding dendrites. The downregulation of OPA1 causes a decrease in membrane potential which leads to an increase in dysfunctional mitochondria that are targets for the competing actions of fusion and mitophagy. In the case of ADOA mitophagy appears to triumph, which is hypothesized to overburden the autophagy system, resulting in apoptosis of the RGCs (White et al., 2009).

1.2.3 General effects of the functional loss of OPA1

ADOA is considered to be a mitochondriopathy as disruption to OPA1 leads to mitochondrial dysfunction, which ultimately gives rise to the disease phenotype. Homozygous inactivation of OPA1 causes embryonic lethality, suggesting a vital role for OPA1 in development (Davies et al., 2007). A loss of OPA1 in the cell results in mitochondrial fragmentation, decreased oxidative phosphorylation, a dissipation of the mitochondrial membrane potential and the initiation of apoptosis (Olichon et al., 2003).

OPA1 may be required for the maintenance of the protein levels and enzymatic activity of complex IV of the electron transport chain. Mice lacking opa1 in β islet cells were shown to have a significant decrease in the protein levels of all subunits of complex IV and a more minor decrease in a subunit of complex I. The remaining complexes were unaffected by the loss of opa1. The specific activity of Complex IV was likewise decreased, while no change was seen in that of the other ETC complexes. Interestingly,

Opa1 loss had no effect on mtDNA copy number, suggesting that the reduction in complex IV does not results from a reduction in mtDNA (Zhang et al., 2011). In mice heterozygous for Opa1, the activities of complex I and IV were found to be decreased from the wild-type, while all other complexes were unaffected. In contrast to the opa1 null β islet cells, the mtDNA was markedly reduced in the heterozygous Opa1 mice (Chen et al., 2012). Furthermore, down regulation of Opa1 in primary cortical neurons lead to a reduction in the levels of reactive oxygen species (ROS).

The levels of expression of pre and post synaptic proteins were reduced with the functional loss of Opa1, thereby, impairing the ability of the neurons to form new synapses (Bertholet et al., 2013). Opa1 loss also resulted in inhibition of dendritic growth essential for neuronal maturation. It is thought that expression of proteins involved in synaptogenesis is dependent on sufficient ROS levels, which are diminished with the loss of Opa1.

1.2.4 The role of OPA1 in apoptosis

The loss of function of OPA1 has been extensively studied, yielding a wealth of information on the importance of this protein in maintaining mitochondrial integrity and cell viability. There appears to be interplay between mitochondrial morphology and apoptosis, however, the underlying molecular events with respect to the role of OPA1 are less well understood.

The structure of the cristae was found to be majorly disrupted in cells devoid of Opa1, which could be the central event leading to apoptosis (Olichon et al., 2003). Approximately 80% of cytochrome *c* is contained within the folds of the cristae and the

remainder is stored in the intermembrane space in a normal non apoptotic cell (Arnoult et al., 2005), (Martinou and Youle, 2006). It is thought that some isoforms of OPA1 such as that which contains exon 5b, form the cristae junctions supporting the sequestration of cytochrome *c*, therefore, when OPA1 expression is inhibited, cytochrome *c* may be released (Lenaers et al., 2009). Perturbations of the inner membrane structure allows the release of cytochrome *c* into the intermembrane space (Olichon et al., 2007). Cristae disorganization could occur prior to the dissipation of the membrane potential, which could open the cristae junctions allowing the release of cytochrome *c*, triggering apoptosis.

Cell demise can be prevented by the overexpression of the anti-apoptotic protein Bcl2, suggesting that OPA1 is a target for pro or anti-apoptotic proteins (Olichon et al., 2007). The interaction of OPA1 with the anti-apoptotic protein Higd-1a has been shown to prevent cleavage of OPA1L; this in turn could prevent the release of cytochrome *c* into the cytosol. It is well known that the induction of the intrinsic apoptotic pathway requires the release of cytochrome *c* into the cytoplasm, and OPA1 is somehow crucial to counteract the intrinsic death signal (Alavi and Fuhrmann, 2013).

The pro-apoptotic proteins Bax and Bak are mediators of the permeabilisation of the mitochondrial outer membrane facilitating the release of cytochrome *c* (Arnoult et al., 2005). Opa1 is also released from the mitochondria and can be detected in the cytosol in apoptotic cells. Moreover, it is thought that the loss of OPA1 from the inner membrane after outer membrane permeabilisation inhibits fusion, allowing mitochondrial fragmentation to occur.

Lastly, the amount of cytochrome *c* required to activate the target caspases of the apoptosome has not been defined and may depend on cell type (Martinou and Youle, 2006). The apoptosome itself can be activated by relatively small amounts of cytochrome *c* that could be released from the intermembrane pool during Bax/Bak mediated mitochondrial outer membrane permeabilisation (MOMP). In neurons (MOMP) can be reversed by antiapoptotic proteins, however, if the remaining cytochrome *c* is released from the cristae folds apoptosis could ensue.

1.2.5 The functional loss of OPA1 with respect to ADOA

With respect to ADOA it is unknown as to why RGCs are exclusively affected by the functional loss of OPA1 considering that the protein is ubiquitously expressed. The highest levels of Opa1 RNA expression were found to occur in the retina and the brain however this does not explain the pathophysiology of ADOA (Alexander et al., 2000). The expression levels of OPA1 does not predominate in RGCs relative to other cells in the retina, nor is there a specific isoform expressed in RGCs, yet, other cells of the retina are unaffected by loss of function of OPA1 and the associated increase in apoptosis (Kamei et al., 2005).

If there is insufficient OPA1 available to maintain the structure of the cristae, cytochrome *c* could be available in the intermembrane space, in amounts sufficient to irreversibly trigger apoptosis. Therefore in the event of exposure to an apoptotic stimulus and the subsequent activation of Bax/Bak cell death would be inevitable.

The retinal ganglion cell may have high levels of antiapoptotic proteins to compensate for the increased exposure to apoptotic stimuli, which would make it more susceptible

to Opa1 loss of function. Further, it was found that neurons can restore normal function after cytochrome *c* release if exposed to nerve growth factor (NGF). Opa1 deficient cells are thought to be lacking in the ROS dependent upregulation of proteins involved in cell growth and survival, rendering them unable to overcome apoptosis (Chen et al., 2012).

1.3 Animal models of ADOA

The availability of retinal tissue from patients with ADOA is low due to the scarcity of patients with the disease. Thus the creation of animal models is necessary to gain insight into the pathology of the disease, as well as testing the efficacy and safety of therapeutic intervention in statistically viable numbers.

1.3.1 Drosophila model of Opa1 deficiency

An eye specific Opa1 mutant *drosophila* was generated by somatic mutagenesis, inactivating two copies of the *Drosophila* ortholog of OPA1, CG8479 (*dOpa1*) in the eye (Yarosh et al., 2008). Eye specific mutants were chosen due to the embryonic lethality of homozygous mutants and the lack of eye phenotype observed with the heterozygous mutants. The eyes in this model were found to be glossy due to decreased lens and pigment disposition by cone and pigment cells. They also had a rough phenotype due to failure of the cells within the ommatidium to develop and pattern properly, which may be due to defective apoptosis during development. The mitochondria were scarce and dysmorphic in mutant cells of this model, which may be caused by the increased ROS production and cell death also observed in these cells. The glossy eye phenotype can be significantly reduced with the over expression of the antioxidant *h*SOD1 however no effect was observed on the rough eye phenotype. The observations in this model support the role of ROS in the pathogenesis of ADOA which would intuitively suggest that antioxidants would ameliorate the disease phenotype.

This model may show the effects of Opa1 loss at a systemic level, however, the reliability of this model in uncovering the pathogenesis of ADOA is questionable. On the other

hand, the mouse is a suitable choice for a disease model due to the relative ease of genetic manipulation and the high homology to the human genome.

1.3.2 Opa1 null β-islet cell mouse

To find out the role of Opa1 in specific tissues a conditional mouse strain must be generated, as homozygous null embryos are not viable. The islet cells were chosen due to the important role of oxidative phosphorylation in regulating glucose levels in the blood. To investigate the role of Opa1 in the pancreatic β-islet cell, Opa1 was deleted from these cells by introducing loxP recombination sites before exon 10 and after exon 13 in the Opa1 gene (Zhang et al., 2011). The intervening sequence which encodes for an essential G3 motif in the GTPase domain is excised, resulting in a dysfunctional Opa1 protein. This model shows a reduction in the activity and the amount of Complex IV activity in the β-islet cells while there is no reduction in the copy number of mtDNA. There was no increase in apoptosis detected in these cells, however cell proliferation was found to be impaired.

1.3.3 Mouse model of RGC loss

Genetic manipulation was employed to create a mouse model whereby RGCs are programmed to be removed after differentiation. This allows a more accurate investigation of the effects of RGC loss on optic nerve degeneration compared to a knockout model that merely prevents normal RGC development. The *Pou4f2* gene which is required for the differentiation and survival of RGCs was knocked out in one allele by the insertion of floxed-lacZ-stop-diphtheria toxin A (dta) cassette in the creation of a heterozygotes mouse (White et al., 2009). This mouse was then crossed with mice with

a tamoxifen-inducible cre strain and the resultant mice were maintained as stock lines. Tamoxifen administration caused successful ablation of the RGCs. The retinas maintained their structural integrity while the model shows characteristic features of retinal degeneration.

1.3.4 Syndromic ADOA mouse model

An *Opa1* knock-in mouse carrying the recurrent *OPA1*c.2708_2711delTTAG mutation, described in patients was generated by deleting the four conserved TTAG base pairs in exon 27 of the murine *Opa1* gene. The gene was integrated by homologous recombination at the *Opa1* gene locus in embryonic stem cells which were subsequently injected into E3.5 blastocysts of C57Bl6/J mice. The $Opa1^{+/-}$ mice have one defective copy of Opa1 in which the last 58 amino acids are deleted due to the presence of a premature stop codon. A progressive loss of visual acuity can be observed in these mice which may be associated to the reduction in the COX activity in the retina. The RGC number was half that of control mice in this model between the ages of 9 and 16 months (Sarzi et al., 2012). The mice also displayed reduced auditory brain stem responses, locomotive and gait abnormalities and disorganised myofibres from both skeletal and cardiac muscle, consistent with the extraocular symptoms observed in ADOA plus patients (Sarzi et al., 2012).

1.3.5 Main mouse models of ADOA

There are two main mouse models of ADOA that have been published: the B6;C3-$Opa1^{Q285STOP}$ Opa1 mutant mouse and the B6;C3-$Opa1^{329\text{-}355del}$ Opa1 mutant mouse (Davies et al., 2007), (Alavi et al., 2007).

1.3.5.1 B6;C3-Opa1$^{329\text{-}355del}$

The B6;C3-Opa1$^{329\text{-}355del}$ Opa1 mutant mouse was generated by screening an *N*-ethyl-N-nitrosourea (ENU)-mutagenized DNA library of mouse DNA and identifying a splice site mutation in murine Opa1 intron 10: c.1065 + 5G → A (Alavi et al., 2007). A purebred C3HeB/FeJ mice carrying the Opa1$^{enu/+}$ mutation were outcrossed with C57BI/6. Subsequent Opa1$^{enu/+\ mice}$ were intercrossed to create a DOA mouse model with the splice site mutation identified in the Opa1 gene and wild-type littermate controls. The mutation in this model is close to three mutations found in DOA patients, namely c.1065 +2T > C, c1065 + 2T > G and c.1065 + 3A > C. Mutations in this region of the Opa1 gene lead to an in-frame deletion of 27 amino acid residues in the dynamin GTPase domain, due to the skipping of exon 10.

1.3.5.2 B6;C3-Opa1^{Q285STOP}

The B6;C3-Opa1^{Q285STOP} mutant mouse model was generated by screening an ENU-mutagenized DNA library of CH3 male mice for point mutations in Opa1 (Davies et al., 2007). A heterozygous nonsense mutation in exon 8 was selected which codes for a C-T transition at 1051 bp. This introduces a stop codon in place of glutamine285, leading to the expression of a truncated protein at the start of the GTPase domain. This mutation is close to the mutation that is the most common cause of ADOA in humans at the 290 amino acid. The Opa1 mutant mice line was then generated via *in vitro* fertilization of C57BI/6J females with mutant sperm. The founder generation was outcrossed to C57BI/6J up to the 4th generation and the heterozygous Opa1+/- mice were then intercrossed to create generation cohorts (Davies et al., 2007). This model shows

premature degeneration of the optic nerve and an increase in the presence of autophagosomes in the RGCs and their axons (White et al., 2009).

1.3.5.3 Validity of B6;C3-Opa1^{Q285STOP} and B6;C3-Opa1$^{329-355del}$ as models of DOA

Both models show a 50% reduction in Opa1 RNA in the retina and a 50% reduction in Opa1 protein in a number of different tissues, supporting the theory that haploinsufficiency is underlying the pathophysiology of DOA.

The B6;C3-Opa1^{Q285STOP} mouse displays a loss in visual acuity noted at 12 months, which is consistent with the age at which dendropathy of RGCs begins to occur (Williams et al., 2011). Abnormalities in myelin distribution in the optic nerve reportedly began at 9 months of age in this model and continued to 18 months (Davies et al., 2007). This is consistent with findings in older ADOA patients whereby demyelination was observed (Davies et al., 2007).

The B6;C3-Opa1$^{329-355del}$ appears to have a more severe phenotype showing total loss of large axons and a significant loss of small axons of the RGCs which make up the optic nerve by the age of 8 months (Alavi et al., 2007). The findings suggest that large RGCs have an increased susceptibility to the Opa1 mutation. However, in some cases the loss of large axons may be due to the shrinkage of RGC axons that occurs prior to cell death. The axonal degeneration in the B6;C3-Opa1^{Q285STOP} mice began at 9 months and the axonal counts were significantly reduced by 24 months (Davies et al., 2007). The RGC layer in the B6;C3-Opa1^{Q285STOP} mouse was compared to littermate controls of up to 24 months and revealed no difference in cell death between the two groups. Similarly there was no change in the retinal architecture or morphology in the mutants compared to the

controls, however, there was a significant increase in the number of autophagosomes in the soma of the RGCs and their axons.

The B6;C3-Opa1$^{329\text{-}355del}$ model shows a slight reduction in the number of RGCs in the mutant mice at 13 months which was exacerbated significantly by 23 months, suggesting a progressive loss of RGCs in the pathophysiology of ADOA (Alavi et al., 2007). Contrastingly, the B6;C3-Opa1^{Q285STOP} model suggests that ADOA results from RGC dysfunction rather than cell loss, as visual function appears to be disrupted in the absence of RGC loss (Williams et al., 2011). Disruption to the visual pathway in these models was revealed by analysis of the visual evoked potentials which are suggestive of RGC loss or dysfunction.

Further, in the B6;C3-Opa1^{Q285STOP} mouse model mitochondria were punctuated and dispersed throughout muscle explant cells (Davies et al., 2007). In cardiac cells of the same model, a reduction in ATP production, oxygen consumption and protein levels of COX, as well as a reduced resistance to oxidative stress was observed (Chen et al., 2012).

1.3.6 Selective dendropathy in the B6;C3-Opa1^{Q285STOP} mouse

Exactly how defective mitochondrial fusion dynamics leads to RGC degeneration has as of yet failed to be established, however the B6;C3-Opa1^{Q285STOP} mice are providing invaluable insight into the underlying mechanisms of ADOA.

The progressive dendritic atrophy in the RGCs of the B6;C3-Opa1^{Q285STOP} mouse beginning from the ages of 10-15 months were localized to those synapsing in the sublamina b (ON layer) of the inner plexiform layer with dendrites synapsing in the outer OFF layer relatively unaffected (Williams et al., 2010b). These findings are suggestive of

a selective effect of the functional loss of Opa1 on On-Centre RGCs, which have different energy demands and neurotransmitter pathways to the resistant Off-Centre cells (Williams et al., 2010b). Findings from the B6;C3-Opa1^{Q285STOP} mouse suggests that RGC loss and optic nerve degeneration occurs secondary to the slow progressive dendritic pruning, causative of the insidious onset of ADOA. The pressing question, regarding the selective atrophy of the On-Centre RGCs remains unanswered.

A decrease in complex I and IV activities and an associated reduction in ATP production was found in the B6;C3-Opa1^{Q285STOP} mouse (Chen et al., 2012). Due to the mitochondrial dysfunction seen in the absence of Opa1, the magnitude of energy demanded of the mitochondria in the RGCs to maintain their function should be considered. There is a large energy demand of RGCs due to the large dendritic field. Each process requires a plentiful supply of mitochondria along its length, in order to be sustained by the cell. Moreover, myelination of the RGC axon begins, merely as the nerve leaves the eye. This puts an additional strain on the energy resources of the cell as the relatively large unmyelinated portion of the axons reduces the conductive capacity of the axon, thereby increasing the amount of ATP needed to carry out the same function (Williams et al., 2012).

Furthermore, the loss of Opa1 and the consequential mitochondrial dysfunction have been shown to result in dysfunctional connectivity in the RGCs (Williams et al., 2012). The dendritic pruning seen in the B6;C3-Opa1^{Q285STOP} mouse is accompanied by atrophy of the synapses of the RGCs, as shown by decreased synaptic density and structural changes. It was also found that there was a decrease in glutamatergic synapses, while

the GABAergic synapses were unaffected by loss of Opa1. On-Centre cells synapse with bipolar cells via glutamatergic receptors, which have high energy requirements while their Off-Centre counterparts use GABAergic transmission which has a much lower energy demand. This finding supports previous findings for selective atrophy of On-Centre RGCs and brings to attention, yet again, to the immense energy demands of the ON-centre RGCs.

Of note, the mitochondria within the synaptic button were found to be fragmented (Williams et al., 2012). As mentioned previously, the fate of fragmented mitochondria is dependent on the cellular environment, i.e. they can be rescued if optimal conditions are restored within the cell. However, with the unceasing energy demands of the On-Centre RGCs and an inadequate number of functioning mitochondria, it is inevitable that the mitochondria will be unable to elongate and will be thus, degraded. The cell may then begin to retract its processes to alleviate the energy burden of the cell, giving rise to the pruning of the dendrites that is seen in this model.

If we could find a way to assist the mitochondria in meeting the, presently, unsurmountable challenge of providing adequate ATP to the On-Centre RGCs, then it may be possible for the RGCs to retain their dendrites. This in turn may prevent the deterioration of visual acuity seen in our model.

1.3.6.1 RGC classification

RGC subtypes have been found to have differential susceptibility to death in diseases associated with RGC degeneration such as glaucoma (Struebing et al., 2016). In ADOA ON-centre RGCs have an increased susceptibility to degeneration compared to OFF-

centre RGCs (Williams et al., 2010b), therefore, it is also possible that further subclasses of RGCs are differentially susceptible to degeneration in ADOA. It is, therefore, important to be able to identify different RGC subtypes and be aware of the percentage of each type in each experimental group to avoid confounding the results.

RGCs can be classified based on their electrophysiology, morphology, anatomy and genetics (Sun et al., 2002) (Baden et al., 2016). RGCs were first classified into ON-centre, OFF-centre and ON-OFF cells based on the response of the cells to light (Baden et al., 2016). Based on their morphology, RGCs can be classified into four main groups, three different groups of monostratified cells (RG_A, RG_B and RG_C) and a group of bistratified cells (RG_D) (Sun et al., 2002). The monostratified cells are classified based on the size of their soma and dendritic field. RG_A cells have a large soma and a large dendritic field, RG_B cells have a small to medium sized soma and a small to medium sized dendritic field, and RG_C cells have a small to medium sized and a medium sized dendritic field (Sun et al., 2002). RGCs can be sub classified based on the morphology, with 10 subclasses of monostratified and 4 subclasses of bistratified cells identified in the mouse based on size shape and branching pattern (Coombs et al., 2006). RGCs in mice have been shown to project to at least 40 different targets, suggesting a large number of RGC subtypes, based on an anatomical classification (Baden et al., 2016). Further, populations of RGCs can be classified based on their genetic profile.

The RGC classification system is based on RGCs from healthy adult and developing retinae (Tribble et al., 2014). Since RGC degeneration in the the B6;C3-Opa1^{Q285STOP} mouse presents as a loss in dendrites and dendritic field size, therefore RGC classification

based on dendritic field size and branching density may be unreliable in this model. However, it is also possible to classify RGCs based on dendritic features that are more resistant to degeneration such as the more proximal dendritic structures, which remain intact during early stage RGC degeneration. It was found that RGCs can be classified based on the RGC soma and proximal dendritic field size, and primary dendrite thickness (Tribble et al., 2014). In addition, asymmetry in the proximal dendritic tree can be used to discriminate between different RGC subtypes.

1.3.7 Limited treatments for ADOA

To date there is no effective treatment available for ADOA. Low visual aids can have some benefit in patients with severely decreased visual acuity, however, there is no effective means of reducing the severity of the symptoms of ADOA (Lenaers et al., 2012).

As the energy deficits appear to be responsible for the cell loss seen in ADOA, targeting the apparent dysfunctional ETC of the mitochondria to increase energy production seems like the most attractive treatment option. Idebenone is an ETC targeting drug that has been shown to have some therapeutic effects, however, these effects are not sufficient for the drug to be recognized as an effective treatment for optic neuropathies including ADOA.

Idebenone is a benzoquinone, a synthetic analogue of Coenzyme Q10 which acts as an exogenous transporter of electrons through the electron transport chain in the mitochondria, thereby, increasing the rate of ATP production. Idebenone acts by transporting electrons directly to Complex III thereby bypassing Complex I which is

defective in ADOA. It is also an antioxidant which can counteract the increase in ROS produced as a result of the defect in complex I (Barboni et al., 2013).

This shows the need to address other underlying features of ADOA as targets for therapeutic intervention, as the effects of bypassing the defective complex I appear to be clinically insufficient. A more effective treatment for ADOA is needed. As complex IV, which is downstream to complex I, has also been shown to be defective in this condition, targeting complex IV could bring about a greater yield of ATP production. As red light is hypothesised to upregulate the activities of complex IV, the possibility of irradiating the RGCs with 670 nm light could provide a simple non-invasive way of ameliorating the condition.

1.4 The potential of red/NIR light therapy in retinal neurodegeneration

1.4.1 History of light therapy

The therapeutic properties of light have been known since antiquity, as far back as 1400 BC, where it was used by Hindus to treat skin disorders (Roelandts, 2002). The ancient Egyptians, Greeks and Romans were also reportedly aware of the beneficial effects of sunlight which they used to treat various ailments (McDonagh, 2001). The evidence for the use of phototherapy in those time, however, is purely anecdotal. It was not until 1903 that the therapeutic power of light gained scientific recognition, when Niels Finsen was awarded the Nobel Prize in medicine for the discovery of UV light as a treatment for skin tuberculosis (*lupus vulgaris*) (Finsen, 1901).

Red light was later found to have biostimulatory effects; an unintentional discovery made by Endre Mester, in 1967, who wanted to assess the ability of 694 nm lasers to

cause carcinogenesis in mice (Mester et al., 1971). The mice in both the light-treated and untreated groups were shaved prior to laser exposure. The results found that the light-treated group did not develop cancer, but more intriguingly, the hair grew back on the laser treated mice at a faster rate than the untreated group.

In more recent times, there has been a surge in the use of red and near infrared (NIR) lasers and LEDs in clinical and preclinical research (Desmet et al., 2006). As red and NIR light have relatively long wavelengths, they have the advantage of a greater penetration depth over shorter wavelengths, making them an ideal choice for the treatment of neural tissue (Hartwig and Van Veen, 1979). In addition to light being able to penetrate into the tissue of interest, another requirement is that the photon energy corresponds to the absorption characteristics of the chromophores responsible for triggering the beneficial effects upon photoexcitation. It appears that red and NIR light correspond the absorption maxima of such chromophores as will be discussed later. For various reasons, LEDs are most commonly used as the light source in these studies. Most importantly, red/NIR LED therapy has been approved for use in humans and has been deemed as a non-significant risk by the U.S. Food and Drug Administration. Although shorter wavelengths of visible light and UV light are also employed for therapeutic purposes, their safety for use in humans, especially for the eye, is less clear (Rozanowska et al., 2009, Rozanowska, 2012). With the ultimate objective of exploring the efficacy of phototherapy as a treatment for neurodegeneration in the human retina, this review will focus only on the use of wavelengths that are least likely to cause adverse effects, that is red and NIR light(Barolet, 2008).

1.4.2 The potential of red/NIR light as a treatment for neurodegeneration

1.4.2.1 Evidence from in vitro studies

Red and NIR light have been shown to provide protection against the deleterious effects of mitochondrial electron transport chain inhibitors and excitotoxic cell death in neurons *in vitro* (Wong-Riley et al., 2005, Ying et al., 2008a, Huang et al., 2014). Since impaired mitochondrial function and excitotoxicity are common causes of cell death in neurodegenerative conditions, the ability of red/NIR light to protect against these challenges *in vitro* has emphasized the potential of this therapy in various neurodegenerative conditions.

1.4.2.2 The effects of red/NIR light in models of neurodegeneration

Red/NIR light therapy has shown great potential in the treatment of acute neurodegenerative conditions, showing neuroprotective effects in rodent models of spinal cord injury, traumatic brain injury and stroke (Byrnes et al., 2005b, Wu et al., 2012, Xuan et al., 2015, Dong et al., 2015a, Oron et al., 2006, Giacci et al., 2014b).

Furthermore, red light has been shown to have beneficial effects in animal models of some of the most prevalent neurodegenerative diseases. A reduction in cell loss and other markers of disease severity was seen with red/NIR light treatment, in rodent models of multiple sclerosis, Alzheimer's and Parkinson's disease (Muili et al., 2013, Muili et al., 2012, Purushothuman et al., 2015, Purushothuman et al., 2013, Oueslati et al., 2015, Johnstone et al., 2014, Peoples et al., 2012b, Shaw et al., 2010).

1.4.2.3 The potential of red/NIR light as a successful treatment for neurodegeneration in humans

While transcranial red/NIR light therapy is yielding remarkable results in numerous rodent models of neurodegeneration, the real question is how well these results will translate when applying this therapy to human patients.

Interestingly, in a neurotoxin-induced monkey model of Parkinson's disease, 670 nm light was delivered directly to the macaque midbrain using an implanted optical fibre which was activated over the period of time of 5-7 days when the neurotoxin precursor, 1-methyl-4-phenyl-1,2,3,6-tetrahydropyridine (MPTP), was injected (Darlot et al., 2016). The study found a reduction in clinically-assessed behavioural impairment with this method of red light delivery in this primate model as well as neuroprotection to the dopaminergic neurons of the substantia nigra. Although a more invasive method of delivery than transcranial red light treatment, no major adverse effects were observed following surgical implantation of the optical fibre. However, it would have been of great interest if the effects of transcranial light delivery were also tested in this model, for comparison.

1.4.3 Red light treatment in retinal degenerative diseases

Since the retina is an extension of the CNS, the neuroprotective effects of red/NIR light, as discussed above, should also be observed in this tissue. In fact, irradiating the retina with red or NIR light seems more likely to be successful as a non-invasive treatment for human patients as the issue of tissue penetration is avoided.

1.4.3.1 The safety of light treatment on the retina

The greatest concern arising when aspiring to use red light therapy to treat retinal degeneration, is the potential retinal damage that may occur upon direct exposure of the retina to light with high levels of irradiance. The dangers of high levels of irradiance on the retina is highlighted in a study on anesthetised monkeys (Friedman and Kuwabara, 1968). It was found that white light with a retinal irradiance of 270 mW/cm^2 caused irreversible damage to the photoreceptors and retinal pigment epithelium. White light is made up of light of all wavelengths in the visible light spectrum, with light of shorter wavelengths and higher frequencies having a greater damaging effect on photoreceptors. Blue light, with a relatively short wavelength, was found to cause irreversible damage to S cones (Harwerth and Sperling, 1975). While exposure to green and red light caused damage to M and L cones, respectively, the damage to these cones was reversible, with a full recovery of function seen after a few weeks. More recent studies on macaque monkey, however, have demonstrated that yellow light of 568 nm wavelength can cause retinal damage manifested as disruption of the retinal pigment epithelium at the dose below the Maximal Permissible Exposure established by the American National Standard Institute's (ANSI) as a standard for the safe use of lasers (Hunter et al., 2012).

Albeit transient and less severe than light of shorter wavelengths, damage to L cones upon exposures to high levels of red light would be a cause for concern when considering red light as a treatment for retinal degeneration. This concern has been addressed with numerous *in vivo* studies. These studies have shown that therapeutic effects were achieved, in the absence of retinal damage, when rodent retinas were exposed to 670

nm light with a therapeutically effective irradiance and exposure times (Albarracin et al., 2013, Albarracin et al., 2011, Giacci et al., 2014a). Further, this included irradiance of 60 mW/cm2 which is the highest irradiance level found in studies of *in vivo* models of retinal degeneration where positive results were achieved using 670 nm light. This demonstrates the safety of using 670 nm light as a treatment for retinal degeneration.

In addition to photoreceptor damage, the possibility of photothermal damage to the retina and surrounding ocular structures evokes further concern when considering using light to treat retinal degeneration (Youssef et al., 2011). Comparing the effects of green, red and NIR laser light exposure on the temperature rise in the human choroid, it was found that the longer wavelengths led to a smaller degree of choroidal heating, due to the decrease in absorption by melanin with increasing wavelength (Vogel and Birngruber, 1992). The variation in choroidal heating between green and red wavelengths was minor compared with the difference between green and NIR wavelengths.

Still the question remains as to which would be the optimal wavelength for use as a neuroprotective agent in the retina. Addressing this, the efficacy of red and NIR light were compared in a model of partial optic nerve transection (Giacci et al., 2014a). It was found that although protective effects were seen in retinae treated with both red and NIR light, 670 nm light was more effective in improving visual function compared with 830 nm light. However, in a rat model of light induced retinal degeneration protective effects were observed with 670 nm light treatment, but no protection was seen with 830 nm light (Giacci et al., 2014a). It is therefore not surprising that most studies testing the

effectiveness of phototherapy on neurodegeneration in the retina use red light at 670 nm.

1.4.3.2 670 nm light therapy in models of photoreceptor damage

As discussed above, exposing the retina to bright light can cause photoreceptor damage, an event that can occur with excessive sunlight exposure or accidental exposure to high intensity artificial light sources. Models of light induced photoreceptor damage are also used to simulate retinal degenerative diseases, involving photoreceptor specific death. Emphasising the vast and diverse effects of light on biological tissue, irradiating the retina with red light provided protection against the structural damage to the outer retina and loss in photoreceptor function in a rat model of light induced photoreceptor degeneration (Albarracin et al., 2011). Methanol can also induce damaging effects on the retina causing photoreceptor toxicity due to the ability of its metabolite, formic acid, to inhibit cytochrome *c* oxidase, the terminal enzyme of the electron transport chain. In a rat model of methanol induced retinal toxicity, red light treatment brought about a significant recovery of rod and cone mediated function, in addition to preventing methanol induced changes to outer retinal morphology (Eells et al., 2003). These studies show the ability of red light to protect against loss in photoreceptor function, an event that would cause severe visual impairment and would otherwise be irreversible.

1.4.3.3 The effects of red light on inflammation in the outer retina

Inflammation in the retina has been implicated in many retinal diseases including age related macular degeneration (AMD) and diabetic retinopathy, and as such, looking at ways to alleviate inflammation in these conditions is thought to reduce the severity of

symptoms associated with these diseases (Whitcup et al., 2013). Also, an upregulation in inflammatory proteins has been observed following light damage in rats, demonstrating pathological features similar to “dry” AMD (Rutar et al., 2012). In addition to its ability to protect against light induced photoreceptor damage, red light treatment was found to reduce the complement propagation that occurs in the retina following light damage. Red light treatment was also tested in an aged genetic mouse model of AMD, the complement factor H knockout, which presents with reduced retinal function and increased inflammation (Begum et al., 2013). In contrast to most studies with red/NIR light where the light source was held directly in front of the animal, the environmental light was supplemented with red light for this study. Even though the red light exposure was indirect, the levels reaching the retina were sufficient to reduce inflammation in the outer retina, in this model.

In addition to inflammation associated with disease pathology, inflammation increases in the retina with age. Red light was effective in reducing proinflammatory cytokines and a chronic marker of inflammation in the aged mouse retina, demonstrating the potential of red light to also alleviate the visual decline associated with normal aging (Kokkinopoulos et al., 2013). These studies draw attention to the ability of red light to produce anti-inflammatory effects associated with outer retinal degeneration, whether by induced damage, disease pathology or normal aging.

1.4.3.3 The effects of red light on neurodegeneration in the inner retina

Retinal ganglion cell (RGC) death and optic nerve degeneration are hallmarks of optic neuropathy, a frequent cause of vision loss, of which the causes are many. Red light

therapy has been trialled in a rat model of diabetic retinopathy and positive outcomes have been reported. There was a significant reduction in the diabetes induced RGC death and a 50% improvement in the diabetes-induced reduction in ERG amplitude with exposure to red light (Tang et al., 2013a). Highlighting the beneficial effects of red light on the retinal vasculature, red light also prevented the diabetes-induced increase in leukostasis in the retinal vasculature, an event which is implicated in the pathogenesis of diabetic retinopathy. Further, the diabetes-induced increase in retinal expression of an adhesion molecule, essential for leukostasis, ICAM-1, was also prevented with red light. Similarly, in a model of secondary degeneration of RGCs, resulting from traumatic injury to the optic nerve, red light was found to be protective (Fitzgerald et al., 2010). The secondary damage, following partial optic nerve transection, normally leads to further loss of RGCs and visual function; however, normal visual function was restored with red light treatment(Fitzgerald et al., 2010). Furthermore, treatment with 670 nm light in a rat model of partial optic nerve transection resulted in improved vision 7 days post injury (Giacci et al., 2014a). Additionally, dendropathy of retinal ganglion cells, an event found to be associated with visual loss in experimental models of glaucoma and autosomal dominant optic atrophy, was partially prevented, in an axotomy model of neurodegeneration, with red light treatment (Beirne et al., 2016). Protection against RGC and optic nerve degeneration, arising from different conditions, appears to be possible with red light treatment. Since RGC dysfunction and optic nerve degeneration are common features among numerous other types of optic neuropathies red light has the potential to provide protection in these conditions also.

However, the successful outcomes achieved in the discussed experimental models were seen when red light was administered immediately after induced optic nerve injury, a treatment strategy that would be unachievable in a real life clinical setting. Although the therapeutic window of opportunity for red/NIR light therapy in models of traumatic optic neuropathy has not been explored, it has been assessed in other CNS injury models. NIR light therapy improved motor function in a rabbit model of embolic stroke when treatment was administered 6 hours post-embolization, but was ineffective when administered 12 hours post embolization (Lapchak et al., 2007). The findings show that neuroprotection can be achieved when red/NIR light is administered for up to 6 hours after the induced injury, showing the therapy to be applicable to a clinical setting. Other studies on animals demonstrated effectiveness of near-infrared light in a mouse model of traumatic brain injury when administered 4 hours after injury, with additional treatments administered at one and two days post injury(Xuan et al., 2016, Thunshelle and Hamblin, 2016). The transcranial treatment upregulated brain-derived neurotrophic factor (BDNF), improved neurological functions, reduced the size of the lesion, stimulated formation of new neurons and stimulated synaptogenenesis. There are also growing body of evidence suggesting that people affected by chronic traumatic brain injury or after stroke can benefit from transcranial irradiation with red/near-infrared light (Naeser et al., 2016, Hamblin et al., 2016)

1.4.3.4 Red/NIR light as a therapy for patients with retinal disease

The protective effects seen with red light treatment, in the absence of adverse effects, in numerous *in vivo* models of retinal degeneration, strongly suggest this non-invasive treatment should be trialled in patients with retinal degeneration. Progress to this end

has commenced with trials of red and NIR light therapy yielding promising results in patients with AMD. In one such study, a brief exposure of NIR light (780 nm), from a semiconductor laser diode, to AMD patients, twice per week for two weeks, resulted in a significant improvement in their visual acuity (Ivandic and Ivandic, 2008). This improvement in vision was seen in patients with both wet and dry AMD and was maintained for 3-36 months after treatment. Moreover, no adverse effects of the treatment were seen. In this study, the laser was applied transconjunctivally to the macula when the eye was in adduction. In another study looking at the effects of photobiomodulation on patients with dry AMD, the retina was irradiated through the pupil with red light (670 nm), from the FDA approved Warp 10 LED light source, 3 times per week for 6 weeks (Merry et al., 2013). The visual acuity and contrast sensitivity remained significantly improved for 12 months after treatment; however, the improvement in visual acuity began to decline after 4 months. The results provide vital information on the time at which patients may benefit from re-treatment, in addition to providing pilot data on the safety and effectiveness of 670 nm light from an LED source. Red/NIR light has also been trialled in diabetic macular edema and Leber's hereditary optic neuropathy, however, there are no results available from these studies. A summary of all the studies using red/NIR light as a treatment intervention in conditions associated with neurodegeneration in the retina is available in Table 1. From all the studies listed, red/NIR light is showing the greatest potential as a treatment for AMD. Since positive outcomes have been observed in patients with AMD, this paves the way for the application of this therapy in other retinal degenerative conditions, particularly those where positive outcomes have been seen in preclinical studies.

Responsible party	Last verified on ClinicalTrials.gov	Condition	Duration of treatment period	Number of patients	Duration of improved vision after treatment	Status
Harry T Whelan	01/09/2013	Diabetic Macular Edema	3 months	20	No results available	Completed
Ivandic and Ivandic 2008	N/A	Wet and dry AMD	2 weeks	203	Up to 36 months	Completed and published(Ivandic and Ivandic, 2008)
Merry, Graham	01/11/2011	Non-exudative Age-related Macular Degeneration	6 weeks	9	Up to 12 months	Completed and published(Merry et al., 2013)
Merry et al., 2016	N/A	Non-exudative Age-related Macular Degeneration	3 weeks	24	3 months	Completed and published(Merry et al., 2016)
University of Sydney	01/06/2014	Diabetic retinopathy	4 weeks	N/A	N/A	Planned
LumiThera, Inc.	01/04/2016	Age-related Macular Degeneration	3 weeks	30	N/A	Planned
Harry T Whelan	01/09/2014	Leber's hereditary optic neuropathy	3 months	4	N/A	Terminated (0/4 patients completed the study)

Table 1.1: A summary of the completed, planned and terminated clinical trials, using red/NIR light as a treatment intervention in conditions associated with retinal neurodegeneration. The table includes the name of the organisation of person responsible for the trial, the date when the trial was last verified on Clinicaltrials.gov, the condition for which red/NIR light is being tested in, the duration of the red/NIR light treatment period, the duration of the improvement in vision after cessation of treatment and the status of the trial.

1.4.4 The effects of red/NIR light on mitochondrial dysfunction

Although the therapeutic benefits of red/NIR light therapy have been demonstrated in a number of different disease models, in addition to AMD patients, the underlying molecular mechanisms are less well understood (Desmet et al., 2006). The question is no longer whether or not light has biological effects, it is rather how these effects are mediated at a cellular and molecular level (Hamblin and Demidova, 2006).

1.4.4.1 Cytochrome c Oxidase: the photoacceptor for red/NIR light

Endeavors to uncover the underlying molecular mechanisms suggest a major role for cytochrome *c* oxidase (COX), which is the terminal enzyme of the electron transport chain, transferring electrons from cytochrome c to molecular oxygen (Chung et al., 2012), (Karu, 1999).

COX is a large multicomponent protein, containing two copper centres (Cu_A and Cu_B) and two heme iron containing centres (heme *a* and heme *a3*), which absorbs photons in the red to NIR region of the electromagnetic spectrum (Karu, 1999). These transition metals are also the intermediate redox sites in the electron transfer pathway from cytochrome *c* to oxygen, a process which is coupled to the pumping of protons across the inner mitochondrial membrane. The electrons pass from cytochrome *c* to Cu_A then passed to heme *a*, from heme *a* to heme a3-Cu_B and finally to molecular oxygen.

1.4.4.2 The absorption of photons by photoacceptors in COX

One theory proposed to explain how photon energy is absorbed by COX, centres on its heme molecules (Zielke, 2014). Heme is comprised of a porphyrin ring with an iron atom at its centre that can continuously switch its oxidation states between ferrous (Fe^{2+}) and

ferric (Fe^{3+}) by accepting or donating an electron. The porphyrin ring is made up of four pyrrole rings that are connected through their carbon atoms via π bonds. The electrons in these π bonds are delocalised, moving back and forth from one configuration to another, creating resonance. Electrons, like photons, have a dual nature, behaving like particles or electromagnetic waves, thereby creating a resonating electromagnetic cloud in the porphyrin ring. Photons with similar wavelengths are absorbed by this cloud, increasing its energy. The energy from these photons causes photoexcitation of electrons of Fe^{2+}, bringing them to an unstable higher energy level. Upon absorption of sufficient energy, these electrons are released from the orbitals of Fe^{2+} causing the oxidation of Fe^{2+} to Fe^{3+}. The oxidised iron atom can then accept electrons from cytochrome c, thus increasing the electron flux through the electron transport chain.

Experimental evidence shows that red/NIR light has the ability to upregulate the enzymatic activity of complex IV, increase the mitochondrial membrane potential and increase ATP production (Karu, 2008, Hamblin and Demidova, 2006, Kokkinopoulos et al., 2013, Begum et al., 2013, Ferraresi et al., 2015a, Ferraresi et al., 2015b, Tina Karu and Hamblin, 2013). These mitochondrial specific effects of photobiomodulation may offer a partial explanation for its beneficial effects in neurodegenerative diseases associated with mitochondrial dysfunction. However, in genetic or toxin induced models of Parkinson's disease, where loss of dopaminergic cells was triggered by complex I dysfunction, neuroprotective effects were seen with red/NIR light treatment. The absorption of photon energy by the heme group in complex IV may explain how photobiomodulation can increase ATP production when complex IV is inhibited, but fails to explain how this effect can be achieved in models with complex I inhibition.

It has been hypothesised by Zielke *et al*. that the electrons released in this oxidation process are free to reduce NAD^+ and FAD, providing substrates for complex I and II, respectively, creating a closed circuit of electron transfer (Zielke, 2014). In the case of aberrant functioning of COX the flux of electrons through this closed circuit would maintain the proton pumping functions of complex I and III, thereby maintaining the electrochemical gradient across the mitochondrial membrane required for ATP synthesis. However, since oxygen is very electronegative it would be most likely that the released electrons would be readily accepted by the oxygen molecule bound to the reduced heme a3-Cu_B component of COX, reducing it to water. In the event of aberrant COX activity the released electron would most likely react with unbound oxygen molecules, forming reactive oxygen species. Therefore, how red/NIR provides neuroprotection against complex I dysfunction is not explained by its direct action on the COX.

1.4.5 The nitric oxide theory of Red/NIR light therapy

1.4.5.1 The role of nitric oxide in mitochondrial respiration

Nitric oxide ($^{\bullet}NO$) has important roles in the regulation of blood pressure and vasculature tone, however, excessive $^{\bullet}NO$ production, as seen in neurodegenerative diseases, can cause impairment of mitochondrial respiration and apoptosis (Zhao, 2005). Mitochondria harbor nitric oxide synthase (NOS) to produce NO, which they use to hinder respiration as an intrinsic mechanism to prevent oxygen from reaching precariously low levels (Barolet, 2008). $^{\bullet}NO$, at low concentrations, competes with oxygen to bind to the reduced heme a3-Cu_B component of COX (Chung et al., 2012). This

prevents COX from reducing molecular oxygen, thus impairing the proton pumping abilities of the enzyme and essentially the energy production ability of the mitochondria. Additionally, •NO was found to cause inhibition of complex I and II and IV-dependent respiration, in mitochondrial suspensions, where the inhibitory action of •NO was found to be more profound at lower oxygen tensions (Cassina and Radi, 1996). Interestingly, this inhibitory action of •NO was overcome by reoxygenation of mitochondrial suspensions for a mere 10 seconds, resulting in complete recovery of complex I and IV dependent oxygen consumption and a 50% recovery of complex II dependent respiration. This shows that the inhibitory actions of •NO are almost completely reversible upon restoration of normal oxygen levels. Therefore, this intrinsic mechanism would protect a tissue if the depleted oxygen supply were temporary, by putting the mitochondria in a state of conservation until the return of normal oxygen levels. However, prolonged inhibition of respiration would deplete ATP levels and bring about cell death (Kalogeris et al., 2012).

1.4.5.2 The effects of red/NIR light on •NO-mediated mitochondrial dysfunction

Red/NIR light has been proposed to influence the photodissociation of •NO from COX, thereby allowing oxygen to reclaim its binding site, permitting the ATP production process to resume (Chung et al., 2012). This would be most beneficial in pathological situations where •NO levels are higher than normal physiological amounts, favouring the binding of •NO rather than O_2 to COX. Experiments have shown that irradiating cells with red/NIR light increases COX activity in normal healthy neurons and restores the activity in COX inhibited neurons (Wong-Riley et al., 2005). However, the increase in COX activity appears to be mediated by an increase in the expression of the proteins in the COX

complex, suggesting that a mechanism, additional to the disinhibition of COX, may also be involved(Lim et al., 2010). Furthermore, exposure of cells to an irreversible COX inhibitor was overcome by NIR light treatment, providing further support to the claim that restoration of activity is mediated by upregulating the expression of COX proteins (Wong-Riley et al., 2005).

An indirect effect of red/NIR light on COX activity helps explain how beneficial effects are also seen in neurodegenerative conditions that are associated with impairment of other electron transport chain complexes. The absorption of photon energy from red/NIR light by COX may indeed have direct effects on the enzyme itself, however, this initial event may trigger further downstream events, which may have more far-reaching effects. As •NO is widely known for its function as an intercellular signaling molecule, the release of •NO upon red/NIR light exposure would increase its bioavailability, allowing it to function as a signaling molecule (Lohr et al., 2009). It has been suggested that •NO intracellular signaling could play a role in the upregulation of COX proteins upon red/NIR light exposure. Intracellular signaling from the mitochondria to the nucleus may be triggered by other byproducts of mitochondrial respiration, levels of which may be altered by red/NIR light, therefore, will be discussed in more detail later in this review.

1.4.5.3 The indirect effects of Red/NIR light on mitochondrial dysfunction

The findings by Cassina and Radi suggest that increasing the delivery of oxygen to the mitochondria, as would occur with increased blood flow to the tissue, would improve mitochondrial function in tissues with •NO-mediated mitochondrial electron transport chain inhibition (Cassina and Radi, 1996). It has been found that the exposure of blood

vessels to red light from an LED source can induce photorelaxation of blood vessels, an event that would increase blood flow and, in turn, oxygen delivery to the irradiated tissue (Plass et al., 2012). Exposure of porcine coronary arteries to red light caused their vasodilation, as measured by wall tension in the exposed vessels. Since nitric oxide is known to have a primary role in the regulation of vasculature tone, and NOS is activated upon absorption of visible light, the vasodilation effect seen upon red light exposure is thought to be mediated through nitric oxide (Samoilova et al., 2008). Additionally, red/NIR light can trigger the photodissociation of •NO from nitrosyl hemoglobin and nitrosyl myoglobin(Lohr et al., 2009). The •NO released from hemoglobin in the blood would contribute to the vasodilation effects of red/NIR light. Depending on the physiological situation, photobiomodulation can either reduce or increase •NO levels, however, the molecular events determining whether the effect will be an inhibitory or a stimulatory one are yet to be identified (Gavish et al., 2008). An increase in •NO upon red light exposure would provide beneficial effects in conditions such as TBI, where increased cerebral blood flow could increase mitochondrial function in hypopxic cells (Figure 1.5) (Naeser et al., 2014). As mentioned earlier in the review, hypoxia can trigger inhibition of respiration through the binding of •NO to COX. The phototdissociation of NO from COX in hypoxic tissue may not cause a significant improvement in mitochondrial function since there would be limited oxygen available to reclaim the binding site on COX. However, if combined with an increase in cerebral blood flow, the associated increase in oxygen levels would lead to a more substantial improvement in mitochondrial function. This proposes a partial explanation for the neuroprotective effects seen upon red/NIR light exposure.

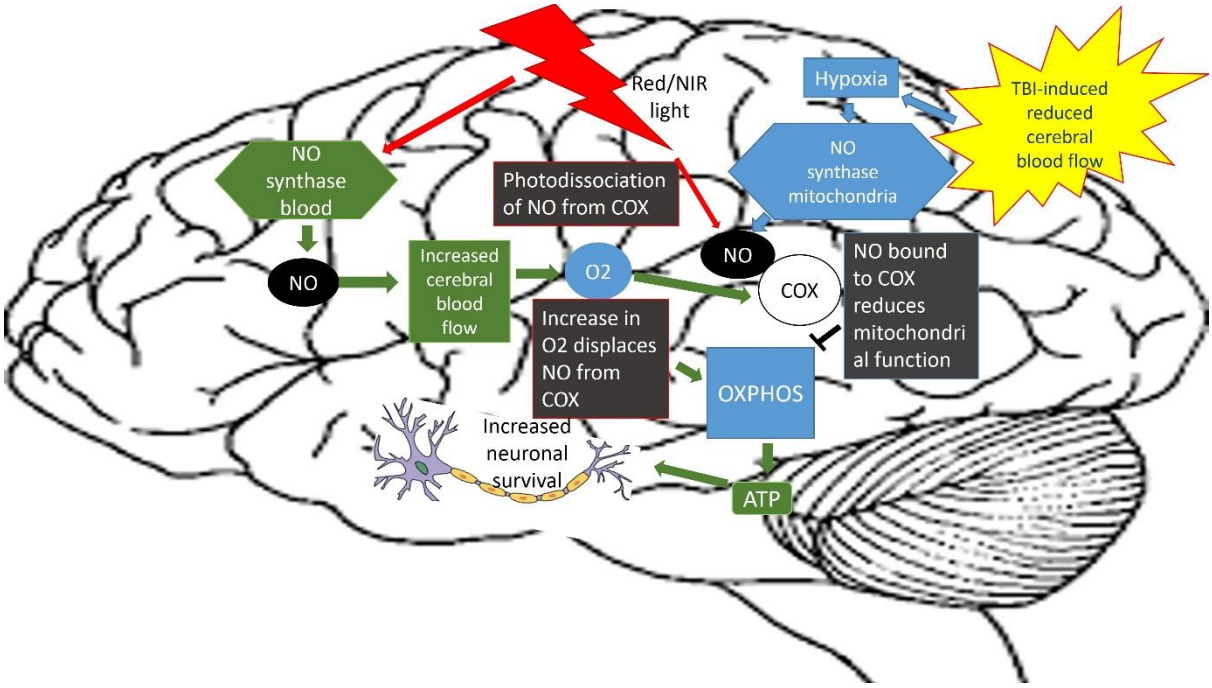

Figure 1.5: The direct and indirect actions of red/NIR light on nitric oxide improve mitochondrial function in neurons vulnerable to degeneration in acute neurodegenerative conditions such as TBI. Cerebral blood flow is reduced by traumatic brain injury, leading to tissue hypoxia. Increased activation of nitric oxide synthase in the mitochondria increases nitric oxide production which can bind to the oxygen binding site on complex IV to slow down oxygen consumption and ATP production. Red/NIR light is absorbed by nitric oxide synthase, triggering the production of nitric oxide which can cause vasodilation, increasing cerebral blood flow. Red/NIR light can also trigger the photodissociation of nitric oxide from the oxygen binding site of complex IV. Increased cerebral blood flow can increase the oxygen supply to the hypoxic tissue and displace nitric oxide from complex IV. The binging of oxygen to complex IV can increase oxidative phosphorylation, thereby increasing ATP production which promotes neuronal survival.

1.4.5.4 The effects of red/NIR light on cellular function

The ability of red/NIR light to increase free •NO can have beneficial effects in cells where mitochondria are dysfunctional. Providing further support to this theory, it was found that red/NIR light was protective against hypoxia and re-oxygenation injury in cultured cardiomyocytes. The observed protection was dependent on an increase in •NO as the protective effects were abolished in the presence of •NO scavengers (Zhang et al., 2009). Further, it was observed that the increase in NO seen upon red/NIR exposure was

partially prevented by the non-selective inhibition of all isoforms of NOS. Of note, there are three isoforms of NOS: Neuronal NOS (nNOS), which is expressed in the central nervous system and plays a role in synaptic plasticity and central regulation of blood pressure, endothelial NOS (eNOS), which is mostly expressed in endothelial cells and primarily functions in controlling blood pressure, and inducible NOS (iNOS), which can be expressed in many cell types in response to cytokines and other agents to generate large amounts of •NO(Förstermann and Sessa, 2012). The findings show that the increase in •NO by red/NIR light is mediated in part by its action on NOS, however, the exact isoform of NOS responsible for the protective effects has not been determined. The source of the remaining NO could be that which is released during the photodisociation of •NO from COX in the mitochondria as discussed above.

This *in vitro* model of cardiac ischemia provides useful insight into how red/NIR light mediates its effects via •NO in ischemic conditions. Since the experiment was done *in vitro,* the observed protective effects most likely arose from the local effects of an increase in intracellular •NO rather than an indirect effect of •NO by increasing blood flow to the ischemic tissue. Although reperfusion is essential to limit cell death after hypoxia, paradoxically, this event itself causes further cell death due to excess ROS production (Keszler et al., 2014). The increase in free •NO upon red/NIR light exposure would increase its availability to bind to COX and cause the reversible S-nitrosation of Complex I, events which would slow down the reactivation of the electron transport chain during the crucial initial stages of reperfusion (Chouchani et al., 2013). In this particular pathological situation red/NIR light, administered upon reoxygenation, could

reduce the harmful levels of ROS produced during reperfusion injury by reversibly inhibiting the electron transport chain.

Contrastingly, in an *in vivo* model of cerebral ischemia, where excess •NO production is said to be associated with neurotoxic effects, red/NIR light has been shown to have the ability to reduce the levels of •NO by down-regulating the activity and expression of all isoforms of NOS (Leung et al., 2002). Both studies focus on •NO to explore the underlying mechanism responsible for the protective effect of red/NIR light in models of ischemia, yet, in these examples, the effects on •NO were found to be conflicting. The respective increase and decrease in •NO levels seen upon red/NIR light irradiation in the discussed models, was dependent on the respective activation and inhibition of NOS. Although theories have been proposed to explain the increase in NOS activity in response to red/NIR light irradiation, how red/NIR light inhibits NOS activity is less clear. Since the expression of the three isoforms of NOS showed a similar trend to the specific activities of the NOS enzymes in response to red/NIR light, red/NIR light must be somehow suppressing the expression of NOS, but the mechanism responsible for this effect is unknown(Leung et al., 2002).

This observed dual effect of red/NIR light on intracellular •NO levels has great relevance in the field of neurodegenerative conditions. •NO at physiological amounts confers neuroprotection, however, if produced in excess, •NO has neurotoxic effects (Calabrese et al., 2007). In the *in vivo* model of cerebral ischemia mentioned above the light was administered immediately after middle cerebral artery occlusion, but the levels of NOS activity were not measured until 4 days post injury, the time at which the NOS levels

peaked before returning to pre-injury levels. In the *in vitro* model of cardiac ischemia the light was also administered immediately after hypoxia but the •NO levels were measured after just 2 hours of reoxygenation. It is possible, therefore, that red/NIR light triggers an initial increase in •NO levels, sufficient to reduce ROS production and bring about the observed cytoprotective effects. Furthermore, as the cell is then in a state of elevated •NO levels and reduced ROS levels this may be sufficient to switch off the endogenous trigger that induces the increased expression of NOS and the subsequent delayed surge in •NO levels, which only contribute to the toxic effects at that late stage of ischemia. However, as shown in Figure 1.6, low levels of •NO are produced during the early stages of ischemia to induce neuroprotective effects in the absence of red/NIR light, yet an increase in •NO is responsible for the neuroprotective effects achieved with red/NIR light in the *in vitro* model of ischemia. Therefore, how does the •NO produced by red/NIR light provide further neuroprotective effects in the early stages of ischemia? Also unanswered is how the increase in •NO by red/NIR light and the associated reduction in ROS production would downregulate the delayed surge in NO production in the later stages of ischemia when the •NO produced in the absence of red/NIR light fails to do so.

There is much evidence to show that •NO acts as a neuroprotective agent through its various cellular effects. One such effect is the induction of the signaling molecule cyclic guanosine 3',5'-monophosphate (cGMP), a molecule with a key role in vasodilation and mitochondrial biogenesis (Tengan et al., 2012). Mitochondrial biogenesis has been found to occur in response to red/NIR light irradiation (Nguyen et al., 2014). Diseases with a mitochondrial origin such as Leber's hereditary optic neuropathy, retinitis pigmentosa

and autosomal dominant optic atrophy would benefit from the associated increase in mitochondrial biogenesis, as a way of supporting neuronal survival.

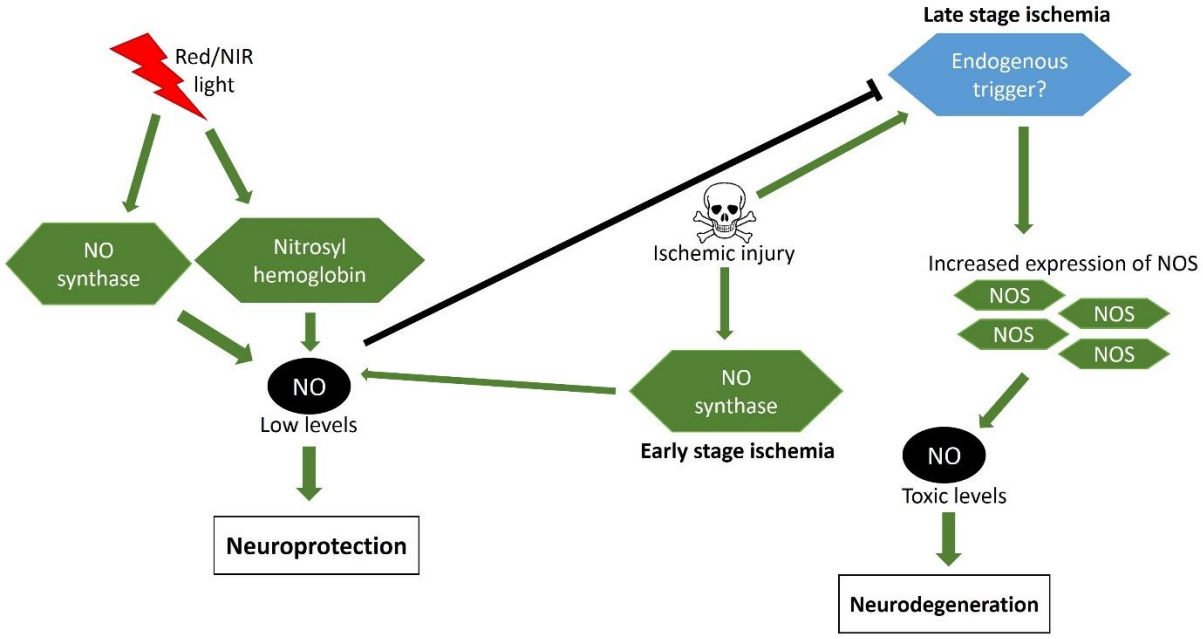

Figure 1.6: A proposed explanation for the observed dual effect of red/NIR light on NO in models of ischemia. Red/NIR light is absorbed by nitric oxide synthase triggering the production of nitric oxide. The photodissociation of nitric oxide from nitrosyl haemoglobin is also triggered by red/NIR light. Low levels of nitric oxide produced by red/NIR light can lead to neuroprotective effects in the early stages of ischemia. This may somehow inhibit the endogenous trigger that causes an increased expression in nitric oxide synthase, leading to the production of toxic levels of nitric oxide that contribute to neurodegeneration during late stage ischemia. However, low levels of nitric oxide are also produced in the early stages of ischemia in the absence of red/NIR light, yet this has no effect on downregulating the delayed surge in nitric oxide production.

1.4.5.5 The effects of reactive nitrogen species on mitochondrial function

There is much evidence to show that •NO, at higher doses, is toxic to neurons; however, this NO-mediated toxicity is not produced by •NO alone, but by the formation of reactive nitrogen species (RNS) (Lipton et al., 1993). As a by-product of mitochondrial respiration the superoxide radical anion ($O_2^{\bullet -}$) is formed when electrons from Complex I or III are transferred to oxygen molecules instead of their respective substrates: ubiquinone and cytochrome c (Lenaz, 2001). If the amount of superoxide produced in the cell increases

to a level that would exceeds the antioxidant capacity of the cell, oxidative stress will result. In that pro-oxidant state, the production of •NO can cause the generation of additional cytotoxic compounds. The reaction of NO with the superoxide radical anion ($O_2^{\bullet -}$) leads to the generation of the powerful oxidant peroxynitrite ($ONOO^-$), which causes detrimental effects in the cell, through its interactions with lipids, proteins and DNA (Lipton et al., 1993).

Nitric oxide, superoxide and peroxynitrite are often generated in excess during inflammatory and pathological conditions, contributing to the associated toxic effects (Rubbo et al., 1994). Peroxynitrite can induce mitochondrial dysfunction and cell death in neurons by its ability to inhibit many mitochondrial proteins including complex I, II and IV, and ATP synthase. It can also increase mitochondrial proton permeability, an effect which may be caused by lipid peroxidation (Brown and Borutaite, 2004). Impairment of normal mitochondrial function causes depletion of ATP and generation of free radicals, causing cellular dysfunction and further oxidative stress. Peroxynitrite has been found to be involved in the pathogenesis of many neurodegenerative disorders (Torreilles et al., 1999). Since the formation of peroxynitrite depends on the availability of •NO, inhibition of nitric oxide synthase activity, as was found to occur in cerebral ischemic-rats irradiated with red light, may reduce the amount of peroxynitrite produced and the associated deleterious effects in neurodegenerative disorders (Leung et al., 2002).

1.4.6 Red/NIR light in the mitochondrial signaling pathway

Causing further controversy in the efforts to uncover the underlying molecular mechanism of red/NIR light therapy, is the effect that it has on ROS and RNS production.

It is also uncertain whether an increase or a decrease in these molecules, in the cell, in response to red/NIR light exposure would be the most therapeutically beneficial. In some physiological situations red light mediates its therapeutic effects by increasing levels of free radicals but in other circumstances by reducing the levels of free radicals. Consequently, a further look at the molecular effects of free radicals in neurodegeneration is required to uncover the underlying mechanism of red/NIR therapy.

1.4.6.1 The role of ROS and RNS in neurodegeneration

Postmortem analysis of the brains of patients with various neurodegenerative diseases shows an increase in ROS and RNS in the affected brain regions (Andersen, 2004, Aslan and Ozben, 2004). It is known that these reactive species can cause oxidative and nitrative damage to cellular components thereby having toxic effects on the cell (Tafur and Mills, 2008). It may be deduced from this association that the increase in ROS and RNS is contributing to cellular death and that an antioxidant may be beneficial in such conditions. Since red/NIR light has been found to be protective in models of such conditions it could, therefore, be possible that the therapeutic benefits of red/NIR light could be due, in part, to an antioxidant effect. One possible mechanism of providing the antioxidant protection is the photodissociation of $^{\bullet}$NO, which at low concentrations can exert an antioxidant effect (Niziolek et al., 2003a, Niziolek et al., 2003b, Niziolek et al., 2005, Niziolek et al., 2006).

Because red/NIR light has been found to increase the activity of the electron transport chain, and ROS/RNS production is a byproduct of such activity, sometimes it is presumed that red/NIR light increases ROS production. It can be argued, however, that by removing

NO-mediated inhibition of COX, the electron flow is restored and therefore the likelihood of donating an electron from Complex I or III to oxygen (which results in generation of superoxide radical anion) is reduced (Lenaz, 2001). Thus by enabling the electron flow in the electron transport chain, the risk of formation of superoxide is decreased.

Investigation into the effects of red/NIR light on ROS production by various groups provides inconsistent results as some found a reduction in ROS upon irradiation while others found that ROS was, in fact, upregulated (Tafur and Mills, 2008). Regardless of the effect of red/NIR light on ROS levels, it is unclear whether an antioxidant or pro-oxidant effect would be most beneficial when employing red/NIR light as a neuroprotective agent. Regulated ROS production could trigger signaling pathways involved in cell protection, but unregulated ROS production could result in cellular damage and cell death (Zorov et al., 2014). In addition, when ROS levels are too low this also has detrimental effects for the cell. The concept that lower, non-toxic levels of ROS are essential for promoting cell survival by inducing an adaptive responses is called mitochondrial hormesis or mitohormesis (Ristow and Schmeisser, 2014). Exposure to red/NIR light may trigger a transient increase in ROS levels, sufficient to induce this adaptive response and provide neuroprotective effects. This explanation seems plausible in situations where light is administered as a pre-treatment as the cells could employ this adaptive response to protect against a subsequent injury-induced increase in ROS levels. However, if the cell is already in a state of elevated ROS levels, as in many pathological situations, it is unclear as to how an additional increase in ROS by red/NIR light would provide neuroprotective effects. From the current literature, it is clear that the mechanism for the effect of red/NIR light on ROS production, in addition to the cellular

mechanisms responsible for balancing the ROS levels required for maintaining optimal mitochondrial and cellular function are not fully understood. However, since maintaining redox homeostasis is paramount for the optimal functioning of the cell and neuronal survival, we suggest that the exposure to red/NIR light may restore redox homeostasis, in pathological conditions where it is perturbed. Therefore, in cells with elevated ROS levels, red/NIR light may cause mild cellular stress by an unknown mechanism that may induce an adaptive response, which includes the upregulation of genes with a role in redox homeostasis. We suggest that the observed increase in •NO upon red/NIR light irradiation, by the various mechanisms discussed in section 5, may facilitate the production of peroxynitrite through the reaction of •NO with ROS. The elevated RNS levels may induce an adaptive response by triggering a different signaling pathway to that which is triggered by ROS.

1.4.6.2 ROS/RNS as signalling intermediates

The upregulation of ROS and RNS, such as peroxynitrite, are thought to promote cell viability and increase proliferation owing to their ability to function as signal intermediates (Figure 1.7). ROS, which is produced by the ETC complexes as a byproduct of cellular respiration permits communication from the mitochondria to the rest of the cell. This mitochondrial signal transduction can activate various signaling pathways resulting in the expression of a plethora of genes including those involved either directly or indirectly in the suppression of apoptosis, cell survival or cell proliferation. Curiously, among the genes affected by red/NIR light irradiation were those with roles in anti-oxidation(Tafur and Mills, 2008).

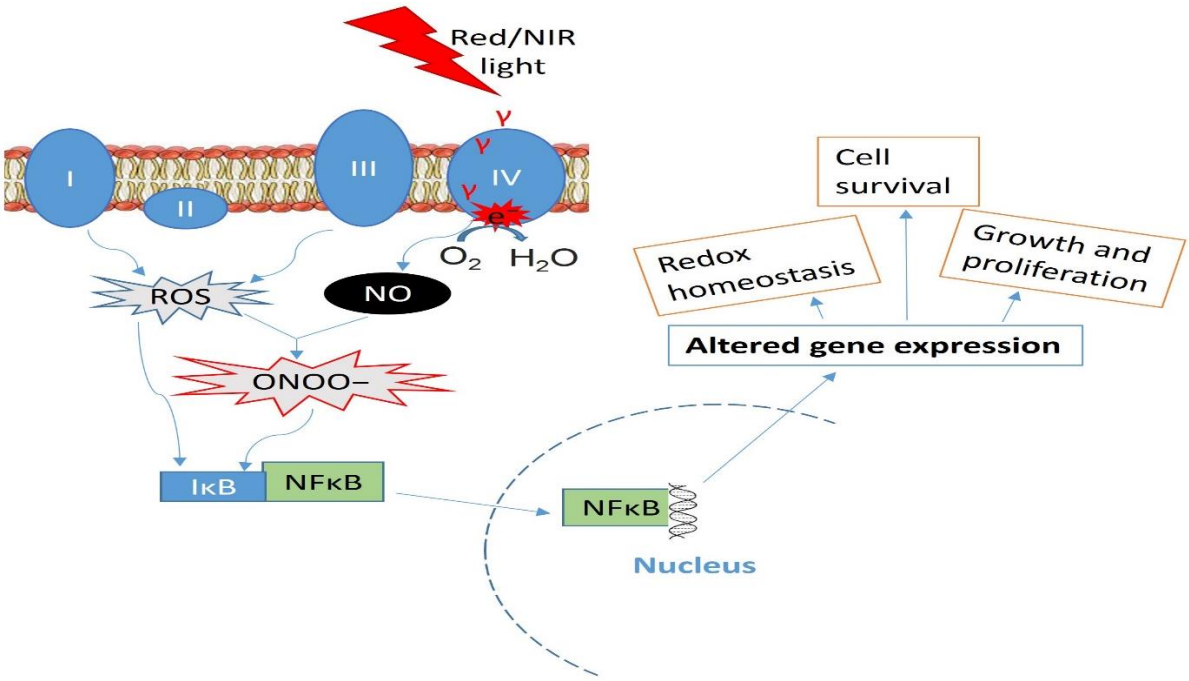

Figure 1.7: The upregulation of ROS or RNS by red/NIR light triggers the translocation of the transcription factor NFκB to the nucleus, enabling NFκB to alter gene expression. Red/NIR light is absorbed by ETC complex IV leading to the photodissociation of nitric oxide from the oxygen binding site of complex IV allowing oxygen to bind to complex IV and accept electrons from complex IV, increasing complex IV activity. This increases the electron flux across the entire electron transport chain and increases ROS production from complex I and III. The free nitric oxide can react with superoxides to produce peroxynitrite. ROS and peroxynirtite can trigger the dissociation of the inhibitor of κB from NFκB, allowing NFκB to translocate to the nucleus where it can alter gene expression of target genes such as those with roles in cell survival and restoring redox homeostasis.

1.4.6.3 The mitochondrial signalling pathway

ROS is thought to mediate its protective effect via the activation of the redox sensitive transcription factor nuclear factor κ-light-chain-enhancer of activated B cells (NFκB) which is proposed to be sensitive to an increase in ROS generation. In support of this theory it was found that an increase in ROS production by mitochondrial inhibitors brought about a concurrent increase in NFκB, while the exposure to antioxidants reduced the NFκB activation (Chen et al., 2011). NFκB can both induce and repress gene expression by binding to κB elements in the promoter and enhancer regions of the gene.

This transcription factor has been shown to induce the expression of numerous genes with functions in cell survival, the stress response and inflammation (Chen et al., 2011). When superoxides are produced in the mitochondria they are metabolized to H_2O_2 which is thought to activate NFκB by triggering the dissociation of inhibitor of κB kinase from NFκB. This allows NFκB to translocate to the nucleus where it can alter gene expression (Figure 1.6) (Gloire et al., 2006). Many of the genes upregulated by NFκB play a role in the immune response, inducing pro-inflammatory genes at the onset of inflammation and anti-inflammatory genes during the resolution of inflammation(Lawrence, 2009).

Therefore, depending on the context, ROS can both activate and inhibit NFκB signaling (Morgan and Liu, 2011). It is no surprise that the results obtained appear to be inconsistent with varying cell type and cellular environment at the time of exposure to red/NIR light. This may provide some explanation for the differential results that have been observed with the use of red/NIR light therapy in different cell types. For example, irradiation of traumatized muscle tissue with red light therapy reduced the levels of ROS and NFκB activation, and the associated increase in the expression of proinflammatory genes (Rizzi et al., 2006). On the other hand, NIR light has been shown to induce ROS production and NFκB activation in murine embryonic fibroblasts (Chen et al., 2011).

In a similar fashion to ROS, peroxynitrite production triggers this stress response, causing the up or downregulation of cell signaling cascades in a cell dependent manner (Liaudet et al., 2009). Peroxynitrite signaling is mediated by tyrosine nitration of proteins, particularly those involved in phosphotyrosine-dependent signaling. The oxidant is also involved in signaling via mitogen activated protein kinase, protein kinase B and C, NFκB

and the insulin receptor. Of note, these pathways which converge on the upregulation of mediators of cell survival, growth and proliferation are also activated by other stress stimuli such as ROS.

It is also possible that nuclear factor erythroid-2 like 2 (Nrf2) may be playing a role in the underlying molecular mechanism of red/NIR light therapy, due to its role in eliciting an adaptive response to oxidative and nitrostrative stress, in a similar manner to NFκB. The Nrf2/Keap1/ARE pathway plays a major role in the regulation of cellular redox homeostasis by regulating the transcription of over 100 genes including those with roles in promoting cell survival, antioxidant production and inhibition of inflammation (David et al., 2017). Under normal cellular conditions Nrf2 is covalently bound to cysteine residues on Keap1 in the cytoplasm, leading to ubquitination and degradation of Nrf2. Nrf2 is thus prevented from translocating to the nucleus and initiating transcription of its gene targets (David et al., 2017). In the presence of oxidative stress, however, ROS modifies the cysteine residues on Keap1, preventing the binding of Keap1 to Nrf2, thereby allowing Nrf2 to translocate to the nucleus and induce transcription by binding to antioxidant response element (ARE) in the promoter element of its target genes (Figure 1.8).

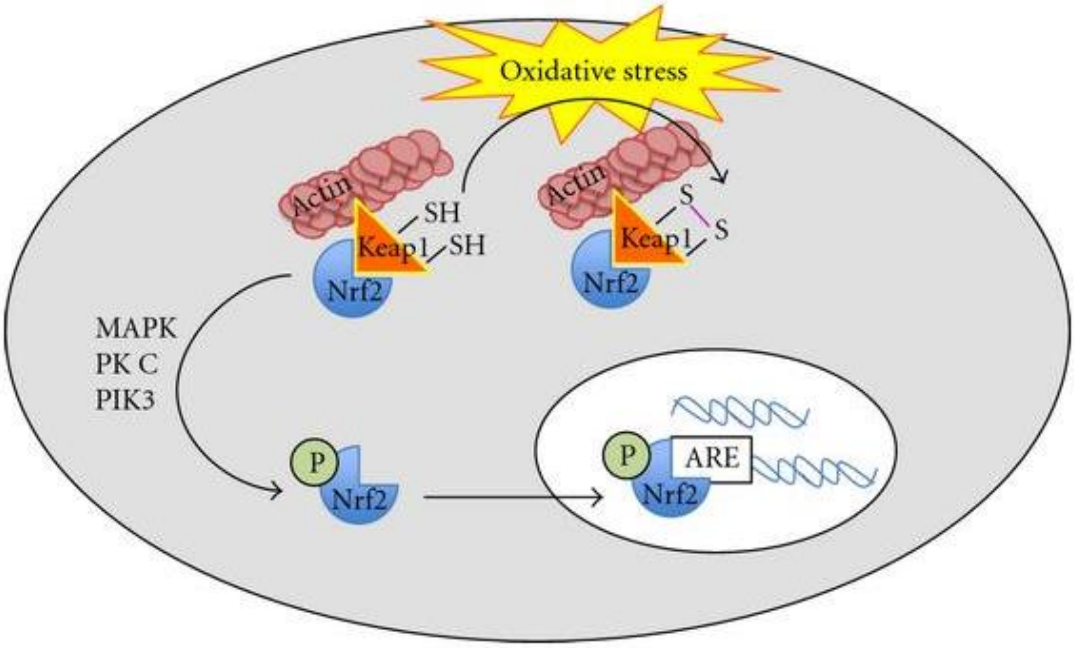

Figure 1.8: Nrf2 activation by oxidative stress (Facecchia et al., 2011). Under normal conditions Nrf2 is sequestered in the cytoplasm by covalent bonding with the cysteine residues on Keap1, preventing Nrf2 from translocating to the nucleus. In the presence of oxidative stress, the cysteine residues on Keap1 are modified, preventing the binging to Nrf2. Nuclear translocation of Nrf2 can then occur allowing Nrf2 to bind to the ARE in the promoter element of target genes and initiate gene transcription.

Another potential molecular effector of red/NRI light is DJ1, a redox responsive protein that increases its expression upon oxidative stress(Ariga et al., 2013). The specific functions of DJ1 and the mechanism of activation remain unclear. It is known, however, that oxidative stress induces the upregulation of endogenous DJ1, an effect that is associated with an increase in the cellular defense mechanism against oxidative stress(Lev et al., 2008). Its subcellular distribution also contributes to its protective effects. Under normal cellular conditions DJ1 is localised to the cytoplasm as a homodimer (Björkblom et al., 2014). During oxidative stress, the dimer is disrupted and

the DJ1 monomer translocates to the mitochondria and nucleus where it can instigate various effects including its antioxidant function and cytoprotective activity.

It is thought that DJ1 is mediating some of its protective effects via the Nrf2 pathway (Im et al., 2012). In support of this finding, activation of the Nrf2 pathway was found to be a critical mechanism by which DJ-1 upregulates antioxidant enzymes and promotes cryoprotection in an *in vitro* model of hypoxia/re-oxygenation (Yan et al., 2015). DJ1 has also been shown to be involved in the modulation of the Akt (protein kinase B) pathway, which is also a major neuroprotective pathway triggered in response to oxidative stress (Aleyasin et al., 2010). Therefore, Akt is another potential molecular effector of red/NIR light that may be responsible, in part, for the neuroprotective effects.

The PI3K-Akt signaling pathway is a critical pathway involved in promoting neuronal survival, which is activated by various mechanism(Brunet et al., 2001). Oxidative stress is one such mechanism by which this pathway is activated in neurons (Uranga et al., 2013). Akt activation requires recruitment to the plasma membrane and subsequent phosphorylation of two key amino acids, Thr303 and Ser473(Song et al., 2005). Upon phosphorylation, it translocates to the nucleus and cytoplasm where it phosphorylates various target proteins to promote neuroprotection (Uranga et al., 2013).

In support of the theory that red/NIR light causes upregulation in the expression of genes associated with cell survival, is the increased neuroprotective effects observed when red/NIR light is administered before the induced injury in models of neurodegeneration, compared to when administered after injury (Ying et al., 2008b). This suggests that red/NIR light could be mediating its protective effects by instigating the production of

ROS/RNS at levels sufficient to cause the upregulation of stress response genes, via the pathways discussed above, with negligible damage to the irradiated tissue. If the same tissue was subsequently exposed to a toxic agent, the cell would be equipped with the appropriate defense mechanisms to cope with such an insult. The destructive effects to the tissue in such an instance would be remarkably less, such as is seen in various pretreatment models (Rutar et al., 2012, Albarracin and Valter, 2012, Albarracin et al., 2013). This knowledge could be exploited in neurodegenerative diseases with a pre-symptomatic phase. The observation demonstrates that red/NIR light therapy would be most effective as a preventative therapeutic treatment, administered before the onset of clinical symptoms and irreversible damage. With respect to retinal degenerative disease this preventative treatment approach would be particularly relevant in inherited optic neuropathies such as Leber's hereditary optic neuropathy. Individuals with a LHON-causing mtDNA pathogenic variant could be monitored so that treatment with red/NIR light could begin upon detection of pre-symptomatic abnormalities as a pre-treatment for the clinical symptoms. In the event of a more acute neurodegenerative condition such as TBI, exploiting the enhanced therapeutic effects of red/NIR light observed when used as a pretreatment would not be feasible. Therefore, the neuroprotective potential of red/NIR light therapy, as seen in the pre-treated animal models, may be somewhat limited in a real life clinical setting.

1.4.7 The effects of red/NIR light on the anti-inflammatory response

Peroxynitrite and ROS are also produced by macrophages during inflammation, which is responsible for the cytotoxic effects (Kang et al., 2002). Red/NIR light has shown the ability to reduce the presence of these reactive species in irradiated tissues, thereby

attenuating some of the cytotoxic effects of the inflammatory response. Furthermore, modulation of the immune response itself was seen in many studies with red/NIR light treatment (Begum et al., 2013, Kokkinopoulos et al., 2013, Gavish et al., 2008). Yet, how red/NIR light mediates this anti-inflammatory effect is poorly understood.

Mitochondria play a major role in the activation of the inflammasome, a molecular platform that activates proapoptotic proteins, cytokines and other mediators of inflammation upon detection of infectious agents or cellular damage (Green et al., 2011). ROS can similarly activate the inflammasome. The production of mitochondrially-derived ROS is known to increase when mitochondria are dysfunctional. Decreased electron flux through the electron transport chain reduces the ability of COX to fully reduce oxygen to water, thereby increasing the formation of ROS. The action of red/NIR light in improving the functions of the mitochondrial electron transport chain could reduce the amount of ROS generated, which may reduce the activation of the inflammasome. Alternatively, the mitochondrial signal transduction triggered by an increase in ROS/RNS as discussed above, could also upregulate the expression of anti-inflammatory or antioxidants proteins, to either directly or indirectly dampen the inflammatory response. However, it has been found that low level laser irradiation (LLLI) can reduce the gene expression of anti-inflammatory cytokines as well as pro-inflammatory cytokines (Gavish et al., 2008). In this particular situation LPS was used to elicit an inflammatory like phenotype, triggering the expression of pro-inflammatory cytokines in addition to the anti-inflammatory cytokine, IL-10. The anti-inflammatory cytokine is also triggered during the inflammatory response to limit the host immune response, thereby minimising the damage caused to the affected tissue during the

inflammatory response (Iyer and Cheng, 2012). The findings demonstrate that LLLI is able to dampen the entire inflammatory response as oppose to specifically downregulating proinflammatory cytokines, suggesting that red/NIR light may be acting further upstream, influencing factors governing the inflammatory response. Also, there appears to be a correlation between the inflammatory level in the tissue and the extent of the inhibition of the inflammatory response (Gavish et al., 2008). It was found that LLLI had little effect on the inflammatory response at low levels of inflammation, but produced a potent anti-inflammatory effect at high levels of inflammation (Gavish et al., 2008). This shows an ability of red/NIR light to restore homeostasis in the tissue. In fact, ROS is produced by the microglia itself and plays an important role in the induction of pro-inflammatory genes (Innamorato et al., 2009). Therefore, restoring the redox balance in microglia may facilitate the transition of the microglia from an activated to a resting state.

It has been suggested that the mitochondrial dysfunction seen in many neurodegenerative diseases not only affects neurons, but also the microglia (Ferger et al., 2010). Experimental findings have shown that complex I inhibition in microglia inhibited the IL-4 mediated reduction in pro-inflammatory cytokines and the secretion of the neuroprotective insulin-like growth factor-1. The inflammatory response triggered by pathogens or damaged neurons functions to protect the neural tissue, but if this response is not attenuated the response would switch from a protective one to a deleterious one (Ramesh et al., 2013). When activated, microglia secrete anti-inflammatory cytokines, in addition to pro-inflammatory cytokines to control the inflammatory response, preventing unnecessary damage to neural tissue. Electron

transport deficiencies in microglia appear to perturb the anti-inflammatory arm of the immune response (Ferger et al., 2010). Since red/NIR light has been shown to improve the function of the electron transport chain in neurons, it can be suggested that a similar effect would be seen in microglia with mitochondrial dysfunction.

1.5 Hypothesis

Since red/NIR light has been found to improve mitochondrial function and increase ATP production, we hypothesise that 670 nm light will restore normal mitochondrial bioenergetics in the B6;C3-Opa1^{Q285STOP} mouse and thereby prevent the associated neurodegeneration. In particular, as red/NIR light has been found to provide neuroprotective effects in numerous models of neurodegenerative conditions we hypothesis that 670 nm light therapy will prevent the dendropathy that occurs in an axotomy model of neurodegeneration. We also hypothesise that 670 nm light will prevent the progressive dendropathy that begins at 12 months in the B6;C3-Opa1^{Q285STOP} mouse. Finally, we hypothesise that 670 nm light produces non-toxic levels of ROS in the neuron that are sufficient to trigger the activation of the NFκB pathway and other signalling pathways to promote cell survival and prevent RGC degeneration.

1.6 General aims

Overall aim: To test the effectiveness of 670 nm light therapy in models of RGC degeneration

Specific aims:

1. To determine whether 670 nm light can improve the energy producing ability of the mitochondria in retinae from aged wild-type and B6;C3-Opa1^{Q285STOP} (het) mice.
2. To test the effects of 670 nm light, delivered post axotomy to the retinal explant, on *ex vivo* RGC dendropathy.

3. To test the effects of 670 nm light treatment, delivered *in vivo*, prior to axotomy, on *ex vivo* RGC dendropathy in the entire population of wild-type RGCs and in the ON-centre RGCs from wild-type and het mice.
4. To explore the effects of 670 nm light on NFκB activation and associated effects on microglial activation in RGCs from wild-type and het mice.
5. To explore the effects of 670 nm light on other transcription factors and signaling intermediates that are upregulated in response to oxidative and nitrostrative stress in wild-type and het mice.

Chapter 2. Materials and Methods

2.1 General methods

2.1.1 Wild-type and Opa1+/- Mice

Mice were kept in a 12 hour light (10 lux) / 12 hour light-dark cycle with food and water available *ad libitum.* Breeding, maintenance and all experimental procedures were in compliance with the *ARVO Statement for the Use of Animals in Ophthalmic and Vision Research* and were approved by the Home Office. The mutant strain, B6; C3-Opa1^{Q285STOP} has been described in detail elsewhere (Davies et al., 2007). The mice were crossed with C57BI6/JCrl mice to move the mutation to a C57BI/6JCrl background (F1) and the experiments were performed on mice bred to F7 generation.

2.1.2 Genotyping

DNA was extracted from mouse ear tissue obtained from ear mark identification procedure. Mouse ear tissue was lysed at 100°C for 5 minutes with 50 mM NaOH before being neutralised with 10 mM Tris. The genotyping of mutant mice involved two separate PCR reactions with two sets of primers. The forward primer was identical for both reactions amplifying wild-type and mutant alleles (F1: 5'- CTCTTCATGTATCTGTGGTC-3'). Two reverse primers were used to specifically amplify either the wild-type or mutant allele (R Wt: 5' TTACCCGTGGTAGGTGATCATG-3' and R Mut: 5'-TTACCCGTGGTAGGTGATCATA-3'). For each reaction 1 µl of DNA was amplified with 1.25 µl (10 µM primer) in a 20 µl reaction mix (BioMix Red; Bioline, UK). PCR reactions were ran on TC-512 Techne Thermal Cycler (Techne Inc., US) under the following conditions; denaturation for 5 minutes at 94°C followed by 35 cycles of denaturation (1 minute at 94°C), annealing (1 minute at 55°C) and elongation (1 minute at 72°C) and a final elongation for 10 minutes at 72 °C. PCR products were separated by 1% agarose gel electrophoresis in TAE (Tris-borate-EDTA)

buffer. 100 bp ladder was added to the gel to allow the size of the PCR products to be determined.

2.1.3 Retinal Dissection

Mice were sacrificed by cervical dislocation. Eyes were immediately enucleated, transferred to a culture dish with ice cold Hanks' balanced salt solution (Invitrogen) and put on ice. A hole was made in the cornea, just above the limbus using a fine needle which allowed for a cut to be made in the cornea. Ophthalmic scissors were used to cut around the cornea, removing the cornea from the eye. Ophthalmic forceps were then employed to pull the lens out of the eye. In aged animals the action of pulling the lens removed most of the vitreous from the eye without damaging the retina, but in younger animals scissors were required to cut the vitreous from the lens to avoid retinal damage. The retina was carefully peeled apart from the sclera, after which care was taken to remove the remaining vitreous using an ophthalmic forceps and scissors. Four radial cuts were made in the retina, towards the optic nerve head, to enable flat mounting onto a 0.4 µm pore PTFE membrane culture plate insert (Sigma). A cut tip 3 mL pasture pipette was used to transfer the retina from the culture dish to the insert and a 1 mL fine tip transfer pipette was then used to carefully remove the excess solution surrounding the retina on the insert. Finally, the retina was gently unfolded with an ophthalmic forceps leaving a flattened out 4 leaf clover structure, with the ganglion cell layer facing up (Figure 2.1). The insert was placed in pre-warmed Neurobasal A media (Invitrogen) and transferred to an incubator at 37 °C, 5% CO_2 for the required *ex vivo* period.

Figure 2.1: Mouse retina on a culture insert post dissection, flattened by four cuts towards the optic nerve head.

2.1.4 DiOlistic labelling of retinal ganglion cells

2.1.4.1 Preparation of DiI and DiO coated tungsten particles

Bullets of 1,10-dioleyl-3,3,3,3 tetramethylindocarbocyanine methanesulphonate (DiO) (Invitrogen) or 3,3'dihexadecyloxacarbocyanine perchlorate (DiI) coated tungsten particles were prepared prior to retinal preparation modified from Gan et al., 2000, with the modified protocol described here (Gan et al., 2000). In a fume cupboard, 100 mg of tungsten particles (1.7 µm) were spread out evenly on two glass slides. In an Eppendorf tube, 4 mg DiI or 8 mg of DiO was weighed out and protected from light with aluminium foil. Each was suspended in 100 µl of dichloromethylene, in a fumehood, and the solution was pipetted onto the tungsten particles. Dichloromethylene evaporated leaving dried DiI or DiO coated tungsten particles, which were then transferred onto filter paper and broken up into a fine powder using a razor blade. The powder was funnelled into a length of tubing (Bio-Rad) and left on a rotator (Bio-Rad) overnight, allowing the powder to

evenly coat the inside of the tubing. The particle coated tubing was stored in the dark and cut into lengths of 1.2 cm prior to use.

2.1.4.2 Preparation of retinae to enable visualisation of RGCs

Retinae were shot once at 100 psi using a Helios gene gun (Bio-Rad) 3 cm from the retina through a 3 µm pore size, high pore density cell culture insert (Milipore) to block clumps of tungsten from coming in contact with the retina. Diolistically labelled retinae were incubated in pre-warmed Neurobasal A for 25 minutes at 37 °C, 5% CO_2 to facilitate dye diffusion before transferring to 4% paraformaldehyde (PFA) for 35 minutes, for fixation. The fixed retinas were then stained with TO-PRO (Invitrogen) (1:500) for 5 minutes before washing three times in PBS. Retinae were then mounted onto a glass slide and coverslipped with Prolong Gold Antifade Reagent (Invitrogen) and left in the dark at room temperature for 1 hour. Finally, an airtight seal was made around the retina before storing in the dark at 4 ^{o}C.

To assess the dendritic complexity at baseline, a group of animals were assigned to a 0 hour group, indicating that retinas were diolistically labelled immediately after dissection. A second group was placed in culture for 8 hours and a third group was cultured for 16 hours before diolistically labelling, to examine the dendritic complexity as function of time and treatment.

2.1.5 Analysis of RGC dendritic complexity

Fluorescent images were collected within 24 hours of labelling. RGCs were identified as having their soma located in the ganglion cell layer, their dendrites stratifying across the inner plexiform layer and a distinct axon projecting towards the optic nerve. Images were

acquired with a Zeiss LSM 510 confocal microscope (Carl Zeiss, Ltd, UK), using a 20X (0.8 NA) objective lens, 543 nm excitation and BP 565-615 nm emission filter for DiI, 488 nm excitation and BP 500-530 nm emission filter for DiO and 633 excitation and 651-704 emission spectral window for TO-PRO.

Images stacks were collected each 1 µm distance along the Z-plane, from the ganglion cell layer to the inner nuclear layer, producing a reconstructed 3-dimensional image. Cells were masked using a Fiji plugin prior to tracing. Dendrites were traced using the Fiji plugin, Simple Neurite Tracer, to facilitate Sholl analysis. Sholl analysis (Sholl, 1953) gives a quantitative measure of dendritic complexity, counting the number of dendritic intersections with concentric rings placed at 10 µm intervals from the soma to the most peripheral dendrite (Sholl, 1953).

The area under the Sholl curve (AUC) was obtained by the trapezoidal method whereby the Sholl curve was divided into trapezoids with a 10 µm base and the sum of the area of each trapezoid from 10 µm to the distance of the most peripheral dendrite was calculated.

The total dendritic length of each RGC was obtained by collecting the length of each dendrite measured in Simple Neurite Tracer and calculating the sum of all the dendrites. The dendritic field area of the RGC was obtained by connecting the ends of each dendrite using a polygon tool in Fiji.

2.2 Exposure of the retinal explant to 670 nm light

2.2.1 Animals used

Twenty five wild-type, 9 week old, male C57 BL/6J mice were used as the source of retinal explants. Each mouse contributed a maximum of one retina per experimental condition. Mice were kept in a 12 hour light (4.88 lux of warm white fluorescent lighting with an irradiance of 0.7 µW/cm^2) / 12 hour light-dark cycle with food and water available *ad libitum.* Maintenance and all experimental procedures were in compliance with the *ARVO Statement for the Use of Animals in Ophthalmic and Vision Research* and were approved by the Home Office, UK.

2.2.2 *Ex vivo* treatment of wild-type retinae with 670 nm light

Mice were killed by cervical dislocation under 275 lux of warm white fluorescent light, providing total irradiance of 74 µW/ cm^2 and an irradiance of 2.8 µW/cm^2 in the 600-780 nm range of the electromagnetic spectrum, as measured using a JETI Specboss 1201 spectroradiometer (JETI Technische Instrumente GmbH, Jena, Germany). Retinae were then dissected under 676 lux of warm white fluorescent light, providing a total irradiance of 250 µW/ cm^2 and an irradiance of 130 µW/cm^2 in the red range. Retinae were dissected as described previously and flat mounted onto a 0.4 µm pore PTFE membrane culture plate insert (Williams et al., 2011). One retina per mouse was assigned to sham treatment and the other to light treatment. The insert was placed in a 6-well plate containing pre-warmed Neurobasal A media (Invitrogen) at 37 °C.

Red light was delivered to the retinae from a WARP 10 light source (Quantum devices, Inc., Wisconsin, USA), immediately after flat mounting. Red light-treated retinae were

exposed to 670 nm with a bandwidth of 30 nm (full width half maximum, FWHM) light with a radiant exposure of 31.7 J/cm², delivered by 6 sequential 88 second exposures of the WARP 10 light device, over a 10 minute period, at room temperature (Figure 2.2). The parameters for 670 nm light delivery were chosen based on an experiment by Liang et al., 2006 where 670 nm light rescued primary visual cortical neurons from apoptosis (Liang et al., 2006). Sham treated retinae were placed at room temperature, in a separate room to the light treatment. Upon cessation of the treatment, the retinae were labelled using DiOlistics, either immediately or after an *ex vivo* period of 8 or 16 hours in a dark incubator, at 37 °C. In the majority of cases, both retinae from a single mouse were assigned to the same time point; one to light treatment and one to sham treatment. Also, the retina assigned to light treatment was alternated between the first and second eye that was dissected, to account for any effect on dissection time on the *ex vivo* dendropathy.

A

B

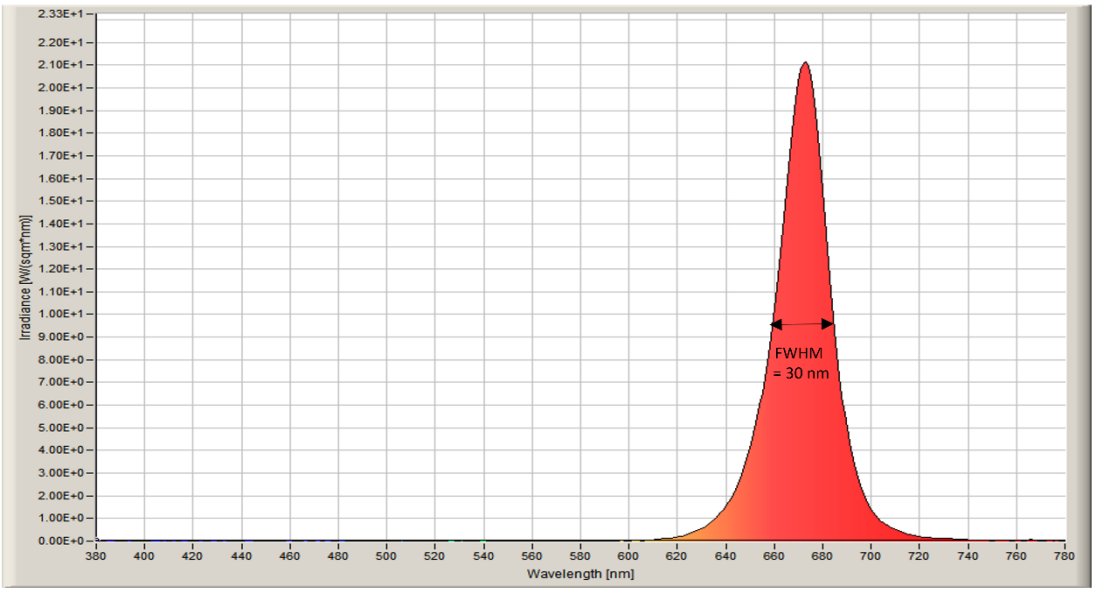

Figure 2.2: Treatment of the mouse retinal explant with 670 nm light. (A) The WARP 10 light device was placed directly under the flat mounted retina in a 6-well plate, containing Neurobasal A media. A total radiant exposure of 26.4 J/cm2 was delivered over a 10 minute period, from 6 serial 88 second exposures of 670 nm light. There was a period of 5 seconds between each exposure. (B) The emission spectrum of the WARP 10 light device was measured with a diffuser, 1 cm from the light source. Peak wavelength: 670 nm. FWHM: 30 nm.

2.3 *In vivo* treatment of 12-15 month old wild-type and het mice with 670 nm light

The mice were divided into 4 experimental groups; WT sham (n=15), WT light (n=16), Het sham (n=11), Het light (n=11). Light treated animals were exposed to 4.4 J/cm^2 of 670 nm light from a WARP 10 light source (Quantum devices, Inc.), which was delivered over 88 seconds. A JETI Specboss 1201 spectroradiometer (JETI Technische Instrumente GmbH, Jena, Germany) was used to measure the irradiance at the level of the eye cornea. Two devices were required to ensure that the radiant exposure delivered to each eye, over the 88 seconds was 4.4 J/cm^2 (Figure 2.3). Light treated mice were light adapted for 30 minutes prior to 670 nm light exposure. The sham treated animals were subjected to the same level of handling as the light treated groups to account for any effect of stress

that may be experienced by the animal upon restraint. The mice were treated daily for 5 consecutive days.

On the fifth day, the final light or sham treatment was administered 30 minutes before culling by cervical dislocation. Thirty minutes was allowed between the final treatment and axotomy as it has been shown that the expression of genes which are induced by nitric oxide signalling peaks 30 minutes after nitric oxide exposure in cultured cells (Hemish et al., 2003).

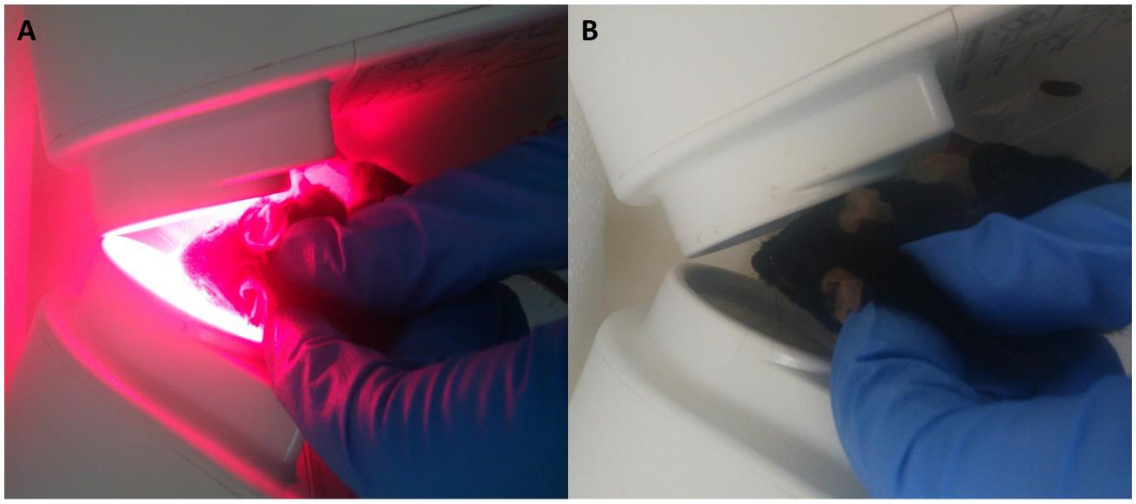

Figure 2.3: Light and sham treatment *in vivo*. (A) Mice assigned to the light treatment group were scruffed in front of two WARP 10 light devices for 88 seconds, positioned as such, ensuring that an irradiance of approximately 50 mW/cm^2 is reaching the cornea. (B) The sham treated mice were scruffed in front of the light source for 88 seconds to ensure the level of stress was uniform throughout the experimental groups.

2.4 *In vivo* treatment of 21-26 month old wild-type and Opa1 (+/-) mice with 670 nm light

Het mice and their wild-type littermate aged between 21 and 26 months were selected for the study. Five wild-type mice were assigned to a sham treatment group (Wild-type

sham). Ten mice heterozygous for Opa1 randomly assigned to either a sham treatment group (Het sham) or a light treatment group (Het light). Light treated animals were exposed to a single WARP 10 for 88 seconds twice daily at 9am and again at 6pm (Figure 2.4B). Measurements were taken with the JETI Specboss 1201 spectroradiometer, taking into account the angle of the eyes relative to the light device (Figure 2.4C-D. An irradiance of 10 mW/cm^2 was measured when the spectroradiometer was placed 1 cm from the light device, at the angle of the mouse eye. To increase the amount of 670 nm light reaching each eye from a single WARP 10 device, an aluminium foil dome was created to reflect some of the 670 nm light back to the eye. The irradiance of the light reaching the eye increased to approximately 19.7 mW/cm^2, with the use aluminium foil dome placed around the spectroradiometer. Thus a foil dome was placed around the head of the mouse during red light exposure, to increase the irradiance reaching each eye.

Sham treatment entailed scruffing in front of a light device for 88 seconds, while the device remained off (Figure 2.4A). Equal handling of all animals was ensured to account for the effect of stress on the results obtained.

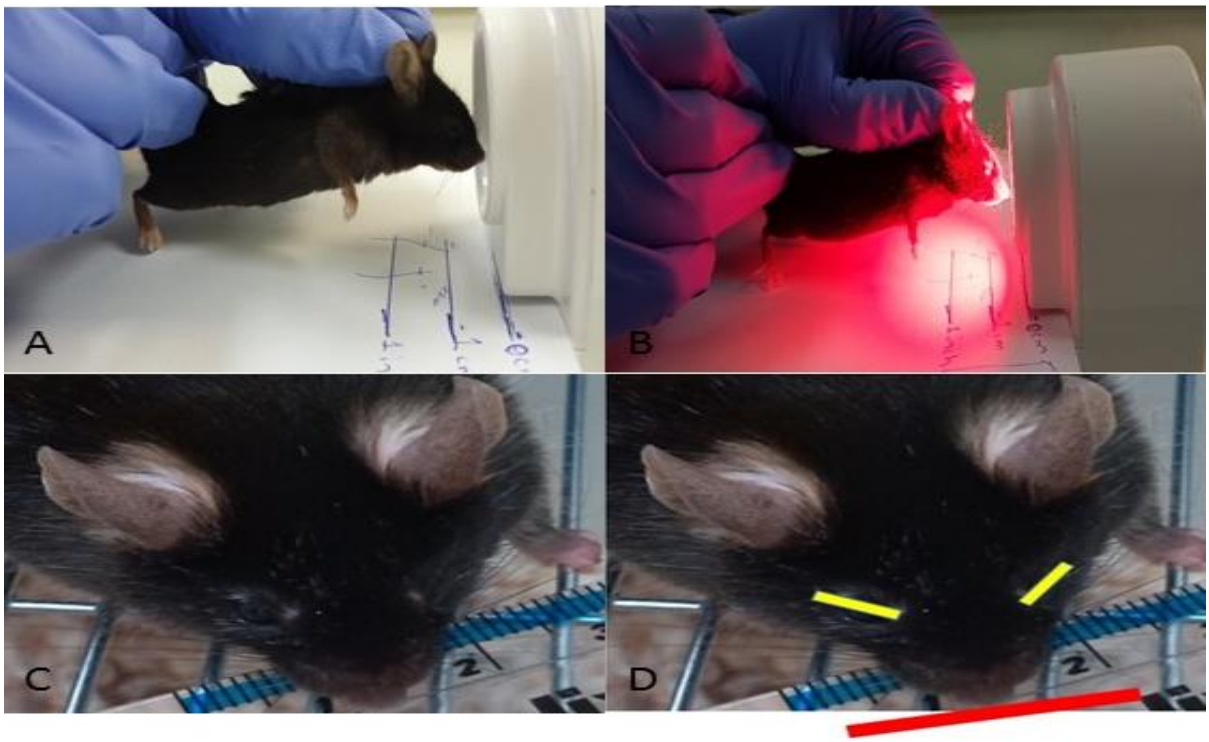

Figure 2.4: In vivo treatment of 21-26 month old wild-type and het with 670 nm light-treated (A) and sham treated (B) mice positioned with their eyes 1 cm from the light source. The mouse head: showing the width of the head and the position of the eyes (C). The angle of the mouse eyes (yellow) relative to the surface of the light (Zhang et al.) (D).

On the seventh day of the trial the mice received one final treatment prior to sacrificing by cervical dislocation. Eyes from an untreated 9 week old wild-type mouse were fixed-frozen and stored to be used as controls for microglial activation (Untreated wild-type).

2.5 Immunohistochemistry

Immunohistochemistry was done to look at the effect of 670 nm light on microglial activation in the GCL and IPL of very aged het mice. This technique was also employed to explore the effect of 670 nm light on the activation or upregulation of transcription factors or signalling intermediates that are upregulated in response to oxidative and nitrostrative stress in aged wild-type and het mice.

2.5.1 Preparation of eyes for Immunohistochemical analysis

Mice were sacrificed by cervical dislocation and the eyes were immediately enucleated and washed in PBS before being placed in 1 mL of 4% PFA and left overnight at 4 ^{o}C. The eyes were transferred to PFA in less than 30 seconds after death. After fixation the eyes were cryoprotected by transferring to a 5% sucrose solution for 1 hour, a 15% sucrose solution until the eye sank to the bottom of the Eppendorf tube and finally to a 30% sucrose solution for a time sufficient to allow the eye to sink. The eyes were then placed in an OCT filled cryomould and transferred to melting isopentane (-160 ^{o}C) until frozen and stored at -80^{o} C. The orientation of the eye was noted and labelled on the mould.

2.5.2 2.5.3 Preparation of eyes for COX/SDH assay

Of the of 21-26 month old wild-type and het mice treated with 670 nm light or sham, one eye was prepared for immunohistochemical analysis, as described above, and other eye was prepared for a COX/SDH assay. One eye from each mouse was transferred rapidly upon death to an Eppendorf tube and immediately placed in a canister containing liquid nitrogen. The eyes were then transferred to the -80 freezer for storage.

2.5.3 Immunostaining procedure

Sagittal sections of 10 µm thickness were cut from fixed-frozen eyes using a Leica 3050 S cryostat and collected on Superfrost Plus Adhesion Slides (Thermo Scientific). Four consecutive sections were placed on each slide and the slides were numbered so that the region of the retina being used for each staining protocol could be approximately known. Sections were allowed to air dry overnight at room temperature before storage at -20 ^{o}C until required.

Sections were selected from each mouse containing comparable regions of the retina by selecting slides labelled with the same number from each mouse. The staining protocol was done three times for each antigen and each slide chosen was 5 slides apart from the others to ensure that 3 different regions of the retina were examined per mouse for each antigen.

The sections were adjusted to room temperature for 20 minutes before rehydrating in 0.1 M PBS for a further 5 minutes. The excess moisture around the sections was wiped off and the tissue sections were encircled with a hydrophobic barrier using a PAP pen. Non-specific binding sites were blocked with 10% fetal calf serum (FCS) (Abcam Ltd, Cambridge, UK) in 0.1 M PBS containing 1% TritonX100 and 1% Tween for 1 hour at room temperature. Sections were then washed three times with 0.1 M Triton-Tween PBS, for 5 minutes each with rocking, before incubation with the primary antibody diluted in 5% FCS in 0.1M Triton-Tween PBS, overnight at 4 ^{o}C. Following three washes in 0.1 M Triton-Tween PBS the secondary antibodies, diluted in 0.1 M Triton-Tween PBS with 5% FCS, were applied to the sections and left for 2 hours at room temperature. The primary and secondary antibody dilutions for each antigen used are listed in Table 2.5. Sections were washed three times in 0.1 M Triton-Tween PBS, as for the primary antibody, to remove excess secondary antibody. Finally sections were stained with Hoechst 33342, trihydrochloride, trihydrate, nuclear stain, diluted to 1:1000 in 0.1 M PBS for 5 minutes at room temperature before coverslipping using Prolong Gold Antifade Reagent (Invitrogen). Sections selected for no primary and no secondary antibody controls were shown identical treatment to the test samples, with the exception of the addition of 5%

FCS in 0.1 M Triton-Tween PBS in place of the primary and secondary antibody, respectively.

For co-staining of two antigens a double staining protocol was used. This staining protocol was identical to the immuno staining protocol described above with the exception that two primary antibodies were applied to the sections simultaneously. Two secondary antibodies were then applied to the sections simultaneously, with care taken to avoid cross reaction of the secondary antibody with a non-specific primary antibody.

For some stains, heat-induced epitope retrieval was required for successful antigen staining. Sections were placed in a large glass beaker filled with 10 mM sodium citrate buffer pH 6.0 and transferred to a heat block for 15 minutes.

Antigen of interest	**Primary antibody**	**Primary antibody dilution**	**Secondary antibody**	**Secondary antibody dilution**	**Antigen retrieval**
Nrf2	Rabbit Anti-Nrf2 (cat no. ab31163; Abcam Ltd, Cambridge, UK)	1 in 100 IHC	Goat Anti-Rabbit IgG H&L (Alexa Fluor® 488)	1 in 500	None
NfkB	Rabbit Anti-NF-kB p65 (phospho S536) antibody (cat no. ab86299; Abcam Ltd, Cambridge, UK)	1 in 150 IHC	Goat Anti-Rabbit IgG H&L (Alexa Fluor® 488)	1 in 500	None
Cytochrome *c* oxidase	Mouse Anti-COX-IV cat no. ab33985; Abcam Ltd, Cambridge, UK)	1 in 100 IHC	Goat Anti-Mouse IgG H&L (Alexa Fluor® 594)	1 in 200	Sodium citrate buffer (pH 6.0)
D-J1	Rabbit Anti-PARK7/DJ1 (cat no. ab18257;	1 in 500 IHC	Goat Anti-Rabbit IgG H&L (Alexa	1 in 500	None

	Abcam Ltd, Cambridge, UK)		Fluor® 488)		
3-nitrotyrosine	Rabbit Anti-Nitrotyrosine antibody (cat no. N0409; Sigma-Aldrich, UK)	1 in 200 IHC	Goat Anti-Rabbit IgG H&L (Alexa Fluor® 488)	1 in 500	Sodium citrate buffer (pH 6.0)
MDA	Rabbit Anti-Malondialdehyde cat no. ab6463; Abcam Ltd, Cambridge, UK)	1 in 200 IHC	Goat Anti-Rabbit IgG H&L (Alexa Fluor® 488)	1 in 500	None
iNOS	Rabbit Anti-iNOS antibody (cat no. ab3523; Abcam Ltd, Cambridge, UK)	1 in 200 IHC	Goat Anti-Rabbit IgG H&L (Alexa Fluor® 488)	1 in 200	Sodium citrate buffer (pH 6.0)
Iba-1	Goat Anti Iba1 (cat no. ab5076; Abcam Ltd, Cambridge, UK)	1 in 500 IHC	Donkey Anti-Goat IgG H&L (Alexa Fluor® 488)	1 in 500	None
Akt1/2/3	Rabbit Anti-AKT1/2/3 antibody (cat no. ab126811; Abcam Ltd, Cambridge, UK))	1 in 1000 WB	Anti-Rabbit-peroxidase antibody produced in goat (Sigma)	1 in 1000	None
p-Akt	Anti-phospho-Akt (pSer473) antibody produced in rabbit (cat no. SAB4504331-100UG; Sigma)	1 in 100 IHC 1 in 750 WB	Goat Anti-Rabbit IgG H&L (Alexa Fluor® 488) Anti-Rabbit-peroxidase antibody produced in goat (Sigma)	1 in 500 IHC 1 in 1000 WB	Sodium citrate buffer (pH 6.0)
Actin	Monoclonal Anti-β-Actin,	1 in 2000 WB	Anti-mouse	1 in 2000	None

	produced in mouse (cat no. A1978; Sigma)		IgG-peroxidase antibody produced in rabbit (cat no. A9044; Sigma)		

Table 2.1: Working conditions for each antigen used in immuniohistochemical staining of fixed-frozen 10 µm retinal sections and western blot analysis. Table includes the primary antibody that was chosen to detect each antigen of interest, the primary antibody dilution, the secondary antibody used to detect the primary antibody and the dilution required. For some antigens, retinal sections were treated with sodium citrated buffer (pH 6.0) for 15 minutes prior to commencement of the staining protocol.

2.6 2.6 Imaging and Fluorescence quantification

2.6.1 Fluorescence microscopy

Images were acquired using an upright fluorescence microscope (Leica WETZLAR DM6000B) with selective FITC filter sets (excitation/emission 495/519 nm), a Rhodamine non-selective filter set (excitation/emission 552/578 nm) and a DAPI filter set (excitation/emission 359/461 nm). The experimental group to which the sections belonged was unknown to the experimenter. Three sections were imaged from each mouse with three images taken per section, one from the centre and two from the periphery using a DFC350 FX camera and a 20X magnification lens. All images were acquired with the same gain, intensity and exposure time. Controls for the primary and secondary antibodies were used to set the gain, intensity and exposure time, ensuring that minimal fluorescence was detected in samples controlling for autofluorescence and non-specific binding of the secondary antibody. This ensured that the images taken contained true fluorescence from the antigen of interest only.

2.6.2 Confocal microscopy

Images were acquired using a Zeiss LSM 510 confocal microscope (Carl Zeiss, Ltd, UK) using a 20X (0.8 NA) objective lens, 488 nm excitation and BP 500-530 nm emission filter for Alexa Fluor 488, 594 nm excitation and BP 599-702 nm emission filter for Alexa Fluor 594 and 350 nm excitation and BP 411-480 nm for Hoechst 33342. Images of 60 X magnification were acquired using a 40X (0.8 NA) objective lens with a zoom value of 1.5. Three sections were imaged from each mouse with one images taken per section. All images were acquired with the same gain, intensity and exposure time.

2.6.3 Fluorescence quantification

Fluorescence quantification was performed using Fiji software. To measure the average fluorescence in the GCL, RGB images with a range of 0-255 for each channel were converted into binary mode and the green and blue channels were split. The green channel was selected and a rectangular box of fixed area was placed on four different regions of the area corresponding to the retinal ganglion cell layer and the mean grey value within each rectangular box was calculated. The mean grey value within the rectangular box was calculated to give the average grey value for all the pixels occupied by the green marker in the selected region.

To measure the nuclear-cytoplasmic ratio of fluorescent markers in the RGCs, the integrated density values were then obtained for the cytoplasmic and nuclear region of RGCs and the ratio between the two was calculated. To measure the integrated density of the RGC nuclei in ImageJ, the blue and green channels were split and the blue channel was overexposed to reveal all the RGCs (Figure 2.5A-B). The threshold function was used

to create a binary image to separate the RGC nuclei from the background (Figure 2.5C). A wand tracing tool was used to select and record the area occupied by each nuclei in the RGC layer and its position on the image (Figure 2.5D). Finally the regions of interest, recorded from the RGC nuclei in the blue channel, were pasted onto the areas corresponding to the RGC nuclei in the green channel, allowing the integrated density values for the antigen of interested in the RGC nuclear region to be measured. The integrated density of the GCL was measured by drawing around the nuclei with a polygon tool; the polygon created was approximately 16 µm in height, the approximate average diameter of the RGC soma. The integrated density value of the RGC nuclei was subtracted from the integrated density value for the GCL region, giving the integrated density values for the RGC cytoplasmic region. The ratio between the integrated density of the nuclear region and the cytoplasmic region of the GCL layer was then calculated.

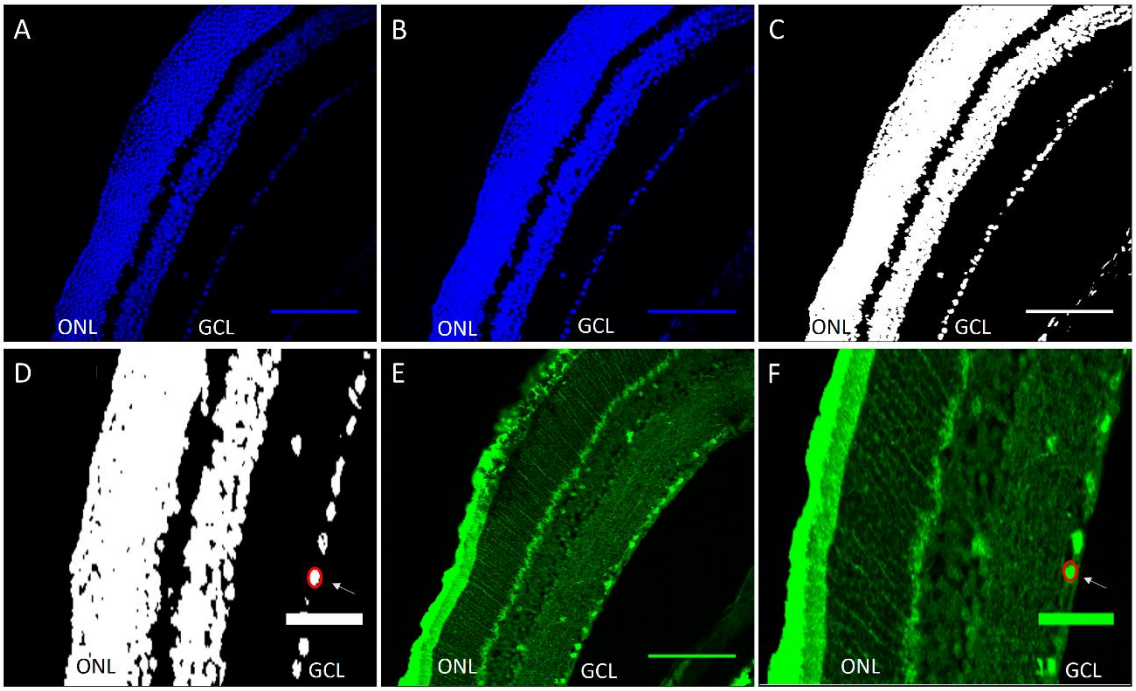

Figure 2.5: Method for calculation of the nuclear-cytoplasmic ratio of fluorescence in RGCs. The blue and green channels were split and the blue channel, showing the nuclear

stain was selected (A). The blue channel was over exposed (B) and the threshold function was used to create a binary image (C). A wand tracing tool was used to select and record the area of each nuclei (D). The green channel was then selected (E) and the area recorded for each nuclei was pasted onto the green channel, allowing the integrated density values for the antigen of interest in the nuclear region to be measured (F). Arrows indicate the selected nuclear region. Scale bars represent 100 µm (A-C and E) and 50 µm (D and F).

2.6.4 Western blotting

Western blot analysis was used to verify the results of the immunohistochemistry in Chapter 6. Mice were sacrificed by cervical dislocation 30 minutes after the final light or sham treatment. The retinae were rapidly removed and placed in 5 µL of phosphatase inhibitor cocktail and 5 µL of protease inhibitor cocktail (Abcam) and immediately transferred to liquid nitrogen. Retinae were stored at -80 until required. Three mice per experimental group were used for each antibody and two retinae from each mouse were pooled together to produce a single sample. Each sample contained enough protein to do the western blot twice.

20 µg of total protein was separated on a 10% SDS–PAGE gel and transferred to a nitrocellulose membrane (0.2 µm) (Bio-Rad laboratories, Hertfordshire, UK). Protein samples were incubated with blocking buffer (5% bovine serum albumen in 1X Tris-buffered saline with 0.5% Tween20- pH 7.2–7.4) for 1 h at room temperature. After washing in wash buffer (1X Tris-buffered saline with 0.5% Tween), the primary antibodies (rabbit Anti-AKT1/2/3 antibody (1:1000), rabbit Anti p-Akt (1in 750) and mouse Anti-actin (1:2000)) were applied to the respective samples in blocking buffer and were incubated overnight at 4 ^{o}C on a mini orbital shaker SO5 (Stuart Scientific, Stratfordshire, UK). After washing three times for 10 minutes each in wash buffer, horseradish peroxidase conjugated secondary antibodies were applied to the samples goat anti-rabbit t at

1:1000 for Akt and p-Akt, and rabbit anti-mouse at 1:2000 for Actin. The samples were incubated with the secondary antibodies for 2 h at room temperature. The blots were developed using the enhanced chemiluminescence detection kit (Biological Industries, Lichfield, UK) and ChemiDOc XRS+ System (Bio-Rad laboratories, Hertfordshire, UK). Bands were quantified using Image Lab software (Bio-Rad laboratories, Hertfordshire, UK) and normalized to actin. The normalised values for p-Akt and Akt were then used to calculate the p-Akt/Akt ratio.

2.7 MTT assay on the retinal flat mount

2.7.1 Reagents used

2.7.1.1 Acidified isopropanol

In the fume cupboard, 3.33 µl of 37% HCL was added to each 1mL isopropanol to make up the required volume of acidified isopropanol with a molarity of 0.04 M. This was done one week prior to use and stored at room temperature.

2.7.1.2 MTT stock solution

A 5 mg/mL stock solution with was made by diluting MTT powder in 0.1M PBS. The solution was passed through a 2 µm pore sterile filter into a sterile 15 mL falcon tube. The falcon tube was foil wrap to protect the solution from light and store in the fridge for up to 4 days before use.

2.7.1.3 Culture medium

Neurobasal A medium without phenol red was used to avoid any potential interference of phenol red with the absorbance readings in the final assay.

2.7.1.4 Triton X 10

TritonX100 was diluted to 1 in 10 in PBS at room temperature to make the solution less viscous allowing the required volumes for the assay to be accurately measured.

2.7.2 Original MTT protocol prior to modifications

Mice were killed by cervical dislocation. Both eyes were removed and placed in ice cold Hanks buffered saline solution. The retinae were dissected and flat mounted onto a membrane culture insert and placed in a 6-well plate containing 1 mL of pre-warmed Neurobasal A medium, as described previously, before being transferred to a at 37 ^{o}C incubator for the required time.

After the incubation period, 110 µL of 5mg/mL (MTT) 3-(4,5-dimethylthiazol-2-yl)-2,5-diphenyltetrazolium bromide) solution was added to the well containing the insert, comprising 10% of the culture medium giving a final concentration of 0.5 mg/mL MTT in each well. The plate was gently swirled to ensure a uniform concentration of MTT within the well. The plate was then returned to the incubator for 2 hours at 37 ^{o}C to allow the reduction of MTT to formazan by active mitochondrial enzymes.

To control for formazan production in the absence of viable cells, a retina was treated with TritonX10 to kill all retinal cells before treatment with MTT, representing 0% cell viability. This was achieved by the addition of 100 µL of Triton X 10 directly on top of the retina which was then left in the incubator at 37 ^{o}C for 30 minutes.

After the MTT incubation period the insert containing the retina was removed from the well and washed with PBS for 5 minutes to remove any traces of MTT whilst taking care not to remove any formazan. Efforts were made to and protecting from light during all

stages of the assay, as light has the potential to cause an accelerated spontaneous of MTT. The insert containing the retina was transferred to a clean well to which 1 mL acidified isopropanol was added. The plate was before put on shaker for 15 minutes to dissolve the formazan crystals. The absorbance of the formazan crystal solution was read at 570 nm in triplicate. A reading was also taken at 690 nm as a reference for each sample, which was subtracted from each reading obtained at 570 nm.

2.8 Measuring oxygen consumption in the retinal explant using the Seahorse XF Analyzer

2.8.1 Original protocol for preparation of retinal explants for use in the Seahorse XF analyser

Mouse retinal explants were flat mounted 16 hours prior to measuring oxygen consumption. A 20 µl drop of chicken plasma was pipetted onto nylon inserts and the retinal explant was centred onto the insert before 20 µl of thrombin was added to fix slices within an O_2 permeable clot. The slices were transferred to a 6 well plate positioned with the slices facing up. The slices were covered with pre-warmed Neurobasal A at 37 °C, 1 ml was sufficient to cover the slice. The plates were then transferred to an incubator at 37 °C and 5% CO_2.

2.8.2 Modified protocol for preparation of retinal punches for use in the Seahorse XF analyser

Mouse retinae were explanted and three 1 mm tissue punches were taken from regions adjacent to the optic nerve. This was to ensure that the readings were taken from the central retina to avoid central to peripheral variations. The retinal punches were placed off centre on the nylon insert and placed in ice cold Ames' medium (pH 7.4) and placed in an igloo with ice. The inserts were positioned off centre so as to place the retinal punch

directly under the O_2 sensor. Ames' solution buffered with 10 mM HEPES was chosen as this medium is optimal for retinal tissue. Retinas remained on in ice cold Ames' medium until the inserts were placed into the wells of the microplate.

2.8.3 XF24 microplate-based respirometry

Respirometry of retinal explants was performed using an XF24 Extracellular Flux Analyzer (Seahorse Bioscience, Billerica, MA). Explants on nylon inserts were individually inserted face down into 16 wells of 24-well XF Islet Capture Microplates that contained 675 µl of Neurobasal A. Eight wells contained inserts but no slices to control for oxygen consumption and extracellular acidification rate. The wide end of a 20 µl pipette tip was used to ensure inserts are even in wells. Once the transfer of inserts was complete, slices in XF Islet Capture Microplates were incubated in a CO_2-free incubator at 37°C for 1hr to allow temperature and pH equilibration. Slices were then loaded into the XF24 and further equilibrated for 15 min by three 3 min mix, 2 min wait cycles prior to the first measurement. XF assays consisted of 3 min mix, 3 min wait, and 2 min measurement cycles and were performed at 37°C as described (Wu et al., 2007). Using this protocol, it was possible to calculate an O_2 consumption rate every 8 minutes. Compounds of interest prepared in Neurobasal A medium (75 µl) were preloaded into reagent delivery chambers A, B, C, and D at 10X, 11X, 12X, and 13X the final working concentration, respectively, and injected sequentially at intervals of 24 minutes, with the first addition occurring after 24 minutes and the final addition occurring after 96 minutes. Chambers A, B, C and D contained oilgomycin, FCCP, Rotenone and Antimycin A, respectively.

2.9 Statistical analyses

The Kolmogorov-Smirnov test was performed in SPSS to test for normality in the data. Normally distributed data were analysed using an unpaired *t*-test in Excel. Non-parametric data were analysed using the Mann Whitney-U test using the SPSS program. *p* values less of than 0.05 were considered statistically significant.

Chapter 3. Modification of cell based assays to assess the effect of 670 nm light on mitochondrial bioenergetics in the retinal explant

3.1 Introduction

Although great progress has been made in uncovering the molecular mechanism responsible for the beneficial effects of 670 nm light, there remains, yet, much controversy and unclarity surrounding this area of research. One of the theories available for the beneficial effects of 670 nm light in neurodegenerative diseases is the increase in Complex IV activity and the restoration of the ATP producing capacities of the mitochondria of cells with defective mitochondrial proteins. Bioenergetic deficiencies have been found in the het mouse model, namely, a reduction in ATP production and oxygen consumption, a reduction in the protein levels of Complex IV and a decrease in the enzymatic activities of Complex I and IV (Chen et al., 2012). RGCs are highly metabolically active and it is hypothesised that the exclusive degeneration of RGCs in ADOA is due to their inability to survive with a reduced capacity to produce ATP. As perturbations in mitochondrial activity are detremental for RGC function, normal mitochondrial activity must be sustained to support the function and survival of the RGCs. We hypothesis that 670 nm light will provide beneficial effects to the degeneration prone RGCs by improving mitochondrial bioenergetics.

Complex IV activity can be measured using the COX/SDH assay. Since many of the beneicial effects of 670 nm light are thought to occur downstream of absorbtion of photon energy at complex IV, we thought exploring the direct effects of 670 nm light on the enzymatic activity of this complex would be a suitable initial experiment.

Mitochondrial electron transport chain activity can be assessed by monitoring the reduction of MTT to formazan. Learning of the effects of 670 nm light on mitochondrial activity or reductive capacity would provide a basic understanding of whether or not 670

nm light can influence mitochondrial function in retinae from het mice; however, the exact components of mitochondrial function altered by 670 nm light would not be identified. A more precise exploration of the effects of 670 nm light on mitochondrial bioenergetics would enable a more detailed analyisis of the effects of 670 nm light on retinal mitochondria. The Seahores XF cell mito stress test measures key parameters of mitochondrial function, including ATP production, proton leak, maximal respiration, spare respiratory capacity and non-mitochondrial respiration, by directly measuring oxygen consumption and cytoplasmic glycolysis.

3.2 Experimental design

3.2.1 COX/SDH assay

The cytochrome c oxidase/succinate dehydrogenase (COX/SDH) assay can be used to measure COX or ETC complex IV activity. The catalytic subunits of COX are encoded by mitochondrial DNA, therefore their correct synthesis is dependent on mtDNA integrity (Ross, 2011). Whereas the subunits of SDH are encoded by nuclear DNA, therefore the proper synthesis of this complex is unaffected by mtDNA mutations.

It was of interest look at the effects of 670 nm light on complex IV activity in in het mice as complex IV activity has been found to be reduced in this model. Very aged mice were chosen for this experiment to test whether or not 670 nm light could produce beneficial effects at the end stage of the disease. Wild-type and het mice were selected in numbers sufficient to have a minimum of five mice in each of the following experimental groups: wild-type sham treated, het sham treated and het 670 nm light treated. The mice were aged until all mice were a minimum of 21 months old to test whether or not 670 nm light could provide therapeutic effects in the very advanced stages of disease in the het mouse.

Thus we treated 21-26 month old het mice (n=6) with 670 nm light twice daily for 7 consecutive days as described in Chapter 2.4. A group of 21-26 month old wild-type (n=5) and het mice (n=4) were sham treated as a control. After the final treatment the mice were killed by cervical dislocation and one eye from each mouse was flash frozen. The second eye was prepared for exploration of the effects of 670 nm light on microglial activation in very aged mice (Chapter 6).

Due to freezer failure the flash frozen tissue was no longer suitable for the assay COX/SDH assay so there are no results for this experiment.

3.2.2 The MTT assay

The MTT reduction assay is a cell viability assay based on the presence of active mitochondrial enzymes. Mitochondrially active viable cells can reduce MTT, which is a yellow solution, into formazan crystals, which are a purple, water insoluble product, in the presence of a mitochondrial reducing molecule, most likely NADH (Riss et al., 2016). NADPH oxidase is also another molecule responsible for MTT reduction. The amount of formazan produced, which absorbs maximally at 570 nm, is considered to be proportional to the number of viable cells, since mitochondrial activity is related to the number of viable cells in most cell populations.

It was most useful to test the effects of 670 nm light on mitochondrial activity at a time when Opa1-related degeneration was present. As degeneration in the het mouse presents as significant dendropathy at 12-15 months, the effects of 670 nm light on mitochondrial activity were tested het mice of that age. Therefore, the mice were treated *in vivo* before culling and explanting the retinae, and the analysis was done on the retinal explant. However, the MTT assay is designed for use in *in vitro* studies, thus it was first necessary to modify the assay for use in the retinal explant.

The degeneration in the het mouse is subtle at 12-15 months, indicating that the Opa1 mutation produces a mild phenotype. In order to find significant differences between both wild-type and het mice, and sham and light treated mice, with a feasible number of retinae, it was necessary to allow the retinae to degenerate *ex vivo* to maximise the

chances of significance being reached between the experimental groups. Significant *ex vivo* dendropathy has been shown to begin to occur in mouse retinal explants after 6 hours and progresses over 3 days (Binley et al., 2016). Sixteen hours was chosen as a suitable time for monitoring the changes in mitochondrial activity between wild-type and het retinae and sham and light treatment. This was considered the ideal time point as the effects of the Opa1 mutation would be exaggerated and the *ex vivo* degeneration in the retinae could be allowed to occur overnight ready for analysis the following morning.

3.2.3 Oxygen consumption measurements

Similar to the MTT assay, it was decided that 16 hours *ex vivo* would be a suitable time point for measuring oxygen consumption in the retinal explant. As the nearest available Seahorse XF24 analyser was in Swansea University, a 16 hour ex vivo time point was considered most suitable for practical reasons. Retinal dissection was done the evening before the assay and retinae were transported to Swansea at 9am the following morning. The time of dissection and transport were carefully considered to ensure that the assay would commence approximately 16 hours post axotomy.

Since there is decreased oxygen consumption *in vivo* in the het mouse, it was hypothesised that there would also be decreased oxygen consumption compared to wild-type after 16 hours *ex vivo*. A statistical reduction in oxygen consumption after 16 hours would provide an ideal platform to test the effects of 670 nm light on this parameter.

Of note, the retinae were placed in suboptimal conditions for transport which may have compromised the tissue quality at the time of the assay. In particular, the 6 well plate

containing the retinae was removed from the incubator and placed in a Styrofoam insulated box that was lined with cotton wool sheets and packed with heat packs at 37 ° C before sealing.

The Seahorse mito stress test kit is used to yield information on various parameters of mitochondrial respiration by the sequential addition of modulators of different components of the electron transport chain, by measuring oxygen consumption (Figure 3.1). Basal respiration shows the energy demand of the cell under normal physiological conditions, maximal respiration occurs when you use an uncoupler so the proton can freely cross the membrane following the concentration gradient so there is no proton gradient to allow for ATP synthesis, spare respiratory capacity demonstrates how well the cell would cope with an increased energy demand, non-mitochondrial "respiration" is the oxygen consumption that remains after the inhibition of the electron transport chain such as generation of superoxide which would be converted to hydrogen peroxide.

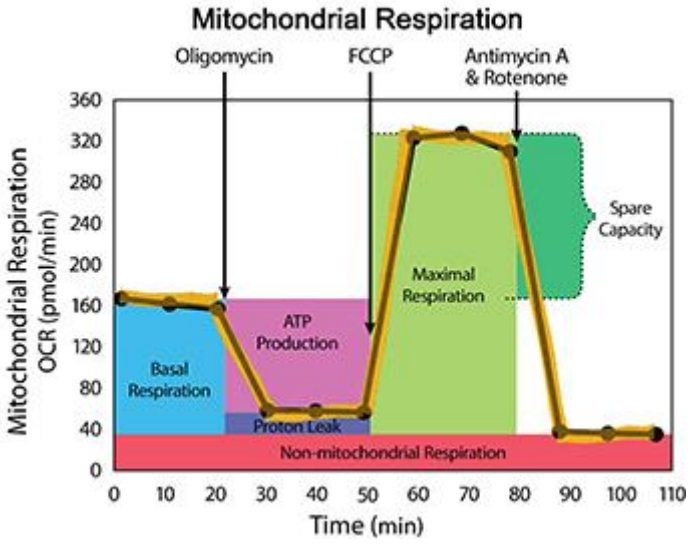

Figure 3.1: An exemplary result from the Seahorse mito stress test on cells *in vitro.* Three readings are taken for the oxygen consumption that results from basal respiration. Another three readings are taken after the addition of oligomycin to show the decrease

in oxygen consumption following the inhibition of ATP synthase. The uncoupler FCCP is then added to uncouple oxidative phosphorylation from ATP synthesis, allowing the protons to flow through the mitochondrial inner membrane, from the intermembrane space back into the matrix, before they can be used to fuel ATP production by ATP synthase. Three readings are taken following FCCP addition to show the oxygen consumption at the maximal respiration ability of the mitochondria. The mitochondrial spare capacity is the difference in between the oxidative phosphorylation thar occurs under basal conditions for ATP production and that which occurs when oxidative phosphorylation is driven to maximum levels The addition of the complex III inhibitor Antimycin A and the complex I inhibitor Rotenone completely supresses oxidative phosphorylation. Three final readings are taken after the addition of Antimycin A and Rotenone to determine the oxygen consumption that occurs in the absence of mitochondrial respiration. The proton leak refers to the oxygen consumption that occurs from mitochondrial respiration under basal conditions that does not result from ATP production.

The Seahorse XF analysers are designed for use with monolayers of cells, cells in suspension or isolated mitochondria, consequently, the assay required modification and optimisation for use in the retinal explant. This assay was previously modified for the measurement of oxygen consumption in both cultured and acute hippocampal slices with some success (Schuh et al., 2011). The hippocampal slices used were 200 µm in thickness, which is the approximate thickness of the mouse retina. The medium used for the culture of hippocampal slices, artificial cerebospinal fluid, was also used as the assay medium, therefore we used retinal explant culture medium, neurobasal A, as the assay medium in our protocol. Plasma and thrombin were used to fix the slices to the nylon insert for measurements on acute hippocampal slices but were not required in the protocol for the cultured hippocampal slices. As the explants were to be placed in culture for only 16 hours, plasma and thrombin were used in the initial test of this assay on the retinal explant to avoid any potential movement of the tissue during oxygen consumption measurements. The concentrations of mito stress test compounds used in

the reference paper were used as the starting point in the optimisation process. Four different concentrations of each compound were tested in attempt to find the optimal concentration for use in the retinal explant. As the retinal explant has a much larger surface area than the hippocampal slices, three different concentrations above those used for the hippocampal slices were selected for testing in the retinal explant (Table 3.1).

	Oligomycin	**FCCP**	**Antimycin A & Rotenone**
Starting concentration from reference paper (Concentration 1)	1 µg/ml	1 and 5 µM	10 µM
Concentration 2	2 µg/ml	2 µM	20 µM
Concentration 3	5 µg/ml	5 µM	30 µM
Concentration 4	10 µg/ml	10 µM	40 µM

Table 3.1: The concentrations of the mito stress test compounds chosen as a starting point for the optimisation of the assay for use in the retinal explant. Four different concentration of each drug were tested as a starting point for the Seahorse assay

3.3 Results

3.3.1 Modification of the cell based cell MTT used to assess cell viability in the retinal explant

Incubation of the retinal explant with 0.5 mg/mL MTT for 2.5 hours resulted in a dense covering of formazan crystals on the retinal explant at different time points up to 24 hours after flat mounting (Figure 3.2A-D). The absorbance at 570 nm of the solubilised formazan crystals, produced by active mitochondria, decreased rapidly as a function of time *ex vivo* (Figure 3.2E). Assessment of the cell viability of RGCs was required from the MTT assay, yet the resulting formazan crystals were formed by the cells of the entire retina. Therefore, visualisation of the formazan crystals around the RGC nuclei was necessary to show the metabolic activity and viability of these cells by the MTT assay.

The concentration of MTT appeared to be too high at 0.5 mg/mL to allow the visualisation of formazan crystal formation around the RGC nuclei. Consequently, the concentration of MTT was reduced to 0.25 mg/mL and the incubation time of the retina with MTT was reduced to 30 minutes. Figure 3.3A shows the formazan formation on the retinal explant when treated with 0.25 mg/mL MTT for 30 minutes. Using this concentration made it possible to visualise the reduction in mitochondrial activity in the explant over time *ex vivo* as shown by the decrease in the purple formazan product on the retinal explant from 0 to 48 hours *ex vivo* (Figure 3.3A-E). This concentration was more suitable to assess whether the formazan crystals can be seen surrounding the RGC nuclei, using confocal microscopy.

Reflective light was used to image the formazan crystals, using Topro as a nuclear counter stain. The results were inconclusive as it was difficult to pick up the reflective light signal

from the RGC layer. In some areas there was some reflected light signal detected around the RGC nuclei however the background signal was very high.

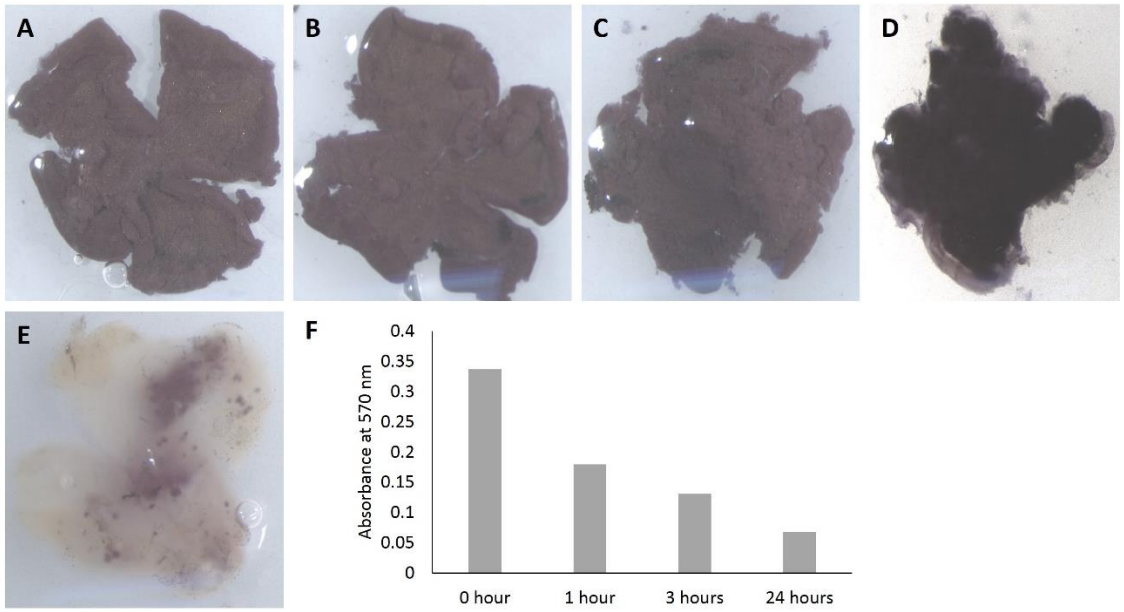

Figure 3.2: Optimisation of the MTT assay to detect reductions in mitochondrial reductive capacity in the retinal explant. The formazan crystal formation on the retinal explant after incubation with 0.5 mg/mL MTT for 2.5 hours immediately after explanting (n=1) (A), 1 hour after explanting (n=1) (B), 3 hours after explanting (n=1) (C) and 24 hours after explanting (n=1) (D). E: The formazan formation on a retina which was treated with TritonX100, to cause almost 100% cell death before incubation with 0.5 mg/mL MTT for 2.5 hours (n=1). F: The absorbance readings of solubilised formazan crystals formed by retinae after various *ex vivo* culture periods.

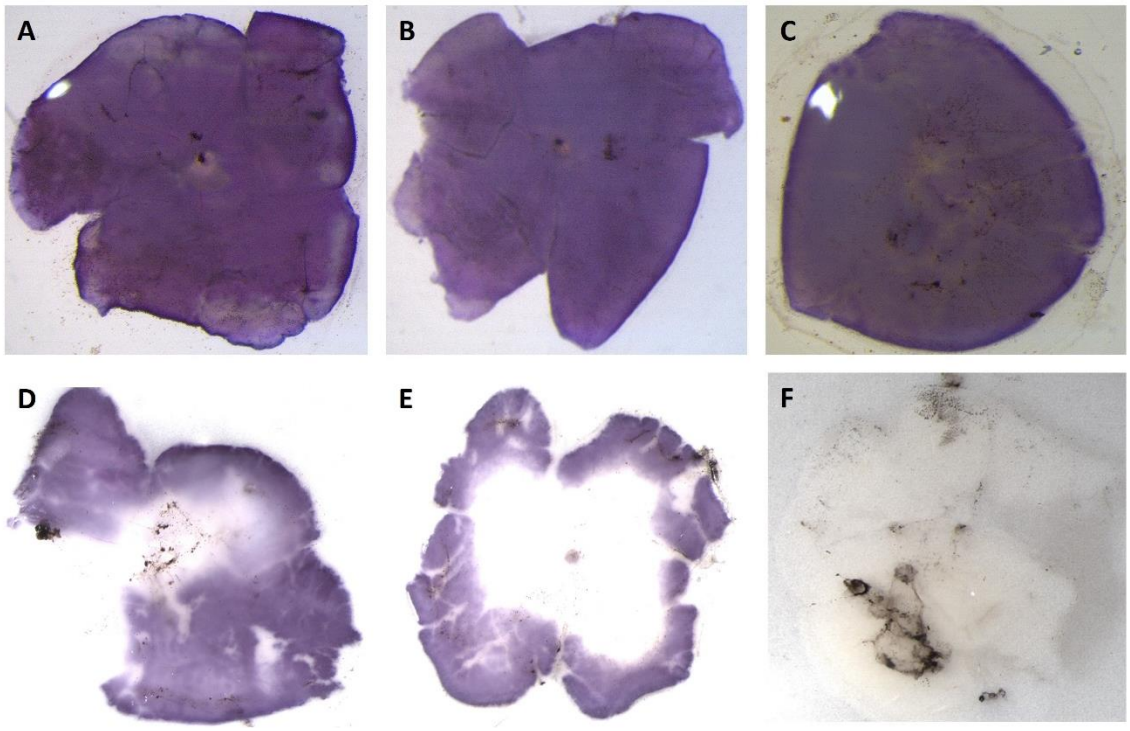

Figure 3.3: Further optimisation of the cell based MTT assay for use on the retinal explant. The explant treated with 0.25 mg/mL MTT immediately after flat mounting (n=1) (A), treated with 0.25 mg/mL MTT 1 hour after flat mounting (n=1) (B), treated with 0.25 mg/mL MTT 16 hour after flat mounting (n=1) (C), treated with 0.25 mg/mL MTT 48 hours after flat mounting (n=1) (D), treated with 0.25 mg/mL MTT 1 week after flat mounting (n=1) (E) and treated with 0.25 mg/mL MTT after treatment with TritonX100, representing as close as possible to 100% cell death (n=1) (F). Images D and E were over exposed, showing the area of the retina with formazan crystals in purple and the unstained area of the retina in white.

The MTT assay was found to have the ability to detect changes in mitochondrial reductive capacity in the retinal explant as observed by the progressive decrease in formazan formation in the explant as it degenerates over time *ex vivo*. Since we were unable to image the formazan crystals surrounding the RGC mitochondria, we were unable to determine the portion of the formazan that was produced exclusively by the RGCs. Therefore, the assay was used to detect changes in the mitochondrial activity of the entire retinal explant.

During the optimisation process much variability was found between the results of the MTT assay in retinae at the same *ex vivo* timepoints. It was noticed that *ex vivo* time points past 16 hours produced the most variable results with the MTT assay. However, a maximum of two retinae were used at each time point in the optimisation stages. To test the reproducibility of this assay on the retinal explant, five retinae each were used at time zero and at 16 hours *ex vivo,* with one retina from each mouse assigned to the 0 hour time point and the other to the 16 hour timepoint. The standard concentration of 0.5 mg/mL MTT was used for this experiment. The mean and standard deviation for the absorbance values at time zero was 0.593 ± 0.125, which was reduced to 0.396 ± 0.142 when the assay was done after 16 hours *ex vivo* (Figure 3.4). The average absorbance value of 5 retinae was reduced from that obtained at 0 hours *ex vivo* to that obtained after 16 hours *ex vivo.* This reduction was in accordance with the reduction in cell viability that occurs over this time. From this result it was concluded that the MTT assay was sensitive enough to detect changes in cell viability in the retinal explant.

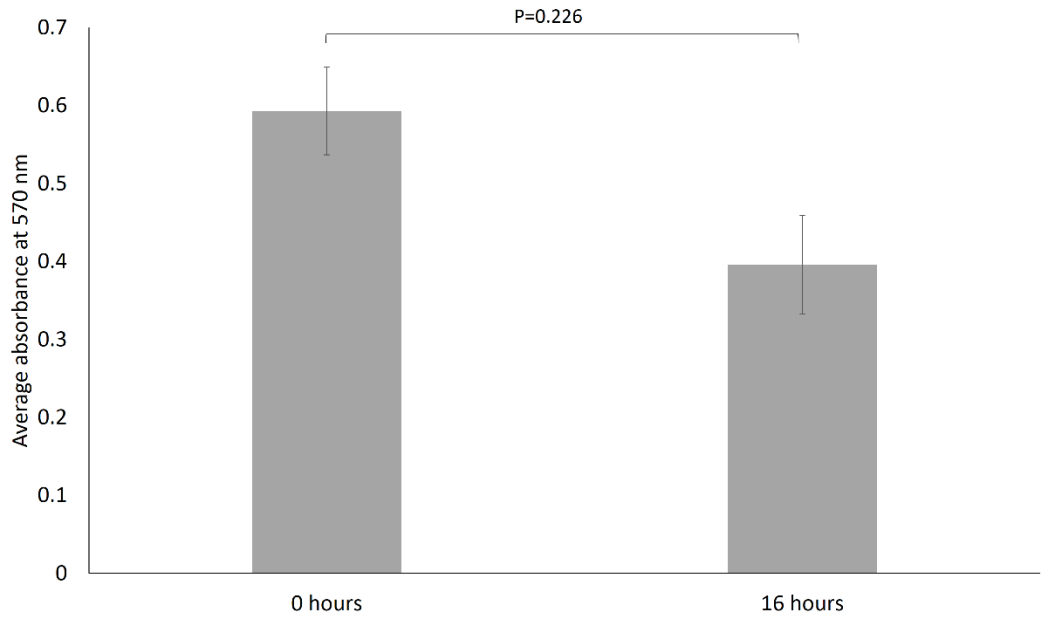

Figure 3.4: Investigating the viability of the wild-type retinal explant from 0 to 16 hours *ex vivo,* based on the mitochondrial reductive capacity, as determined by the MTT assay. The average absorbance of formazan at 570 nm was measured in retinal explants treated with MTT at 0 (n=5) and 16 (n=5) hours after flat mounting. Error bars represent SEM.

The MTT assay was then used to explore differences in the cell viability of the retinal explant from wild-type and het mice after 16 hours *ex vivo*. The assay was also employed to look at the effect of 670 nm light on mitochondrial reductive capacity in aged wild-type and het mice. Retinae from wild-type and het mice were treated *in vivo* with 670 nm light, for 5 consecutive days, and the effects on the cell viability of the retinal explant after 16 hours *ex vivo* was monitored. There were no significant differences between any of the groups investigated, using three mice per experimental group (Figure 3.5). Further, no trend emerged to show that 670 nm light can increase mitochondrial activity in either wild-type and het retinae. Also, there was no decrease in mitochondrial activity in the het retinae, showing an inability of the MTT assay to detect differences between

wild-type and het retinae or sham treated and light treated retinae. This pilot experiment was therefore not pursued further.

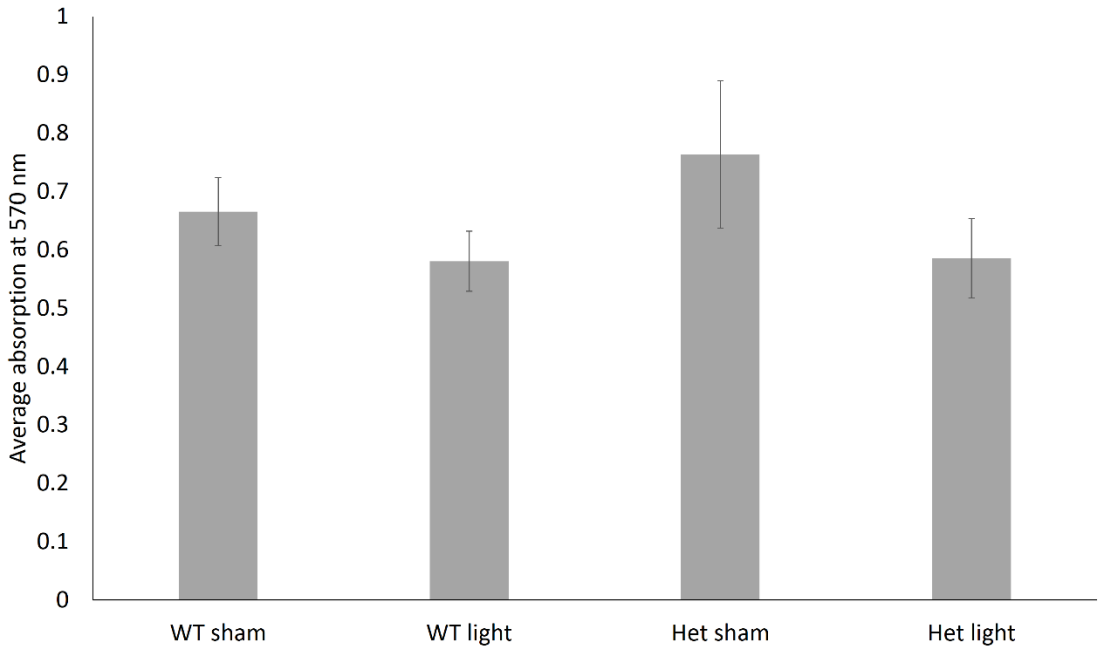

Figure 3.5: Mitochondrial reductive capacity was unchanged in retinal explants from het mice after 16 hours *ex vivo* compared to wild-type. Similarly, *in vivo* treatment with 670 nm light had no effect on the mitochondrial reductive capacity of wild-type or het retinae, when assayed after 16 hours *ex vivo*. The average absorbance of formazan at 570 nm of retinae from sham treated wild-type (n=5), light treated wild-type (n=6), sham treated het (n=4) and light treated het (n=4) mice is presented. Error bars represent SEM.

3.3.2 Development of a method to measure oxygen consumption in the retinal explant using the Seahorse XF analyser

As the retina is almost the same diameter as the microchamber of the Seahorse XF24 Islet cell microplate, it was thought that the design would be suitable for measuring oxygen consumption of the entire retinal explant (Figure 3.6A-C). Plasma and thrombin were used to prevent the retina moving during measurements by creating an oxygen permeable tissue clot between the retina and the porous nylon insert (Figure 3.6B-C). Different concentrations of compounds from the mitochondrial stress test (oligomycin,

FCCP, rotenone and antimycin A) were tested to find the best concentration of each for use on the retinal explant. The basal rate of oxygen consumption was very low for a large piece of tissue such as the retina (Figure 3.7). Additionally, there was only a minor effect of oligomycin and FCCP in most of the retinae, however, the respective decrease and increase in oxygen consumption was not as steep as that seen with a monolayers of cells (Figure 3.1). All concentrations of rotenone and antimycin A were found to be ineffective in supressing mitochondrial respiration as the oxygen consumption rates began to rise after the addition of the uncoupler, FCCP, and continued to rise despite the addition of the Complex I inhibitor, rotenone, and the Complex III inhibitor, antimycin A.

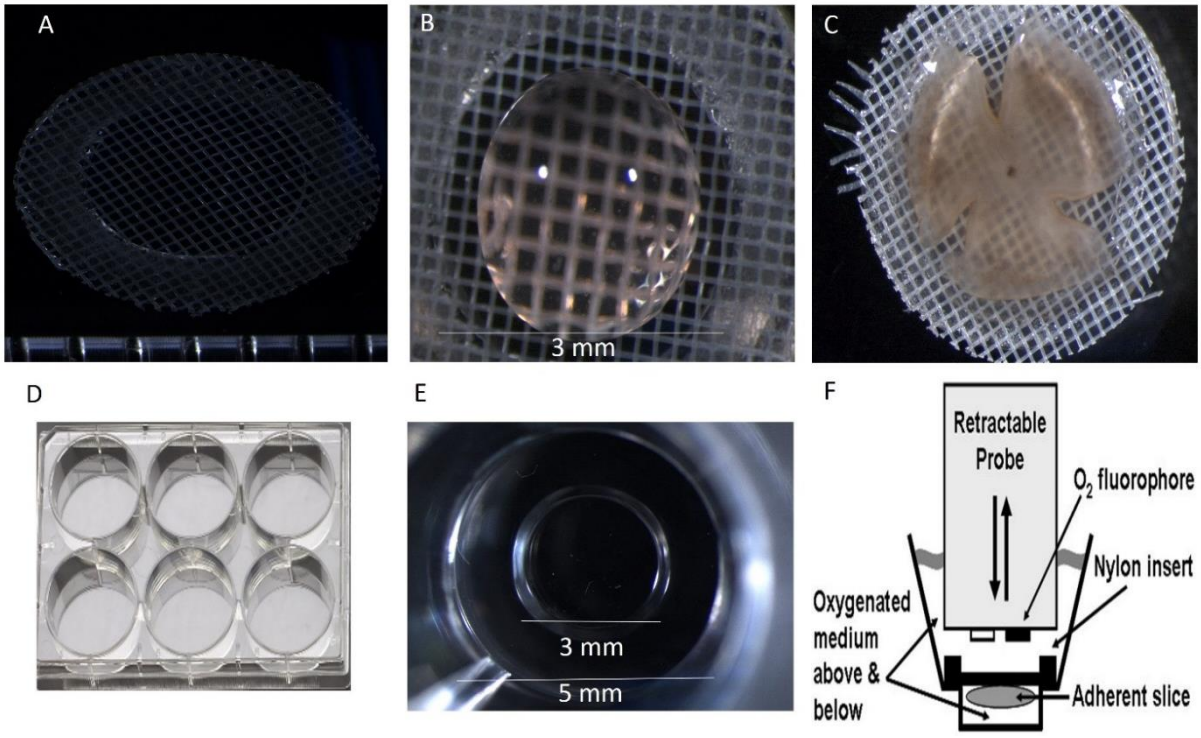

Figure 3.6: Preparation of the retinal flat mount for measurement of oxygen consumption using the Seahorse XF Analyser and the Seahorse XF24 Islet Capture Microplate. The nylon insert (A), 10 µl of chicken plasma placed on the nylon insert (B), the retina flat-mounted onto the nylon insert (C), the 6 well plate containing the retina atop the nylon insert and neurobasal A medium (D), the bottom of the Islet Capture Microplate (E) and a diagram of the retina attached to the nylon insert placed in the Islet

Capture Microplate for the creation of a transient microchamber with the retractable probe (F).

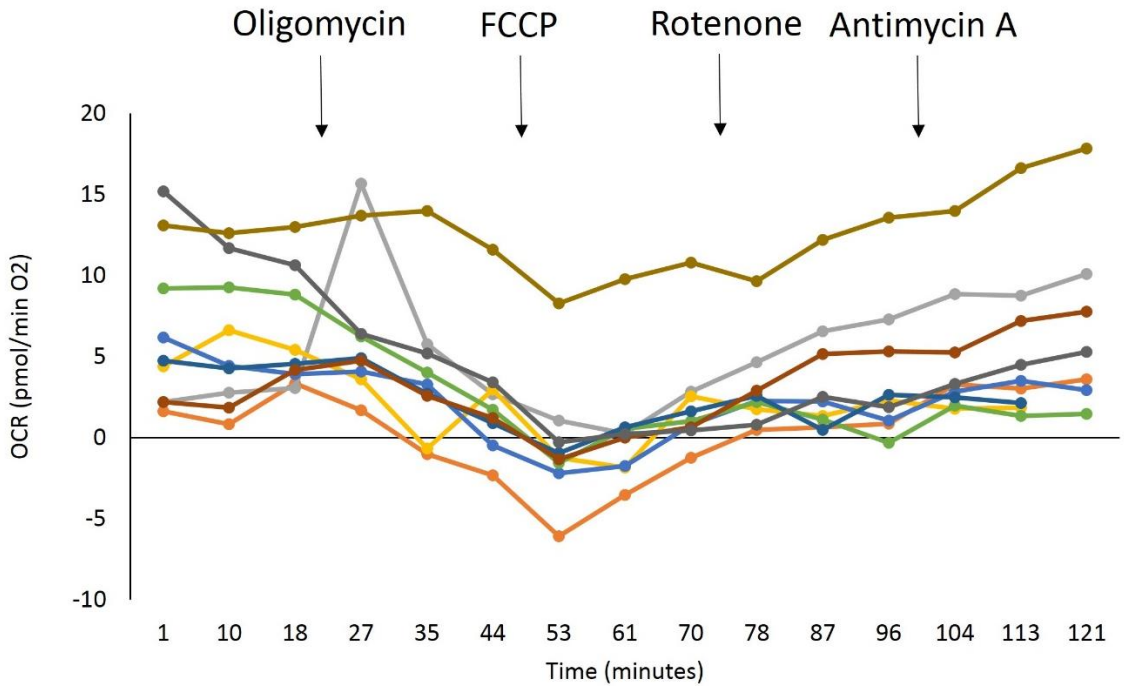

Figure 3.7: The oxygen consumption rates of whole retinal flatmounts measured using the Seahorse XF Analyser. Three measurements were taken for basal respiration before the addition of oligomycin, FCCP, rotenone and antimycin A at the times indicated by the arrows. Each plot shows the oxygen consumption over time for one retinal explant.

The use of 20 µL of plasma and thrombin, as used previously to adhere the retina to the nylon insert, appeared to be too large of a volume for the retina, therefore, smaller volumes of 5 µL and 10 µL were tested (Figure 3.8A-B). Furthermore, as the tissue clot was formed prior to incubation of the explant for 16 hours, the effect of this condition on oxygen consumption measurements was examined (Figure 3.8). The baseline oxygen consumption measurements were, on average, higher in retinas not fixed to the nylon

insert with plasma and thrombin. Further, some retinae treated with 10 µL of plasma and thrombin had negative oxygen consumption readings. Based on this result, the use of plasma and thrombin on the retinal explant either caused a disruption to the oxygen consumption readings during the assay or the incubation of the retina with plasma and thrombin for 16 hours compromised the viability of the retinal explant leading to low oxygen consumption rates. However, even without the use of plasma and thrombin, the response of the retinae to the mitochondrial stress test compound was limited. This highlighted the possibility that waiting 16 hours between explanting the retina and measuring the oxygen consumption compromised the ability of the retina to respond to the mitochondrial stress test compound.

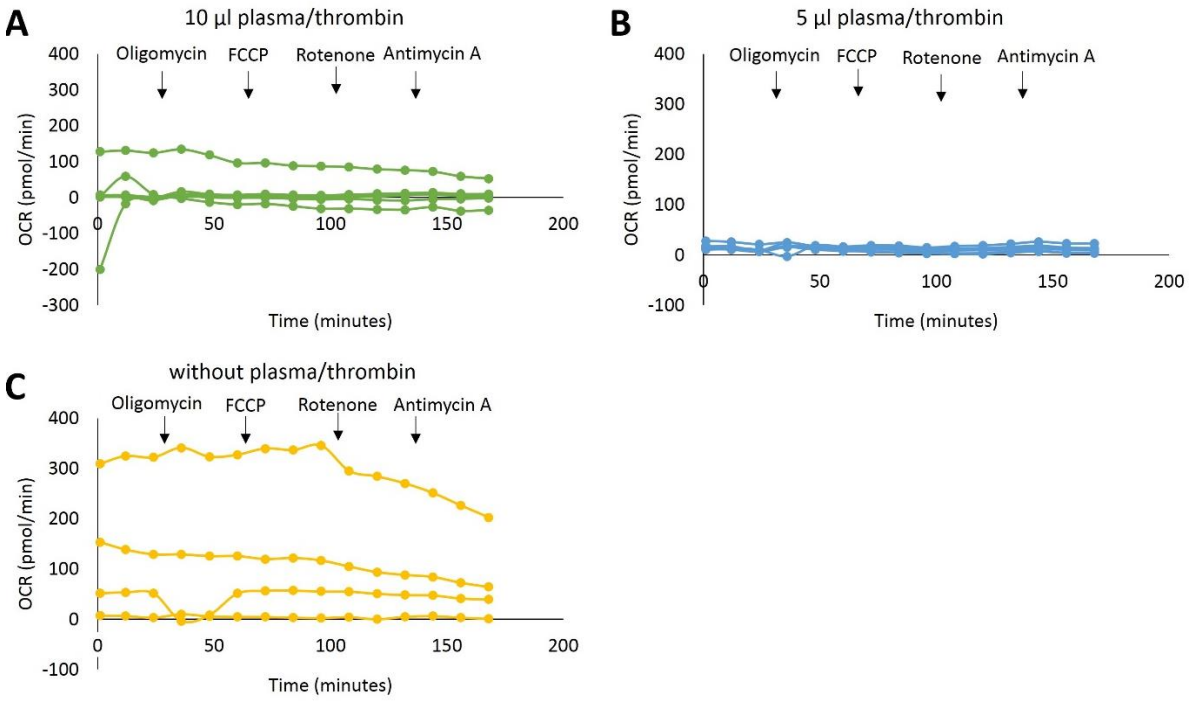

Figure 3.8: A comparison of the effect of 10 µl plasma/thrombin, 5 µl plasma/thrombin or no plasma/thrombin on the oxygen consumption rates of whole retinal flatmounts as measured using the Seahorse XF analyser. Three measurements were taken for basal respiration before the addition of oligomycin, FCCP, rotenone and antimycin A at the times indicated by the arrows.

The MTT assay was employed to assess the viability of the retinal explant at the time of oxygen consumption measurements, taking into consideration the 15 hour incubation period at 37 ˚C in a 5% CO_2 incubator and 1 hour transport conditions. The retina was incubated for 15 hours in a 37 ˚C 5% CO_2 incubator then the 6-well plate was transferred to a sealed polystyrene box containing a heat pack at 37 °C and an inner insulating layer of cotton wool sheets. After an hour the plate was removed and an MTT assay was done. Figure 3.9D shows the cell viability of the retina represented by the formazan formation after normal 16 hour incubation conditions and Figure 3.9E shows the cell viability of the retina after 15 hours normal incubation conditions and one hour of simulated transport conditions. The large region of the retina without formazan crystals was indicative of a substantial loss in the number of viable cells with active mitochondria, in retinae where transport conditions were simulated (Figure 3.9E). A 16 hour incubation period with the additional challenge of the suboptimal transport conditions were found to have too of severe an effect on cell viability to be suitable for an assay where optimally functioning mitochondria are required.

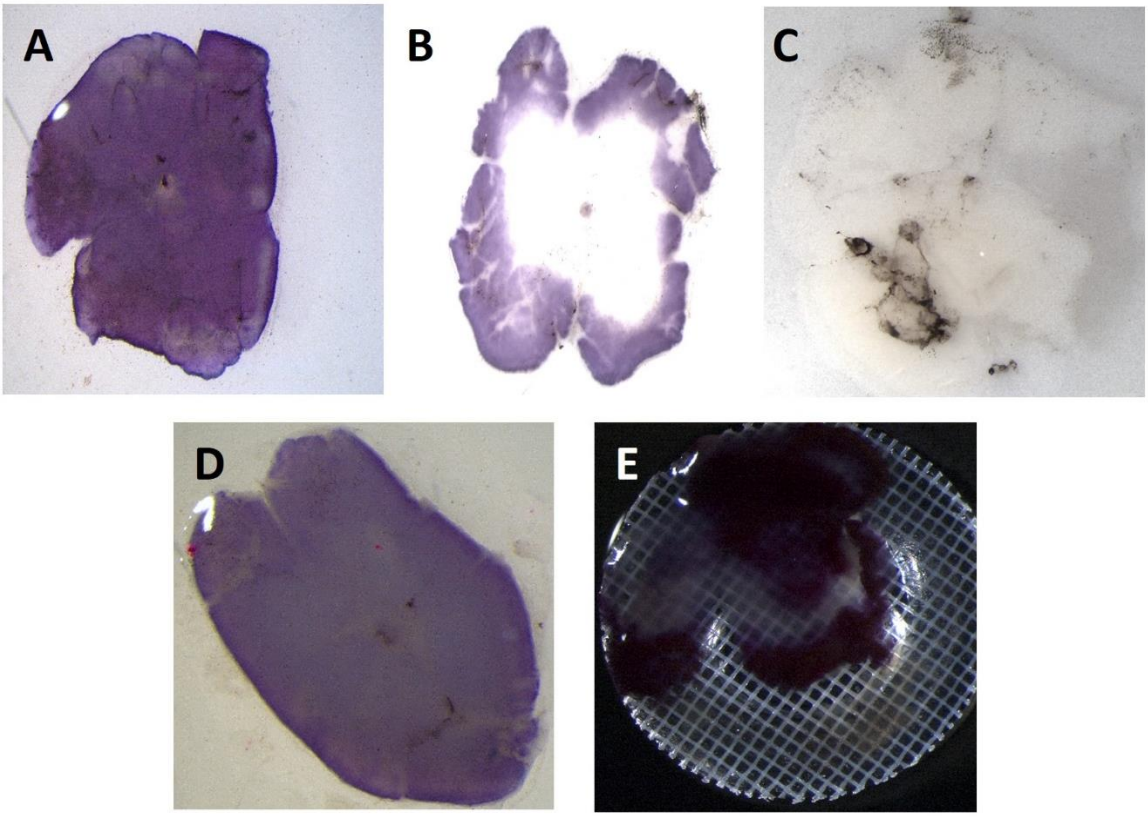

3.9: The MTT assay revealed that 16 hours *ex vivo* and suboptimal culture conditions prior to the seahorse assay severely reduced mitochondrial function in the retinal explants. A: The retinal flat mount treated with MTT immediately after flat-mounting. B: The retinal flat mount treated with MTT 1 week after flat mounting. The image was over exposed, showing the area of the retina with formazan crystals in purple and the unstained area of the retina in white. C: The retinal flat mount treated with MTT after TritonX100 treatment to represent 100% retinal cell death. D: The retinal flat mount treated with MTT 16 hours after flat mounting under normal tissue culture conditions. E: The retinal flat mount treated with MTT 16 hours after flat mounting under normal tissue culture conditions for 15 hours and simulated transport conditions for an hour.

The measurement of oxygen consumption on the retinal explant was then tested 2 hours after explanting the retina, with one hour of transport conditions included in this incubation period (Figure 3.10A). Examination of the condition of the retinal wholemount on the nylon insert after completion of the assay revealed that although the flatmounts had cuts to allow the media to flow unimpeded through the porous insert

into the microchamber at the beginning of the assay, the entire insert was covered with retinal tissue upon cessation of the assay (Figure 3.10B). This uncovered a potential limitation of the protocol as the tissue itself may have restricted fresh media being delivered to the microchamber before each measurement, which may have limited the oxygen consumption capacity of the explant in the previous tests. To address this concern, the retina was cut into thirds to ensure that a fresh supply of media could enter the microchamber after each oxygen consumption measurement (Figure 3.10C).

The basal oxygen consumption rates in many of the samples were between 200 and 500 pmol O_2 (Figure 3.10A). Of those samples, the majority showed a response to the mitochondrial stress test compound; the oxygen consumption decreased after the addition of the inhibitor of ATP synthase, oligomycin, increased after the addition of the mitochondrial membrane uncoupler, FCCP, began to rapidly decrease after the addition of the complex I inhibitor, rotenone, and continued to decrease after the addition of the Complex III inhibitor, antimycin A. However, with the exception of two samples, the response to oligomycin and FCCP was weak compared to that which occurs when the assay is done using cell monolayers. The retina appeared to respond appropriately to rotenone, as the oxygen consumption rates were brought down below basal respiration rates. The effect of antimycin A is unclear as the oxygen consumption rate continued to decrease with each measurement after the addition of rotenone, but the rate of the decrease remained unchanged after the addition of antimycin A.

The high oxygen consumption rate after the addition of oligomycin indicates that much of the oxygen consumption in these retinal samples is due to non-mitochondrial

respiration. It is also possible that the concentration of oligomycin used was too low or the time allotted for the inhibition of ATP synthase was too short. The high oxygen consumption levels after the addition of rotenone and antimycin A were a further indication of high non-mitochondrial respiration levels in the retinal samples.

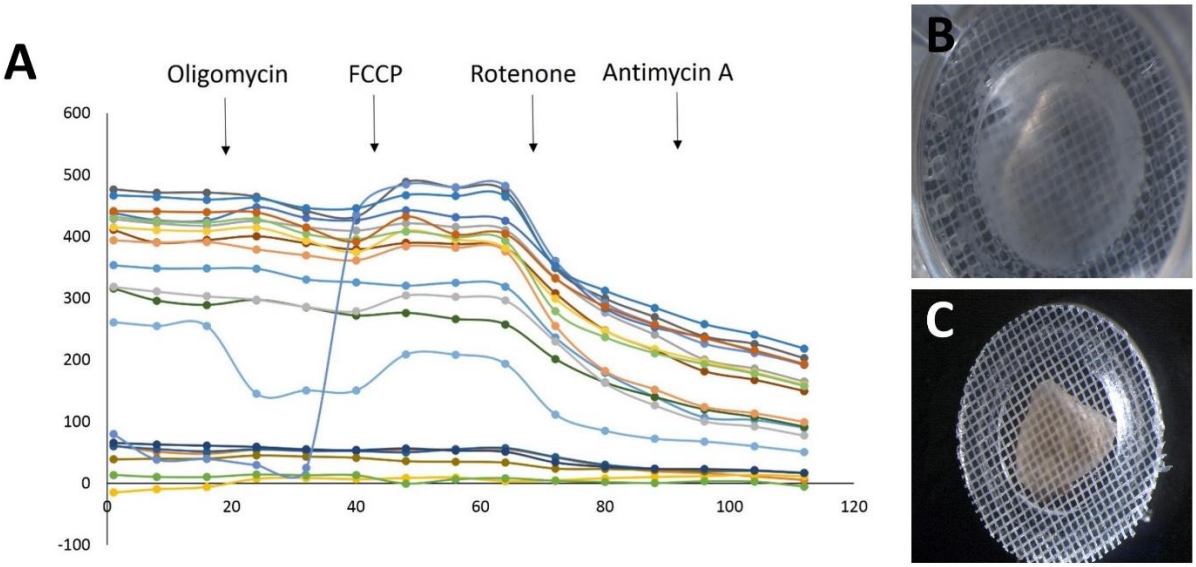

Figure 3.10: The oxygen consumption rates of retinal flatmount thirds were measured using the Seahorse XF Analyser. A: Three measurements were taken for basal respiration before the addition of oligomycin, FCCP, rotenone and antimycin A at the times indicated by the arrows. B: The whole retinal flatmount after the assay. C: The retinal flatmount third placed on the nylon insert.

It was thought that the amount of tissue used to measure retinal oxygen consumption was too large as the concentration of compound used in the assay is dependent on the number of cells, therefore decreasing the tissue size will increase the likelihood of seeing standard changes in the oxygen consumption rate in response to the compound. The method from the paper using hippocampal slices was used as our starting point because the slices were approximately 200 µm in thickness, which is the approximate thickness of the mouse retina. However, comparing our method to that used to measure oxygen

consumption in hippocampal slices using Seahorse XF technology, the area of the retinal section, with an area of 3.2 mm^2, was much greater than that of the hippocampal slice, with an area of 0.33 mm (Schuh et al., 2011).

It was possible to cut the retina into 8 radial sections with an approximate area of 1.2 mm each, which was 3.6 times larger than the hippocampal slice. The drug concentrations used for hippocampal slices were then adjusted to achieve a 3.6 times larger concentration for the retinal section. Two concentrations higher and two concentrations lower than the concentration predicted to be suitable for the retinal section were tested (Table 3.2).

Drug	**Concentration hippocampal slice titration**	**Predicted suitable concentration for retina (3.6X)**	**Rep1**	**Rep2**	**Rep3**	**Rep4**
Oligomycin	3 µM	11 µM	5 µM	10 µM	15 µM	20 µM
FCCP	<5 µM	11, 14 or 18 µM	5 µM	10 µM	15 µM	20 µM
Rotenone	Not tested	36 µM	10 µM	20 µM	30 µM	40 µM
Antimycin A	10 µM	36 µM	10 µM	20 µM	30 µM	40 µM

Table 3.2: Predicted suitable drug concentrations for use on retinal sections, based on reference paper. The optimisation of the best concentration of compound to use on the retinal explant was tested using two concentrations above and two concentrations below the concentration predicted to be suitable for a retinal section of 1.2 mm in area.

The protocol used in the preceding attempts had taken three measurements after each drug injection, with each measurement taking 8 minutes. This may not have been sufficient time for a molecule with such a high molecular weight such as oligomycin (790.523113 g/mol) (exact mass, Pubchem) to penetrate a large tissue section. Schuh et al. 2011 has shown that the OCR continues to decrease after the addition of oligomycin for up to 9 measurements (Schuh et al., 2011). FCCP (254.041545 g/mol) has a lower molecular weight and may not need as many measurements. Also, since the OCR increased after the first measurement of FCCP but steadily decreased with subsequent measurements, fewer measurements may be sufficient (Schuh et al., 2011). Antimycin A (548.273381 g/mol) has been shown to decrease OCR using the protocol from our previous attempt, however, since it has a relatively large molecular weight and the decrease seen was not as steep as expected, an additional measurement was added.

The Seahorse XF Analyser simultaneously records changes in oxygen consumption and pH rate to monitor rates of respiration and glycolysis, respectively. A pH of between 8 and 9 was recorded in the samples which may be responsible for the limited effect of the drugs. The tissue, which should be maintained at pH 7.4, may not have responded to the drug a such a high pH. The assay medium Neurobasal A, which is buffered with sodium bicarbonate, was not suitable for use for the Seahorse assay which is done in a CO_2 free incubator. The Neurobasal A medium was replaced by non-buffered Seahorse assay medium supplemented with 25 mM glucose and 0.23 mM pyruvate. Furthermore, the potential movement of the smaller retinal section during oxygen consumption measurements raised concerns about increasing variability in the readings. The effect of using plasma and thrombin on the sections was therefore explored again; the findings

showing a negative effect of plasma and thrombin on the baseline oxygen consumption levels, as rates of those treated with plasma and thrombin were mainly lower that those without (Figure 3.11).

There were no effects of oligomycin or antimycin A in any of the samples. There was a subtle increase in oxygen consumption after the addition of FCCP in most samples and a transient decrease in oxygen consumption after the addition of rotenone. Reducing the tissue size and increasing the concentrations of compound used reduced the success of the mitochondrial stress test assay compared to the previous attempt. The oxygen consumption rates decreased steadily over time, a trend which was minimally altered by the addition of high concentrations of mitochondrial compound. Curiously, the oxygen consumption readings rapidly increase or decrease in some retinal samples after approximately 25 minutes. This event coincides with the addition of oligomycin, as a rapid and transient change in oxygen consumption readings is seen between the final measurement of basal respiration and the first reading after the addition of oligomycin.

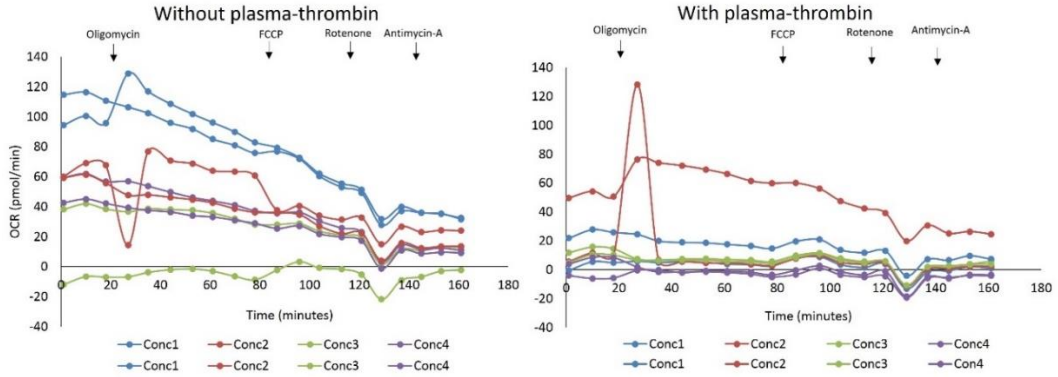

Drug	Conc1	Conc2	Conc3	Conc4
Oligomycin	5 µM	10 µM	15 µM	20 µM
FCCP	5 µM	10 µM	15 µM	20 µM
Rotenone	10 µM	20 µM	30 µM	40 µM
Antimycin A	10 µM	20 µM	30 µM	40 µM

Figure 3.11: Plasma/thrombin reduced the oxygen consumption rates of retinal flatmount eights as measured using the Seahorse XF analyser. Three measurements were taken for basal respiration before the addition of varying concentrations (as shown in the table) of oligomycin, FCCP, rotenone and antimycin A at the times indicated by the arrows.

The publication of a paper to measure the oxygen consumption in the retinal explant showed some success in using the mitochondrial stress test compound on the retinal explant (Kooragayala et al., 2015). The adapted method has been described in detail in Chapter 2 using 1 mm retinal punches. Of note, three punches each were taken from the central and peripheral retina. The retinal punches were placed off centre onto the nylon insert and placed in ice cold Ames' medium pH 7.4 and placed in an igloo with ice for transport. The inserts were positioned so as to place the retinal punch directly under the O_2 sensor. As some studies omit oligomycin from their protocol the assay was tested adding the uncoupler, FCCP, directly after the basal respiration measurements, and

compared the result to the effect of adding the uncoupler after the addition of oligomycin.

The effect on the oxygen consumption measurements of the placement of the retinal punch on the insert was also investigated, with some peripheral retinal punches placed with the GCL facing down and others with the GCL facing up (Figure 3.12B). Following this method, oligomycin and FCCP failed to have any effect on the oxygen consumption levels of the retinal punches (Figure 3.12). The rates declined steadily with an increase in this rate of decline after the addition of rotenone in some of the samples. The results from the published paper were not replicated indicating that the transport conditions for the retinae may have compromised the mitochondrial function of the retinal cells as seen by their inability to respond to the mitochondrial stress test compound (Kooragayala et al., 2015).

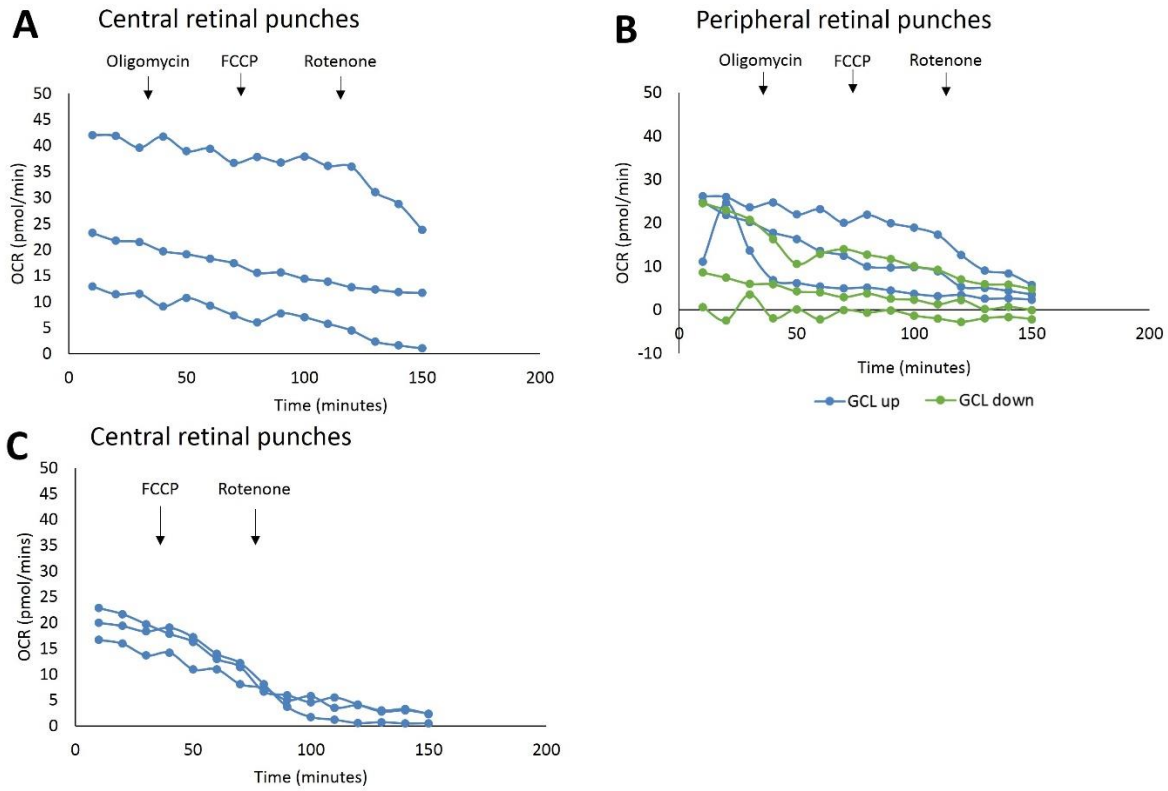

Figure 3.12: The mito stress test compounds did not have an appropriate effect on oxygen consumption rates in retinal punches of 1 mm in diameter, as measured using the Seahorse XF Analyser. Three measurements were taken for basal respiration before the addition of oligomycin, FCCP and rotenone at the times indicated by the arrows: central retinal punches (A) and peripheral retinal punches (B). Three measurements were taken for basal respiration before the addition of FCCP and rotenone at the times indicated by the arrows (C).

3.4 Discussion

3.4.1 Modification of the cell based cell viability assay MTT for use in the retinal explant

Dendropathy is associated with a loss in visual acuity in the het mouse, in the absence of apoptosis (Williams et al., 2010a). The MTT assay was therefore employed to explore the effects of 670 nm light on the more subtle reductions in mitochondrial activity.

The energy demands in the inner segment of photoreceptor cells, the outer plexiform layer and the nerve fibre layer are greater than in the inner plexiform layer and ganglion cell layer. This is denoted by the density of the distribution of cytochrome *c* oxidase and the active energy consuming-enzyme Na^+K^+ATPase in these layers (Wong-Riley, 2010). As the readings from the MTT assay reflected the mitochondrial activity of the entire population of retinal cells, the majority of the formazan produced was most likely due to the mitochondrial activity of the retinal cells other than RGCs. To overcome this confounding factor, we sought to quantify the formazan produced exclusively from RGCs.

Unfortunately, endeavours to quantify the extent of formazan crystal formation surrounding the nuclei in the ganglion cell layer, required for the specific quantification of mitochondrial activity of RGCs, were not met with success. Whilst not equipped to yield information on mitochondrial activity from RGCs only, the assay was capable of detecting reductions in mitochondrial activity over time *ex vivo* from the entire retina, as shown by a progressive decrease in formazan production from 0 to 48 hours *ex vivo* (Figure 3.3). However, high variability was observed between readings at the same time point, therefore large numbers of retinae were predicted to be required for detecting

statistically significant differences between groups. Using 5 retinae per group, the assay was capable of detecting a difference in mitochondrial activity from the entire explant between 0 and 16 hours *ex vivo,* however this difference was not statistically significant (Figure 3.4). This result showed that the assay was capable of detecting reductions in mitochondrial reductive capacity but would most likely not be the most feasible in terms of the amount of tissue required to achieve statistically meaningful results.

The pilot study carried out to see if it was possible to detect differences in mitochondrial activity between wild-type and het retinae in response to 670 nm light treatment and provide pilot data to perform a sample size calculation to determine how many retinae would be required to achieve statistically significant differences between groups. The pilot study, found there to be no reduction in mitochondrial activity in het retinae or an increase in either wild-type or het retinae when pre-treated with 670 nm light (Figure 3.5). Since this pilot study had 5 retinae per experimental group but revealed no emerging trend, it was deemed that it was not worthwhile investing more retinae into this assay.

The results revealed that there is high variability between retinae of the same genotype, in terms of mitochondrial activity. This has important implications when testing the effects of a therapy that targets mitochondria as each retina may respond differently to the same treatment. Additionally, the dendropathy, that is associated with the mutation in Opa1, may vary in terms of severity between mice. The method of analysis used to test the effectiveness of 670 nm light in the het mouse must, therefore, be most accurate so that it limits the variability to that produced by the biological situation.

3.4.2 Development of a method to measure oxygen consumption in the retinal explant using the Seahorse

The most success was achieved with the Seahorse assay when retinal thirds were assayed approximately 2 hours after explantation (Figure 3.10). Dividing the retina into 8 radial sections had a negative effect on the oxygen consumption measurements (Figure 3.11), with most basal rates of oxygen consumption measurements of retinal thirds showing readings of 200-500 pmol O_2/min and measurements of retinal eighths showing readings of 0-100 pmol O_2/min. The tissue was also much more responsive to the mitochondrial stress test compounds when retinal thirds were used compared to retinal eighths. Thus using a retinal section large enough to cover most of the nylon insert yet not large enough to impede the flow of media into the microchamber, proved to be the most appropriately sized retinal section for this assay (Figure 3.10C). Endeavours to improve on the result achieved using retinal thirds by using less tissue, increasing the concentrations of compounds and increasing the time allowed for the compounds to penetrate the tissue were not successful as these modifications to the protocol abolished the effects of the mito stress test compounds (Figure 3.11). This implies that sectioning the retina into eight radial sections before placing in culture for 2 hours compromised the ability of the mitochondria to respond to the compounds, therefore sections of this size proved to be less suitable than retinal thirds.

Despite all efforts to optimise the Seahorse assay for use in the retinal explant, the practical challenges which prevented using freshly explanted retinae compromised the careful consideration of all other factors. This was proven in the final test which followed a published protocol that was successful in measuring oxygen consumption in the retinal

explant with somewhat appropriate responses to the mito stress test compounds (Kooragayala et al., 2015). The published protocol used fresh retinae, yet achieved less than ideal responses to some of the mito stress test compounds, bringing to light the additional challenges faced when tissue was placed in suboptimal culture conditions before commencement of the assay. This shows that if the assay were to be used for the assessment of the effects of 670 nm light on oxygen consumption in the retina, the freshest tissue possible would be required before attempting to address other limiting factors.

Chapter 4. Red light treatment in an axotomy model of neurodegeneration

4.1 Introduction

Evidence is continually mounting in support of the potential of red and near infrared (NIR) light therapy to provide protective effects in various neurodegenerative diseases including Parkinson's disease and multiple sclerosis (Fitzgerald et al., 2013, Byrnes et al., 2005a, Wu et al., 2012, Xuan et al., 2015, Naeser and Hamblin, 2011, Naeser and Hamblin, 2015, Dong et al., 2015b, Ando and Hamblin, 2013, Nivaldo A. Parizotto and Hamblin, 2013). Red/NIR light therapy has also shown great potential in the treatment of the more acute neurodegenerative conditions such as stroke, spinal cord injury and traumatic brain injury (Fitzgerald et al., 2013, Byrnes et al., 2005a, Wu et al., 2012, Xuan et al., 2015, Naeser and Hamblin, 2011, Naeser and Hamblin, 2015, Dong et al., 2015b, Ando and Hamblin, 2013, Nivaldo A. Parizotto and Hamblin, 2013).

Since longer wavelengths have the ability to penetrate deeper than shorter wavelengths, NIR light is the preferred choice for irradiating brain tissue (Jagdeo et al., 2012). When irradiating the retina, however, the issue of tissue penetration, when using shorter wavelengths, is avoided. Consequently, the beneficial effects of red light have been reported in the retina. Treatment with 670 nm light has provided protection against cell loss in various rodent models of photoreceptor damage whilst demonstrating the safety of using 670 nm light with an irradiance of 60 mW/cm^2 on this light sensitive tissue (Albarracin et al., 2013, Albarracin et al., 2011). Also, 670 nm light provided protection in other models retinal damage or dysfunction (Peoples et al., 2012a, Tang et al., 2013b, Barbosa et al., 2014, Natoli et al., 2013). In particular, treatment with 670 nm light in a rat model of partial axotomy (optic nerve transection) resulted in improved vision, 7 days post injury (Giacci et al., 2014a).

Apoptosis, the primary mechanism of retinal ganglion cell (RGC) death following axotomy, is not detectable until 3-4 days after axotomy, *in vivo* (Magharious et al., 2011). RGC dendritic pruning, as characterized by a reduction in dendritic complexity, reduced dendritic arbor area and shrinkage of dendrites, has been observed in mouse models of both glaucoma and Alzheimer's disease and this event has been suggested to precede cell loss (Berry et al., 2015, Votruba et al., 2012, Williams et al., 2013b).

Until recently, the mechanisms by which dendrites are eliminated from the neuron were largely unknown. Newly emerging data has provided some mechanistic insight into this process. The findings of one such study has suggested that dendrite degeneration occurs in a process independent of apoptosis involving a local loss of mitochondrial membrane potential and ATP decline, which precede dendrite loss (Ikegami and Koike, 2003). Inflammation is, likewise, thought to play a prominent role in this process, as an increase in the pro-inflammatory cytokine, interferon γ, and an upregulation in complement proteins were found to be associated with the dendritic pruning that occurs in neurodegenerative diseases and neural injury (Kim et al., 2002, Stephan et al., 2012). Other findings have shown the inhibition of mTOR, the key signal integrator for a variety of extracellular signals including growth factors, to be involved in dendritic pruning (Di Polo, 2015). Notably, cellular stressors such as low ATP levels and inflammation have been shown to inhibit mTOR, and optic nerve lesion has been shown to bring about the inhibition of an mTOR complex, an event which has been shown to coincide with dendritic retraction.

Red/NIR light, which is absorbed by complex IV of the mitochondrial electron transport chain, has been shown to upregulate the enzymatic activity of complex IV, increase the

mitochondrial membrane potential and increase ATP production (Karu, 2008, Hamblin and Demidova, 2006, Kokkinopoulos et al., 2013, Begum et al., 2013, Ferraresi et al., 2015a, Ferraresi et al., 2015b, Tina Karu and Hamblin, 2013). Red light was also found to have an anti-inflammatory effect as markers of inflammation, including complement proteins, were significantly reduced in the outer retina following 670 nm light treatment (Kokkinopoulos et al., 2013, Begum et al., 2013, Fernandes et al., 2015, Rutar et al., 2012, Calaza et al., 2015). Additionally, red/NIR light was found to modify cell growth by modulating the Akt/mTOR signaling pathway in cancer cells (Sperandio et al., 2013). In fact, the PI3K/Akt/mTOR pathway, which is involved with cell growth, proliferation, differentiation and survival, has been reported to be one of the most studied pathways that is influenced by red/NIR light (Sonis et al., 2016).

4.2 Experimental design

Since many of the mechanisms proposed to be involved in the dendritic pruning process are potential therapeutic targets of the molecular mechanism responsible for the beneficial effects of 670 nm light, we have hypothesised that 670 nm light can delay the dendritic pruning that is initiated upon axotomy. To test this hypothesis we used an *ex vivo* model of dendritic pruning in the mouse retinal explant. Explanting the retina which involves axotomy of the entire population of RGCs by complete severing of their axons, is rapidly followed by pruning of the RGC dendrites (Di Polo, 2015). The retinal explant, consequently, provides a platform upon which to test the effects of 670 nm light on dendritic pruning in a substantially shorter timeframe than would be possible in the models of RGC degeneration, mentioned in the introduction. The effect of 670 nm light on the RGC dendritic pruning in the retinal explant was monitored at 40 minutes, 8 hours and 16 hours post axotomy. Changes in RGC dendritic morphology over time were investigated by employing various methods to analyze dendritic complexity, including Sholl analysis, area under the Sholl curve, the maximum peak of the Sholl curve, average total dendritic length and average dendritic field area.

4.3 Results

A total of 31 retinae out of 50 included RGCs with fluorescent labeling that allowed for accurate tracing of their dendrites (Figure 4.1).

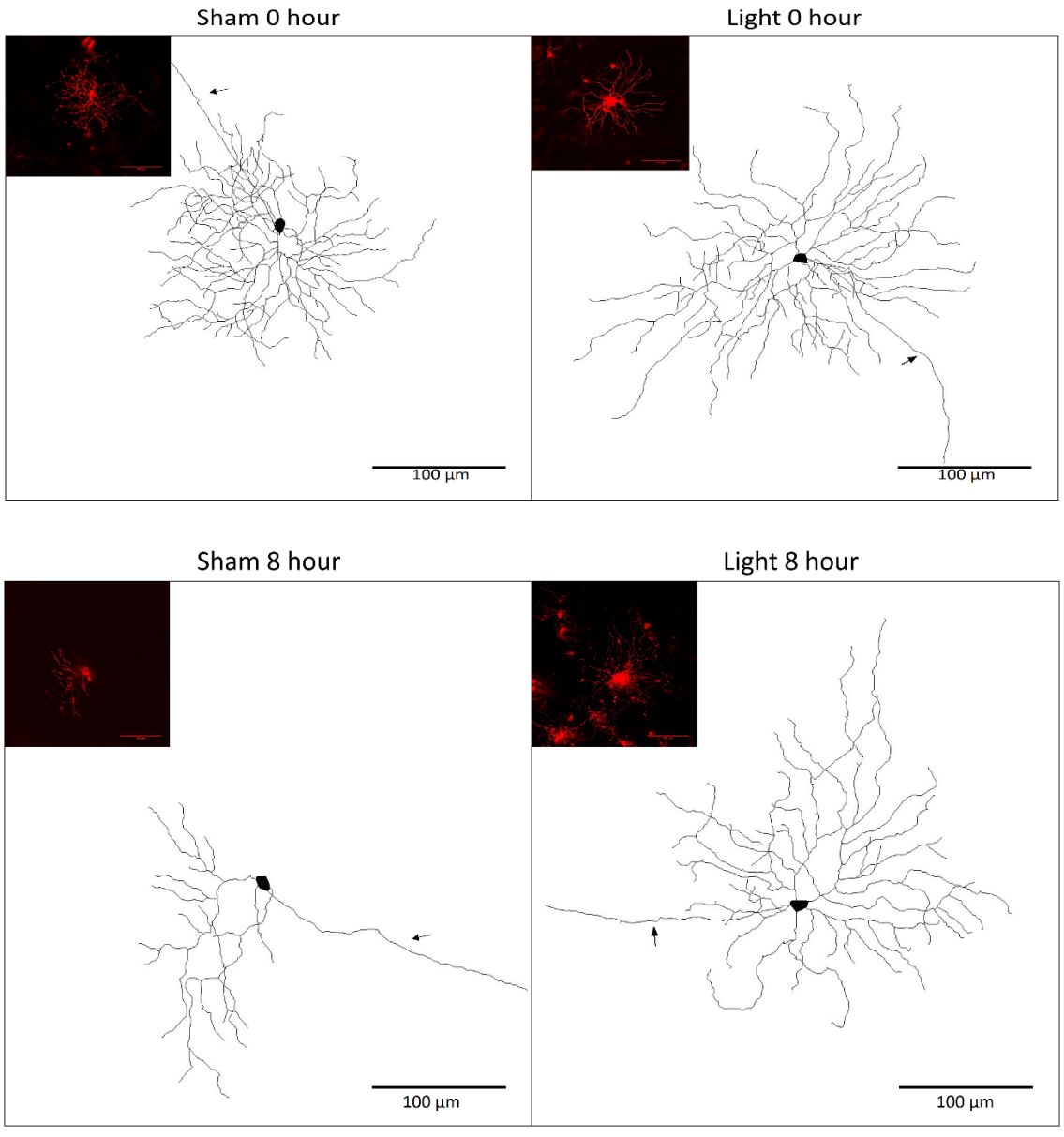

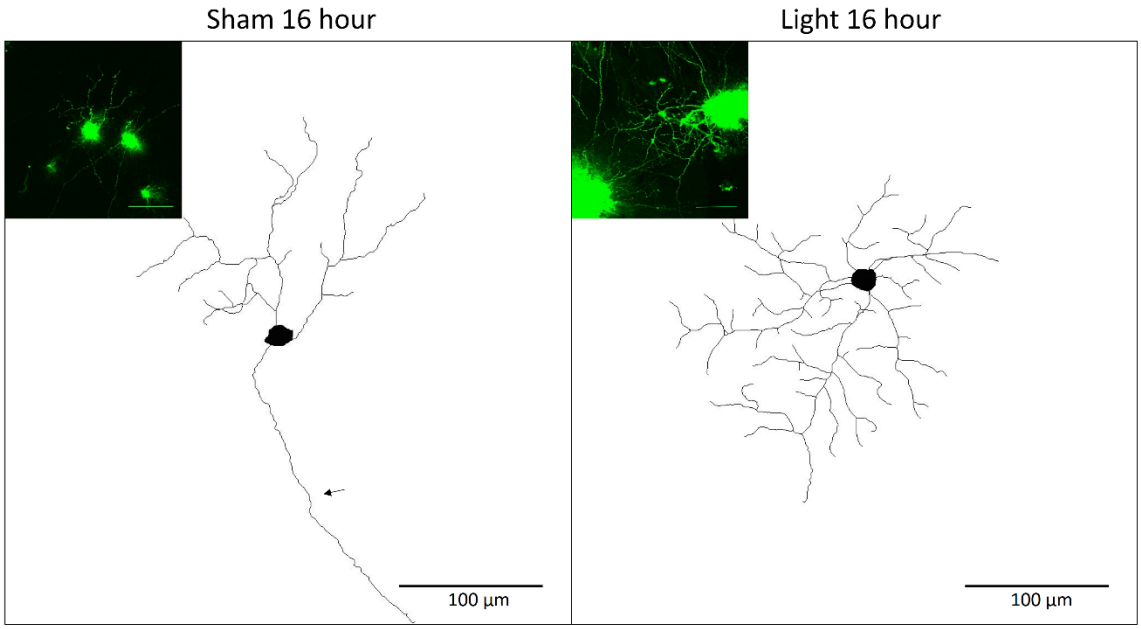

Figure 4.1: Representative images of RGCs from sham and light treated retinae over time *ex vivo*. The main image shows the Z-projected tracing of the Diolistically labelled RGC and inset is the original confocal image of the Diolistically labelled RGC. Scale bars represent 100 µm. Arrows indicate the axon.

Tracing of the RGC dendrites facilitated Sholl analysis to be done. Sholl analysis is a method used to analyze dendritic morphology, which gives information on the functionality of the neuron and its ability communicate effectively with other cells (Langhammer et al., 2010). Since dendrites are the main regions of information input into neurons, reductions in the number of dendrites could hinder the ability of the RCG to receive information from the preceding bipolar and amacrine cells. Changes in dendritic morphology are associated with malfunction in neurons, as seen in neurodegenerative diseases. Sholl analysis enables the monitoring of these changes quantitatively by producing the data in the form of a Sholl profile. Although 3D tracings of the RGCs were obtained, the Sholl analysis was done in 2D on the Z-projected tracings of RGCs, which have a planar stratification of dendrites. Of note, it is also possible to do

Sholl Analysis in 3D, which is more appropriate in studies on non-planar neurons where 2D Sholls may introduce error (Binley et al., 2014).

In this experiment, the Sholl profile, which illustrates the number of intersections of dendrites with concentric rings placed at each 10 µm distance from the cell soma, of RGCs from sham treated retinae showed a downward and leftward shift after both 8 and 16 hours *ex vivo*, indicating a loss of RGC dendritic complexity over time (Figure 4.2A-B). In retinae treated with red light, the leftward shift in the RGC Sholl profile over time was less profound (Figure 4.2C-D). There was a statistically significant reduction in the number of dendritic intersections at 70, 90 and 130 µm from the soma after 8 hours (p<0.05) and at 30 (p<0.05), 40 (p<0.01), 50 (p<0.05), 60-70 (p<0.01) and 80-110 µm (p<0.05) after 16 hours *ex vivo* for sham-treated retinae. In contrast, RGCs from light treated retinae had no statistically significant reductions in the number of dendritic intersections at any point on the Sholl curve after 8 or 16 hours. However, there was no statistically significant reduction between sham- and light-treated RGCs after 16 hours *ex vivo* (Figure 4.2F).

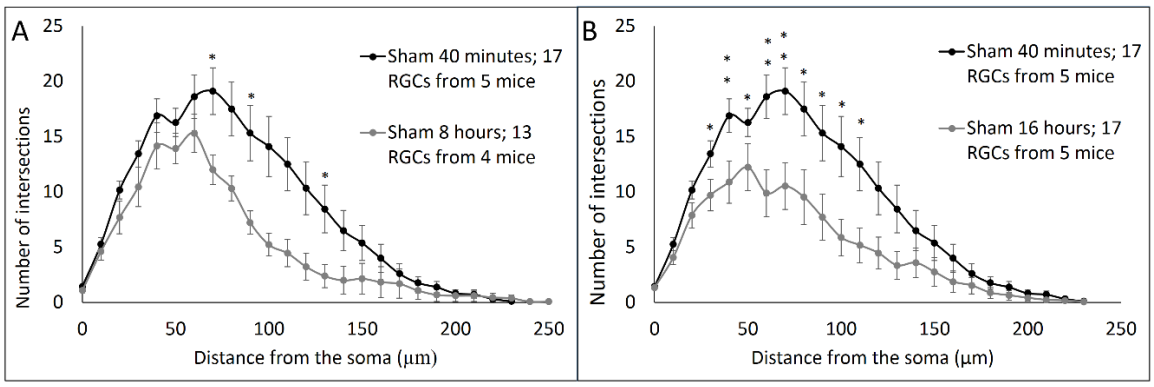

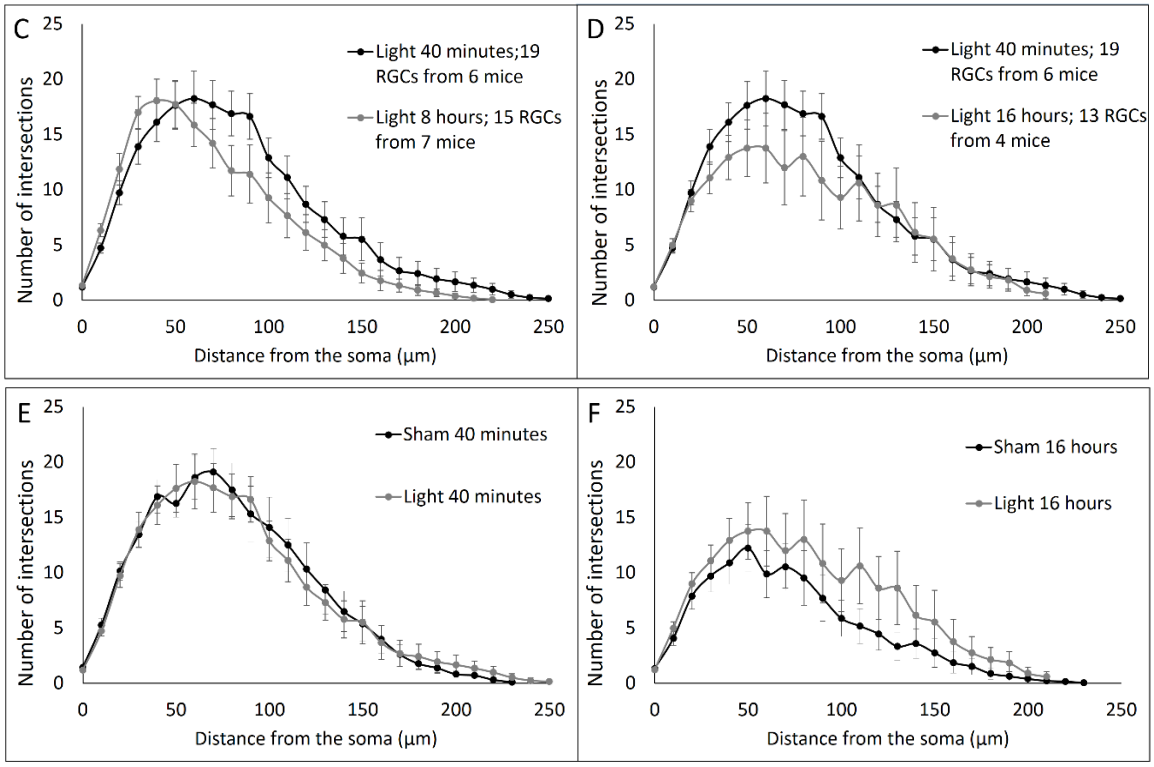

Figure 4.2: Treatment with 670 nm light prevents statistically significant reductions in various points on the Sholl plot of RGCs after 8 and 16 hours *ex vivo.* The Sholl profiles of sham-treated RGCs after 8 hours (A) and after 16 hours (B) *ex vivo*. The Sholl profiles of light-treated RGCs after 8 hours (C) and 16 hours (D) *ex vivo*. At 40 minute sham (17 RGCs from 5 mice), 8 hours sham (13 RGCs from 4 mice), 16 hours sham (17 RGCs from 5 mice), 40 minutes light (19 RGCs from 6 mice), 8 hours light (15 RGCs from 7 mice) and 16 hours light (13 RGCs from 4 mice) were used * $p<0.05$, ** $p<0.01$; Mann-Whitney U test. Error bars represent SEM.

The Sholl profile suggests that there is a difference in the areas under the Sholl curves and the maximum number of dendritic intersections in the Sholl plot of sham treated and light treated RGCs. For statistical comparison, however, it was necessary to compare the Sholl profiles of the individual RGCs used to create the Sholl plots in Figure 4.2. This was achieved by doing subsequent analysis on the Sholl plot of each cell, allowing statistical comparisons to be made.

The average area under the Sholl curves was calculated by the trapezoidal method. The average area under the Sholl curves of RGCs from sham treated retinae was reduced by

39% after 8 hours *ex vivo* (p=0.018) and by 43% after 16 hours (p=0.007) (Figure 4.3A). For light-treated retinae the values were reduced by 17% after 8 hours and by 18% after 16 hours but none of the differences were significant (p=0.286 and p=0.223, respectively) (Figure 4.3A).

The average maximum peak of the Sholl curves for RGCs from sham-treated retinae was significantly reduced from 24.4 intersections at 40 minutes to 17.1 intersections at 8 hours (p=0.005) and to 15.1 intersections at 16 hours (p=0.001) (Figure 4.3B). In RGCs from light-treated retinae, the average maximum peak of the Sholl curves was reduced from 23.0 at 40 minutes to only 22.0 intersections after 8 hours and to 18.3 intersections after 16 hours (p=0.986 and p=0.136, respectively) (Figure 4.3B).

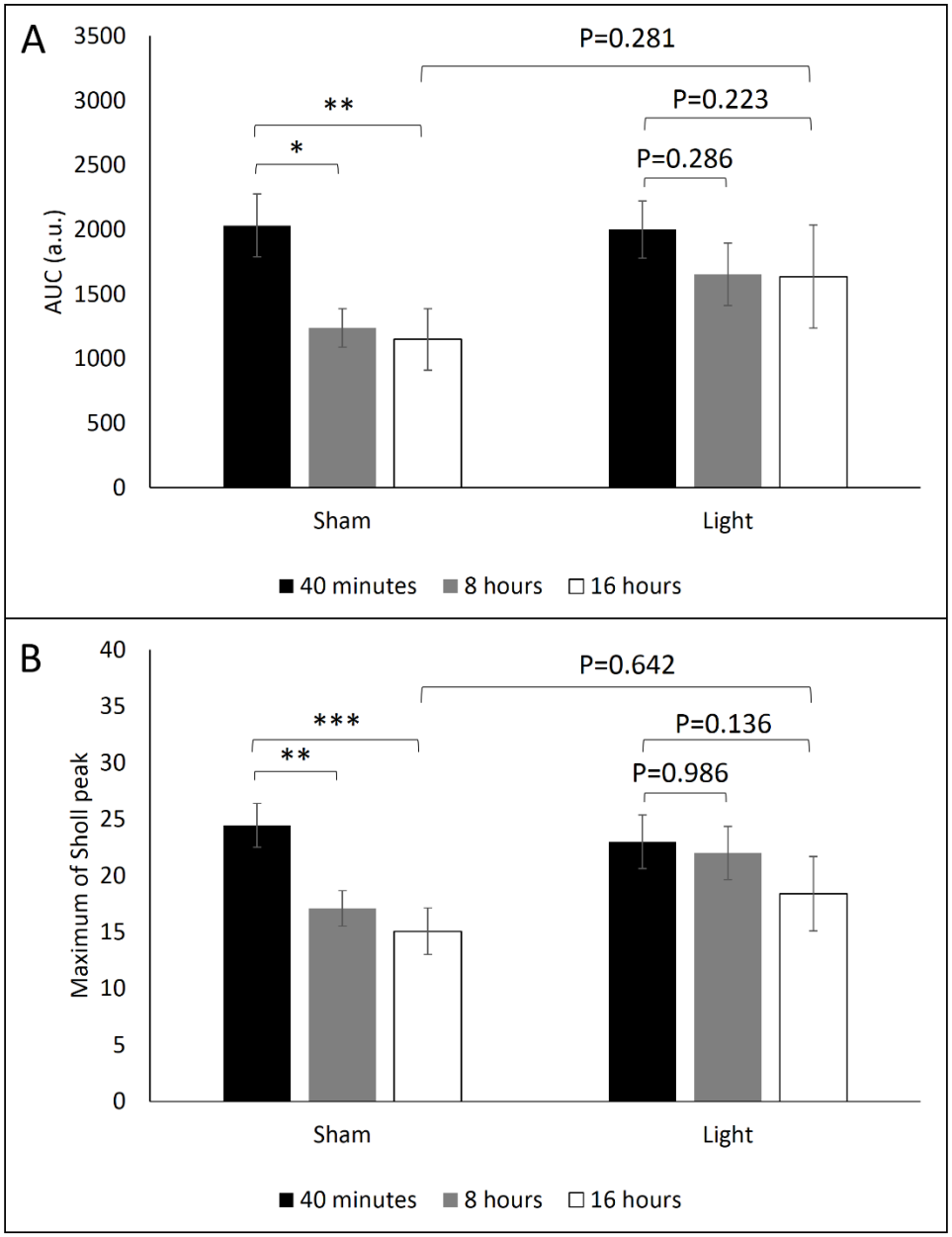

Figure 4.3: Treatment with 670 nm light partially prevents reductions in the Area under the Sholl curve and the peak of the Sholl curve of RGCs after 8 and 16 hours *ex vivo*. The effect of time *ex vivo*, up to 16 hours, on the average area under the Sholl curves (A) and average maximum Sholl peaks (B) of sham and light treated RGCs. At 40 minute sham (17 RGCs from 5 mice), 8 hours sham (13 RGCs from 4 mice), 16 hours sham (17 RGCs from 5 mice), 40 minutes light (19 RGCs from 6 mice), 8 hours light (15 RGCs from 7 mice) and 16 hours light (13 RGCs from 4 mice) were used. * $p<0.05$, ** $p<0.01$, *** $p<0.001$; Mann-Whitney U test. Error bars represent SEM.

To further investigate the effects of red light on RGC dendrites after axotomy, measurements of dendritic field area and total dendritic length, which are additional measures of RGC dendritic complexity were obtained. Dendritic field area provides information on how widely the cell spreads over the retina and relates to the size of its receptive field. Since RGCs are the final neurons in the visual pathway before the light signal is transmitted to the brain, a reduction in the area of the RGC dendritic field could diminish photosensitivity, impeding the entire visual process. Similarly, since total dendritic length has been found to be positively correlated with whole-neuron capacitance (Gertler et al., 2008), a decrease in this parameter could negatively impact on the ability of the cell to reach the threshold for electrical stimulation, thereby reducing the likelihood of an action potential being formed.

The average dendritic field area for RGCs from sham-treated retinae decreased significantly from 31204 μm^2 at 40 minutes to 17402 μm^2 after 16 hours *ex vivo* (p=0.019). Contrastingly, where retinae were treated with 670 nm light, the RGCs did not experience a statistically significant reduction in their average dendritic field area (28971 to 22540 μm^2, p=0.195) (Figure 4.4B).

A statistically significant decrease in the average total dendritic length was also seen in RGCs from sham treated retinae, from 3007 µm at 40 minutes to 1851 µm at 8 hours (p=0.038) and to 1640 µm at 16 hours (p=0.006). The values for dendritic length decreased from 2943 µm to 2430 µm after 8 hours (p=0.286) and 2362 after 16 hours (p=0.170), in RGCs that were exposed to 670 nm light, but the differences were not statistically significant (Figure 4.5B).

Although the average total dendritic field area of red light-treated retinae was 30% greater than in the sham-treated retinae after 16 hours, the difference was not statistically significant (p=0.385). To determine the number of retinae required to obtain a statistically significant difference between red light and sham-treated retinae after 16 hours, a sample size calculation was done. It was determined that 40 additional retinae would be required for the sham-treated group and 61 for the red light-treated group to achieve a statistically significant difference in the dendritic field area between sham and red light-treated retinae after 16 hours at 0.8 power.

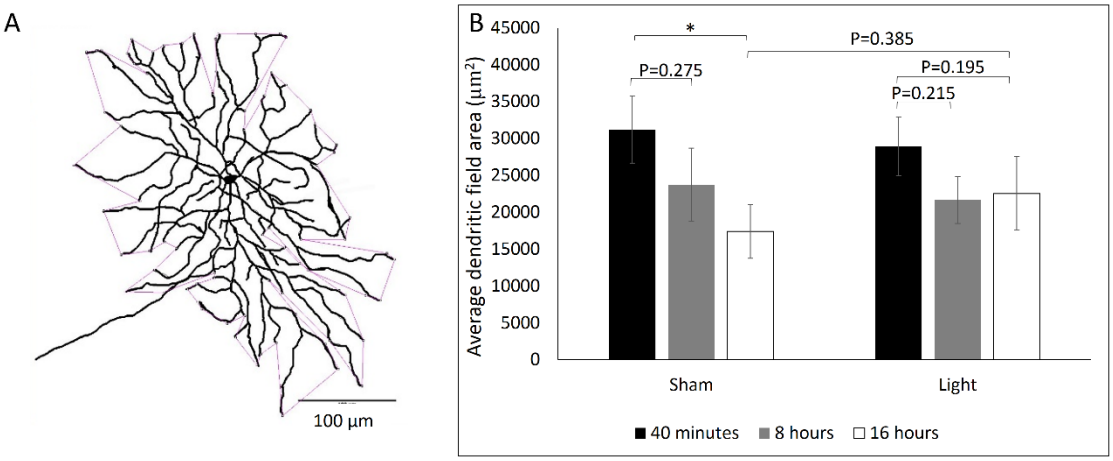

Figure 4.4: Treatment with 670 nm light prevented the reduction in the dendritic field area of RGCs after 16 hours. The effect of time *ex vivo*, up to 16 hours, on the average dendritic field area of light and sham treated RGCs. (A) The Z-projected image of an RGC showing the dendritic field area measurement using a concave polygon tool in ImageJ. (B) Stars indicate statistically significant reductions in the average dendritic field area, occurring *ex vivo* at the times indicated in the legends. At 40 minute sham (17 RGCs from 5 mice), 8 hours sham (13 RGCs from 4 mice), 16 hours sham (17 RGCs from 5 mice), 40 minutes light (19 RGCs from 6 mice), 8 hours light (15 RGCs from 7 mice) and 16 hours light (13 RGCs from 4 mice) were used. * p<0.05; Mann-Whitney U test. Error bars represent SEM. Arrow indicates the axon. Scale bar represents 100 µm.

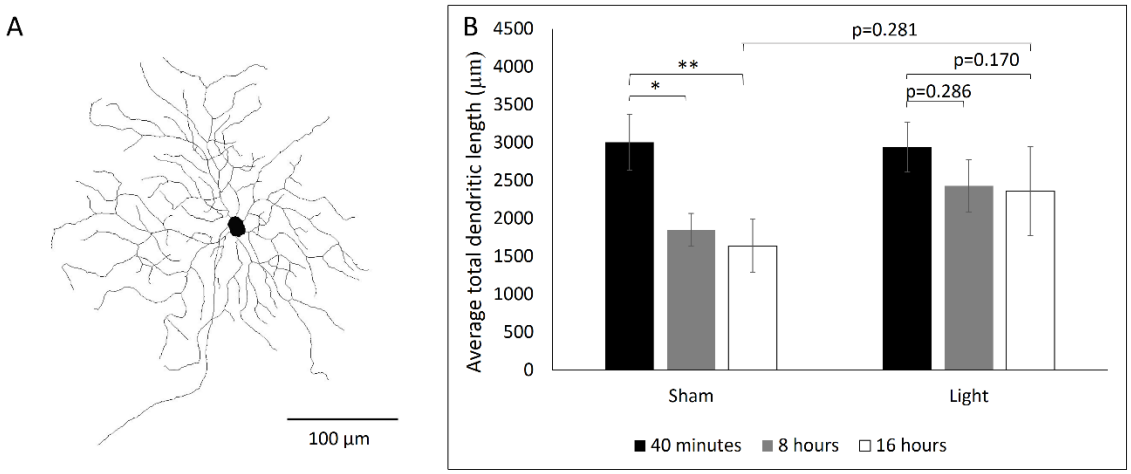

Figure 4.5: Treatment with 670 nm light prevented the reductions in total dendritic length of RGCs from RGCs after 8 and 16 hours *ex vivo*. The effect of time *ex vivo*, up to 16 hours, on the average dendritic field length of RGCs from sham and light treated retinae. (A) A 3-D image of an RGC tracing used to calculate dendritic field length measurements. (B) Stars indicate statistically significant reductions in the average dendritic field length, occurring *ex vivo* at the times indicated in the legends. At 40 minute sham (17 RGCs from 5 mice), 8 hours sham (13 RGCs from 4 mice), 16 hours sham (17 RGCs from 5 mice), 40 minutes light (19 RGCs from 6 mice), 8 hours light (15 RGCs from 7 mice) and 16 hours light (13 RGCs from 4 mice) were used. ** $p<0.01$; Mann-Whitney U test. Error bars represent SEM. Arrow indicates the axon.

In summary, the statistically significant reductions in the number of RGC dendritic intersections at various points on the Sholl plot were observed after 8 and 16 hours in sham-treated retinae but were not seen in red light-treated retinae. Treatment with red light also prevented a statistically significant reduction to the area under the Sholl curve and to the peak of the Sholl curve. The results for average dendritic field area and average total dendritic length measurements were consistent with Sholl analysis data, showing the ability of 670 nm light to prevent statistically significant decreases in further parameters of dendritic complexity. Red light prevented statistically significant reductions in the total loss of dendrites form the entire RGC dendritic arbor, the total

area of the dendritic field and the loss of dendrites from the most densely branched region of the RGC dendritic arbor.

4.4 Discussion

Herein we report, for the first time, of the ability of 670 nm light to prevent the dendritic pruning that occurs upon axonal injury. In this study, we investigated the effect of 670 nm light on RGC dendritic pruning which occurs in the mouse retinal explant upon axotomy of the optic nerve. This degeneration was detectable by analysis of dendritic morphology after 8 hours and again after 16 hours, where statistically significant decreases from initial values were observed in sham-treated explants. Sholl analysis revealed statistically significant reductions in the number of dendritic intersections at various points of the Sholl curve after both 8 and 16 hours. The area under the Sholl curve, the average peak of the fitted Sholl curve, the average total dendritic length and average dendritic field area after 16 hours also showed statistically significant reductions from the values at 40 minutes by 40.56% (p<0.008), 33.9% (p<0.007), 45.43% (p<0.006), and 44.23% (p<0.019), respectively. Our results have demonstrated that 670 nm light can prevent the statistically significant reductions in these measurements up to 16 hours post axotomy, since the reductions seen in RGCs from light treated retinae were smaller and not statistically significant. The results revealed that rapid intervention with 670 nm light, when administered immediately after the acute optic nerve lesion, axotomy, prevented significant neuronal damage.

Although 670 nm light prevents statistically significant reductions from 0 to 16 hours *ex vivo,* the lack of statistical significance between the sham- and light-treated retinae after 16 hours *ex vivo* restricts the conclusions that can be made from this experiment. There is a reduction in each parameter in sham-treated retinae after 16 hours compared to light-treated retinae, however with the numbers of cells used statistical significance was

not achieved. It was not possible to obtain the cell numbers required to achieve statistical significance based on the power calculation due to limited resources. However, since the results were not based on a particular RGC subtype it may be possible to reduce the number of cells required in future experiments by classifying cells based the proximal dendrites (Tribble et al., 2014). Genetic identification of RGC subtypes can also be used to selectively label a particular cell type, thereby reducing the numbers of retinae required (Huberman et al., 2009). However, there may be limitations to this method when labelling degenerating cells due to possible changes in gene expression during degeneration.

Evidence has been gathered, suggestive of a role for dendritic abnormalities in the pathology associated with the initial clinical symptoms of a range of neurodegenerative diseases (Di Polo, 2015). Degeneration of RGCs is a hallmark of devastating retinal degenerative diseases such as glaucoma and autosomal dominant optic atrophy (ADOA). A progressive degeneration of the RGCs in such diseases coincides with deterioration in visual acuity, eventually resulting in blindness. In experimental glaucoma, dendritic pruning has been suggested to precede selective loss of RGCs (Liu et al., 2010, Williams et al., 2013a, Pavlidis et al., 2003). Also in ADOA, dendritic pruning was found to begin at a time when a loss in visual acuity was observed, in a mouse model of the disease (Williams et al., 2010a).

The effect of changes to the dendritic morphology of neurons has also been observed in some of the most common and debilitating, neurodegenerative diseases, including Alzheimer's disease. In the postmortem brains of Alzheimer's disease patients, there was

a marked decrease in the number of dendritic branches in the majority of neurons from the visual and acoustic cortices compared to normal controls (Baloyannis, 2009). In addition, there was a 45% decrease in the dendritic field area compared with controls in these neurons. Alterations in dendritic morphology has also been found in Parkinson's disease (Bertram and Tanzi, 2005). In the *substantia nigra pars compacta* of *post mortem* tissue from Parkinson's disease patients, there was a severe reduction in the dendritic length of dopaminergic type I neurons compared with healthy controls (Patt et al., 1991). Similarly, in post mortem tissue from patients with multiple sclerosis (MS), a loss in dendritic arborization was observed in cortical lesions (Peterson et al., 2001). This pathology was thought to contribute to the clinical symptoms of MS by decreasing the synaptic input to the cortex. Since these relatively subtle changes to the neurons are thought play a role in the clinical symptoms, mild beneficial effect on the survival ability of the dendrites could translate into a significant clinical effect. Delaying the dendritic pruning that occurs in the early stages of these neurodegenerative diseases could delay the onset of clinical symptoms, thereby providing an invaluable improvement to the quality of life of patients.

The pathology for the initial symptoms in the discussed diseases appears to be due to a loss of dendrites as opposed to cell death. Moreover, dendritic degeneration appears to occur via a process independent of neuronal loss. It was found that the inhibition of pro-apoptotic proteins was sufficient to delay neuronal somal death while failing to have any preventative effect on dendritic pruning (Koike et al., 2008). Therefore, looking at ways of preventing dendritic pruning may require a unique approach and may also be a more fruitful treatment strategy than merely endeavoring to keep dysfunctional cells alive. As

we have found that 670 nm light can prevent axotomy induced dendritic pruning in RGCs this therapy may be of greater benefit than an anti-apoptotic therapy.

Our understanding of the pathology of neurodegenerative diseases seems to be changing from one of progressive cell loss to one whereby more subtle alterations in the dendritic morphology are associated with the initial clinical symptoms. The alterations to the dendritic morphology reported in the aforesaid neurodegenerative diseases were similar to those changes observed in the current experiment after 16 hours post axotomy, in the retinal explant. Since rapid intervention with 670 nm light treatment prevented such statistically significant alterations in the dendritic morphology for up to 16 hours *ex vivo*, it is possible that it may prevent or slow down the changes to the dendrites associated with the pathology of the said neurodegenerative diseases.

Chapter 5. The effect of 670 nm light treatment *in vivo* on dendropathy in the retinal explant from aged wild-type and het mice

5.1 Introduction

We have shown in the previous chapter that 670 nm light was partially effective in preventing axotomy-induced dendropathy in RGCs from young wild-type mice. However, the dendritic pruning associated with the initial clinical symptoms of neurodegenerative diseases, discussed in 3.4, begins at an advanced age. It has been shown that treatment with 670 nm light has the potential to protect against age related degeneration in the outer retina as suggested by the increase in ATP production, a decrease in the expression of a marker of oxidative stress and a reduction in the expression in a marker of inflammation, in the outer retina of aged mice (Gkotsi et al., 2014, Begum et al., 2013). However, the effects of 670 nm light in aged mice has not yet been explored in RGCs. It is therefore worth testing if 670 nm light can provide protection against dendropathy in RGCs from aged mice, similar to those effects achieved in the retinae from young wild-type mice.

As described in Chapter 1, the mutation in Opa1 in the het mouse leads to progressive pruning of the RGC dendrites, which occurs predominantly in the ON-centre sub-type, beginning at 12 months (Williams et al., 2010a). The commencement of dendropathy at this age suggests a gradual loss in the ability of RGCs, particularly ON-centre RGCs, to cope with the effects of the mutation in Opa1. When the mice reach 12 months, the long battle for survival is eventually lost by the RGCs as they succumb to their suboptimal cellular environment, which results in an impaired ability to maintain their dendrites. Since 670 nm light has been shown to improve mitochondrial bioenergetics and ATP production, and the exclusive susceptibility of RGCs to degeneration in ADOA has being theorised to be due to the high energy demands of this cell type; we hypothesise that

670 nm light will be effective in preventing RGC dendritic pruning in retinae from het mice.

5.2 Experimental design

The dendropathy seen to occur in the het mouse progresses slowly, from mild at 12-15 month months to severe after 20 months(Williams et al., 2010a). As dendropathy *in vivo* progresses slowly over many months, treatment would be required for several months to allow differences between sham- and light-treated RGCs to be detected. With a more acute model of RGC dendritic pruning available in the retinal explant, whereby significant dendritic pruning occurs in less than 24 hours, we have an opportunity to test 670 nm light treatment in the het mouse in a much shorter timeframe.

As described in the previous chapter, the post axotomy treatment provided only partial protection against *ex vivo* dendropathy in young wild-type mice. It has been suggested that red/NIR light triggers a stress response, upregulating pro-survival pathways; therefore applying 670 nm light to the cells prior to trauma would enhance their ability to survive during a subsequent trauma. This theory has been discussed in the final paragraph of 1.6.3 with evidence to show that pre-treatment with red/NIR light before the induced damaged has been shown to provide enhanced neuroprotective effects compared to treatment with red/NIR light post damage. Due to the added challenge of using retinal explants from much older mice and a mutation that increases susceptibility to dendrite loss, an *in vivo* treatment protocol was chosen to enhance the neuroprotective effects of 670 nm light against dendropathy in the current experiment.

Thus we tested the protective effects of 670 nm light against the RGC dendritic pruning that occurs *ex vivo,* upon axotomy, in cultured retinal flat mounts from 12-15 month old Opa1 $^{(+/-)}$ (Het) mice. The effectiveness of 670 nm light was also tested on retinal flat-mounts from 12-15 month old wild-type mice (WT) to control for the effect of increased

age on the response of the RGCs to 670 nm. Therefore, WT and Het mice were treated *in vivo* with 670 nm light daily for 5 consecutive days with the final treatment delivered 30 minutes before culling and axotomy. A 30 minute delay between the final treatment and culling was chosen as it has been shown that the expression of genes which are induced by nitric oxide signalling peaks 30 minutes after nitric oxide exposure in cultured cells (Hemish et al. 2003).

5.3 Results

5.3.1 The effects of 670 nm light on *ex vivo* dendropathy in RGCs

RGCs from WT and Het mice, pre-treated with 4.4 J/cm^2 of 670 nm light or sham for five consecutive days, were diolistically labelled either immediately (0 hour), 8 or 16 hours after flat mounting, before confocal images were obtained (Figure 5.1).

In order to quantitatively analyse the dendritic complexity of the RGCs, Sholl analysis was employed. The Sholl profiles, depicting the average dendritic complexity for the RGCs in each experimental group, showed a loss of dendritic complexity in RGCs from sham wild-type mice, which increased from 8 to 16 hours *ex vivo* (Figure 5.2). There was a statistically significant reduction in the number of dendritic intersections at 50 and 60 µm from the soma after 8 hours ($p<0.05$), and at 20-50 µm ($p<0.01$) and at 60-90 µm ($p<0.05$) from the soma after 16 hours *ex vivo*. There were no statistically significant reductions in any point on the Sholl curve in RGCs from light-treated wild-type mice. This shows the ability of 670 nm light to prevent the statistically significant reductions in the number of dendritic intersections from 20 to 90 µm from the soma in RGCs from wild-type mice.

In RGCs from sham treated het mice there were not statistically significant reductions in the number or dendritic intersections at any point on the Sholl curve, even after 16 hours *ex vivo*. Therefore the effects of 670 nm light on preventing the changes of the Sholl curve of RGCs from het mice could not be determined by this method of analysis.

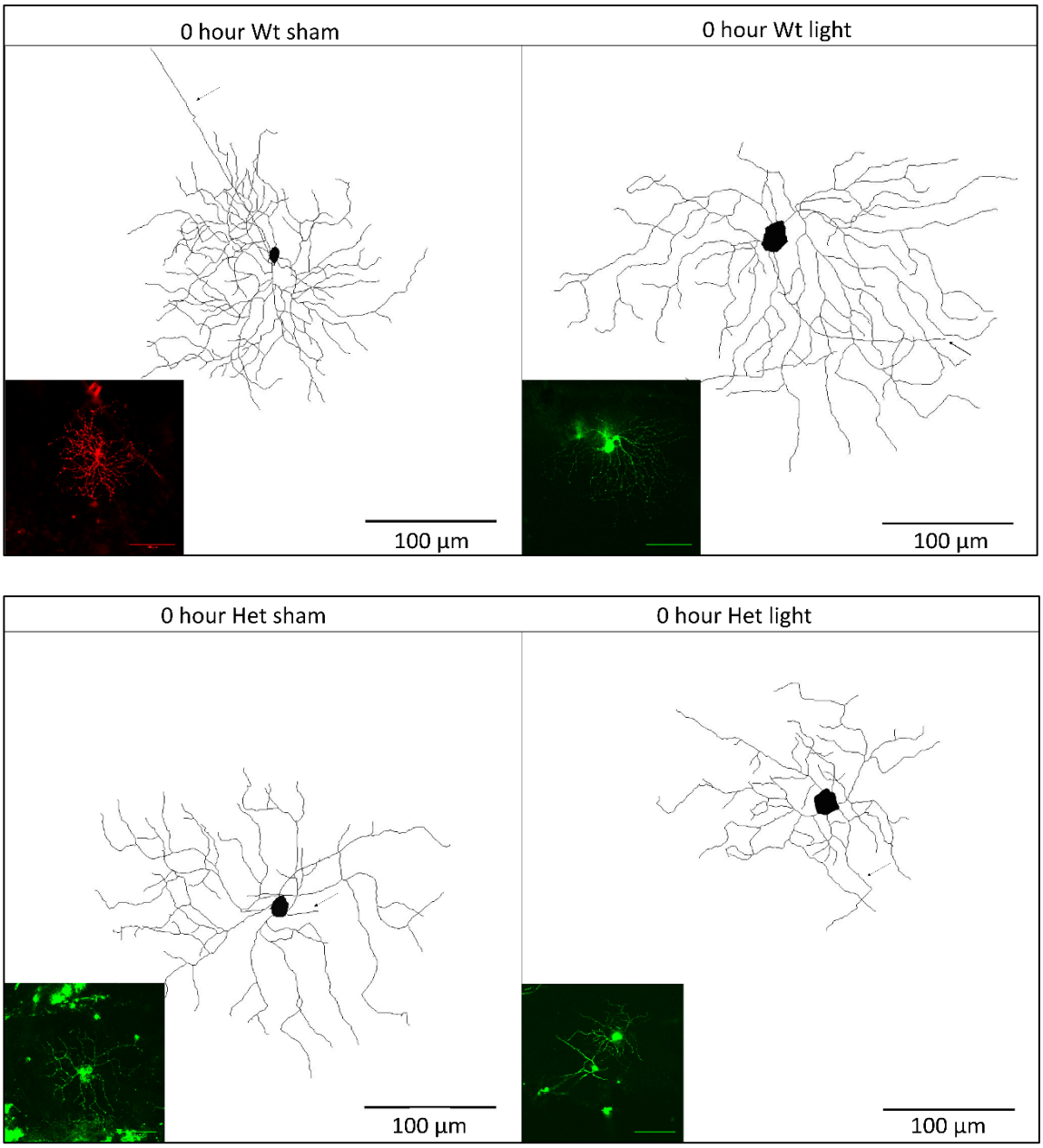
0 hour Wt sham
0 hour Wt light
100 µm
100 µm
0 hour Het sham
0 hour Het light
100 µm
100 µm

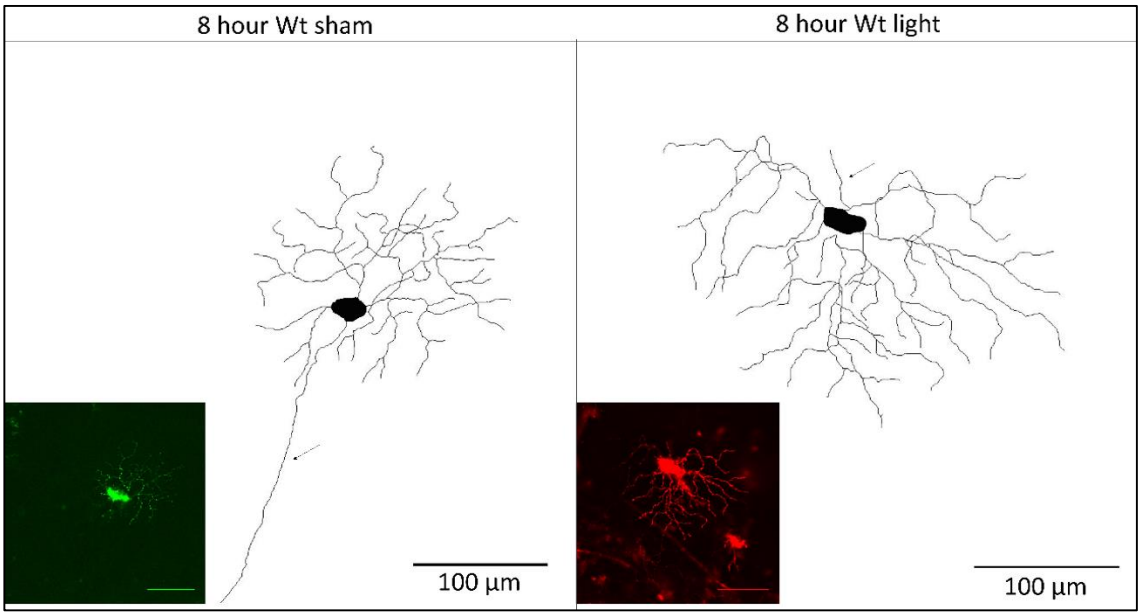
8 hour Wt sham
8 hour Wt light
100 µm
100 µm

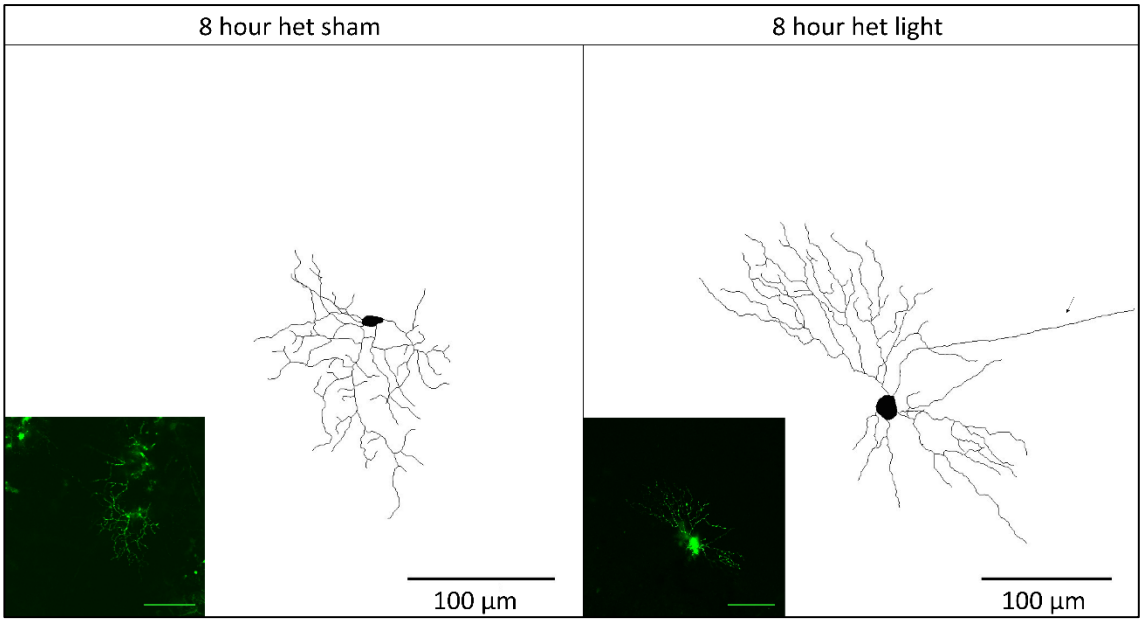
8 hour het sham
8 hour het light
100 µm
100 µm

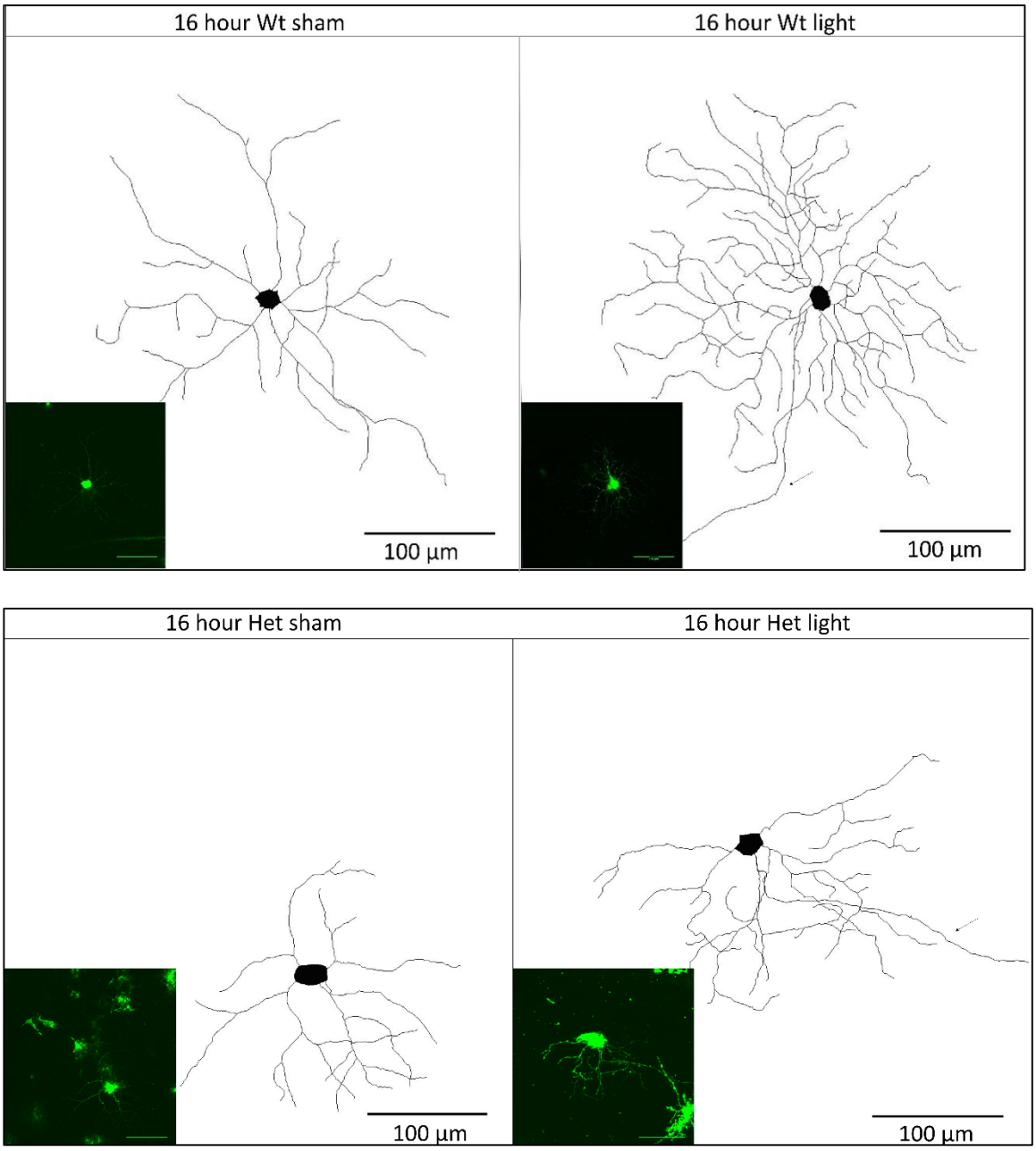

Figure 5.1: Representative images of RGCs from sham and light treated WT and Het mice over time *ex vivo*. The main image shows the tracing of the Diolistically labelled RGC and inset is the original confocal image. Time points represent time post axotomy at which cells were labelled. Scale bars represent 100 µm. Arrows indicate the axon.

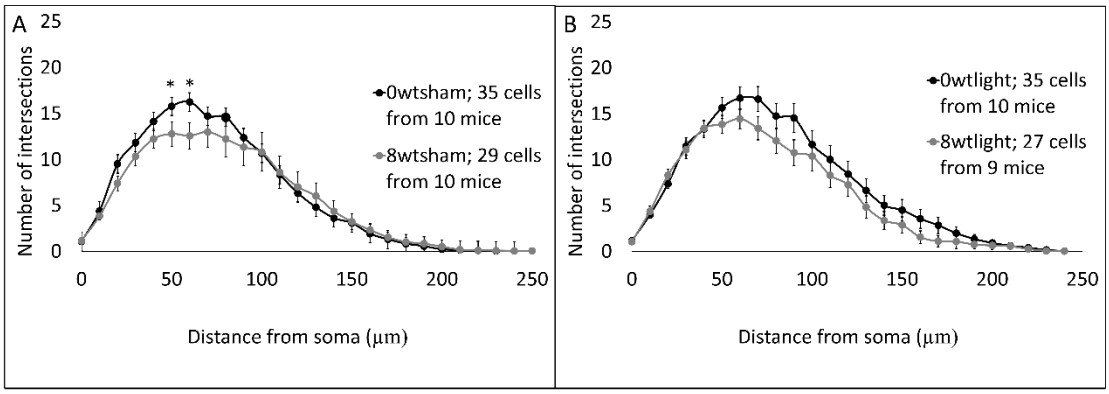
A
Number of intersections
Distance from soma (μm)
0wtsham; 35 cells from 10 mice
8wtsham; 29 cells from 10 mice
B
Number of intersections
Distance from soma (μm)
0wtlight; 35 cells from 10 mice
8wtlight; 27 cells from 9 mice

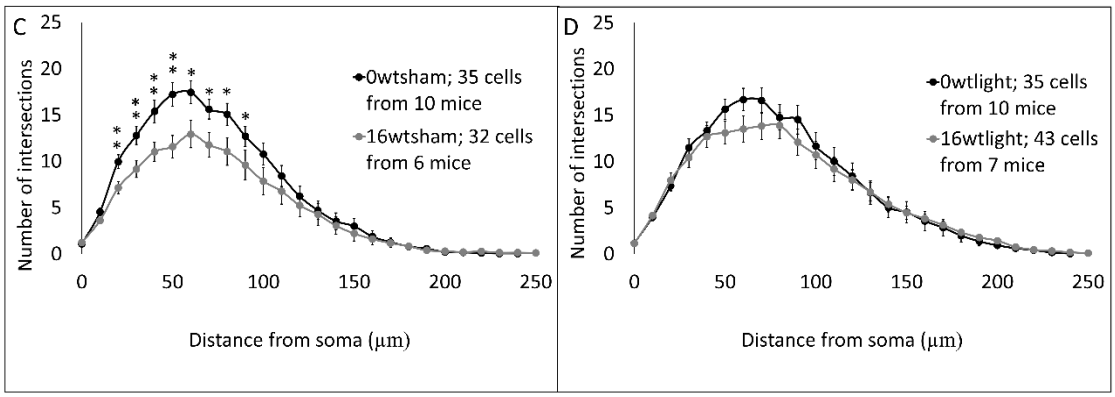
C
Number of intersections
Distance from soma (μm)
0wtsham; 35 cells from 10 mice
16wtsham; 32 cells from 6 mice
D
Number of intersections
Distance from soma (μm)
0wtlight; 35 cells from 10 mice
16wtlight; 43 cells from 7 mice

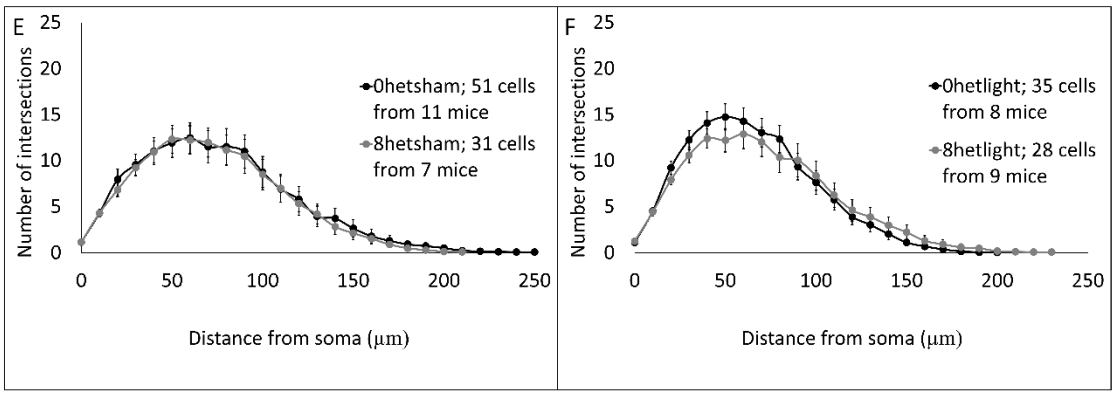
E
Number of intersections
Distance from soma (μm)
0hetsham; 51 cells from 11 mice
8hetsham; 31 cells from 7 mice
F
Number of intersections
Distance from soma (μm)
0hetlight; 35 cells from 8 mice
8hetlight; 28 cells from 9 mice

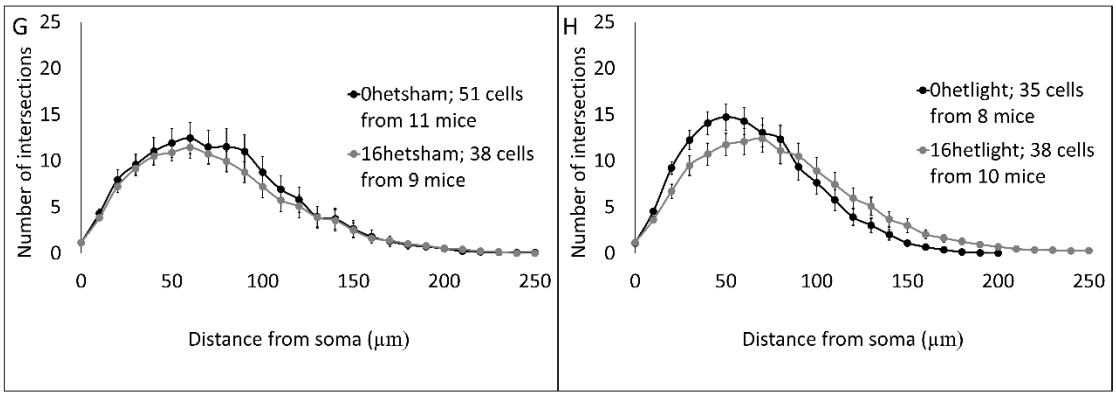
G
Number of intersections
Distance from soma (μm)
0hetsham; 51 cells from 11 mice
16hetsham; 38 cells from 9 mice
H
Number of intersections
Distance from soma (μm)
0hetlight; 35 cells from 8 mice
16hetlight; 38 cells from 10 mice

Figure 5.2: Red light treatment prevented the significant reductions seen after 8 and 16 hours in various points of the Sholl profile of RGCs from wild-type mice, however, the effect of 670 nm light on the Sholl profiles of Het RGCs could not be determined. Sholl profile of RGCs from (A) sham treated WT at 0 and 8 hours, (B) light treated WT at 0 and 8 hours, (C) sham treated WT at 0 and 16 hours, (D) light treated WT at 0 and 16 hours, (E) sham treated Het at 0 and 8 hours, (F) light treated Het at 0 and 8 hours, (G) sham treated Het at 0 and 16 hours, (H) light treated Het at 0 and 16 hours over time *ex vivo*. Stars indicate statistically significant reduction in the number of dendritic intersections over time *ex vivo*. * $p<0.05$, ** $p<0.01$; Mann-Whitney *U* test. Error bars represent SEM.

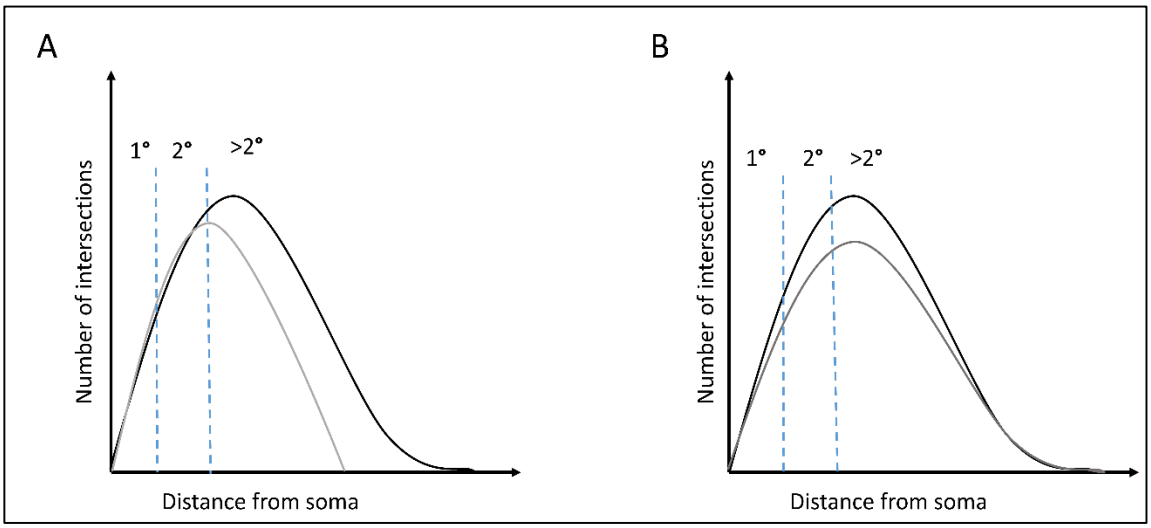

Figure 5.3: Cartoon diagram of a Sholl profile of RGC degeneration showing the primary, secondary and tertiary dendrites. (A) An example of a typical change in the Sholl profile of a degenerating RGC. The black curve represents the healthy RGC before dendrite loss. The grey curve represents the Sholl profile after dendropathy. The loss of dendrites occurs from the region of the Sholl curve that represents the tertiary dendrites. (B) An example of an atypical change in the Sholl profile of degenerating RGCs. The black curve shows the healthy RGC before dendrite loss. The grey curve represents the Sholl profile after dendropathy. The loss of dendrites appears to affect the primary and secondary dendrites while the tertiary dendrites are still present. This is due to high variability in the degeneration, with some cells appearing to have lost the majority of their dendrites and other cells appearing resistant to *ex vivo* degeneration. To overcome this problem a higher cell number is required.

After 16 hours *ex vivo* the AUC decreased by 26% in sham treated wild-type RGCs ($p<0.01$) (Figure 5.3A). However, the AUC of RGCs from light treated wild-type mice after 16 hours *ex vivo* was not significantly different from the value at 0 hours ($p=0.205$).

Further, there was a statistically significant difference in the AUC of RGCs from sham treated wild-type mice and light treated wild-type mice after 16 hours *ex vivo* ($p<0.05$). There was a significant reduction in the AUC by 17% in RGCs from het mice when compared to wild-type mice at baseline, however, a further statistically significant reduction in the AUC in RGCs from sham treated het mice was not observed after 16 hours *ex vivo* ($p=0.347$) (Figure 5.4A).

The average maximum peak of the Sholl curve at baseline was 21 intersections in RGCs from sham treated wild-type mice and 21 intersections in RGCs from light treated wild-type mice (Figure 5.4B). A decrease to 15 intersections was observed after 16 hours *ex vivo* with sham treatment ($p<0.001$), however, with light treatment the AUC decreased to 19 intersections, which was less that the decrease in wild-type and was not statistically significant ($p=0.125$). There was a significant reduction in the average maximum of the Sholl peak from 21 intersections in sham treated wild-type RGCs to 18 intersections in sham treated het RGCs at baseline ($p<0.01$). However, there was no further statistically significant reduction in the average maximum Sholl peak in RGCs from sham treated mice after 16 hours *ex vivo* ($p=0.124$).

To further support the findings of Sholl analysis on the dendritic complexity of the RGCs the average total dendritic length was computed, as an additional measures of dendritic complexity. Total dendritic length (Figure 5.4C), presented a similar pattern to the Sholl analysis data, with sham-treated wild-type RGCs showing a decrease from 2348 µm at 0 hours to 1748 µm after 16 hours *ex vivo* ($p<0.01$). Conversely, light treated wild-type RGCs did not experience a significant reduction in dendritic length after 16 hours,

showing an insignificant decrease from 2466 µm at 0 hours to 2373 µm at 16 hours *ex vivo* (p=0.247). Further, a significant difference was seen between light and sham treated wild-type RGCs after 16 hours ($p<0.05$). Although a significant decrease was observed from 2348 µm in RGCs from sham treated wild-type mice to 1926 µm in RGCs from sham treated het mice ($p<0.01$), the dendritic length did not decrease further after 16 hours in RCGs from sham treated het mice.

670 nm light provided partial protection against the dendropathy that occurs in RGCs from sham treated wild-type mice after 16 hours *ex vivo.* Since there was no further statistically significant reduction in the AUC, maximum peak of the Sholl curve or dendritic length after 16 hours *ex vivo* in RGCs from het mice, the effects of 670 nm light on these parameters in RGCs from the het could not be determined by this analysis.

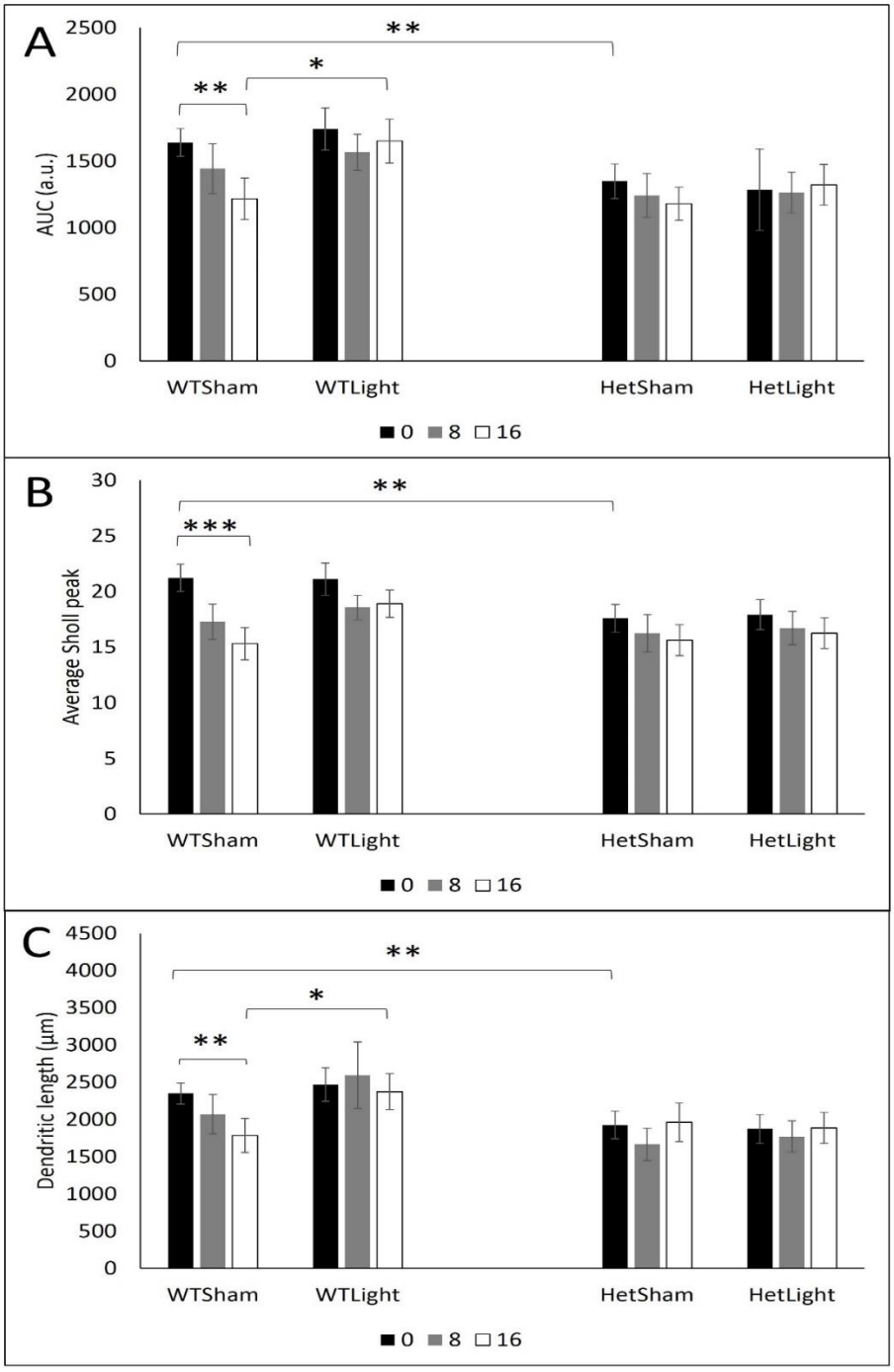

Figure 5.4: Pre-treatment with 670 nm light prevented the statistically significant reductions in the Area under the curve, and dendritic length and partially prevented the reduction in the Sholl peak, seen in wild-type RGCs after 16 hours. The effects of 670 nm light on these parameters could not be determined in het RGCs. Area under the Sholl curve (A), Average maximum peak of Sholl curve (B) and Average dendritic length (C) of light and sham treated WT and Het RGCs over time *ex vivo*. Wt sham 0 hours (n=35), Wt sham 8 hours (n=29), Wt sham 16 hours (n=32), Wt light 0 hours (n=35), Wt light 8 hours (n=27), Wt light 16 hours (n=43), Het sham 0 hours (n=51), Het sham 8 hours

(n=31), Het sham 16 hours (n=38), Het light 0 hours (n=35), Het light 8 hours (n=28) and Het light 16 hours (n=38). Error bars represent SEM.* p<0.05, ** p<0.01, *** p<0.001.

5.3.2 The effects of 670 nm light on dendropathy in ON-centre RGCs

Analysis of the entire population of RGCs from het mice did not allow the evaluation of the potential protective effect of 670 nm light on *ex vivo* dendropathy due to the lack of significant *ex vivo* dendropathy from 0 hours to 16 hours in sham-treated RGCs from these mice. It has been shown previously that ON-centre RGCs from het mice degenerate faster than OFF-centre RGCs (Williams, Morgan and Votruba, 2010). Consequently, the ON-centre RGCs from the sample population were selected for sub-analysis.

There was a statistically significant reduction in the number of dendritic intersections at 50 µm (p<0.01), 60 µm (p<0.05) and 80 µm (p<0.05) from the soma after 8 hours (Figure 5.5A), and at 30-40 µm (p<0.01) and at 50-80 µm (p<0.05) from the soma after 16 hours (Figure 5.5C) *ex vivo* in RGCs from sham treated WT mice. In RGCs from light treated wild-type mice there were no statistically significant reductions in any point on the Sholl curve, with the exception of 90 µm from the soma in RGCs from light treated wild-type mice (Figure 5.5 B and D). This shows the ability of 670 nm light to partially prevent the statistically significant reductions in the number of dendritic intersections from 20 to 90 µm from the soma that occur over time *ex vivo* in the ON-centre RGCs in wild-type mice. In RGCs from sham treated het mice, there were no statistically significant reductions in the number or dendritic intersections, even after 16 hours *ex vivo* (Figure 5.5 E-H).

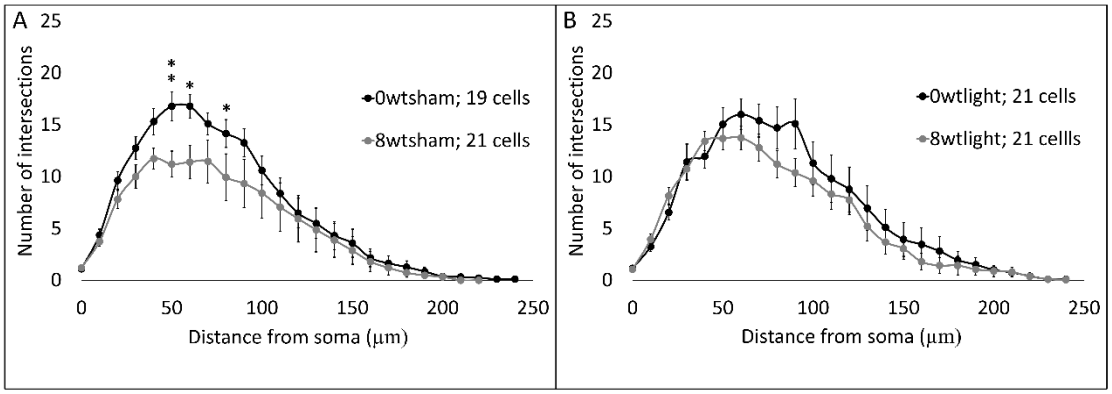
A
Number of intersections
Distance from soma (μm)
0wtsham; 19 cells
8wtsham; 21 cells
B
0wtlight; 21 cells
8wtlight; 21 cellls

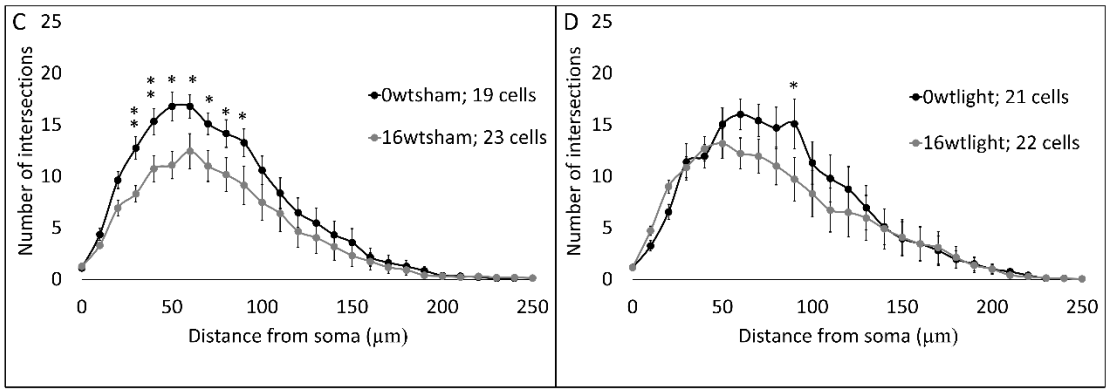
C
Number of intersections
Distance from soma (μm)
0wtsham; 19 cells
16wtsham; 23 cells
D
0wtlight; 21 cells
16wtlight; 22 cells

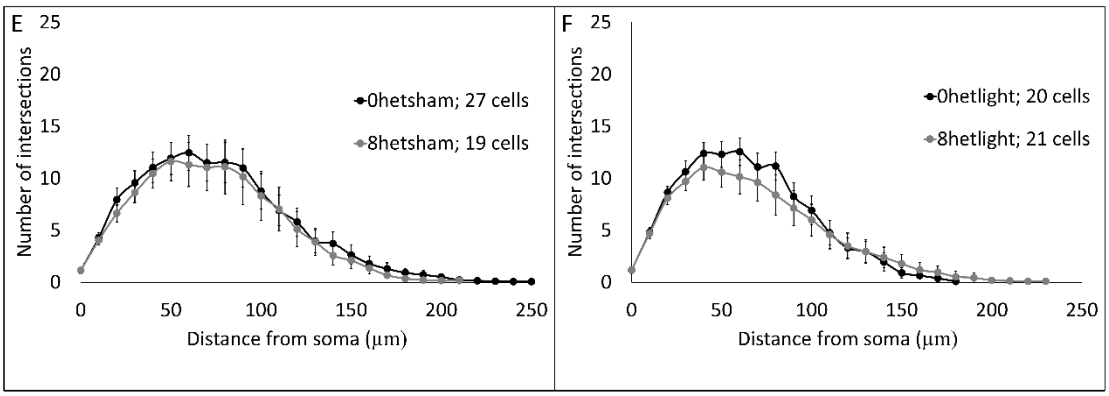
E
Number of intersections
Distance from soma (μm)
0hetsham; 27 cells
8hetsham; 19 cells
F
0hetlight; 20 cells
8hetlight; 21 cells

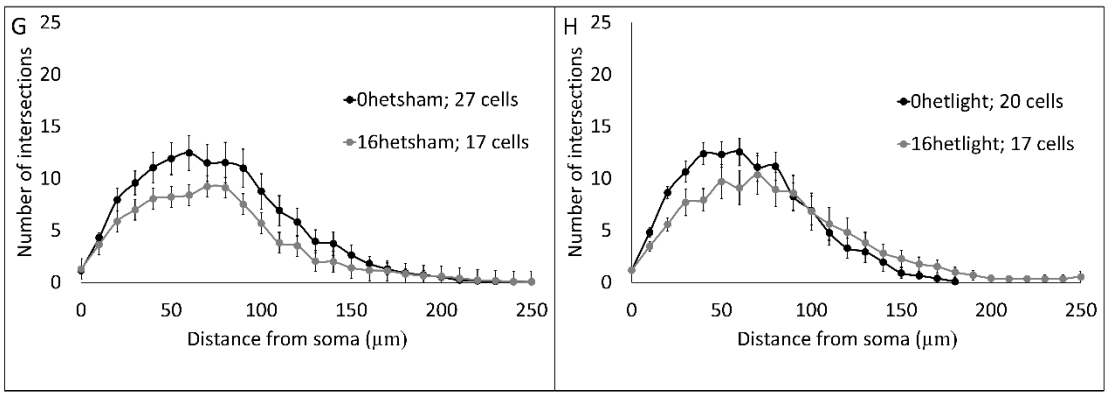
G
Number of intersections
Distance from soma (μm)
0hetsham; 27 cells
16hetsham; 17 cells
H
0hetlight; 20 cells
16hetlight; 17 cells

Figure 5.5: Pre-treatment with 670 nm light prevented the significant reductions seen after 8 and 16 hours in various points of the Sholl profile of ON-centre RGCs from wild-type mice, however, the effect of 670 nm light on the Sholl profiles of ON-centre Het RGCs could not be determined. Sholl profile of ON-centre RGCs from (A) sham treated WT at 0 and 8 hours, (B) light treated WT at 0 and 8 hours, (C) sham treated WT at 0 and 16 hours, (D) light treated WT at 0 and 16 hours, (E) sham treated Het at 0 and 8 hours, (F) light treated Het at 0 and 8 hours, (G) sham treated Het at 0 and 16 hours, (H) light treated Het at 0 and 16 hours over time *ex vivo*. Stars indicate statistically significant reduction in the number of dendritic intersections over time *ex vivo*. * $p<0.05$, ** $p<0.01$; Mann-Whitney *U* test. Error bars represent SEM.

The area under the Sholl curve (AUC) was 1650 a.u. in RGCs from sham treated wild-type mice and 1684 a.u. in RGCs from light treated wild-type mice ($p=0.224$) at 0 hours *ex vivo*. After 16 hours *ex vivo* the AUC decreased to 1183 a.u. in sham treated wild-type RGCs ($p<0.01$) (Figure 5.6A). The AUC of RGCs from light treated wild-type mice after 16 hours *ex vivo* was 1452 a.u., which was not significantly different from the value at 0 hours ($p=0.129$). There was a reduction in the AUC from 1650 a.u. in sham treated wild-type RGCs to 1303 a.u. in sham treated RGCs from het mice at baseline, however, this reduction did not reach statistical significance ($p=0.558$). There was a further reduction in the AUC in RGCs from sham treated het mice to 922 a.u. after 16 hours *ex vivo* ($p<0.05$). The decrease in the AUC of RCGs from light treated het mice from 1150 a.u. at 0 hours to 1064 a.u. after 16 hours was smaller than that observed with sham treatment and was not statistically significant (p=0.331).

The average maximum of the Sholl peak was 20.5 intersections and 21 intersections at 0 hours *ex vivo* for RGCs from sham and light treated wild-type mice, respectively (Figure 5.6B). The value decreased after 16 hours to 15 intersections in sham treated RGCs (p<0.01). The decrease in light treated RGCs to 18 intersections after 16 hours was less than in sham treated RGCs and was not statistically significant ($p=0.122$). The average

maximum of the Sholl peak was reduced to 17.7 intersections in RGCs from sham treated het mice at 0 hours when compared with 20.5 intersections in the wild-type controls (p<0.05). There was also a statistically significant reduction in the maximum of the Sholl peak in RGCs from sham treated Opa1 $^{(+/-)}$ mice after 16 hours *ex vivo*, to 11.9 intersections (p<0.05). Light treated RGCs from het mice had an average maximum of the Sholl peak of 16.4 intersections at 0 hours. After 16 hours a reduction in this value to 13.7 intersections was observed, which was less than that which was observed over the same *ex vivo* period in RCGs that were sham treated and did not reach statistical significance (p=0.0986).

The average total dendritic length was 2320 µm at 0 hours in RGCs from sham treated wild-type mice and 2433 µm in RGCs from light treated wild-type mice (p=0.315). The dendritic length decreased to 1650 µm with sham treatment (p<0.05) and to 2066 µm with light treatment (p=0.147) after 16 hours *ex vivo* (Figure 5.6C). In RGCs from het mice, the average total dendritic length was reduced to 1794 µm at 0 hours when compared to the wild-type value (p<0.05). A further statistically significant reduction in dendritic length was observed after 16 hours (p<0.05) in RGCS from sham treated Opa1 $^{(+/-)}$ mice. In RGCs from light treated het mice, the reduction in dendritic length from 1617 µm to 1502 µm after 16 hours *ex vivo* was much less than that observed with sham treatment and was not statistically significant (p=0.344).

Treatment with 670 nm light prevented the statistically significant reductions in all measures of dendritic complexity explored in ON-centre RGCs from wild-type mice. In ON-centre RGCs from Opa1 $^{(+/-)}$ mice 670 nm light provided protection against statistically

significant reductions in the AUC, maximum of the Sholl peak and dendritic length. This shows the ability of 670 nm light to provide partial protection against dendropathy in ON-centre RGCs from het mice.

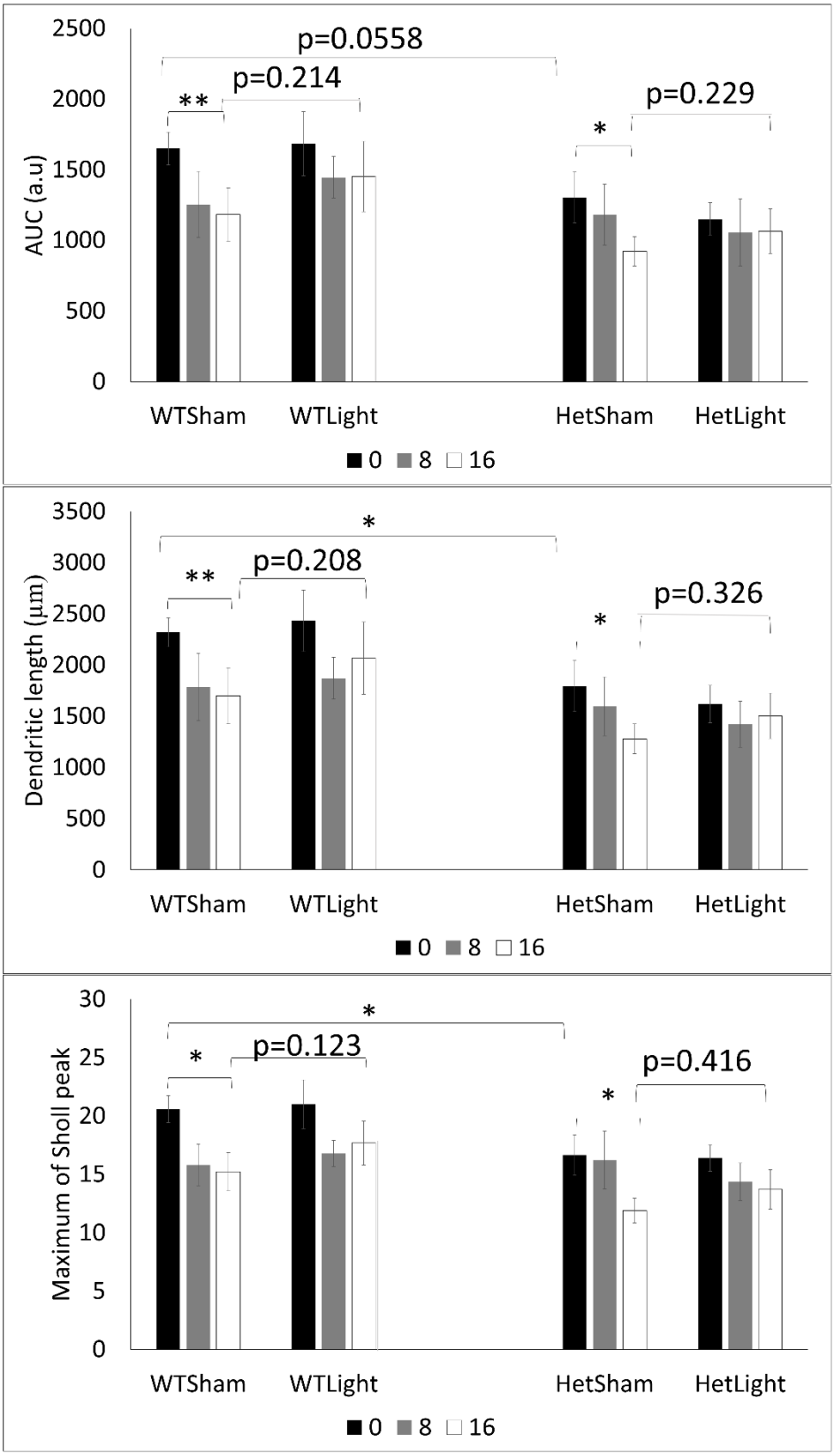
AUC (a.u)
2500
2000
1500
1000
500
0
p=0.0558
p=0.214
p=0.229
**
*
WTSham
WTLight
HetSham
HetLight
0 8 16
Dendritic length (µm)
3500
3000
2500
2000
1500
1000
500
0
*
**
p=0.208
p=0.326
*
WTSham
WTLight
HetSham
HetLight
0 8 16
Maximum of Sholl peak
30
25
20
15
10
5
0
*
*
p=0.123
p=0.416
*
WTSham
WTLight
HetSham
HetLight
0 8 16

Figure 5.6: Pre-treatment with 670 nm light partially prevented the statistically significant reductions in the Area under the curve, dendritic length and the Sholl peak, seen in wild-type and Het ON-centre RGCs after 16 hours *ex vivo*. AUC (A), Sholl peak (B) and Dendritic length (C) of ON-centre RGCs from sham and light treated WT and Het mice, over time *ex vivo.* Wt sham 0 hours (n=19), Wt sham 8 hours (n=21), Wt sham 16 hours (n=23), Wt light 0 hours (n=21), Wt light 8 hours (n=21), Wt light 16 hours (n=22), Het sham 0 hours (n=27), Het sham 8 hours (n=19), Het sham 16 hours (n=17), Het light 0 hours (n=20), Het light 8 hours (n=21) and Het light 16 hours (n=17). Error bars represent SEM. * $p<0.05$, ** $p<0.01$.

5.4 Discussion

5.4.1 The effects of 670 nm light on RGC dendritic pruning in the aged WT retinal explant

In the retinal explants from aged wild-type mice, the RGC dendritic complexity, as quantified by Sholl analysis (AUC and Sholl peak) and total dendritic length, experiences a marked decrease 16 hours post axotomy. Reductions in these parameters were not seen in RGCs from aged wild-type mice pre-treated with 670 nm light. The results demonstrate the ability of 670 nm light to prevent dendropathy in the aged wild-type when delivered *in vivo* for 5 days, prior to axotomy. In Chapter 4, a single 10 minute exposure to 670 nm light provided partial protection against *ex vivo* dendropathy in RGCs from young wild-type mice. This was shown by the ability of 670 nm light to prevent statistically significant reductions in various measures of dendritic complexity, for up to 16 hours *ex vivo*, in the absence of a statistically significant difference in those measures between sham and light treated young wild-type retinae after 16 hours. Delivery of 5 exposures of red light to aged wild-type retinae *in vivo,* as a pre-treatment to axotomy, the trigger of *ex vivo* degeneration, had a more potent effect on protecting RGCs from *ex vivo* dendropathy than exposure to 670 nm light post axotomy. This was demonstrated by the statistically significant differences in the measures of dendropathy between light and sham treated aged wild-type retinae, for up to 16 hours *ex vivo*. The results suggest that 670 nm light is effective in preventing *ex vivo* dendropathy in retinae from 12-15 month old mice, which is an important finding in terms of expanding on the potential of this therapy as an effective treatment for the dendropathy that is associated with age related neurodegenerative diseases.

5.4.2 Effects of 670 nm light on dendritic pruning in the aged Het retinal explant

Although the results revealed a significant difference in the dendritic complexity in RGCs between sham-treated WT and sham-treated Het mice at time zero, there was no further significant reduction in the dendritic complexity of the entire subpopulation of Het RGCs from time zero to 16 hours *ex vivo*. Considering that there was a statistically significant reduction after 16 hours in the dendritic complexity in the entire subpopulation of RGCs from young wild-type mice and aged wild-type mice, and the Opa1 mutation has been shown to cause a reduction in the ability of RGCs to maintain their dendrites in mice of 12-15 months, it was intriguing that *ex vivo* dendropathy was hindered rather than intensified in Het RGCs. As Het RGCs may struggle to meet the energy demands required for the maintenance of their dendrites it may be possible that Het RGCs had already upregulated survival pathways *in vivo* to compensate for their compromised ability to function optimally. The Het RGCs may have a greater resistance to further degeneration at the time of axotomy compared to wild-type RGCs, resulting in a delay in the axotomy-induced dendropathy in aged Het RGCs.

As ON-centre RGCs were the most vulnerable to the effects of the Opa1 mutation, ON-centre RCGs were analysed separately. There was significant dendropathy after 16 hours *ex vivo* in Het ON-centre RGCs, similar to the results obtained from the entire RGC population in young and aged wild-type RGCs. Pre-treatment with 670 nm light brought about partial protection from *ex vivo* dendropathy in ON-centre Het RGCs. Comparing the effects of 670 nm light on ON-centre cells from Het to those from aged matched WT controls, there was a reduction in the protection achieved in the in ON-centre RGCs from

Het. The reduced effectiveness could be due to the increased challenge of preventing *ex vivo* dendropathy in cells with an increased vulnerability to dendrite loss.

The extent of the *ex vivo* RGC degeneration observed after 16 hours, triggered by mechanical insult, is comparable to that which occurs *in vivo* in the het mouse, beginning at 12 months, triggered by a loss in the RGCs ability to function normally with reduced Opa1. As 670 nm light has been shown here to partially protect against RGC dendritic pruning *ex vivo* in ON-centre Het RGCs, at an aged when Opa1 induced-dendropathy is ongoing, a similar protection against the dendropathy that takes place after 12 months in the het mouse could be achieved with 670 nm light. The increased effectiveness of pre-treatment in the prevention of *ex vivo* dendropathy provides further support to the theory that survival pathways are upregulated at the time of axotomy, enhancing the neuroprotective effects. Therefore, it may be may be most beneficial, when testing this therapy on *in vivo* dendropathy in the het mouse, to commence treatment in younger mice before the initiation of dendropathy.

Chapter 6. The underlying cellular and molecular effects of 670 nm light

6.1 Introduction

6.1.1 The underlying molecular and cellular effects of 670 nm light in retinas of 12-15 month old wildtype and het mice

As discussed in Chapter 5, morphological changes are seen in RGCs after 16 hours post axotomy, *ex vivo*. Yet, the change in dendritic architecture that we see after 16 hours, occurs downstream of a series of molecular changes (Wang et al., 2012). Firstly, axotomy of the RGCs results in depriving the cells of neurotrophic factors that support cell survival (Lieven and Levin, 2007). In addition, explanting the retina transfers the RGCs from a low oxygen environment to one rich in oxygen, fuelling the surge in the generation of reactive oxygen species (ROS), which may play a role in the initial stages of degeneration (Lieven and Levin, 2007). Modifying the molecular environment of the RGCs in such a way as to reduce their vulnerability to the molecular changes that precede dendropathy may offer some resistance against dendropathy.

As discussed in detail in Chapter 1, the underlying molecular mechanisms responsible for the neuroprotective effects of 670 nm light are not fully understood. There are, however, four main theories available which attempt to explain the mechanism underlying the observed therapeutic effects, mechanisms that may also be responsible for countering the degeneration-inducing molecular events initiated by axotomy. Each potential mechanisms of action of red light, discussed in Chapter 1, could all theoretically play a role in delaying the many molecular events that contribute to RGC dendritic pruning that occurs post axotomy. The results of Chapter 5 suggested that genes are upregulated to support survival in the presence of the Opa1 mutation, and that a similar survival response may be triggered by 670 nm light exposure. We hypothesise that 670 nm light

is hijacking the same cell survival response employed by cells to aid their survival during challenging conditions, by inducing a transient increase in oxidative and nitrostrative stress. To explore this hypothesis we investigated the effects of 670 nm light and the Opa1 mutation on the expression levels of a section of particular genes known to be influenced by oxidative and nitrostrative stress.

The presence of 3-nitrotyrosine is used as a marker of oxidative damage mediated by peroxynitrite, and therefore is considered as a biomarker for endogenous peroxynitrite activity (Ahsan, 2013). Low levels of peroxynitrite can trigger signalling pathways that promote neuroprotection, with minimal damage to the cell, whereas high levels are detremental to the cell. We hypothesised in Chapter 1 that upregulation of reactive nitrogen species such as peroxynitrite may be playing a role in the upregulation of genes involved in neuroprotection in response to 670 nm light. Of the genes upregulated in response to peroxynitrite signaling are those with roles in reducing oxidative and nitrostrative stress. This may explain the seemingly contradictory results on the effects of red/NIR light on 3-nitrotyrosine in the literature. For example, an increase in 3-nitrotyrosine was found in spinal cord slice cultures from neonatal rats following a partial transection, an effect that was reduced with 660 nm light (Ashworth et al., 2016).

We sought to investigate the effect of 670 nm light on a marker of peroxynitrite activity in RGCs. Also, the transcription factor, nuclear factor kappa B (NFκB), which is well known for its role in the regulation of immune and inflammatory responses, is activated in response an increase in oxidative/nitrostrative stress. More recently its pivotal role in the regulation of energy metabolism has been uncovered (Tornatore et al., 2012).

Previous studies have shown that NfκB was activated in response to NIR light exposure in murine embryonic fibroblasts (Chen et al., 2011).

The activation of Nrf2 by oxidative and nitrostrative stress leads to the transcription of genes involved in antioxidant defence and cell survival, as discussed in 1.4.6.3. Due to its role in promoting the resistance of the cell to oxidative stress and promoting its survival under challenging conditions, Nrf2 was also hypothesized to be playing a role in the neuroprotective effects of 670 nm light observed in axotomised RGCs (Ma, 2013).

DJ1 is another potential molecular effector of 670 nm light as it is upregulated and activated in response to an increase in oxidative stress, which triggers a downstream anti-oxidant defence mechanism, as described in 1.4.6.3. Further, there are reports of increased expression of DJ1 in the brain under conditions of oxidative stress and in post mortem brains of AD patients (Baulac et al., 2009). Other studies have found that DJ1 can regulate the expression of anti-oxidants and attenuate oxidative stress in cardiomyocytes (Yan et al., 2015).

Akt activation is known to promote neuronal survival which is supported by the findings in a mouse model of dementia where a decrease in phosphorylated Akt was found in the hippocampus (Snigdha et al., 2012). The PI3K-Akt-mTOR pathway plays an essential role in dendrite formation (Kumar et al., 2005). It has been shown that the phosphorylation of Akt is required for BDNF induced dendrite formation in cortical neurons (Dijkhuizen and Ghosh, 2005). However, it must be mentioned that in the hippocampus there is constant formation of new synapses, a process that is not required in the retina. Therefore, a downregulation of Akt in the retina may have different effects than in the

hippocampus. However, phosphorylated Akt supports neuronal survival, therefore we hypothesise that increasing the levels of Akt in the RGCs pre axotomy will promote their ability to resist degeneration.

The results of Chapter 5 suggested that genes are upregulated to support survival in the presence of the Opa1 mutation. In support of this, nuclear Nrf2 fluorescence, as reported to represent Nrf2 activation, was upregulated in primary cortical neurons transfected with siRNA directed against Opa1 (Millet et al., 2016). However, as mentioned in 1.2, cells deficient in Opa1 are thought to lack the ROS dependent upregulation of genes involved in promoting cell survival, an effect that is hypothesised to contribute to their increased susceptibility to cell death in ADOA. This hypothesis was based on results from cells *in vitro*, however, in the drosophila model of ADOA, discussed in 1.3.1, an increase in ROS was found. In our aged model, therefore, it is likely that ROS is produced as the result of aberrant mitochondrial functioning. We hypothesise that the ROS present in the RGCs of the het mice upregulates signalling pathways that support cell survival, increasing the resistance of those RGCs to axotomy induced degeneration.

6.1.2 The effect of 670 nm light treatment on microglial activation in the retinae of 21-26 month old het mice

As mentioned above and in Chapter 1, both pro- and anti-inflammatory effects can occur downstream of NFκB activation, depending on the particular state of the cell at the time of activation. Therefore, if 670 nm light is mediating its protective effects via NFκB, the effect of 670 nm light on inflammation would also depend on the cellular environment upon 670 nm light exposure. Neuroinflammation is a characteristic feature of retinal neurodegenerative diseases including glaucoma, AMD and diabetic retinopathy, with

evidence for the involvement of activated microglia in the initiation and progression of the degenerative process (Madeira et al., 2015). There is also much evidence available to associate the activation of microglia with the degeneration of RGCs in diseases associated with optic atrophy such as glaucoma (Wang et al., 2016). Although our group have previously shown that RGC dysfunction in 12-15 month old het mice was found to occur in the absence of soma loss and microglial activation, the activation of microglia in het mice over 20 months, when severe dendropathy is present, has not been investigated (Williams et al., 2011). As

The dendropathy in the het mouse is accompanied by synaptic atrophy (Williams et al., 2012). It is known that microglial activation plays a role in the removal of dysfunctional synapses (Kettenmann et al., 2013). Further, there is evidence from animal studies to show that there are changes in microglial morphology and an increase in lectin reactivity for microglia in the retina as a result of nonpathological aging (Conde et al., 2006). It was therefore hypothesised that ativated microglial would be present in wild-type mice above 20 months and het mice over 20 months. Additionally, as microglial activation is associated with other optic atrophies, it was hypothesised that there would be increased microglial activation in the very aged het mouse compared to the very aged wild-type mouse. As discussed in Chapter 1 red/NIR light has been shown to modulate the immune response; however, the particular effect produced by 670 nm light appears to be dependent upon extent of the inflammatory response in the cell or tissue at the time of exposure. Therefore, we sought to explore the effects of 670 nm light on microglial activation in very aged wild-type and het mice.

6.2 Experimental design

6.2.1 The underlying molecular and cellular effects of 670 nm light in retinas of 12-15 month old wildtype and het mice

We investigated changes in expression or activation of the potential molecular effectors of 670 nm light, discussed in the introduction. As we were particularly interested in the effects of delivering 670nnm light to RGCs prior to axotomy as discussed in chapter 5, we sought to explore molecular changes in sham- and light-treated RGCs from wild-type and het mice that were present upon axotomy. Therefore, 12-15 month old wild-type and het mice were sham- or light-treated for 5 consecutive days before axotomy. Of the mice assigned to the 0 hour time point in the dendropathy study from which one eye was taken for Diolistic labelling of RGCs, the fellow eye was placed in 4% PFA immediately after axotomy for immunohistochemical analysis. The activation of transcription factors NFκB and Nrf2 is dependent on their translocation from the cytoplasm to the nucleus. Therefore, we calculated the nuclear-cytoplasmic ratio of the integrated density values to obtain a measure for the activation of each transcription factor in response to 670 nm light treatment. The protective effect that occur downstream of DJ1 are triggered by both an upregulation of endogenous DJ1 and its translocation to the mitochondria. Therefore, we measured the mean fluorescence of DJ1 in RGCs from 12-15 month old wild-type and het mice in response to 670 nm light treatment. We also measured the amount of DJ1 co-localised with a mitochondrial marker to measure the extent of translocation of DJ1 to the mitochondria. The phosphorylation of Akt on its Ser473 is required for its full activation upregulation, before it can produce its cytoprotective effects. Thus the mean fluorescence of p-Akt was measured in the RGCs in response to

670 nm light. To back up the findings of the immunohistochemistry data for Akt, wild-type mice were 670 nm light treated (n=3) and sham-treated (n=3) to find the ratio between p-Akt and total Akt in the entire retina, to explore the effect of 670 nm light on p-Akt activation in the entire retina. As 3-nitrotyrosine is a marker of peroynitrite activity, the mean fluorescence of 3-nitrotyrosine in RGCs was measured in response to 670 nm light treatment in wild-type and het mice.

6.2.2 The effect of 670 nm light treatment on microglial activation in the retinae of 21-26 month old het mice

Wild-type and het mice were selected in numbers sufficient to have a minimum of five mice in each of the following experimental groups: wild-type sham treated, het sham treated and het 670 nm light treated. The mice were aged until all mice were a minimum of 21 months old to test whether or not 670 nm light could provide therapeutic effects in the very advanced stages of disease in the het mouse. As such we sought to explore the involvement of microglial activation in end stage dendropathy, which may be associated with the synaptic and dendritic atrophy found in this model and investigate the effect of 670 nm light on microglial activation.

Accordingly, we treated 21-26 month old het mice (n=6) with 670 nm light twice daily for 7 consecutive days as described in Chapter 2. As therapeutic effects were found with seven 90s exposures of 670 nm light with an irradiance of 40 mW/cm^2, and our single device gave an irradiance of approximately 20 mW/cm^2 (Gkotsi et al., 2014), we delivered 670 nm light to our mice over 14, 90 s exposures. A group of 21-26 month old wild-type (n=5) and het mice (n=4) were sham treated to compare the levels of microglial activation between very aged wild-type and het mice and as a control for the effects of

normal aging on microglial activation. After the final treatment the mice were killed by cervical dislocation and one eye from each mouse was fixed in 4% PFA before cryopreservation. The second eye was prepared for exploration of mitochondrial bioenergetics as mentioned in Chapter 3. Microglia were labelled with an Iba1 antibody using immunohistochemistry to enable the identification of both resting and activated microglia in the retina.

Amoeboid microglia are associated with maximum pro-inflammatory activation and are characterised by a rounded morphology with few or no processes (Crews and Vetreno, 2016). Ramified or “resting” microglia can be identified by long ramified processes; mildly activated hyper ramified microglia can be identified by increased branching of dendrites; and microglia with intermediate activation can be identified as being branched but having swollen truncated processes. For analysis, the microglial states were divided into fully activated and all other stages of microglial activation, which were identified by amoeboid microglia and ramified microglia, respectively.

6.3 Results

6.3.1 The underlying molecular and cellular effects of 670 nm light in retinas of 12-15 month old wildtype and het mice

Reactive oxygen and nitrogen species can trigger the translocation of NfkB to the nucleus where it can induce the trancription of genes involved in the regulation of the inflammatory response and cytoprotection. NfkB staining was present in retinae from all experimental groups (Figure 6.1). The staining was particularly noticable in the GCL and was detectable in the nuclear region and cytoplasmic region of the RGCs. The overall expression of NfkB in the GCL was unaffected by the Opa1 mutation or 670 nm light treatment (Figure 6.2A). The mean fluorescence values of NFkB in the nuclear and cytoplasmic region of wild-type RGCs were both significantly reduced with light treatment (Figure 6.2B-C). Similarly, the mean fluorescence of NFkB in the cytoplasmic region was reduced significantly with the Opa1 mutation (Figure 6.2C). The nuclear-cytoplasmic ratio of NFκB, representing the extent of NfκB translocation from the cytoplasm to the nucleus, (Figure 6.2D) was significantly reduced in RGCs from sham treated het mice compared to sham treated wild-type mice (Figure 6.2D). The nuclear to cytoplasmic ratio of NFκB increased with 670 nm light treatment in RGCs from het, restoring the ratio up to wild-type levels. However, despite the reports of NFκB activation in response to 670 nm light treatment in the literature, we found no effect of 670 nm light treatment on the nuclear to cytoplasmic ratio of NFκB in RGCs from wildtype mice. Therefore, 670 nm light significantly increased the activation of NfkB in RGCs from het mice but had no effect on wild-type RGCs.

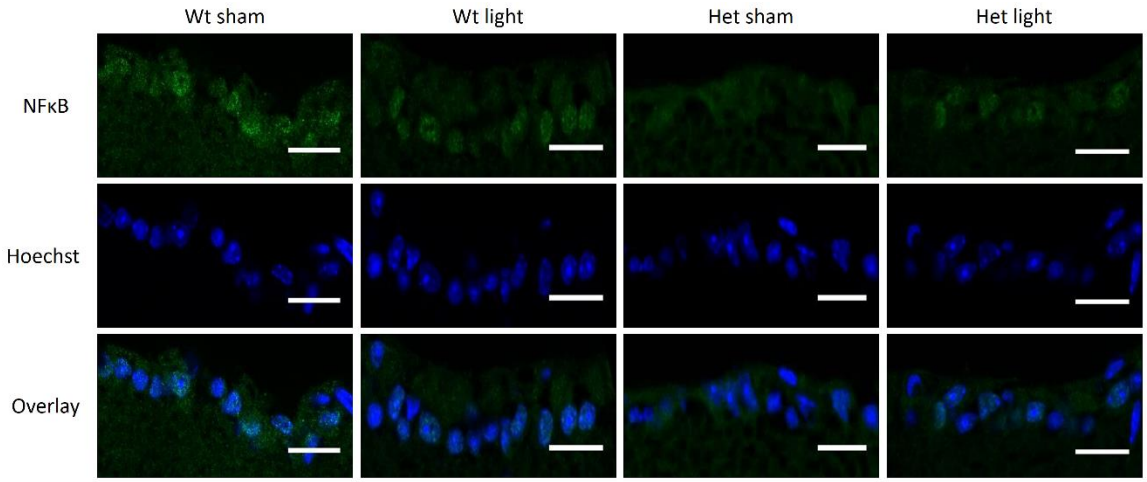

Figure 6.1: Representative images of NFκB expression in the wild-type sham treated (n=3), wild-type light treated (n=6), het sham treated (n=4) and het light treated (n=3) retinae. Images are presented at 60X magnification to show the staining in the nuclear region of the RGCs. The top row shows NFκB staining with an example image of a retina from each group, the middle row shows the nuclear stain and the bottom row shows an overlay of the two stains. Scale bar represents 20 µm.

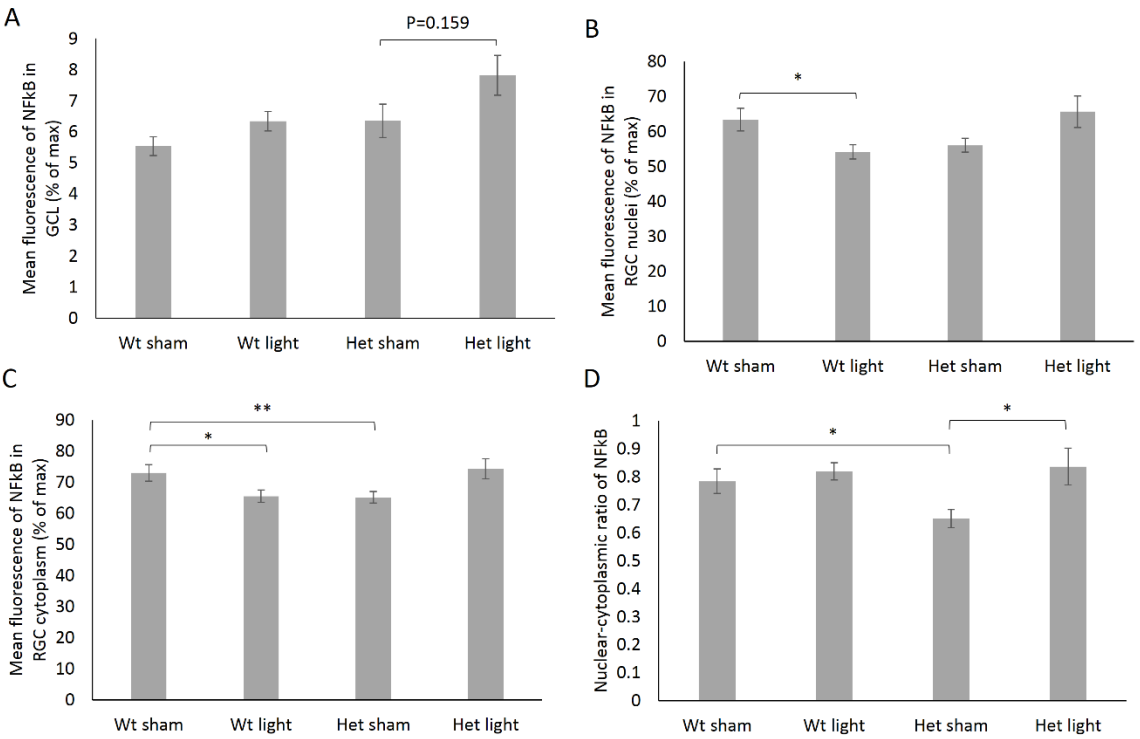

Figure 6.2: The activation of NFκB is reduced by the Opa1 mutation and is restored with 670 nm light treatment, in the absence of a change in the overall expression levels of this protein. (A) The mean fluorescence of NFκB in the GCL. (B) The mean fluorescence of NFκB in RGC nuclei. (C) The mean fluorescence of NFκB in RGC cytoplasm. (D) The average nuclear-cytoplasmic ratio of the integrated density of NFκB fluorescence in the GCL of retinae from each experimental group. Error bars represent SEM. * $p<0.05$, ** $p<0.01$.

6.3.2 The effect of 670 nm light treatment on microglial activation in the retinae of 20-26 month old het mice

NFκB activation can bring about both pro- and anti-inflammatory responses depending on the cellular state at the time of activation, therefore as 670 nm light induced NFκB activation in het mice, we sought to explore the effects of 670 nm light exposure on microglial activation in very aged het mice. Iba1 staining, which labels microglia of all activation states, was present in the GCL, the IPL and the OPL (Figure 6.3).

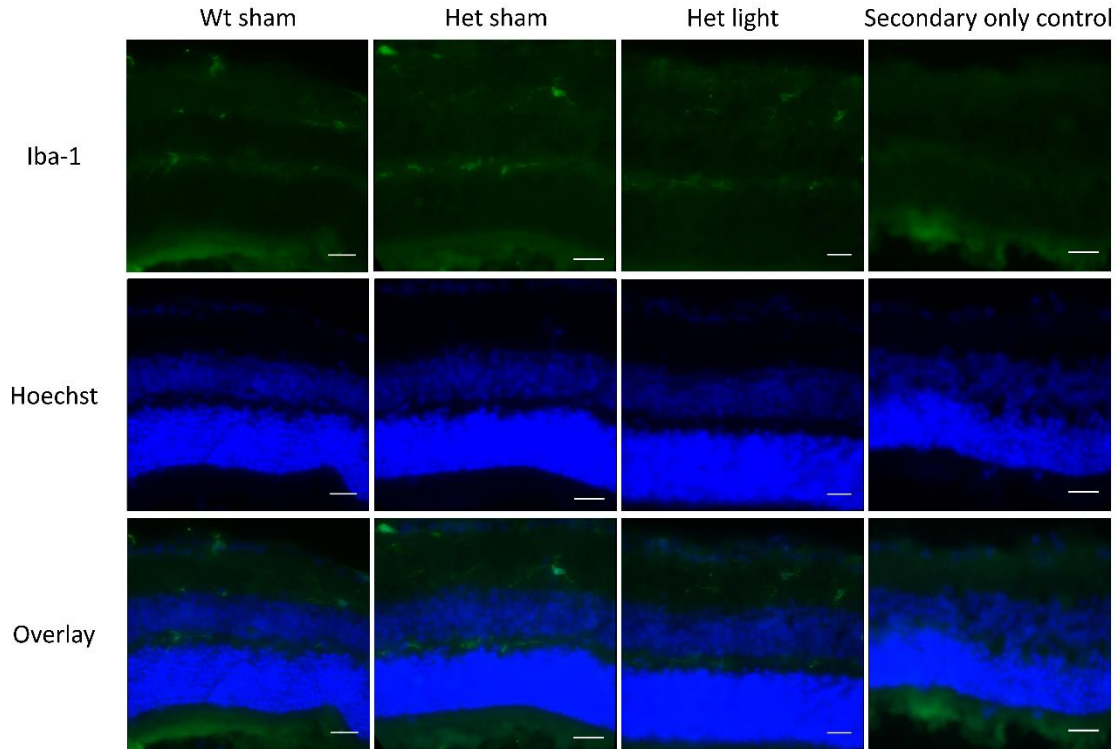

Figure 6.3: Representative images of Iba-1 expression in the wild-type sham treated (n=5), het sham treated (n=4) and het light treated (n=6) retinae. The top row shows Iba-1 staining with an example image of a retina from each group, the middle row shows the nuclear stain and the bottom row shows an overlay of the two stains. The secondary only control image shows the non-specific staining that occurs in the absence of the primary antibody. Scale bar represents 20 µm.

For analysis the microglial states were divided into fully activated (amoeboid microglia) and all other stages of microglial activation (ramified microglia) (Figure 6.4).

There was no significant difference in the percentage of ameboid microglia in the GCL or IPL of retinae from sham treated wild-type and sham treated het mice (Figure 6.5A-B). Similarly, there was no significant difference in in the percentage of ameboid microglia in the GCL or IPL of retinae from sham and light treated het mice.

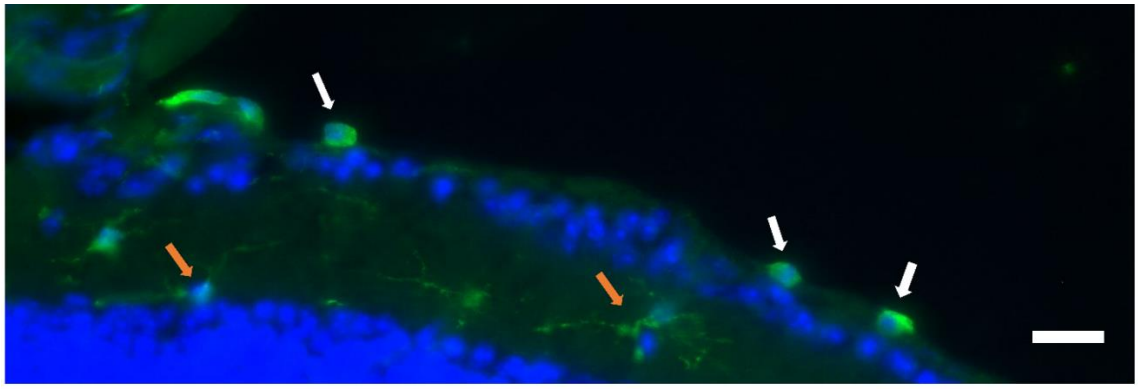

Figure 6.4: Examples of amoeboid and ramified microglia on the GCL and IPL of the retina. Amoeboid microglia in the GCL are indicated by the white arrows and ramified microglia in the IPL are indicated by the orange arrows. Scale bar represents 20 µm.

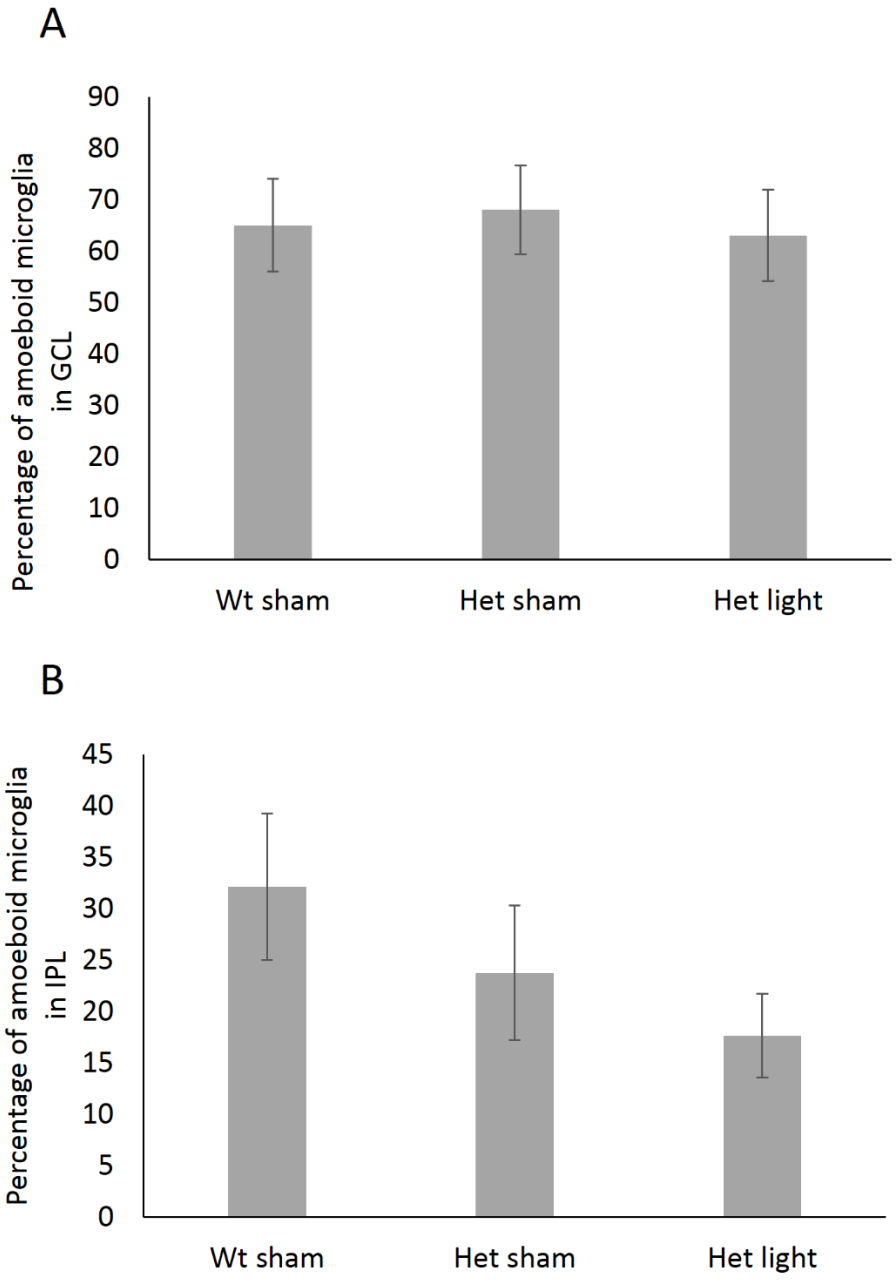

Figure 6.5: In very aged mice 670 nm light had no significant effect on the activation of microglia in het RGCs. The the percentage of ameboid microglia in the GCL or (A) and IPL (B) of retinae from each experimental group. Error bars represent SEM.

6.3.3 Further exploration of the underlying molecular and cellular effects of 670 nm light in retinas of 12-15 month old wildtype and het mice

The unexpected lack of NfkB activation in WT mice and the lack of an effect on microglial activation in het mice prompted us to test other transcription factors activated by oxidative stress which lead to upregulation of antioxidant and pro-survival pathways, namely Nrf2 and DJ1. We sought to explore the translocation of Nrf2 from the cytoplasm to the nucleus of RGCs by measuring the nuclear to cytoplasmic ratio of Nrf2. We also measured the expression of Nrf2 in the nuclear region, the cytoplasmic region and the entire GCL. Nrf2 staining was present in the retina, most noticeably in the GCL, IPL and INL in each experimental group (Figure 6.6A). Much of the Nrf2 staining in the RGCs was present in the nuclear region, with most of the Nrf2 fluorescence co-localised with the nuclear stain (Figure 6.6B). There was no significant difference in any of these measurements between sham treated wild-type and het mice or in either genotype in response to 670 nm light exposure (Figure 6.7). Of note, we observed an increase in nuclear Nrf2 fluorescence represent Nrf2 activation, in RGCs from het mice when compared to wild-type, however this increase was not statistically significant (Figure 6.4B).

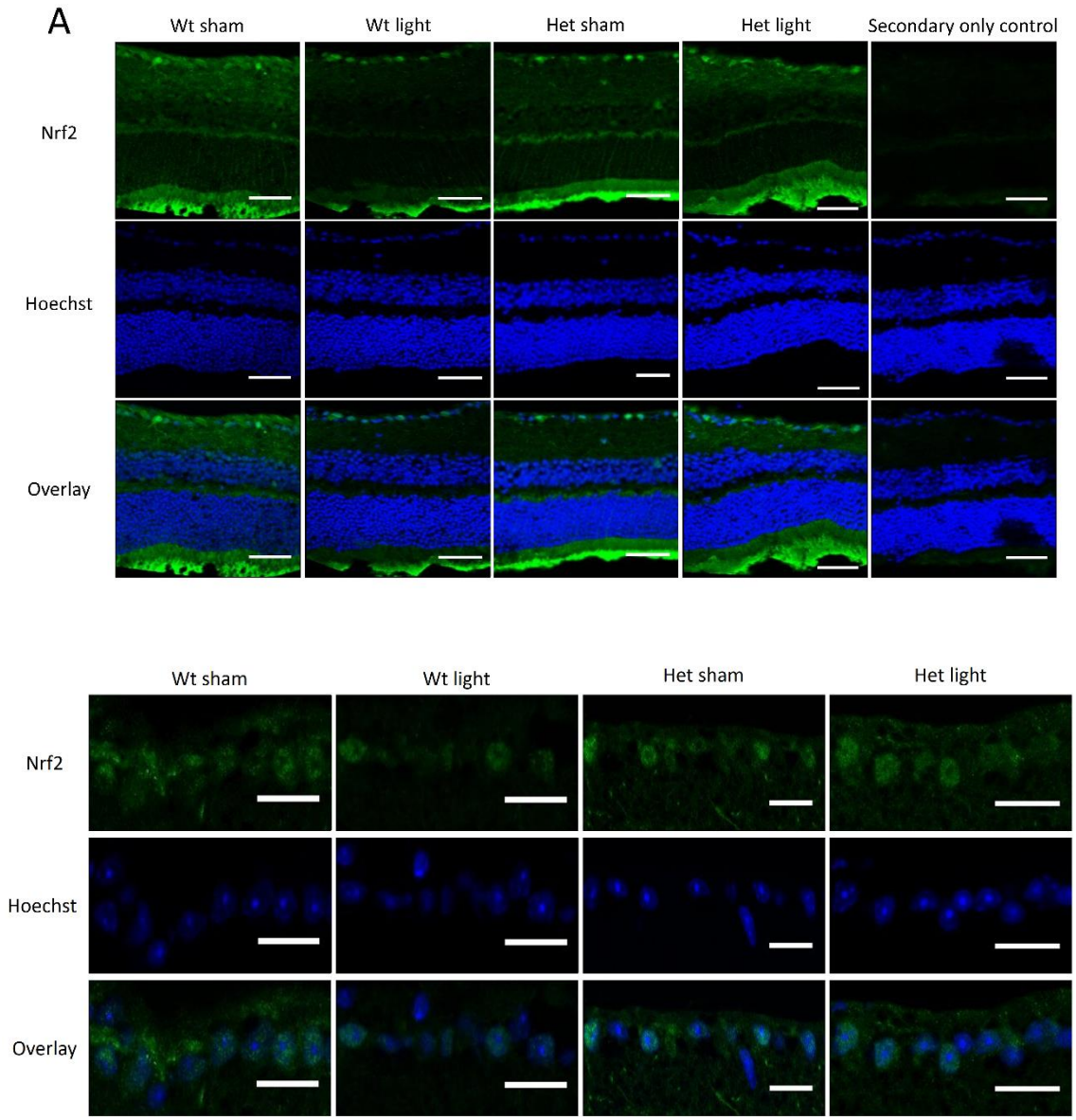

Figure 6.6: Representative images of Nrf-2 expression in the wild-type sham treated (n=6), wild-type light treated (n=6), het sham treated (n=5) and het light treated (n=3) retinae. A: images taken at 20X magnification, B: images taken at 60X magnification. The top row shows Nrf-2 staining with an example image of a retina from each group, the middle row shows the nuclear stain and the bottom row shows an overlay of the two stains. The secondary only control image shows the non-specific staining that occurs in the absence of the primary antibody. Scale bar represents 20 µm.

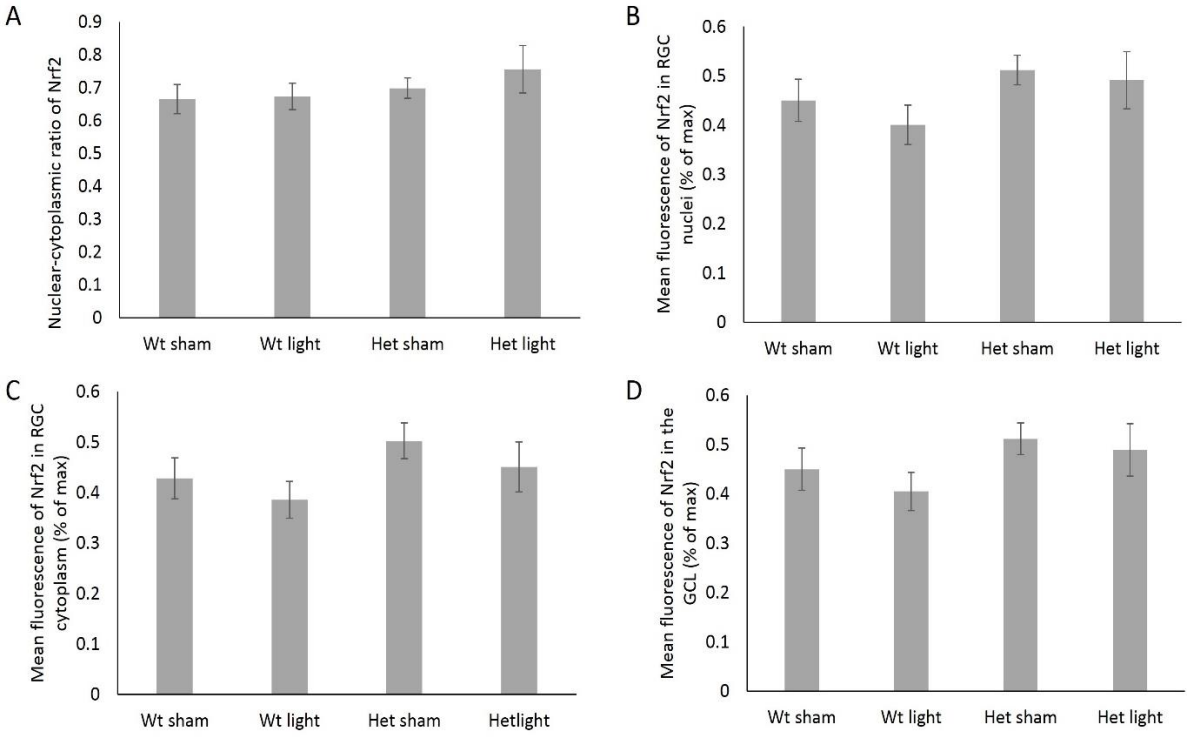

Figure 6.7: There was no significant difference in Nrf2 expression or activation in aged RGCs as a result of the het mutation or from treatment with 670 nm. (A) The average nuclear-cytoplasmic ratio of the integrated density of Nrf-2 fluorescence in RGCs from each experimental group. (B) The mean fluorescence of Nrf2 in RGC nuclei. (C) The mean fluorescence of Nrf2 in the RGC cytoplasm. (D) The mean fluorescence of Nrf2 in the GCL. Error bars represent SEM.

The upregulation of Dj1 by oxidative and nitrostrative stress triggers a cellular defence mechanism to support cell survival during unfavourable conditions. DJ1 staining was found in the retinae from each experimental group, which was most intense in the GCL, the INL and the ONL (Figure 6.8). Much of the staining was colocalised with the nuclear stain. DJ1 was found to be upregulated in the GCL of retinae from het mice compared to wild-type (Figure 6.9A). There was also an increase in DJ1 expression in the GCL in response to 670 nm light treatment in retinae from wild-type mice. There was, however, no observed effect of 670 nm light treatment on total DJ1 expression in RGCs from het

mice. Upon exploration of the expression of DJ1 in the IPL, there was no significant difference between wild-type and het mice, but a significant increase was seen with 670 nm light treatment in retinae from both wild-type and het mice (Figure 6.9B).

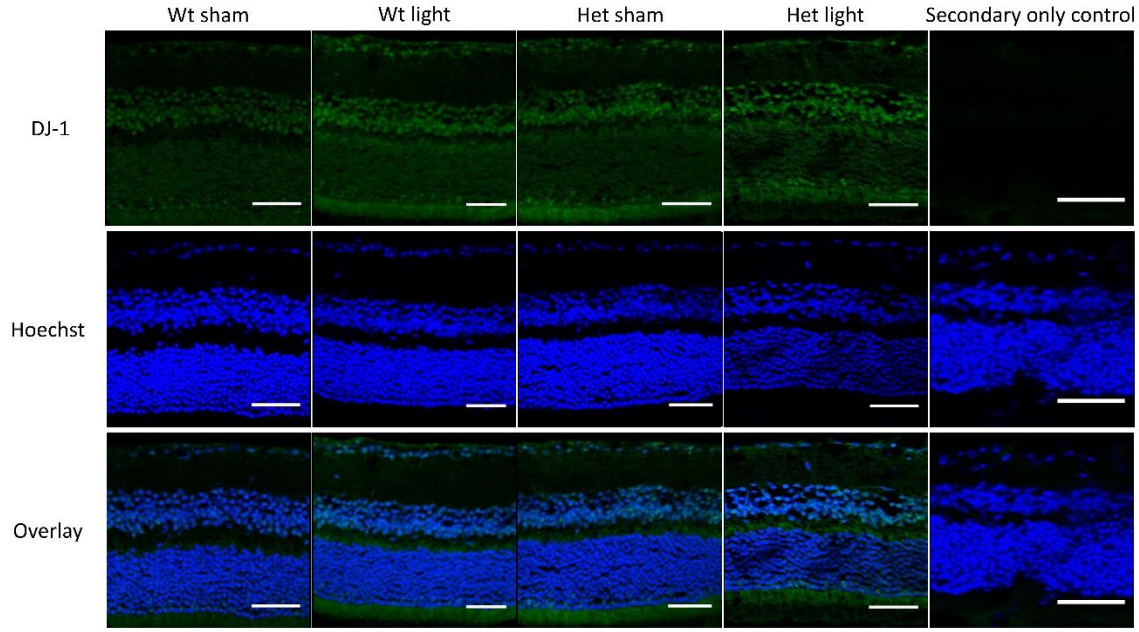

Figure 6.8: Representative images of DJ-1 expression in the wild-type sham treated (n=4), wild-type light treated (n=6), het sham treated (n=6) and het light treated (n=3) retinae. The top row shows DJ-1 staining with an example image of a retina from each group, the middle row shows the nuclear stain and the bottom row shows an overlay of the two stains. The secondary only control image shows the non-specific staining that occurs in the absence of the primary antibody. Scale bar represents 20 μm.

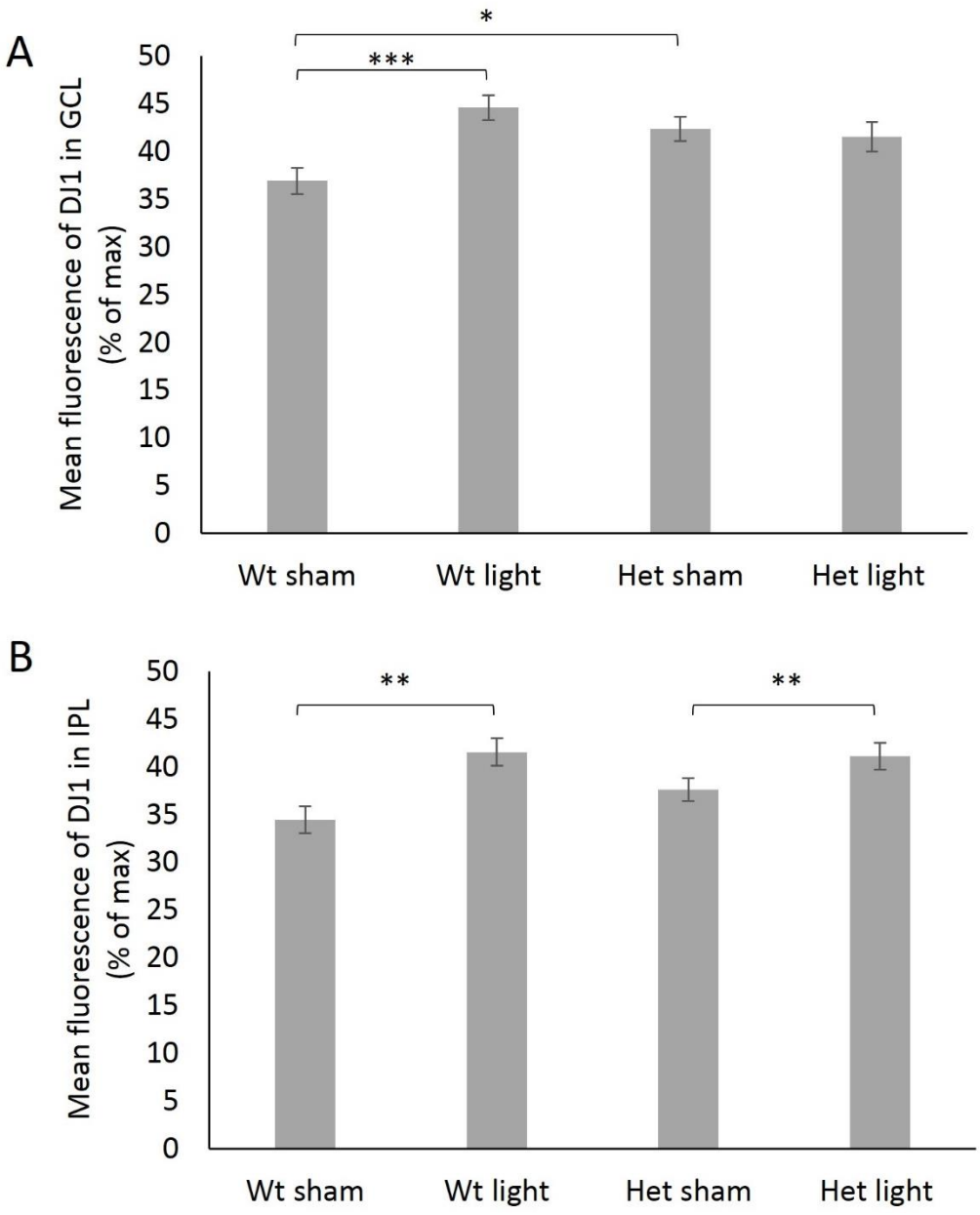

Figure 6.9: DJ1 was upregulated in the GCL of retinae from sham treated het mice and 670 nm light treated wild-type mice, and in the IPL of retinae from wild-type and het mice in response to 670 nm light treatment. Average mean values of DJ-1 fluorescence presented as a percentage of the maximum fluorescence reading from each group in the GCL (A) and the IPL (B). Error bars represent SEM. * $p<0.05$, ** $p<0.01$, *** $p<0.001$.

The data presented above show total DJ1 expression in the GCL and IPL layer. We next sought to further explore the subcellular distribution of DJ1 as this contributes to the

triggering of the associated downstream protective effects. We looked at the localisation of DJ1 to the mitochondria in response to 670 nm light in RGCs (Figure 6.10).

The results show that the percentage of RGCs with DJ1 staining colocalised with the mitochondrial marker was not significantly changed with either the Opa1 mutation or 670 nm light treatment (Figure 6.11A). The percentage of RGCs with DJ1 staining that was not colocalised with the mitochondrial marker was significantly reduced in het mice that received 670 nm light treatment compared to sham treatment (Figure 6.11B). The results suggests that although 670 nm light can increase the expression of DJ1 in RGCs of wild-type mice it does not influence its localisation to the mitochondria, an event associated with enhanced neuroprotection. In het RGCs where DJ1 expression is upregulated, 670 nm light does little to influence the localisation of Dj1 to the mitochondria to enhance neuroprotection.

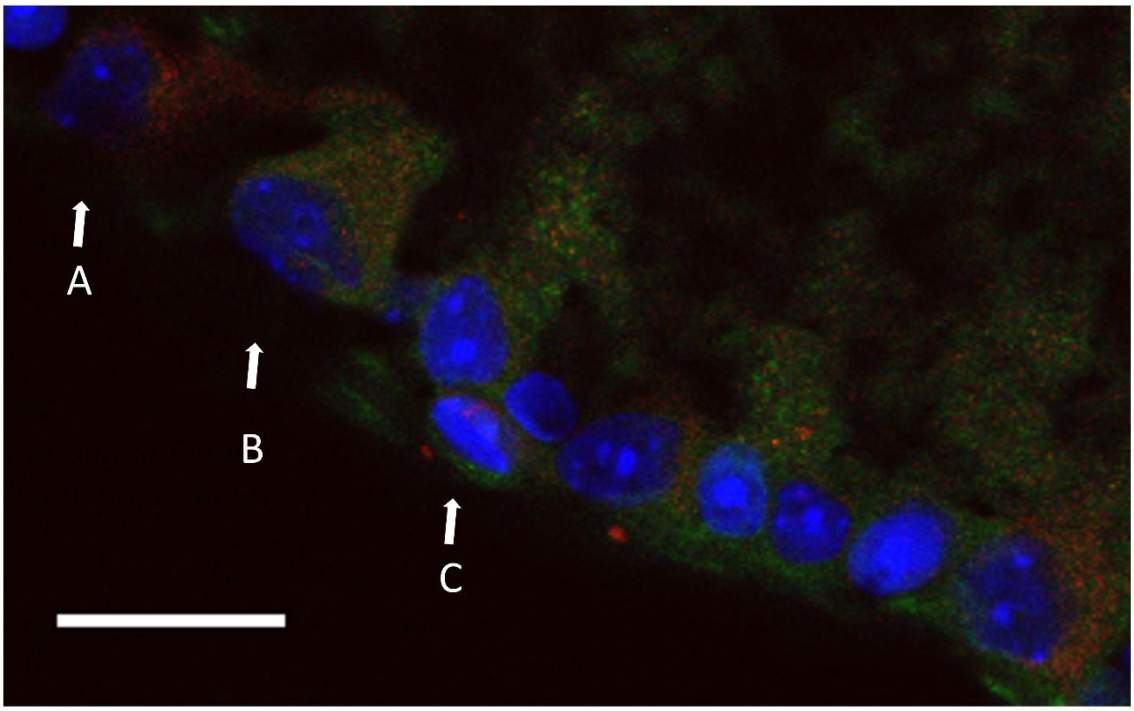

Figure 6.10: An example of DJ1 and COX IV expression in RGCs to enable identification of cells where DJ1 is localised to the mitochondria. (A) A cell with weak DJ1 staining. (B) A cell where DJ1 is co-localised with cytochrome c oxidase which is used as a mitochondrial marker. (C) A cell where DJ1 is non-colocalised with the mitochondrial marker. Scale bar represents 20 μm.

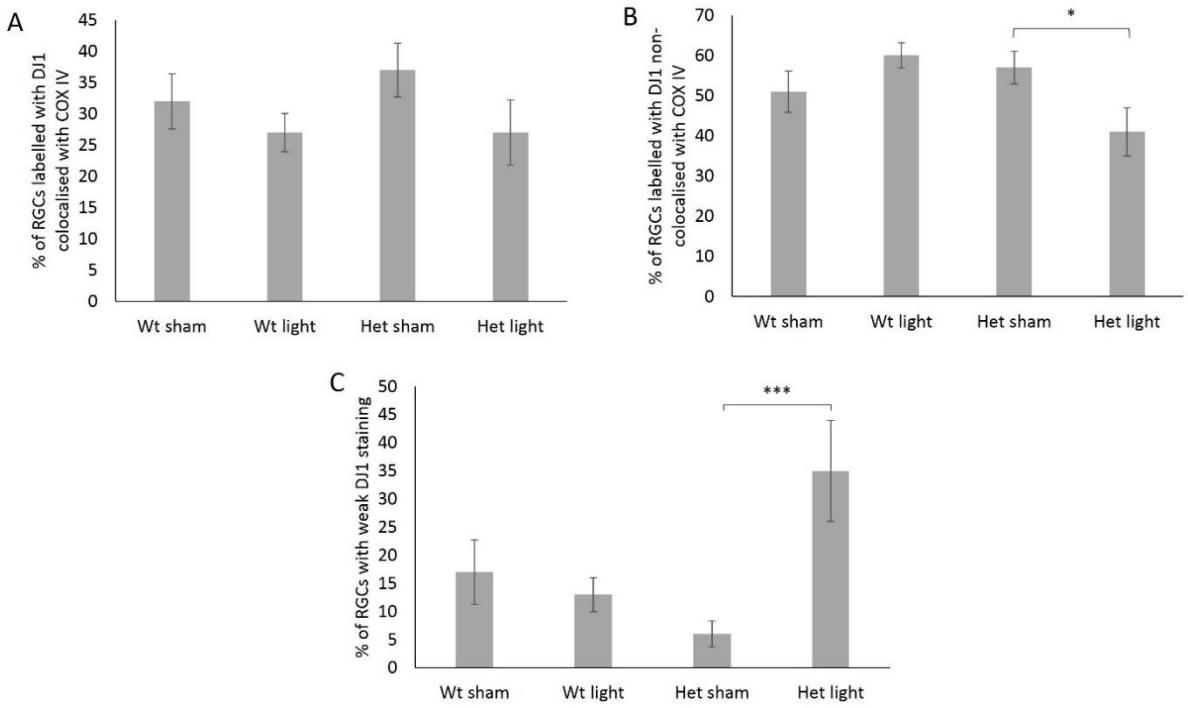

Figure 6.11: Analysis of DJ1 co-localisation with the mitochondrial marker, COX IV, in the GCL of retina from wild-type sham (n=3), wild-type light (n=3), het sham (n=3) and het light (n=2). (A) The percentage of cells labelled strongly with DJ1 and co-localised with COX IV staining. (B) The percentage of cells strongly labelled with DJ1 but not co-localised with COX IV. (C) The percentage of cells with weak DJ1 staining.

As described in Chapter 1.4.6.3, activation of DJ-1 can upregulate antioxidant defences, and therefore we investigated whether an increased expression of DJ-1 can protect from nitration of tyrosine residues. There was no effect of 670 nm light on 3-nityrosine levels in RGCs from aged wild-type or het mice (Figure 6.12-13). We did, however, find that the amount of 3-nitrotyrosine was upregulated in RGCs of retinas of aged het mice.

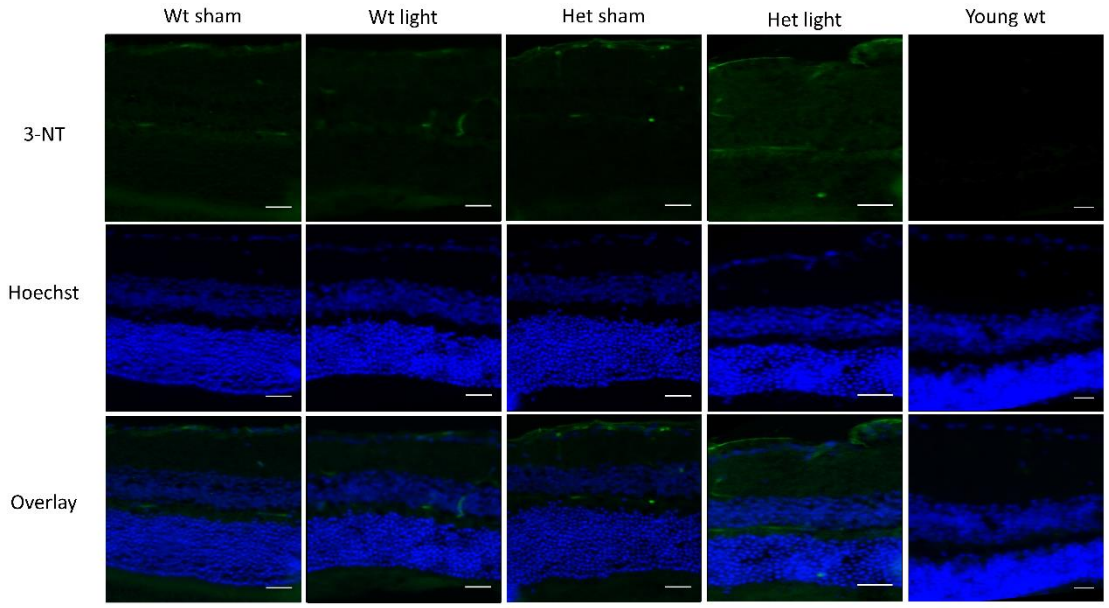

Figure 6.12: Representative images of 3-nitrotyrosine expression in the wild-type sham treated (n=3), wild-type light treated (n=4), het sham treated (n=4) and het light treated (n=2) and young wild-type untreated (n=1) retinae. The top row shows 3-nitrotyrosine staining with an example image of a retina from each group, the middle row shows the nuclear stain and the bottom row shows an overlay of the two stains. The young wild-type retina was used as a negative control for 3-nitrotyrosine staining in the retina. Scale bar represents 20 μm.

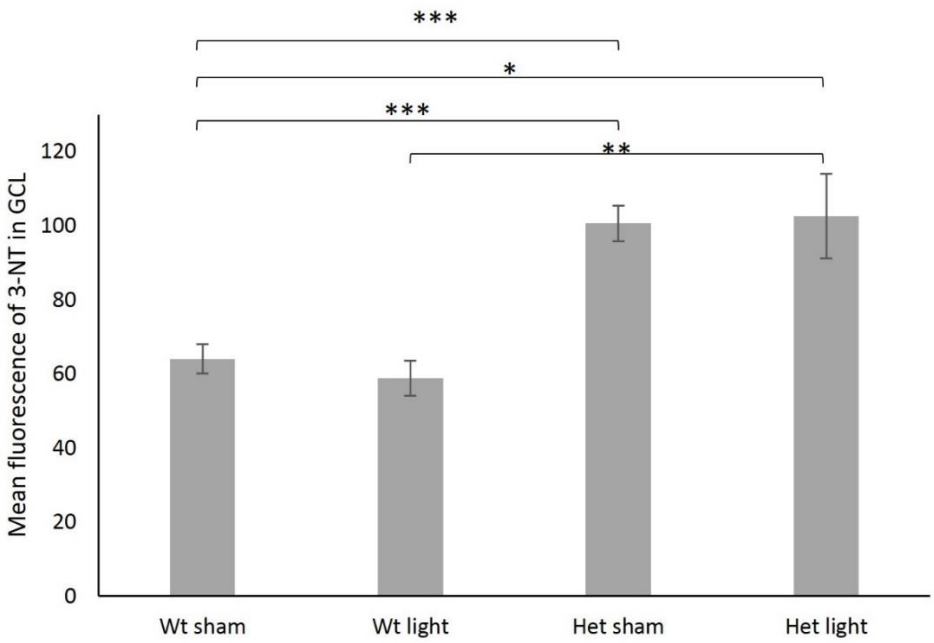

Figure 6.13: The expression of 3-nitrotyrosine was increased in RGCs from het mice. Average mean values of 3-nitrotyrosine fluorescence in the GCL from each experimental group. Error bars represent SEM. * p<0.05, ** p<0.01, *** p<0.001.

The activation of Akt can be quantified by the phosphorylation of Ser473, an effect that is associated with increased protection against oxidative stress and increased cell survival. Phosphorylated Akt staining was present in the retinae of both sham and light treated wild-type mice, with an increase in staining intensity noticeable in the GCL of wild-type retinae (Figure 6.14). Most unexpectedly, p-Akt was found to be significantly down-regulated in the GCL and IPL of retinae from wild-type aged mice treated with 670 nm light (Figure 6.15A-B). The increased activation of p-Akt was exclusive to the GCL and IPL as there was no significant difference in p-Akt expression in the INL or ONL (Figure 6.15C-D). Similarly, after comparing the protein expression levels of Akt and p-Akt from the entire retinae, there was no significant difference in the p-AKt/Akt ratio between light treated and sham treated retinae (Figure 6.16A-B).

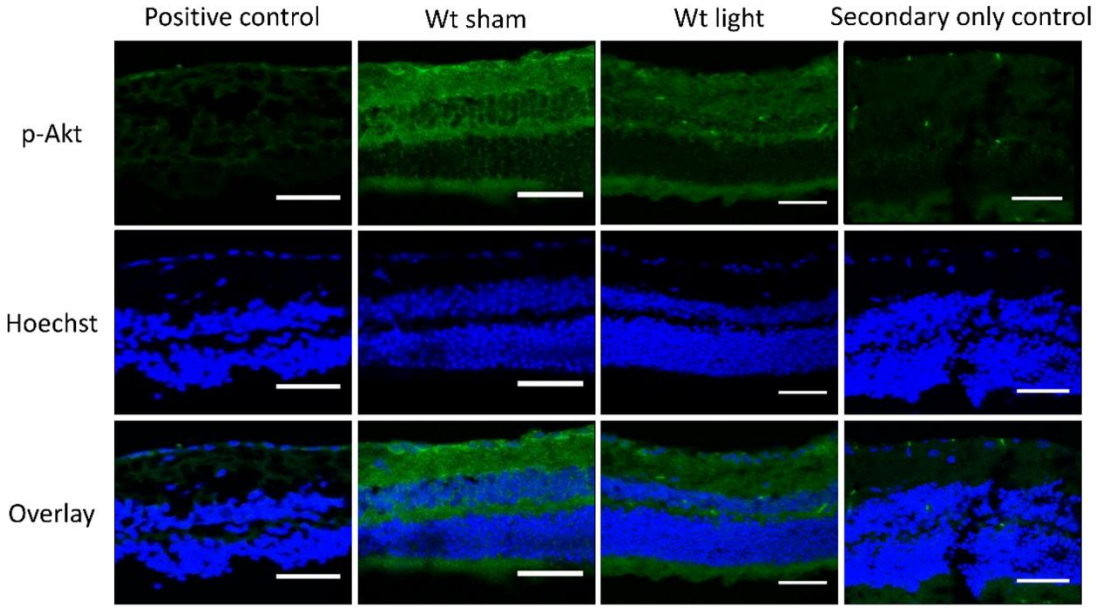

Figure 6.14: Representative images of p-Akt expression in aged wild-type sham treated (n=3) and aged wild-type light treated (n=3) retinae. The top row shows p-Akt staining with an example image of a retina from each group, the middle row shows the nuclear stain and the bottom row shows an overlay of the two stains. The positive control shows p-Akt staining in a retinal flat mount from a young adult mount treated with 10 nM insulin for 5 minutes to upregulate p-Akt. There is higher background staining in the Wt sham and Wt light sections than in the control sections. This may be due to differences in fixation as the control sections were obtained from a fixed froxen explants while the experimental samples were obtained from fixed frozen whole eyes. The secondary only control image shows the non-specific staining that occurs in the absence of the primary antibody. Scale bar represents 20 μm.

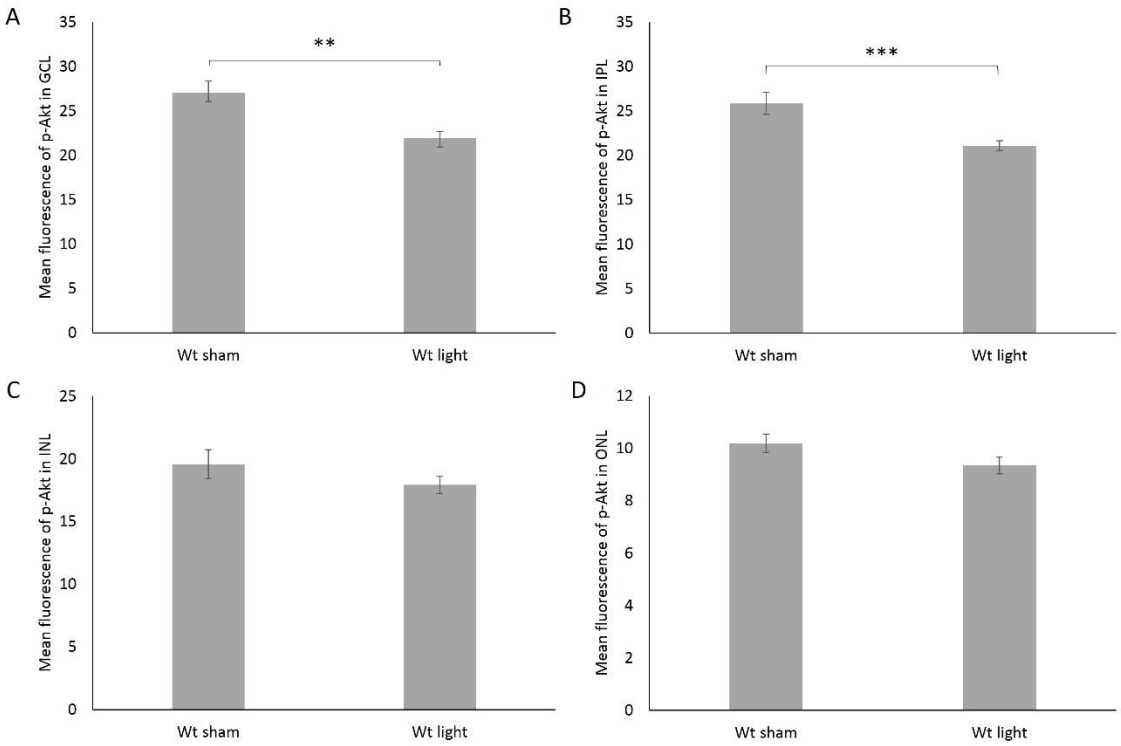

Figure 6.15: The expression of p-Akt was significantly reduced in the GCL and IPL of aged wild-type mice treated with 670 nm light but was unchanged in the other retinal layers. Average mean values of p-Akt fluorescence in the GCL from each experimental group. Error bars represent SEM. ** $p<0.01$.

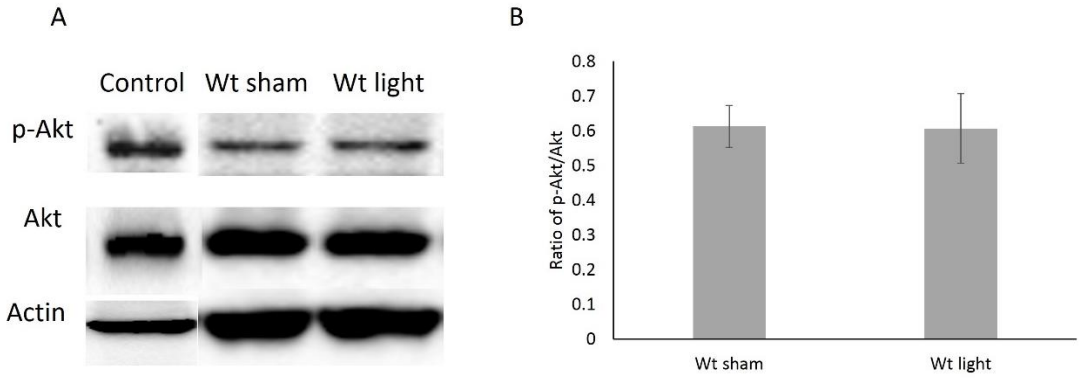

Figure 6.16: Akt activation was unchanged in the wild-type retina with 670 nm light treatment. The protein expression levels of p-Akt and Akt were analysed by western blot (A) and the ratio of the protein levels of p-Akt and Akt was calculated (B). Results are based on 3 biological samples per experimental group and the western blots were ran twice. Control represents the protein expression of of p-Akt and Akt from a retina treated with insulin as a positive control for Akt activation. Error bars represent SEM.

6.4 Discussion

6.4.1 The underlying molecular and cellular effects of 670 nm light in retinas of 12-15 month old wild-type and het mice

In wild-type RGCs 670 nm light had no effect on the activation of NFκB. The results differ to that published previously by Chen et al who found that 810 nm light increased NFκB activation in mouse embryonic fibroblasts via the generation of ROS (Chen et al., 2011). As the experiment was done on fibroblasts, the authors suggest that different cell types may show a different pattern of NFκB activation in response to LLLT. We found this predicted varying effect in our work as although 670 nm light treatment had no effect on the activation of NFκB in wild-type, it increased NFκB activation in RGCs from het mice up to wild-type levels. As NFκB activity is known to be increased with aging and is associated with neurodegenerative diseases it was intriguing that NFκB was downregulated in aged het mice (Tilstra et al., 2011). There are many molecules that are known activators of NFκB within neurons, some of which act as repressors of NFκB activity at higher concentrations, revealing an essential role for NFκB in preconditioning (Kaltschmidt et al., 2005). Aged het RGCs may have had suboptimal levels of NFκB activation which may have contributed to their *in vivo* neurodegeneration. Treatment with 670 nm light increased NFκB activity in het RGCs to a level which may be optimal for neuroprotection so that upon axotomy the RGCs were more resistant to *ex vivo* degeneration. The result for the het RGCs is in accord with the result found by Chen et al, showing an increase in NFκB activation following red/NIR light treatment. In wild-type RGCs, since NFκB activity is not altered with 670 nm light treatment, NFκB activity may already be at the optimal

level required for neuroprotection in wild-type RGCs, therefore altering NFκB activation is not a mechanism by which 670 nm light is providing neuroprotection against *ex vivo* degeneration in wild-type RGCs.

6.4.2 The effect of 670 nm light treatment on microglial activation in the retinae of 21-26 month old het mice

In 21-26 month old mice there was no significant difference in the number of activated microglia surrounding the RGC cell soma or dendrites in very aged wild-type and het mice, as assessed by the numbers of amoeboid microglia in the GCL and IPL. In another mouse model of ADOA, microglial activation has been found to be involved in phagocytosing dying RGCs from 18 month old mice (Heiduschka et al., 2010). In our mouse model of ADOA, however, the extent of microglial activation in GCL and IPL, even at this late stage of the disease was no different from that associated with normal aging. However, NFκB activation was downregulated in aged het mice. Since microglia are one of the downstream effectors of NFκB activation it was interesting that the downregulation of NFκB activation had no effect on microglial activation.

Due to the less severe phenotype of our mouse model of ADOA, showing dendrite degeneration without RGC death, microglial activation may be playing a less prominent role in the progression of the disease phenotype. Also, microglial activation increases as a result of normal aging (Sloane et al., 1999). Therefore, microglial activation may be playing a role in RGC degeneration in het mice, but the increase in microglial activation with normal aging in addition to the limited

availability of such aged mice may have resulted in any real increase in microglial activation to evade detection by our analysis.

Albeit not increased in het RGCs compared to wild-type, it was of interest to explore the effects of 670 nm light therapy on the microglial activation associated with normal aging in RGCs from wild-type and het mice. Red light therapy has been shown to inhibit microglial activation in a model of TBI (Khuman et al., 2012). Additionally, NFκB activation appears to be playing a role in providing protection to het mice and microglia are one of the downstream effectors of NFκB activation. However, in the current experiment, there was no significant effect of 670 nm light treatment on microglial activation in the GCL or IPL of het mice.

The lack of effect of 670 nm light on microglial activation in very aged (21-26 months) het mice may be due to the advanced age of the mice. It would have been of great interest to explore the effect of 670 nm light on complex IV activity as was planned for the fellow eye in Chapter 3. As an increase in complex IV activity is a well-documented effect of 670 nm light, this experiment would have shown whether or not 670 nm light can produce therapeutic effects in aged mice with mitochondrial dysfunction. This would have determined whether 670 nm light is simply having no effect on microglial activation in het mice or whether the mice are too old to receive therapeutic benefits from 670 nm light.

6.4.3 Further exploration of the underlying molecular and cellular effects of 670 nm light in retinas of 12-15 month old wildtype and het

There was no significant effect of 670 nm light treatment on Nrf2 activation in either wild-type or het RGCs. Despite an increase in Nrf2 activation in cortical neurons with reduced Opa1 (Millet et al., 2016), the haploinsufficiency of Opa1 in our aged mice had no effect Nrf2 on activation. This may be explained by one experiment using neurons *in vitro* and the other experiment using neurons from aged mice. It is known that Nrf2 activation is impaired with ageing, therefore the cell of an aged organism cannot effectively respond to oxidative insults via Nrf2 signalling (Zhang et al., 2015). Due to the age of the RGCs from het mice, Nrf2 activation may be impaired, which may explain why we don't see an increase in the activation of Nrf2 in this study. The fact that Nrf2 activation may be impaired with ageing may also explain why we don't see an increase in its activation in response to 670 nm light treatment in either wild-type or het mice. Our theory that 670 nm light is triggering upregulation of cell survival genes in response to transient oxidative stress may therefore involve an alternative signalling pathway in aged tissue.

Red light brought about an upregulation of DJ1 expression in the GCL and IPL of retinae from wild-type mice and in the IPL of retina from het mice. DJ1 expression is triggered by oxidative stress inducing events to protect the cell against such stress. Mutations in Opa1 in some models of ADOA can increase ROS production, therefore the RGCs from het mice may have increased DJ1 expression in an attempt to mitigate the resulting oxidative stress. Pre-treatment of the wild-type RGCs with 670 nm light appears to have increased the DJ1 expression to that of the het RGCs, an effect which

may have helped them to cope with the increased ROS that accompanies axotomy and therefore delay the associated dendropathy. Investigating the total cellular DJ1 levels in RGCs provides information on the ability of 670 nm light to induce the upregulation of DJ1, an event that may equip the cell to better cope with subsequent oxidative stress inducing events.

Upregulating endogenous DJ1 is one mechanism by which the RGCs may have increased their defence against oxidative stress. Another mechanism by which cells can increase their antioxidant defence is increasing the translocation of DJ1 to the nucleus or the mitochondria. It has been found that localisation of DJ1 to the mitochondria can bring about greater neuroprotection than its localisation to the nucleus or cytoplasm in the battle against oxidative stress (Junn et al., 2009). However, we did not find any significant difference in the number of RGCs where DJ1 was colocalised with mitochondria, in response to 670 nm light treatment in wild-type or het RGCs. This suggests that 670 nm induced neuroprotective effects by upregulating DJ1, but further enhancement of such effects was not achieved by increased mitochondrial localisation of DJ1.

There was no effect of 670 nm light on 3-nitrotyrosine expression in the GCL of wild-type retinae. Although 3-nitrotyrosine expression was upregulated in the GCL of retina from het mice, 670 nm light had no effect on the expression levels of 3-nitrotyrosine as they were up-regulated in the GCL from both sham treated and light treated het mice. Therefore, there was no involvement of 3-nitrotyrosine in the

underlying molecular mechanism 0f 670 nm light responsible for neuroprotective effects seen on aged wild-type and het mice.

Despite not revealing any effects of 670 nm light our experiment on 3-nitrotyprosine expression did reveal an interesting finding. We show for the first time that 3-nitrotyrosine is upregulated in the presence of the Opa1 mutation, as we found an increase in 3-nitrotyrosine in the GCL of aged het mice. It has been shown that 3-nitrotyrosine can elicit neurodegenerative effects *in vivo* (Mihm et al., 2001). Free 3-nitrotyrosine inhibited complex I, decreased ATP production and increased superoxide production in neurons *in vitro* (Ma et al., 2007). Therefore 3-nitrotyrosine may contribute to the mitochondrial deficits in ADOA and the associated RGC degeneration.

Although Akt is known to promote cell survival and has been shown to protect against neurodegeneration, we found that 670 nm light treatment caused a downregulation in the expression of p-Akt in the GCL of wild-type retinae. The findings were unexpected or rather counterintuitive since 670 nm light protected the RGCs from neurodegeneration, yet neuroprotection is commonly associated with an up-regulation of p-Akt. However, another study showed that preconditioning of PC12 cells with 6hr of oxygen and glucose deprivation (OGD) on day one significantly reduced basal p-Akt expression during a second exposure to OGD 24 hours later (Hillion et al., 2006). The initial exposure to OGD induced a strong increase in p-Akt after 2hr but went back to basal levels after 6 hr. Although the second exposure to

OGD increased p-Akt expression after 2 hours the increase was significantly lower than in preconditioned cells compared to non-preconditioned cells.

This may also be happening with 670 nm light treated retinae; there may have been an initial increase in p-Akt in response to 670 nm light treatment, however, after each of the five treatments, the p-Akt level in light treated retinae may have been reduced to below basal levels. This seems like a plausible explanation for why light is reducing instead of increasing levels of p-Akt, but it does not explain how reducing p-Akt can increase the RGC resistance against degeneration. Nevertheless, in the OGD model, the preconditioning that was associated with reduced levels of p-Akt was associated with a significant decreased in cell death induced by 15 hours of OGD (Hillion et al., 2006). The cell death induced by OGD was reported to be induced predominantly by apoptosis, with the involvement of caspase-3.

The authors state their awareness of the evidence that has been gathered over the past decade that consistently show the role of Akt in counteracting apoptotic stimuli and that their results seem counterintuitive, but claim that their results suggest that too much activation of Akt is damaging (Hillion et al., 2006). Decreased activation of the downstream targets of Akt can trigger apoptosis, an effect which is well known, however, this effect can also regulate cell proliferation and trigger growth arrest. In situations of stress or low energy, driving cells into a state of quiescence may provide neuroprotective effects.

A similar unexpected effect was seen with the pro-apoptotic protein caspase-3; in mice where caspase-3 was inhibited or knocked out there was increased cell death

in response to chemical and environmental stressors (Khalil et al., 2012). This reveals that caspase-3 plays an important role as a cell stress sensor, triggering responses that either result in apoptosis, as has been well documented, or triggering a cellular programme that promotes increased cell survival in response to cellular stressors.

The studies are counterintuitive regarding the effects of anti-apoptotic p-Akt and pro-apoptotic caspase-3 downregulation. The studies highlight the need for further exploration into the precise functions of these proteins as the terms anti and pro-apoptotic are over simplistic. The evidence suggests that the functions of these proteins are vast and are highly dependent on the state of the cell and its environment at the time of analysis. In terms of the effects of 670 nm light on p-Akt proteins, our results also seem counter-intuitive based on our original hypothesis. However, in support of our findings, 670 nm light has previously been shown to prevent the upregulation of p-Akt in RGC5 cells in response to 30 mM glucose, an effect that was associated with inhibition of RGC degeneration (Tang et al., 2013b).

The results reveal the enormity of the challenge presented when trying to uncover the mechanism of action of 670 nm light that is responsible for its neuroprotective effects. If the role of its molecular effectors are complex and vary depending on the state of the neuron at the time of exposure, this makes it increasingly difficult to predict the effect that 670 nm light would have on any given neuronal tissue.

Chapter 7. General discussion

7.1 Conclusions

Light at 670 nm was found to produce neuroprotective effects in models of RGC degeneration. As the therapy was found to provide resistance against RGC dendropathy in retinal explants from a mouse model of ADOA, it has great potential to be effective in preventing the RGC dendropathy that is associated with a loss in visual acuity in the ADOA mouse. However, the underlying cellular and molecular mechanism responsible for the neuroprotective effects remain unclear. In particular:

1. The effects of 670 nm light on mitochondrial function in retinal explants from 12-15 month old wild-type and het mice could not be determine due to the practical limitations of the experiment.
2. A single exposure of 670 nm with a radiant exposure of 31.7 J/cm², delivered post axotomy to young wild-type retinal explants provided partial protection from dendropathy in the entire population of RGCs for up to 16 hours *ex vivo*.
3. Five daily exposures to 670 nm light with a total radiant exposure of 22 J/cm² to the eyes of 12-15 month old wild-type and het mice prior to axotomy provide protection against *ex vivo* dendropathy in the entire population of wild-type RGCs and a partial protection from *ex vivo* dendropathy in ON-centre RGCs from wild-type and het mice.
4. Exposure of the eyes of 12-15 month old wild-type mice to a total of 22 J/cm² of 670 nm light for 5 consecutive days had no effect on NFκB activation. The same treatment in 12-15 month old het mice caused an increase in NFκB activation. No downstream effects of NFκB activation were seen on microglial

activation in 21-26 month old het mice approximately 23 J/cm² of 670 nm light treatment.

5. A total *in vivo* radiant exposure of 22 J/cm² of 670 nm light for 5 consecutive days caused an upregulation of DJ1 expression in RGCs from 12-15 month old wild-type and het mice. This treatment had no effect on Nrf2 activation or the levels of 3-nitrotyrosine in RGCs from 12-15 month old wild-type or het mice. There was a reduction in Akt activation in response to this treatment in 12-15 month old wild-type mice.

The findings of this thesis show for the first time a protective effect of 670 nm light in ON-centre RGCs from a mouse model of ADOA at an age when these RGCs show an increased susceptibility to degeneration. However, to ensure maximum protective effects are achieved from this therapy *in vivo*, a greater understanding of the mechanism of action is necessary.

7.2 Future work

7.2.1 The effect of 670 nm light on caspase 3 activation in wild-type and het mouse

In Chapter 6 we found an upregulation of DJ1 in response to 670 nm light. DJ1 has been shown to inhibit the extrinsic apoptotic pathway by blocking Fas-associated protein death domain-mediated caspase-8 activation (Fu et al., 2012). It also inhibits p53, decreases the expression of Bax and inhibits caspase-3 activation. Experimental evidence from hippocampal cultures demonstrates that caspase 3 can be activated locally within distal dendrites and dendritic spines in the absence of neuronal cell death for the regulation of spine density and dendritic morphology in a process essential for development and synaptic plasticity (Ertürk et al., 2014). Since pharmacological inhibition of caspase-3 activity rescued the dendritic spine degeneration that is associated with a deficiency in hippocampal-dependent memory in a mouse model of AD, this suggests an essential role for caspase 3 activation in the degeneration of dendritic spines that is associated with the early stages of neurodegeneration (D'amelio et al., 2011). Similarly, in post mortem brains of AD patients there was increased activated caspase 3 in the post synaptic density fractions of synapses, providing more evidence to suggest an important role for caspase3 in synapse degeneration during disease progression (Louneva et al., 2008).

Although there is experimental evidence to show that caspase 3 plays a primary role in the execution of dendritic degeneration both in neurons i*n vitro* and *in vivo,* and from post mortem neural tissue, there is insufficient evidence for the role of caspase 3 in RGC dendropathy that occurs post axotomy. Exploration of caspase 3 activation

by Binley et al. found that there was no significant increase in the expression of caspase 3 in the GCL or IPL of explanted retinae from zero to 14 days *ex vivo* (Binley et al., 2016). However, the expression level was not explored at any time point between zero and three days, a critical period during which significant dendropathy occurs. Therefore, although it is most likely, it is impossible to say whether or not caspase 3 is also required for the initiation of the *ex vivo* dendropathy that occurs post axotomy.

If the activation of caspase 3 is required for the initiation of dendritic pruning then inhibiting this activation may play a role in protecting the cells against axotomy induced dendropathy. As DJ1 can inhibit caspase 3 activation and prevent apoptosis, then the upregulation of DJ1 in the IPL in response to 670 nm light treatment may be preventing *ex vivo* dendropathy by inhibiting the activation of caspase 3 in the dendrites of wild-type and het mice.

It would be very interesting to look at the expression levels of caspase-3 at a time before significant dendropathy is established to confirm that caspase 3 is involved in triggering *ex vivo* dendritic pruning. We therefore want to look at the expression of activated caspase 3 in the GCL and IPL at a number of time points between 0 and 16 hours to establish whether or not caspase 3 activation in dendrites is involved in dendropathy. If we find that caspase 3 activation is involved, we will then select the time point with the highest expression of activated caspase 3 and chose this *ex vivo* time point to explore the effects of 670 nm light treatment on caspase 3 activation.

As we plan to do this work using immunohistochemistry, we have commenced with the optimisation of the antibody to detect activated caspase 3 on fixed frozen sections. We used mouse spleen sections to optimise the antibody (Figure 7.1). However, we need to optimise the antibody on retinal sections and establish a suitable positive control. Therefore, we treated retinal explants with 5 µM staurosporine and fixed after 4 hours *ex vivo*, cryopreserved and stored at -80 °C. We will use these retinae to establish a positive control as our starting point for this work. To back up the findings of the immunohistochemistry we will use western blot analysis. Staurosporine treated retinal explants have also been flash frozen as a positive control for the western blot of activated caspase.

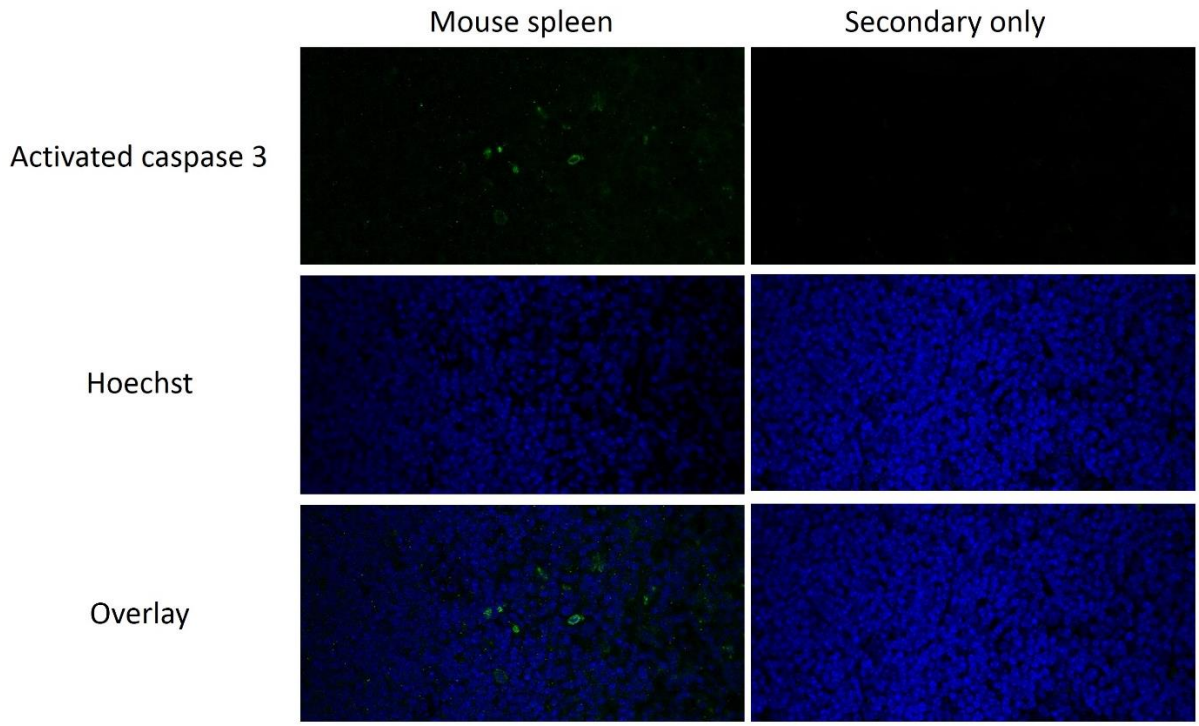

Figure 7.1: Optimisation of activated caspase 3 antibody on fixed frozen mouse spleen sections. The left column shows the mouse spleen sections that were

probed for anti-activated caspase 3. The right column shows mouse spleen sections where the primary antibody was omitted from the staining protocol.

7.2.1.1 Retinal shaves for Western blot analysis

Any results seen with immunohistochemistry should be confirmed with Western blot analysis. This was done for Akt activation, however, the results shown are based on the entire retina, yet the RGCs make up a relatively small percentage of retinal cells. Therefore, the results from the Western blot analysis is most likely coming from photoreceptors which are the most abundant cell in the retina. Since we are only interested in the RGCs it would be most useful to perform retinal shaves to localise the GCL and IPL. Western blot analysis on the RGC portion of the retina would allow for a more reliable confirmation of immunohistochemistry results.

7.2.2 Testing the effects of 670 nm light treatment on in vivo dendropathy in the het mouse

As success was found on *ex vivo* dendropathy in ON-centre RGCs from aged het mice in the therapy has high potential for success on *in vivo* dendropathy in this model. *In vivo* treatment prior to axotomy, the trigger of ex vivo dendropathy, enhanced the neuroprotective effects of the therapy. This result is very valuable when applying this therapy to the *in vivo* situation, in terms of the age at which we should begin treatment to yield the greatest neuroprotective effects. Treatment should therefore commence before significant dendropathy is present in this model. It has been reported that although dendropathy is significant after 12 months in the het mouse,

it has been shown to present as early as 10 months. Therefore, treatment should commence no later than 9 months in this model.

7.2.3 Establishing the optimal dose for maximum efficacy *in vivo* in the retina

The results of the thesis show that 670 nm light can alter the activity of various effector proteins to produce downstream neuroprotective effects. However, as we only looked at the activity of these markers at one specific time point after exposure, we do not know how long the increased activation of the effector proteins was sustained for. Additionally, the effector proteins that were not found to be activated in the RGCs after five exposures may have been activated after fewer exposures, but returned to baseline levels before fixation. Although we found beneficial effects of 670 nm light with a daily radiant exposure of 4.4 J/cm² this may not be the optimal dose for the prevention of RGC degeneration in aged het mice.

A more thorough understanding of the mechanism of action of 670 nm light is required to enable the design of an efficacious therapy for ADOA. To achieve this, the effect of different parameter combinations, such as irradiance and radiant exposure, on the molecular effectors that are responsible for the neuroprotective effects, need to be tested. A comparison could then be made to find the combination that results in the activation of the molecular effectors for the longest period of time before downregulation occurs. This would provide valuable information on the dose required per treatment and the treatment frequency.

7.2.4 Assessing the possible thermal effects of 670 nm

Red/NIR light may be producing neuroprotective effects by inducing mild heat stress in the irradiated tissue. Heat stress can upregulate the expression of heat shock proteins (HSPs) that that function as molecular chaperones, assisting the cell in the presence of stress (Jolly and Morimoto 2000). During cellular stress misfolded proteins can accumulate in the cell leading to apoptosis. Upregulation of heat shock proteins can help to repair the damaged proteins or facilitate degeneration, thereby restoring cellular homeostasis and preventing apoptosis. The mild heat produced during 670 nm light exposure may be sufficient to produce heat shock in the cells which induces the expression of heat shock proteins, with negligible damage to the irradiated tissue.

There are many different HSPs that are named according to their molecular weight. High molecular weight HSPs such as HSP60 HSP70 and HSP90 are dependent on ATP for chaperone activity whereas low molecular weight HSPs such as HSP27 are ATP independent (Lanneau et al., 2008). HSP70 and HSP90 appear to be upregulated in response to heat acclimation, which is an adaptive response that occurs in response to heat stress (Jee, 2016). It would be of great interest to monitor the expression levels of HSP70 and HSP90 in response to 670 nm light to explore a possible thermal effect of 670 nm light. However, HSPs are upregulated by a various other cellular stressors including oxidative stress which is also hypothesised to be responsible for triggering a stress response following red/NIR light exposure. Therefore, exploring the effects of 670 nm light on HSPs alone will not be sufficient to determine whether or not the therapeutic effects are as a result of a thermal effect of light exposure.

References

AHSAN, H. 2013. 3-Nitrotyrosine: a biomarker of nitrogen free radical species modified proteins in systemic autoimmunogenic conditions. *Human Immunology,* 74**,** 1392-1399.

ALAVI, M. V., BETTE, S., SCHIMPF, S., SCHUETTAUF, F., SCHRAERMEYER, U., WEHRL, H. F., RUTTIGER, L., BECK, S. C., TONAGEL, F. & PICHLER, B. J. 2007. A splice site mutation in the murine Opa1 gene features pathology of autosomal dominant optic atrophy. *Brain,* 130**,** 1029-1042.

ALAVI, M. V. & FUHRMANN, N. 2013. Dominant optic atrophy, OPA1, and mitochondrial quality control: understanding mitochondrial network dynamics. *Molecular Neurodegeneration,* 8**,** 32.

ALBARRACIN, R., EELLS, J. & VALTER, K. 2011. Photobiomodulation protects the retina from light-induced photoreceptor degeneration. *Investigative Ophthalmology & Visual Science,* 52**,** 3582-3592.

ALBARRACIN, R., NATOLI, R., RUTAR, M., VALTER, K. & PROVIS, J. 2013. 670 nm light mitigates oxygen-induced degeneration in C57BL/6J mouse retina. *BMC Neuroscience,* 14**,** 1.

ALBARRACIN, R. & VALTER, K. 2012. 670 nm red light preconditioning supports Müller cell function: evidence from the white light-induced damage model in the rat retina. *Photochemistry and Photobiology,* 88**,** 1418-1427.

ALEXANDER, C., VOTRUBA, M., PESCH, U. E., THISELTON, D. L., MAYER, S., MOORE, A., RODRIGUEZ, M., KELLNER, U., LEO-KOTTLER, B., AUBURGER, G., BHATTACHARYA, S. S. & WISSINGER, B. 2000. OPA1, encoding a dynamin-related GTPase, is mutated in autosomal dominant optic atrophy linked to chromosome 3q28. *Nature Genetics,* 26**,** 211-5.

ALEYASIN, H., ROUSSEAUX, M. W., MARCOGLIESE, P. C., HEWITT, S. J., IRRCHER, I., JOSELIN, A. P., PARSANEJAD, M., KIM, R. H., RIZZU, P., CALLAGHAN, S. M., SLACK, R. S., MAK, T. W. & PARK, D. S. 2010. DJ-1 protects the nigrostriatal axis from the neurotoxin MPTP by modulation of the AKT pathway. *Proceedings of the National Academy of Sciences,* 107(7)**,** 3186-91.

AN, H.-J., CHO, G., LEE, J.-O., PAIK, S.-G., KIM, Y. S. & LEE, H. 2013. Higd-1a interacts with Opa1 and is required for the morphological and functional integrity of mitochondria. *Proceedings of the National Academy of Sciences,* 110**,** 13014-13019.

ANDERSEN, J. K. 2004. Oxidative stress in neurodegeneration: cause or consequence? Nature Medicine, 10.

ANDO, T., Y-Y. HUANG & HAMBLIN, M. R. 2013. *LLLT for Stroke and Brain Disease. In: Hamblin MR, Huang Y-Y (eds), Handbook of Photomedicine,* Boca Raton, CRC Press.

ARIGA, H., TAKAHASHI-NIKI, K., KATO, I., MAITA, H., NIKI, T. & IGUCHI-ARIGA, S. M. 2013. Neuroprotective function of DJ-1 in Parkinson's disease. *Oxidative Medicine and Cellular Longevity,* 2013.

ARNOULT, D., GRODET, A., LEE, Y.-J., ESTAQUIER, J. & BLACKSTONE, C. 2005. Release of OPA1 during apoptosis participates in the rapid and complete release of cytochrome c and subsequent mitochondrial fragmentation. *Journal of Biological Chemistry,* 280**,** 35742-35750.

ASHWORTH, B. E., STEPHENS, E., BARTLETT, C. A., SERGHIOU, S., GIACCI, M. K., WILLIAMS, A., HART, N. S. & FITZGERALD, M. 2016. Comparative assessment of phototherapy protocols for reduction of oxidative stress in partially transected spinal cord slices undergoing secondary degeneration. *BMC Neuroscience,* 17**,** 21.

ASLAN, M. & OZBEN, T. 2004. Reactive oxygen and nitrogen species in Alzheimer's disease. *Current Alzheimer Research,* 1**,** 111-119.

BALOYANNIS, S. 2009. Dendritic pathology in Alzheimer's disease. *Journal of the Neurological Sciences,* 283**,** 153-157.

BARBONI, P., VALENTINO, M. L., LA MORGIA, C., CARBONELLI, M., SAVINI, G., DE NEGRI, A., SIMONELLI, F., SADUN, F., CAPORALI, L. & MARESCA, A. 2013. Idebenone treatment in patients with OPA1-mutant dominant optic atrophy. *Brain,* 136**,** e231-e231.

BARBOSA, M., NATOLI, R., VALTER, K., PROVIS, J. & MADDESS, T. 2014. Integral-geometry characterization of photobiomodulation effects on retinal vessel morphology. *Biomedical Optics Express,* 5**,** 2317-2332.

BAROLET, D. Light-emitting diodes (LEDs) in dermatology. Seminars in Cutaneous Medicine and Surgery, 2008. Elsevier, 227-238.

BAULAC, S., LU, H., STRAHLE, J., YANG, T., GOLDBERG, M. S., SHEN, J., SCHLOSSMACHER, M. G., LEMERE, C. A., LU, Q. & XIA, W. 2009. Increased DJ-1 expression under oxidative stress and in Alzheimer's disease brains. *Molecular Neurodegeneration,* 4**,** 12.

BEGUM, R., POWNER, M. B., HUDSON, N., HOGG, C. & JEFFERY, G. 2013. Treatment with 670 nm light up regulates cytochrome C oxidase expression and reduces inflammation in an age-related macular degeneration model. *PloS one,* 8**,** e57828.

BEIRNE, K., ROZANOWSKA, M. & VOTRUBA, M. 2016. Red light treatment in an axotomy model of neurodegeneration. *Photochemistry and Photobiology*. 92(4), 624-631.

BERRY, R. H., QU, J., JOHN, S. W., HOWELL, G. R. & JAKOBS, T. C. 2015. Synapse Loss and Dendrite Remodeling in a Mouse Model of Glaucoma. *PloS one,* 10**,** e0144341.

BERTHOLET, A. M., MILLET, A. M., GUILLERMIN, O., DALOYAU, M., DAVEZAC, N., MIQUEL, M.-C. & BELENGUER, P. 2013. OPA1 loss of function affects in vitro neuronal maturation. *Brain,* 136**,** 1518-1533.

BERTRAM, L. & TANZI, R. E. 2005. The genetic epidemiology of neurodegenerative disease. *The Journal of Clinical Investigation,* 115**,** 1449-1457.

Binley, K.E., Ng, W.S., Tribble, J.R., Song, B. and Morgan, J.E., 2014. Sholl analysis: a quantitative comparison of semi-automated methods. Journal of neuroscience methods, 225, 65-70.

BINLEY, K. E., NG, W. S., BARDE, Y. A., SONG, B. & MORGAN, J. E. 2016. Brain-derived neurotrophic factor prevents dendritic retraction of adult mouse retinal ganglion cells. *European Journal of Neuroscience,* 44**,** 2028-2039.

BJÖRKBLOM, B., MAPLE-GRØDEM, J., PUNO, M. R., ODELL, M., LARSEN, J. P. & MØLLER, S. G. 2014. Reactive Oxygen Species-Mediated DJ-1 Monomerization Modulates Intracellular Trafficking Involving Karyopherin β2. *Molecular and Cellular Biology,* 34**,** 3024-3040.

BROWN, G. C. & BORUTAITE, V. 2004. Inhibition of mitochondrial respiratory complex I by nitric oxide, peroxynitrite and S-nitrosothiols. *Biochimica et Biophysica Acta (BBA) - Bioenergetics,* 1658**,** 44-49.

BRUNET, A., DATTA, S. R. & GREENBERG, M. E. 2001. Transcription-dependent and -independent control of neuronal survival by the PI3K–Akt signaling pathway. *Current Opinion in Neurobiology,* 11**,** 297-305.

BYRNES, K. R., WAYNANT, R. W., ILEV, I. K., WU, X., BARNA, L., SMITH, K., HECKERT, R., GERST, H. & ANDERS, J. J. 2005a. Light promotes regeneration and functional recovery and alters the immune response after spinal cord injury. *Lasers in Surgery and Medicine,* 36**,** 171-185.

BYRNES, K. R., WAYNANT, R. W., ILEV, I. K., WU, X., BARNA, L., SMITH, K., HECKERT, R., GERST, H. & ANDERS, J. J. 2005b. Light promotes regeneration and functional recovery and alters the immune response after spinal cord injury. *Lasers in Surgery Medicine,* 36**,** 171-85.

CALABRESE, V., MANCUSO, C., CALVANI, M., RIZZARELLI, E., BUTTERFIELD, D. A. & STELLA, A. M. G. 2007. Nitric oxide in the ventral nervous system: Neuroprotection versus neurotoxicity. *Nature Reviews Neuroscience,* 8**,** 766-775.

CALAZA, K. C., KAM, J. H., HOGG, C. & JEFFERY, G. 2015. Mitochondrial decline precedes phenotype development in the complement factor H mouse model of retinal degeneration but can be corrected by near infrared light. *Neurobiology of Aging,* 36**,** 2869-2876.

CASSINA, A. & RADI, R. 1996. Differential inhibitory action of nitric oxide and peroxynitrite on mitochondrial electron transport. *Archives of Biochemistry and Biophysics,* 328**,** 309-316.

CHEN, A. C., ARANY, P. R., HUANG, Y. Y., TOMKINSON, E. M., SHARMA, S. K., KHARKWAL, G. B., SALEEM, T., MOONEY, D., YULL, F. E., BLACKWELL, T. S. & HAMBLIN, M. R. 2011. Low-level laser therapy activates NF-kB via generation of reactive oxygen species in mouse embryonic fibroblasts. *PLoS One,* 6**,** e22453.

CHEN, H. & CHAN, D. C. 2005. Emerging functions of mammalian mitochondrial fusion and fission. *Human Molecular Genetics,* 14**,** R283-R289.

CHEN, H. & CHAN, D. C. 2009. Mitochondrial dynamics–fusion, fission, movement, and mitophagy–in neurodegenerative diseases. *Human Molecular Genetics,* 18**,** R169-R176.

CHEN, L., LIU, T., TRAN, A., LU, X., TOMILOV, A. A., DAVIES, V., CORTOPASSI, G., CHIAMVIMONVAT, N., BERS, D. M. & VOTRUBA, M. 2012. OPA1 mutation and

late-onset cardiomyopathy: mitochondrial dysfunction and mtDNA instability. *Journal of the American Heart Association,* 1(5), e003012.

CHEN, Y., JIA, X., WANG, P., XIAO, X., LI, S., GUO, X. & ZHANG, Q. 2013. Mutation survey of the optic atrophy 1 gene in 193 Chinese families with suspected hereditary optic neuropathy. *Molecular Vision,* 19**,** 292.

CHOUCHANI, E. T., METHNER, C., NADTOCHIY, S. M., LOGAN, A., PELL, V. R., DING, S., JAMES, A. M., COCHEMÉ, H. M., REINHOLD, J. & LILLEY, K. S. 2013. Cardioprotection by S-nitrosation of a cysteine switch on mitochondrial Complex I. *Nature Medicine,* 19**,** 753.

CHUNG, H., DAI, T., SHARMA, S. K., HUANG, Y.-Y., CARROLL, J. D. & HAMBLIN, M. R. 2012. The nuts and bolts of low-level laser (light) therapy. *Annals of Biomedical Engineering,* 40**,** 516-533.

CIPOLAT, S., DE BRITO, O. M., DAL ZILIO, B. & SCORRANO, L. 2004. OPA1 requires mitofusin 1 to promote mitochondrial fusion. *Proceedings of the National Academy of Sciences of the United States of America,* 101**,** 15927-15932.

CREWS, F. T. & VETRENO, R. P. 2016. Mechanisms of neuroimmune gene induction in alcoholism. *Psychopharmacology,* 233**,** 1543-1557.

D'AMELIO, M., CAVALLUCCI, V., MIDDEI, S., MARCHETTI, C., PACIONI, S., FERRI, A., DIAMANTINI, A., DE ZIO, D., CARRARA, P. & BATTISTINI, L. 2011. Caspase-3 triggers early synaptic dysfunction in a mouse model of Alzheimer's disease. *Nature Neuroscience,* 14**,** 69.

DARLOT, F., MORO, C., MASSRI, N., CHABROL, C., JOHNSTONE, D. M., REINHART, F., AGAY, D., TORRES, N., BEKHA, D. & AUBOIROUX, V. 2016. Near-infrared light is neuroprotective in a monkey model of Parkinson disease. *Annals of Neurology,* 79**,** 59-75.

DAVID, J. A., RIFKIN, W. J., RABBANI, P. S. & CERADINI, D. J. 2017. The Nrf2/Keap1/ARE Pathway and Oxidative Stress as a Therapeutic Target in Type II Diabetes Mellitus. *Journal of Diabetes Research,* 2017.

DAVIES, V. & VOTRUBA, M. 2006. Focus on molecules: the OPA1 protein. *Experimental eye research,* 83**,** 1003-1004.

DAVIES, V. J., HOLLINS, A. J., PIECHOTA, M. J., YIP, W., DAVIES, J. R., WHITE, K. E., NICOLS, P. P., BOULTON, M. E. & VOTRUBA, M. 2007. Opa1 deficiency in a mouse model of autosomal dominant optic atrophy impairs mitochondrial morphology, optic nerve structure and visual function. *Human Molecular Genetics,* 16**,** 1307-1318.

DELETTRE, C., LENAERS, G., PELLOQUIN, L., BELENGUER, P. & HAMEL, C. P. 2002. OPA1 (Kjer type) dominant optic atrophy: a novel mitochondrial disease. *Molecular Genetics and Metabolism,* 75**,** 97-107.

DESMET, K. D., PAZ, D. A., CORRY, J. J., EELLS, J. T., WONG-RILEY, M. T., HENRY, M. M., BUCHMANN, E. V., CONNELLY, M. P., DOVI, J. V. & LIANG, H. L. 2006. Clinical and experimental applications of NIR-LED photobiomodulation. *Photomedicine and Laser Therapy,* 24**,** 121-128.

DI POLO, A. 2015. Dendrite pathology and neurodegeneration: focus on mTOR. *Neural Regeneration Research,* 10**,** 559.

DIJKHUIZEN, P. A. & GHOSH, A. 2005. BDNF regulates primary dendrite formation in cortical neurons via the PI3-kinase and MAP kinase signaling pathways. *Developmental Neurobiology,* 62**,** 278-288.

DONG, T., ZHANG, Q., HAMBLIN, M. R. & WU, M. X. 2015a. Low-level light in combination with metabolic modulators for effective therapy of injured brain. *Journal of Cerebral Blood Flow & Metabolism*. 35(9), 1435-1444.

DONG, T., ZHANG, Q., HAMBLIN, M. R. & WU, M. X. Low level light in combination with metabolic modulators for effective therapy. SPIE BiOS, 2015b. International Society for Optics and Photonics, 93090A-93090A-22.

EELLS, J., HENRY, M., SUMMERFELT, P., WONG-RILEY, M., BUCHMANN, E., KANE, M., WHELAN, N. & WHELAN, H. 2003. Therapeutic photobiomodulation for methanol-induced retinal toxicity. *Proceedings of the National Academy of Sciences,* 100**,** 3439-3444.

EIBERG, H., HANSEN, L., KJER, B., HANSEN, T., PEDERSEN, O., BILLE, M., ROSENBERG, T. & TRANEBJAERG, L. 2006. Autosomal dominant optic atrophy associated with hearing impairment and impaired glucose regulation caused by a missense mutation in the WFS1 gene. *Journal of Medical Genetics,* 43**,** 435-40.

ERTÜRK, A., WANG, Y. & SHENG, M. 2014. Local pruning of dendrites and spines by caspase-3-dependent and proteasome-limited mechanisms. *Journal of Neuroscience,* 34**,** 1672-1688.

Facecchia, K., Fochesato, L.A., Ray, S.D., Stohs, S.J. and Pandey, S., 2011. Oxidative toxicity in neurodegenerative diseases: role of mitochondrial dysfunction and therapeutic strategies. *Journal of Toxicology*, *2011*.

FERGER, A. I., CAMPANELLI, L., REIMER, V., MUTH, K. N., MERDIAN, I., LUDOLPH, A. C. & WITTING, A. 2010. Effects of mitochondrial dysfunction on the immunological properties of microglia. *Journal of Neuroinflammation,* 7**,** 1.

FERNANDES, K. P. S., SOUZA, N. H. C., MESQUITA-FERRARI, R. A., DA SILVA, D. D. F. T., ROCHA, L. A., ALVES, A. N., DE BRITO SOUSA, K., BUSSADORI, S. K., HAMBLIN, M. R. & NUNES, F. D. 2015. Photobiomodulation with 660-nm and 780-nm laser on activated J774 macrophage-like cells: Effect on M1 inflammatory markers. *Journal of Photochemistry and Photobiology B: Biology,* 153**,** 344-351.

FERRARESI, C., DE SOUSA, M. V. P., HUANG, Y.-Y., BAGNATO, V. S., PARIZOTTO, N. A. & HAMBLIN, M. R. 2015a. Time response of increases in ATP and muscle resistance to fatigue after low-level laser (light) therapy (LLLT) in mice. *Lasers in Medical Science,* 30**,** 1259-1267.

FERRARESI, C., PARIZOTTO, N. A., PIRES DE SOUSA, M. V., KAIPPERT, B., HUANG, Y. Y., KOISO, T., BAGNATO, V. S. & HAMBLIN, M. R. 2015b. Light-emitting diode therapy in exercise-trained mice increases muscle performance, cytochrome c oxidase activity, ATP and cell proliferation. *Journal of Biophotonics,* 8**,** 740-754.

FINSEN, N. 1901. The treatment of lupus vulgaris by concentrated chemical rays. *Phototherapy. London: Edward Arnold,* 27**,** 73.

FITZGERALD, M., BARTLETT, C. A., PAYNE, S. C., HART, N. S., RODGER, J., HARVEY, A. R. & DUNLOP, S. A. 2010. Near infrared light reduces oxidative stress and preserves function in CNS tissue vulnerable to secondary degeneration following partial transection of the optic nerve. *Journal of Neurotrauma,* 27**,** 2107-2119.

FITZGERALD, M., HODGETTS, S., VAN DEN HEUVEL, C., NATOLI, R., HART, N. S., VALTER, K., HARVEY, A. R., VINK, R., PROVIS, J. & DUNLOP, S. A. 2013. Red/near-infrared irradiation therapy for treatment of central nervous system injuries and disorders. *Reviews in the Neurosciences,* 24**,** 205-226.

FÖRSTERMANN, U. & SESSA, W. C. 2012. Nitric oxide synthases: regulation and function. *European Heart Journal,* 33**,** 829-837.

FRIEDMAN, E. & KUWABARA, T. 1968. The retinal pigment epithelium: IV. The damaging effects of radiant energy. *Archives of Ophthalmology,* 80**,** 265-279.

FU, K., REN, H., WANG, Y., FEI, E., WANG, H. & WANG, G. 2012. DJ-1 inhibits TRAIL-induced apoptosis by blocking pro-caspase-8 recruitment to FADD. *Oncogene,* 31**,** 1311.

GAN, W.-B., GRUTZENDLER, J., WONG, W. T., WONG, R. O. & LICHTMAN, J. W. 2000. Multicolor "DiOlistic" labeling of the nervous system using lipophilic dye combinations. *Neuron,* 27**,** 219-225.

GAVISH, L., PEREZ, L. S., REISSMAN, P. & GERTZ, S. D. 2008. Irradiation with 780 nm diode laser attenuates inflammatory cytokines but upregulates nitric oxide in lipopolysaccharide-stimulated macrophages: Implications for the prevention of aneurysm progression. *Lasers in Surgery and Medicine,* 40**,** 371-378.

GERTLER, T. S., CHAN, C. S. & SURMEIER, D. J. 2008. Dichotomous anatomical properties of adult striatal medium spiny neurons. *The Journal of Neuroscience,* 28**,** 10814-10824.

GIACCI, M. K., WHEELER, L., LOVETT, S., DISHINGTON, E., MAJDA, B., BARTLETT, C. A., THORNTON, E., HARFORD-WRIGHT, E., LEONARD, A., VINK, R., HARVEY, A. R., PROVIS, J., DUNLOP, S. A., HART, N. S., HODGETTS, S., NATOLI, R., VAN DEN HEUVEL, C. & FITZGERALD, M. 2014. Differential effects of 670 and 830 nm red near infrared irradiation therapy: a comparative study of optic nerve injury, retinal degeneration, traumatic brain and spinal cord injury. *PLoS One,* 9**,** e104565.

GKOTSI, D., BEGUM, R., SALT, T., LASCARATOS, G., HOGG, C., CHAU, K.-Y., SCHAPIRA, A. H. & JEFFERY, G. 2014. Recharging mitochondrial batteries in old eyes. Near infra-red increases ATP. *Experimental Eye Research,* 122**,** 50-53.

GLOIRE, G., LEGRAND-POELS, S. & PIETTE, J. 2006. NF-κB activation by reactive oxygen species: fifteen years later. *Biochemical Pharmacology,* 72**,** 1493-1505.

GRAY, J. J., ZOMMER, A. E., BOUCHARD, R. J., DUVAL, N., BLACKSTONE, C. & LINSEMAN, D. A. 2013. N-terminal cleavage of the mitochondrial fusion GTPase OPA1 occurs via a caspase-independent mechanism in cerebellar granule neurons exposed to oxidative or nitrosative stress. *Brain Research,* 1494**,** 28-43.

GREEN, D. R., GALLUZZI, L. & KROEMER, G. 2011. Mitochondria and the autophagy–inflammation–cell death axis in organismal aging. *Science,* 333**,** 1109-1112.

HAMBLIN, M. R. & DEMIDOVA, T. N. Mechanisms of low level light therapy. Biomedical Optics 2006, 2006. International Society for Optics and Photonics, 614001-614001-12.

HAMBLIN, M. R., TABOADA, L. D. & HUANG, Y.-Y. 2016. Chapter 21 Transcranial Low-Level Laser (Light) Therapy for Stroke and Traumatic Brain Injury in Animal Models. *Handbook of Low-Level Laser Therapy.* Pan Stanford Publishing Pte. Ltd.

HARTWIG, H. & VAN VEEN, T. 1979. Spectral characteristics of visible radiation penetrating into the brain and stimulating extraretinal photoreceptors. *Journal of Comparative Physiology,* 130**,** 277-282.

HARWERTH, R. & SPERLING, H. 1975. Effects of intense visible radiation on the increment-threshold spectral sensitivity of the rhesus monkey eye. *Vision Research,* 15**,** 1193-1204.

HEAD, B., GRIPARIC, L., AMIRI, M., GANDRE-BABBE, S. & VAN DER BLIEK, A. M. 2009. Inducible proteolytic inactivation of OPA1 mediated by the OMA1 protease in mammalian cells. *The Journal of Cell Biology,* 187**,** 959-966.

HEIDUSCHKA, P., SCHNICHELS, S., FUHRMANN, N., HOFMEISTER, S., SCHRAERMEYER, U., WISSINGER, B. & ALAVI, M. V. 2010. Electrophysiological and histologic assessment of retinal ganglion cell fate in a mouse model for OPA1-associated autosomal dominant optic atrophy. *Investigative Ophthalmology & Visual Science,* 51**,** 1424-1431.

HEMISH, J., NAKAYA, N., MITTAL, V. & ENIKOLOPOV, G. 2003. Nitric oxide activates diverse signaling pathways to regulate gene expression. *Journal of Biological Chemistry*.

HILLION, J. A., LI, Y., MARIE, D., TAKANOHASHI, A., KLIMANIS, D., BARKER, J. L. & HALLENBEEK, J. M. 2006. Involvement of Akt in preconditioning-induced tolerance to ischemia in PC12 cells. *Journal of Cerebral Blood Flow & Metabolism,* 26**,** 1323-1331.

HUANG, Y. Y., NAGATA, K. & TEDFORD, C. E. 2014. Low-level laser therapy (810 nm) protects primary cortical neurons against excitotoxicity in vitro. *Journal of Biophotonics,* 7**,** 656-664.

HUNTER, J. J., MORGAN, J. I., MERIGAN, W. H., SLINEY, D. H., SPARROW, J. R. & WILLIAMS, D. R. 2012. The susceptibility of the retina to photochemical damage from visible light. *Progress in Retinal and Eye Research,* 31**,** 28-42.

IKEGAMI, K. & KOIKE, T. 2003. Non-apoptotic neurite degeneration in apoptotic neuronal death: pivotal role of mitochondrial function in neurites. *Neuroscience,* 122**,** 617-626.

IM, J.-Y., LEE, K.-W., WOO, J.-M., JUNN, E. & MOURADIAN, M. M. 2012. DJ-1 induces thioredoxin 1 expression through the Nrf2 pathway. *Human Molecular Genetics,* 21**,** 3013-3024.

INNAMORATO, N. G., LASTRES-BECKER, I. & CUADRADO, A. 2009. Role of microglial redox balance in modulation of neuroinflammation. *Current Opinion in Neurology,* 22**,** 308-314.

IVANDIC, B. T. & IVANDIC, T. 2008. Low-level laser therapy improves vision in patients with age-related macular degeneration. *Photomedicine and Laser Surgery,* 26**,** 241-245.

IYER, S. S. & CHENG, G. 2012. Role of interleukin 10 transcriptional regulation in inflammation and autoimmune disease. *Critical Reviews™ in Immunology,* 32.

JAGDEO, J. R., ADAMS, L. E., BRODY, N. I. & SIEGEL, D. M. 2012. Transcranial red and near infrared light transmission in a cadaveric model. *PloS one,* 7**,** e47460.

Jee, H., 2016. Size dependent classification of heat shock proteins: a mini-review. Journal of exercise rehabilitation, 12(4), p.255.

JOHNSTON, P. B., GASTER, R. N., SMITH, V. C. & TRIPATHI, R. C. 1979. A clinicopathologic study of autosomal dominant optic atrophy. *American Journal of Ophthalmology,* 88**,** 868-75.

JOHNSTONE, D., EL MASSRI, N., MORO, C., SPANA, S., WANG, X., TORRES, N., CHABROL, C., DE JAEGER, X., REINHART, F. & PURUSHOTHUMAN, S. 2014. Indirect application of near infrared light induces neuroprotection in a mouse model of parkinsonism–an abscopal neuroprotective effect. *Neuroscience,* 274**,** 93-101.

Jolly, C. and Morimoto, R.I., 2000. Role of the heat shock response and molecular chaperones in oncogenesis and cell death. Journal of the National Cancer Institute, 92(19), pp.1564-1572.

JUNN, E., JANG, W. H., ZHAO, X., JEONG, B. S. & MOURADIAN, M. M. 2009. Mitochondrial localization of DJ-1 leads to enhanced neuroprotection. *Journal of Neuroscience Research,* 87**,** 123-129.

KALOGERIS, T., BAINES, C. P., KRENZ, M. & KORTHUIS, R. J. 2012. Cell biology of ischemia/reperfusion injury. *International Review of Cell and Molecular Biology,* 298**,** 229.

KALTSCHMIDT, B., WIDERA, D. & KALTSCHMIDT, C. 2005. Signaling via NF-κB in the nervous system. *Biochimica et Biophysica Acta (BBA) - Molecular Cell Research,* 1745**,** 287-299.

KAMEI, S., CHEN-KUO-CHANG, M., CAZEVIEILLE, C., LENAERS, G., OLICHON, A., BÉLENGUER, P., ROUSSIGNOL, G., RENARD, N., EYBALIN, M. & MICHELIN, A. 2005. Expression of the Opa1 mitochondrial protein in retinal ganglion cells: its downregulation causes aggregation of the mitochondrial network. *Investigative Ophthalmology & Visual Science,* 46**,** 4288-4294.

KANG, K. W., CHOI, S. H. & KIM, S. G. 2002. Peroxynitrite activates NF-E2-related factor 2/antioxidant response element through the pathway of phosphatidylinositol 3-kinase: The role of nitric oxide synthase in rat glutathione S-transferase A2 induction. *Nitric Oxide,* 7**,** 244-253.

KARU, T. 1999. Primary and secondary mechanisms of action of visible to near-IR radiation on cells. *Journal of Photochemistry and photobiology B: Biology,* 49**,** 1-17.

KARU, T. 2008. Action spectra: their importance for low level light therapy. *Photobiological Sciences Online (KC Smith, editor) American Society for Photobiology, http://www. photobiology. info*.

KESZLER, A., BRANDAL, G., BAUMGARDT, S., GE, Z.-D., PRATT, P. F., RIESS, M. L. & BIENENGRAEBER, M. 2014. Far red/near infrared light-induced protection against cardiac ischemia and reperfusion injury remains intact under diabetic conditions and is independent of nitric oxide synthase. *Frontiers in Physiology,* 5**,** 305.

KETTENMANN, H., KIRCHHOFF, F. & VERKHRATSKY, A. 2013. Microglia: new roles for the synaptic stripper. *Neuron,* 77**,** 10-18.

KHALIL, H., PELTZER, N., WALICKI, J., YANG, J.-Y., DUBUIS, G., GARDIOL, N., HELD, W., BIGLIARDI, P., MARSLAND, B. & LIAUDET, L. 2012. Caspase-3 protects stressed organs against cell death. *Molecular and Cellular Biology,* 32**,** 4523-4533.

KHUMAN, J., ZHANG, J., PARK, J., CARROLL, J. D., DONAHUE, C. & WHALEN, M. J. 2012. Low-level laser light therapy improves cognitive deficits and inhibits microglial activation after controlled cortical impact in mice. *Journal of neurotrauma,* 29**,** 408-417.

KIM, I.-J., BECK, H. N., LEIN, P. J. & HIGGINS, D. 2002. Interferon γ induces retrograde dendritic retraction and inhibits synapse formation. *The Journal of Neuroscience,* 22**,** 4530-4539.

KJER, P., JENSEN, O. A. & KLINKEN, L. 1983. Histopathology of eye, optic nerve and brain in a case of dominant optic atrophy. *Acta Ophthalmol,* 61**,** 300-12.

KOIKE, T., YANG, Y., SUZUKI, K. & ZHENG, X. 2008. Axon & dendrite degeneration: its mechanisms and protective experimental paradigms. *Neurochemistry International,* 52**,** 751-760.

KOKKINOPOULOS, I., COLMAN, A., HOGG, C., HECKENLIVELY, J. & JEFFERY, G. 2013. Age-related retinal inflammation is reduced by 670 nm light via increased mitochondrial membrane potential. *Neurobiology of Aging,* 34**,** 602-609.

KOORAGAYALA, K., GOTOH, N., COGLIATI, T., NELLISSERY, J., KADEN, T. R., FRENCH, S., BALABAN, R., LI, W., COVIAN, R. & SWAROOP, A. 2015. Quantification of Oxygen Consumption in Retina Ex Vivo Demonstrates Limited Reserve Capacity of Photoreceptor MitochondriaQuantification of Retinal Oxygen Consumption. *Investigative Ophthalmology & Visual Science,* 56**,** 8428-8436.

KUMAR, V., ZHANG, M.-X., SWANK, M. W., KUNZ, J. & WU, G.-Y. 2005. Regulation of dendritic morphogenesis by Ras–PI3K–Akt–mTOR and Ras–MAPK signaling pathways. *Journal of Neuroscience,* 25**,** 11288-11299.

LANDES, T., EMORINE, L. J., COURILLEAU, D., ROJO, M., BELENGUER, P. & ARNAUNÉ-PELLOQUIN, L. 2010. The BH3-only Bnip3 binds to the dynamin Opa1 to promote mitochondrial fragmentation and apoptosis by distinct mechanisms. *EMBO reports,* 11**,** 459-465.

LANGHAMMER, C. G., PREVITERA, M. L., SWEET, E. S., SRAN, S. S., CHEN, M. & FIRESTEIN, B. L. 2010. Automated Sholl analysis of digitized neuronal morphology at multiple scales: whole cell Sholl analysis versus Sholl analysis of arbor subregions. *Cytometry Part A,* 77**,** 1160-1168.

Lanneau, D., Brunet, M., Frisan, E., Solary, E., Fontenay, M. and Garrido, C., 2008. Heat shock proteins: essential proteins for apoptosis regulation. Journal of cellular and molecular medicine, 12(3), pp.743-761.

LAPCHAK, P. A., SALGADO, K. F., CHAO, C. H. & ZIVIN, J. A. 2007. Transcranial near-infrared light therapy improves motor function following embolic strokes in rabbits: An extended therapeutic window study using continuous and pulse frequency delivery modes. *Neuroscience,* 148**,** 907-914.

LAWRENCE, T. 2009. The Nuclear Factor NF-κB Pathway in Inflammation. *Cold Spring Harbor Perspectives in Biology,* 1**,** a001651.

LEE, Y.-J., JEONG, S.-Y., KARBOWSKI, M., SMITH, C. L. & YOULE, R. J. 2004. Roles of the mammalian mitochondrial fission and fusion mediators Fis1, Drp1, and Opa1 in apoptosis. *Molecular Biology of the Cell,* 15**,** 5001-5011.

LENAERS, G., HAMEL, C., DELETTRE, C., AMATI-BONNEAU, P., PROCACCIO, V., BONNEAU, D., REYNIER, P. & MILEA, D. 2012. Dominant optic atrophy. *Orphanet Journal of Rare Diseases,* 7**,** 46.

LENAERS, G., REYNIER, P., ELACHOURI, G., SOUKKARIEH, C., OLICHON, A., BELENGUER, P., BARICAULT, L., DUCOMMUN, B., HAMEL, C. & DELETTRE, C. 2009. OPA1 functions in mitochondria and dysfunctions in optic nerve. *The International Journal of Biochemistry & Cell Biology,* 41**,** 1866-1874.

LENAZ, G. 2001. The mitochondrial production of reactive oxygen species: mechanisms and implications in human pathology. *IUBMB Life,* 52**,** 159-164.

LEUNG, M. C., LO, S. C., SIU, F. K. & SO, K. F. 2002. Treatment of experimentally induced transient cerebral ischemia with low energy laser inhibits nitric oxide synthase activity and up-regulates the expression of transforming growth factor-beta 1. *Lasers in Surgery and Medicine,* 31**,** 283-288.

LEV, N., ICKOWICZ, D., MELAMED, E. & OFFEN, D. 2008. Oxidative insults induce DJ-1 upregulation and redistribution: Implications for neuroprotection. *NeuroToxicology,* 29**,** 397-405.

Liang, H.L., Whelan, H.T., Eells, J.T. and Wong-Riley, M.T., 2008. Near-infrared light via light-emitting diode treatment is therapeutic against rotenone-and 1-methyl-4-phenylpyridinium ion-induced neurotoxicity. Neuroscience, 153(4), pp.963-974.

LIAUDET, L., VASSALLI, G. & PACHER, P. 2009. Role of peroxynitrite in the redox regulation of cell signal transduction pathways. *Frontiers in Bioscience: A Journal and Virtual Library,* 14**,** 4809.

LIEVEN, C. & LEVIN, L. 2007. Tools for studying early events in optic neuropathies. *Eye,* 21**,** S21.

LIM, J., SANDERS, R. A., SNYDER, A. C., EELLS, J. T., HENSHEL, D. S. & WATKINS III, J. B. 2010. Effects of low-level light therapy on streptozotocin-induced diabetic kidney. *Journal of Photochemistry and Photobiology B: Biology,* 99**,** 105-110.

LIPTON, S. A., CHOI, Y.-B., PAN, Z.-H., LEI, S. Z., CHEN, H.-S. V., SUCHER, N. J., LOSCALZO, J., SINGEL, D. J. & STAMLER, J. S. 1993. A redox-based mechanism for the neuroprotective and neurodestructive effects of nitric oxide and related nitroso-compounds. *Nature*, 364(64380, pp. 626-632.

LIU, M., GUO, L., SALT, T. & CORDEIRO, M. 2010. Dendritic Changes in the Retinal Ganglion Cells in a Rat Model of Experimental Glaucoma. *Investigative Ophthalmology & Visual Science,* 51**,** 5217-5217.

LOHR, N. L., KESZLER, A., PRATT, P., BIENENGRABER, M., WARLTIER, D. C. & HOGG, N. 2009. Enhancement of nitric oxide release from nitrosyl hemoglobin and nitrosyl myoglobin by red/near infrared radiation: potential role in cardioprotection. *Journal of Molecular and Cellular Cardiology,* 47**,** 256-263.

LOUNEVA, N., COHEN, J. W., HAN, L.-Y., TALBOT, K., WILSON, R. S., BENNETT, D. A., TROJANOWSKI, J. Q. & ARNOLD, S. E. 2008. Caspase-3 is enriched in postsynaptic densities and increased in Alzheimer's disease. *The American Journal of Pathology,* 173**,** 1488-1495.

MA, Q. 2013. Role of nrf2 in oxidative stress and toxicity. *Annual Review of Pharmacology and Toxicology,* 53**,** 401-426.

MA, T. C., MIHM, M. J., BAUER, J. A. & HOYT, K. R. 2007. Bioenergetic and oxidative effects of free 3-nitrotyrosine in culture: selective vulnerability of dopaminergic neurons and increased sensitivity of non-dopaminergic neurons to dopamine oxidation. *Journal of Neurochemistry,* 103**,** 131-44.

MADEIRA, M. H., BOIA, R., SANTOS, P. F., AMBRÓSIO, A. F. & SANTIAGO, A. R. 2015. Contribution of microglia-mediated neuroinflammation to retinal degenerative diseases. *Mediators of Inflammation,* 2015.

MAGHARIOUS, M. M., D'ONOFRIO, P. M. & KOEBERLE, P. D. 2011. Optic nerve transection: a model of adult neuron apoptosis in the central nervous system. *Journal of visualized experiments: JoVE*, 51.

MARTINOU, J. & YOULE, R. 2006. Which came first, the cytochrome c release or the mitochondrial fission? *Cell Death & Differentiation,* 13**,** 1291-1295.

MCDONAGH, A. F. 2001. Phototherapy: from ancient Egypt to the new millennium. *Journal of Perinatology,* 21(s1), p.S7.

MERRY, G., DEVENYI, R., DOTSON, R., MARKOWITZ, S. & REYES, S. Treatment of dry age-related-macular degeneration with photobiomodulation. Proceedings of the 9th WALT Congress, 2013. Medimond, Bologna, 81-84.

MERRY, G. F., MUNK, M. R., DOTSON, R. S., WALKER, M. G. & DEVENYI, R. G. 2016. Photobiomodulation reduces drusen volume and improves visual acuity and contrast sensitivity in dry age-related macular degeneration. *Acta Ophthalmologica*.

MESTER, E., SZENDE, B., SPIRY, T. & SCHER, A. 1971. Stimulation of wound healing by laser rays. *Acta Chirurgica Academiae Scientiarum Hungaricae,* 13**,** 315-324.

MIHM, M. J., SCHANBACHER, B. L., WALLACE, B. L., WALLACE, L. J., URETSKY, N. J. & BAUER, J. A. 2001. Free 3-nitrotyrosine causes striatal neurodegeneration in vivo. *Journal of Neuroscience,* 21**,** Rc149.

MILLET, A., BERTHOLET, A. M., DALOYAU, M., REYNIER, P., GALINIER, A., DEVIN, A., WISSINGUER, B., BELENGUER, P. & DAVEZAC, N. 2016. Loss of functional OPA1 unbalances redox state: implications in dominant optic atrophy pathogenesis. *Annals of Clinical and Translational Neurology,* 3**,** 408-421.

MORGAN, M. J. & LIU, Z.-G. 2011. Crosstalk of reactive oxygen species and NF-κB signaling. *Cell Research,* 21**,** 103-115.

MUILI, K. A., GOPALAKRISHNAN, S., EELLS, J. T. & LYONS, J.-A. 2013. Photobiomodulation induced by 670 nm light ameliorates MOG35-55

induced EAE in female C57BL/6 mice: a role for remediation of nitrosative stress. *PloS one,* 8**,** e67358.

MUILI, K. A., GOPALAKRISHNAN, S., MEYER, S. L., EELLS, J. T. & LYONS, J.-A. 2012. Amelioration of experimental autoimmune encephalomyelitis in C57BL/6 mice by photobiomodulation induced by 670 nm light. *PloS one,* 7**,** e30655.

NAESER, M. A. & HAMBLIN, M. R. 2011. Potential for transcranial laser or LED therapy to treat stroke, traumatic brain injury, and neurodegenerative disease. *Photomedicine and Laser Surgery,* 29**,** 443-446.

NAESER, M. A. & HAMBLIN, M. R. 2015. Traumatic brain injury: a major medical problem that could be treated using transcranial, red/near-infrared LED photobiomodulation. *Photomedicine and Laser Surgery,* 33**,** 443-446.

NAESER, M. A., MARTIN, P. I., HO, M. D., KRENGEL, M. H., BOGDANOVA, Y., KNIGHT, J. A., YEE, M. K., ZAFONTE, R., FRAZIER, J. & HAMBLIN, M. R. 2016. Transcranial, Red/Near-Infrared Light-Emitting Diode Therapy to Improve Cognition in Chronic Traumatic Brain Injury. *Photomedicine and Laser Surgery,* 34**,** 610-626.

NAESER, M. A., ZAFONTE, R., KRENGEL, M. H., MARTIN, P. I., FRAZIER, J., HAMBLIN, M. R., KNIGHT, J. A., MEEHAN III, W. P. & BAKER, E. H. 2014. Significant improvements in cognitive performance post-transcranial, red/near-infrared light-emitting diode treatments in chronic, mild traumatic brain injury: open-protocol study. *Journal of Neurotrauma,* 31**,** 1008-1017.

NATOLI, R., VALTER, K., BARBOSA, M., DAHLSTROM, J., RUTAR, M., KENT, A. & PROVIS, J. 2013. 670nm Photobiomodulation as a Novel Protection against Retinopathy of Prematurity: Evidence from Oxygen Induced Retinopathy Models. *PLOS ONE,* 8**,** e72135.

NGUYEN, L. M.-D., MALAMO, A. G., LARKIN-KAISER, K. A., BORSA, P. A. & ADHIHETTY, P. J. 2014. Effect of near-infrared light exposure on mitochondrial signaling in C 2 C 12 muscle cells. *Mitochondrion,* 14**,** 42-48.

NIVALDO A. PARIZOTTO, H., YING-YING & HAMBLIN, M. R. 2013. *LLLT for Nerve and Spinal Cord Regeneration. In: Hamblin MR, Huang Y-Y (eds), Handbook of Photomedicine,* Boca Raton, CRC Press.

NIZIOLEK, M., KORYTOWSKI, W. & GIROTTI, A. W. 2003a. Chain-breaking antioxidant and cytoprotective action of nitric oxide on photodynamically stressed tumor cells. *Photochemistry and Photobiology,* 78**,** 262-70.

NIZIOLEK, M., KORYTOWSKI, W. & GIROTTI, A. W. 2003b. Nitric oxide inhibition of free radical-mediated lipid peroxidation in photodynamically treated membranes and cells. *Free Radical Biology and Mededicine,* 34**,** 997-1005.

NIZIOLEK, M., KORYTOWSKI, W. & GIROTTI, A. W. 2005. Self-sensitized photodegradation of membrane-bound protoporphyrin mediated by chain lipid peroxidation: inhibition by nitric oxide with sustained singlet oxygen damage. *Photochemistry and Photobiology,* 81**,** 299-305.

NIZIOLEK, M., KORYTOWSKI, W. & GIROTTI, A. W. 2006. Nitric oxide-induced resistance to lethal photooxidative damage in a breast tumor cell line. *Free Radical Biology and Medicine,* 40**,** 1323-31.

OLICHON, A., BARICAULT, L., GAS, N., GUILLOU, E., VALETTE, A., BELENGUER, P. & LENAERS, G. 2003. Loss of OPA1 perturbates the mitochondrial inner membrane structure and integrity, leading to cytochrome c release and apoptosis. *Journal of Biological Chemistry,* 278**,** 7743-7746.

OLICHON, A., GUILLOU, E., DELETTRE, C., LANDES, T., ARNAUNÉ-PELLOQUIN, L., EMORINE, L. J., MILS, V., DALOYAU, M., HAMEL, C. & AMATI-BONNEAU, P. 2006. Mitochondrial dynamics and disease, OPA1. *Biochimica et Biophysica Acta (BBA)-Molecular Cell Research,* 1763**,** 500-509.

OLICHON, A., LANDES, T., ARNAUNÉ-PELLOQUIN, L., EMORINE, L. J., MILS, V., GUICHET, A., DELETTRE, C., HAMEL, C., AMATI-BONNEAU, P. & BONNEAU, D. 2007. Effects of OPA1 mutations on mitochondrial morphology and apoptosis: relevance to ADOA pathogenesis. *Journal of Cellular Physiology,* 211**,** 423-430.

ORON, A., ORON, U., CHEN, J., EILAM, A., ZHANG, C., SADEH, M., LAMPL, Y., STREETER, J., DETABOADA, L. & CHOPP, M. 2006. Low-level laser therapy applied transcranially to rats after induction of stroke significantly reduces long-term neurological deficits. *Stroke,* 37**,** 2620-2624.

OUESLATI, A., LOVISA, B., PERRIN, J., WAGNIÈRES, G., VAN DEN BERGH, H., TARDY, Y. & LASHUEL, H. A. 2015. Photobiomodulation Suppresses Alpha-Synuclein-Induced Toxicity in an AAV-Based Rat Genetic Model of Parkinson's Disease. *PloS one,* 10**,** e0140880.

PATT, S., GERTZ, H.-J., GERHARD, L. & CERVOS-NAVARRO, J. 1991. Pathological changes in dendrites of substantia nigra neurons in Parkinson's disease: a Golgi study. *Histology and Histopathology.* 6(3), 373-380.

PAVLIDIS, M., STUPP, T., NASKAR, R., CENGIZ, C. & THANOS, S. 2003. Retinal ganglion cells resistant to advanced glaucoma: a postmortem study of human retinas with the carbocyanine dye DiI. *Investigative Ophthalmology & Visual Science,* 44**,** 5196-5205.

PEOPLES, C., SHAW, V. E., STONE, J., JEFFERY, G., BAKER, G. E. & MITROFANIS, J. 2012a. Survival of dopaminergic amacrine cells after near-infrared light treatment in MPTP-treated mice. *ISRN neurology,* 2012.

PEOPLES, C., SPANA, S., ASHKAN, K., BENABID, A.-L., STONE, J., BAKER, G. E. & MITROFANIS, J. 2012b. Photobiomodulation enhances nigral dopaminergic cell survival in a chronic MPTP mouse model of Parkinson's disease. *Parkinsonism & Related Disorders,* 18**,** 469-476.

PETERSON, J. W., BÖ, L., MÖRK, S., CHANG, A. & TRAPP, B. D. 2001. Transected neurites, apoptotic neurons, and reduced inflammation in cortical multiple sclerosis lesions. *Annals of Neurology,* 50**,** 389-400.

PLASS, C. A., LOEW, H. G., PODESSER, B. K. & PRUSA, A. M. 2012. Light-induced vasodilation of coronary arteries and its possible clinical implication. *The Annals of Thoracic Surgery,* 93**,** 1181-1186.

PURUSHOTHUMAN, S., JOHNSTONE, D. M., NANDASENA, C., VAN EERSEL, J., ITTNER, L. M., MITROFANIS, J. & STONE, J. 2015. Near infrared light mitigates cerebellar pathology in transgenic mouse models of dementia. *Neuroscience Letters,* 591**,** 155-159.

PURUSHOTHUMAN, S., NANDASENA, C., JOHNSTONE, D. M., STONE, J. & MITROFANIS, J. 2013. The impact of near-infrared light on dopaminergic cell survival in a transgenic mouse model of parkinsonism. *Brain Research,* 1535**,** 61-70.

RAMESH, G., MACLEAN, A. G. & PHILIPP, M. T. 2013. Cytokines and chemokines at the crossroads of neuroinflammation, neurodegeneration, and neuropathic pain. *Mediators of Inflammation,* 2013.

REYNIER, P., AMATI-BONNEAU, P., VERNY, C., OLICHON, A., SIMARD, G., GUICHET, A., BONNEMAINS, C., MALECAZE, F., MALINGE, M. C., PELLETIER, J. B., CALVAS, P., DOLLFUS, H., BELENGUER, P., MALTHIERY, Y., LENAERS, G. & BONNEAU, D. 2004. OPA3 gene mutations responsible for autosomal dominant optic atrophy and cataract. *Journal of Medical Genetics,* 41(9)**,** e110.

RISS, T. L., MORAVEC, R. A., NILES, A. L., DUELLMAN, S., BENINK, H. A., WORZELLA, T. J. & MINOR, L. 2016. Cell viability assays.

RISTOW, M. & SCHMEISSER, K. 2014. Mitohormesis: promoting health and lifespan by increased levels of reactive oxygen species (ROS). *Dose-Response,* 12(2).

RIZZI, C. F., MAURIZ, J. L., FREITAS CORRÊA, D. S., MOREIRA, A. J., ZETTLER, C. G., FILIPPIN, L. I., MARRONI, N. P. & GONZÁLEZ-GALLEGO, J. 2006. Effects of low-level laser therapy (LLLT) on the nuclear factor (NF)-κB signaling pathway in traumatized muscle. *Lasers in Surgery and Medicine,* 38**,** 704-713.

ROELANDTS, R. 2002. The history of phototherapy: Something new under the sun? *Journal of the American Academy of Dermatology,* 46**,** 926-930.

ROSS, J. M. 2011. Visualization of Mitochondrial Respiratory Function using Cytochrome C Oxidase / Succinate Dehydrogenase (COX/SDH) Double-labeling Histochemistry. *Journal of Visualized Experiments : JoVE***,** 3266.

ROZANOWSKA, M., ROZANOWSKI, B. & BOULTON, M. 2009. Light-induced damage to the retina. *In:* SMITH, K. C. (ed.) *Photobiological Sciences Online.* www.photobiology.info: American Society for Photobiology.

ROZANOWSKA, M. B. 2012. Light-induced damage to the retina: current understanding of the mechanisms and unresolved questions: a symposium-in-print. *Photochemistry and Photobiology,* 88**,** 1303-8.

RUBBO, H., RADI, R., TRUJILLO, M., TELLERI, R., KALYANARAMAN, B., BARNES, S., KIRK, M. & FREEMAN, B. A. 1994. Nitric oxide regulation of superoxide and peroxynitrite-dependent lipid peroxidation. Formation of novel nitrogen-containing oxidized lipid derivatives. *Journal of Biological Chemistry,* 269**,** 26066-26075.

RUTAR, M., NATOLI, R., ALBARRACIN, R., VALTER, K. & PROVIS, J. 2012. 670-nm light treatment reduces complement propagation following retinal degeneration. *Journal of Neuroinflammation,* 9**,** 257.

SAMOILOVA, K. A., ZHEVAGO, N. A., PETRISHCHEV, N. N. & ZIMIN, A. A. 2008. Role of nitric oxide in the visible light-induced rapid increase of human skin microcirculation at the local and systemic levels: II. healthy volunteers. *Photomedicine and Laser Surgery,* 26**,** 443-449.

SANJUÁN SZKLARZ, L. K. & SCORRANO, L. 2012. The antiapoptotic OPA1/Parl couple participates in mitochondrial adaptation to heat shock. *Biochimica et Biophysica Acta (BBA)-Bioenergetics,* 1817**,** 1886-1893.

SARZI, E., ANGEBAULT, C., SEVENO, M., GUEGUEN, N., CHAIX, B., BIELICKI, G., BODDAERT, N., MAUSSET-BONNEFONT, A.-L., CAZEVIEILLE, C. & RIGAU, V. 2012. The human OPA1delTTAG mutation induces premature age-related systemic neurodegeneration in mouse. *Brain,* 135**,** 3599-3613.

SATOH, M., HAMAMOTO, T., SEO, N., KAGAWA, Y. & ENDO, H. 2003. Differential sublocalization of the dynamin-related protein OPA1 isoforms in mitochondria. *Biochemical and Biophysical Research Communications,* 300**,** 482-493.

SCHUH, R. A., CLERC, P., HWANG, H., MEHRABIAN, Z., BITTMAN, K., CHEN, H. & POLSTER, B. M. 2011. Adaptation of microplate-based respirometry for hippocampal slices and analysis of respiratory capacity. *Journal of Neuroscience Research,* 89**,** 1979-1988.

SHAW, V. E., SPANA, S., ASHKAN, K., BENABID, A. L., STONE, J., BAKER, G. E. & MITROFANIS, J. 2010. Neuroprotection of midbrain dopaminergic cells in MPTP-treated mice after near-infrared light treatment. *Journal of Comparative Neurology,* 518**,** 25-40.

SHOLL, D. A. 1953. Dendritic organization in the neurons of the visual and motor cortices of the cat. *Journal of Anatomy,* 87**,** 387.

SLOANE, J. A., HOLLANDER, W., MOSS, M. B., ROSENE, D. L. & ABRAHAM, C. R. 1999. Increased microglial activation and protein nitration in white matter of the aging monkey☆. *Neurobiology of Aging,* 20**,** 395-405.

SNIGDHA, S., SMITH, E. D., PRIETO, G. A. & COTMAN, C. W. 2012. Caspase-3 activation as a bifurcation point between plasticity and cell death. *Neuroscience Bulletin,* 28**,** 14-24.

SONG, G., OUYANG, G. & BAO, S. 2005. The activation of Akt/PKB signaling pathway and cell survival. *Journal of Cellular and Molecular Medicine,* 9**,** 59-71.

SONG, Z., GHOCHANI, M., MCCAFFERY, J. M., FREY, T. G. & CHAN, D. C. 2009. Mitofusins and OPA1 mediate sequential steps in mitochondrial membrane fusion. *Molecular Biology of the Cell,* 20**,** 3525-3532.

SONIS, S. T., HASHEMI, S., EPSTEIN, J. B., NAIR, R. G. & RABER-DURLACHER, J. E. 2016. Could the biological robustness of low level laser therapy (Photobiomodulation) impact its use in the management of mucositis in head and neck cancer patients. *Oral Oncology,* 54**,** 7-14.

SPERANDIO, F. F., GIUDICE, F. S., CORRÊA, L., PINTO, D. S., HAMBLIN, M. R. & DE SOUSA, S. C. 2013. Low-level laser therapy can produce increased aggressiveness of dysplastic and oral cancer cell lines by modulation of Akt/mTOR signaling pathway. *Journal of Biophotonics,* 6**,** 839-847.

STEPHAN, A. H., BARRES, B. A. & STEVENS, B. 2012. The complement system: an unexpected role in synaptic pruning during development and disease. *Annual Review of Neuroscience,* 35**,** 369-389.

TAFUR, J. & MILLS, P. J. 2008. Low-intensity light therapy: Exploring the role of redox mechanisms. *Photomedicine and Laser Surgery,* 26**,** 323-328.

TANG, J., DU, Y., LEE, C. A., TALAHALLI, R., EELLS, J. T. & KERN, T. S. 2013a. Low-intensity far-red light inhibits early lesions that contribute to diabetic retinopathy: in vivo and in vitro. *Investigative Ophthalmology & Visual Science,* 54**,** 3681-3690.

TANG, J., DU, Y., LEE, C. A., TALAHALLI, R., EELLS, J. T. & KERN, T. S. 2013b. Low-Intensity Far-Red Light Inhibits Early Lesions That Contribute to Diabetic Retinopathy: In Vivo and In VitroFar-Red Light Inhibits DR. *Investigative Ophthalmology & Visual Science,* 54**,** 3681-3690.

TENGAN, C. H., RODRIGUES, G. S. & GODINHO, R. O. 2012. Nitric oxide in skeletal muscle: role on mitochondrial biogenesis and function. *International Journal of Molecular Sciences,* 13**,** 17160-17184.

THISELTON, D. L., ALEXANDER, C., TAANMAN, J.-W., BROOKS, S., ROSENBERG, T., EIBERG, H., ANDREASSON, S., VAN REGEMORTER, N., MUNIER, F. L. & MOORE, A. T. 2002. A comprehensive survey of mutations in the OPA1 gene in patients with autosomal dominant optic atrophy. *Investigative Ophthalmology & Visual Science,* 43**,** 1715-1724.

THUNSHELLE, C. & HAMBLIN, M. R. 2016. Transcranial low-level laser (light) therapy for brain injury. *Photomedicine and Laser Surgery,* 34**,** 587-598.

TILSTRA, J. S., CLAUSON, C. L., NIEDERNHOFER, L. J. & ROBBINS, P. D. 2011. NF-κB in aging and disease. *Aging and Disease,* 2**,** 449.

TINA KARU, H., YING-YING & HAMBLIN, M. R. 2013. *Chromophores (Photoacceptors) for LLLT. In: Hamblin MR, Huang Y-Y (eds), Handbook of Photomedicine,* Boca Raton, CRC Press.

TORNATORE, L., THOTAKURA, A. K., BENNETT, J., MORETTI, M. & FRANZOSO, G. 2012. The nuclear factor kappa B signaling pathway: integrating metabolism with inflammation. *Trends in Cell Biology,* 22**,** 557-566.

TORREILLES, F., SALMAN-TABCHEH, S. D., GUÉRIN, M.-C. & TORREILLES, J. 1999. Neurodegenerative disorders: the role of peroxynitrite. *Brain Research Reviews,* 30**,** 153-163.

TWIG, G. & SHIRIHAI, O. S. 2011. The interplay between mitochondrial dynamics and mitophagy. *Antioxidants & Redox Signaling,* 14**,** 1939-1951.

URANGA, R. M., KATZ, S. & SALVADOR, G. A. 2013. Enhanced phosphatidylinositol 3-kinase (PI3K)/Akt signaling has pleiotropic targets in hippocampal neurons exposed to iron-induced oxidative stress. *Journal of Biological Chemistry,* 288**,** 19773-19784.

VOGEL, A. & BIRNGRUBER, R. 1992. Temperature profiles in human retina and choroid during laser coagulation with different wavelengths ranging from 514 to 810 nm. *Lasers and Light in Ophthalmology,* 5**,** 9-16.

VOTRUBA, M., MOORE, A. T. & BHATTACHARYA, S. S. 1998. Clinical features, molecular genetics, and pathophysiology of dominant optic atrophy. *Journal of Medical Genetics,* 35**,** 793-800.

VOTRUBA, M., WILLIAMS, P. A., THIRGOOD, R. A., OLIPHANT, H., GOOD, M. A., WILLIAMS, J. & MORGAN, J. E. 2012. Retinal Ganglion Cell Dendritic Degeneration in a Mouse Model Of Alzheimer's Disease. *Investigative Ophthalmology & Visual Science,* 53**,** 4650-4650.

WANG, J.-W., CHEN, S.-D., ZHANG, X.-L. & JONAS, J. B. 2016. Retinal microglia in glaucoma. *Journal of Glaucoma,* 25**,** 459-465.

WANG, J. T., MEDRESS, Z. A. & BARRES, B. A. 2012. Axon degeneration: molecular mechanisms of a self-destruction pathway. *Journal of Cell Biology,* 196**,** 7-18.

WHITCUP, S. M., SODHI, A., ATKINSON, J. P., HOLERS, V. M., SINHA, D., ROHRER, B. & DICK, A. D. 2013. The role of the immune response in age-related macular degeneration. *International Journal of Inflammation,* 2013.

WHITE, K. E., DAVIES, V. J., HOGAN, V. E., PIECHOTA, M. J., NICHOLS, P. P., TURNBULL, D. M. & VOTRUBA, M. 2009. OPA1 deficiency associated with increased autophagy in retinal ganglion cells in a murine model of dominant optic atrophy. *Investigative Ophthalmology & Visual Science,* 50**,** 2567-2571.

WILLIAMS, P., MORGAN, J. & VOTRUBA, M. 2011. Mouse models of dominant optic atrophy: what do they tell us about the pathophysiology of visual loss? *Vision Research,* 51**,** 229-234.

WILLIAMS, P. A., HOWELL, G. R., BARBAY, J. M., BRAINE, C. E., SOUSA, G. L., JOHN, S. W. & MORGAN, J. E. 2013a. Retinal ganglion cell dendritic atrophy in DBA/2J glaucoma. *PloS one,* 8**,** e72282.

WILLIAMS, P. A., MORGAN, J. E. & VOTRUBA, M. 2010a. Opa1 deficiency in a mouse model of dominant optic atrophy leads to retinal ganglion cell dendropathy. *Brain***,** 133(10), pp2942-2951.

WILLIAMS, P. A., PIECHOTA, M., VON RUHLAND, C., TAYLOR, E., MORGAN, J. E. & VOTRUBA, M. 2012. Opa1 is essential for retinal ganglion cell synaptic architecture and connectivity. *Brain***,** 135(2), 493-505.

WILLIAMS, P. A., THIRGOOD, R. A., OLIPHANT, H., FRIZZATI, A., LITTLEWOOD, E., VOTRUBA, M., GOOD, M. A., WILLIAMS, J. & MORGAN, J. E. 2013b. Retinal ganglion cell dendritic degeneration in a mouse model of Alzheimer's disease. *Neurobiology of Aging,* 34**,** 1799-1806.

WONG-RILEY, M. T. 2010. Energy metabolism of the visual system. *Eye and Brain,* 2**,** 99.

WONG-RILEY, M. T., LIANG, H. L., EELLS, J. T., CHANCE, B., HENRY, M. M., BUCHMANN, E., KANE, M. & WHELAN, H. T. 2005. Photobiomodulation Directly Benefits Primary Neurons Functionally Inactivated by Toxins ROLE OF CYTOCHROME c OXIDASE. *Journal of Biological Chemistry,* 280**,** 4761-4771.

WU, Q., XUAN, W., ANDO, T., XU, T., HUANG, L., HUANG, Y. Y., DAI, T., DHITAL, S., SHARMA, S. K. & WHALEN, M. J. 2012. Low-Level Laser Therapy for Closed-Head Traumatic Brain Injury in Mice: Effect of Different Wavelengths. *Lasers in Surgery and Medicine,* 44**,** 218-226.

XUAN, W., AGRAWAL, T., HUANG, L., GUPTA, G. K. & HAMBLIN, M. R. 2015. Low-level laser therapy for traumatic brain injury in mice increases brain derived neurotrophic factor (BDNF) and synaptogenesis. *Journal of Biophotonics,* 8**,** 502-511.

XUAN, W., HUANG, L. & HAMBLIN, M. R. 2016. Repeated transcranial low-level laser therapy for traumatic brain injury in mice: biphasic dose response and long-term treatment outcome. *Journal of Biophotonics,* 9**,** 1263-1272.

YAN, Y.-F., YANG, W.-J., XU, Q., CHEN, H.-P., HUANG, X.-S., QIU, L.-Y., LIAO, Z.-P. & HUANG, Q.-R. 2015. DJ-1 upregulates anti-oxidant enzymes and attenuates hypoxia/re-oxygenation-induced oxidative stress by activation of the nuclear factor erythroid 2-like 2 signaling pathway. *Molecular Medicine Reports,* 12**,** 4734-4742.

YAROSH, W., MONSERRATE, J., TONG, J. J., TSE, S., LE, P. K., NGUYEN, K., BRACHMANN, C. B., WALLACE, D. C. & HUANG, T. 2008. The molecular mechanisms of OPA1-mediated optic atrophy in Drosophila model and prospects for antioxidant treatment. *PLoS genetics,* 4**,** e6.

YING, R., LIANG, H. L., WHELAN, H. T., EELLS, J. T. & WONG-RILEY, M. T. 2008a. Pretreatment with near-infrared light via light-emitting diode provides added benefit against rotenone-and MPP^+-induced neurotoxicity. *Brain Research,* 1243**,** 167-173.

YING, R., LIANG, H. L., WHELAN, H. T., EELLS, J. T. & WONG-RILEY, M. T. 2008b. Pretreatment with near-infrared light via light-emitting diode provides added benefit against rotenone-and MPP^+-induced neurotoxicity. *Brain Research,* 1243**,** 167-173.

YOUSSEF, P., SHEIBANI, N. & ALBERT, D. 2011. Retinal Light Toxicity. *Eye,* 25**,** 1-14.

YU-WAI-MAN, P., GRIFFITHS, P. G., BURKE, A., SELLAR, P. W., CLARKE, M. P., GNANARAJ, L., AH-KINE, D., HUDSON, G., CZERMIN, B. & TAYLOR, R. W. 2010. The Prevalence and Natural History of Dominant Optic Atrophy Due to OPA1 Mutations. *Ophthalmology,* 117**,** 1538-1546. e1.

ZHANG, H., DAVIES, K. J. A. & FORMAN, H. J. 2015. Oxidative stress response and Nrf2 signaling in aging. *Free Radical Biology and Medicine,* 88**,** 314-336.

ZHANG, R., MIO, Y., PRATT, P. F., LOHR, N., WARLTIER, D. C., WHELAN, H. T., ZHU, D., JACOBS, E. R., MEDHORA, M. & BIENENGRAEBER, M. 2009. Near infrared light protects cardiomyocytes from hypoxia and reoxygenation injury by a nitric oxide dependent mechanism. *Journal of Molecular and Cellular Cardiology,* 46**,** 4-14.

ZHANG, Z., WAKABAYASHI, N., WAKABAYASHI, J., TAMURA, Y., SONG, W.-J., SEREDA, S., CLERC, P., POLSTER, B. M., AJA, S. M. & PLETNIKOV, M. V. 2011. The dynamin-related GTPase Opa1 is required for glucose-stimulated ATP production in pancreatic beta cells. *Molecular Biology of the Cell,* 22**,** 2235-2245.

ZHAO, B. 2005. Nitric oxide in neurodegenerative diseases. *Frontiers in Bioscience,* 10**,** 454-461.

ZIELKE, A. Photo-excitation of electrons in cytochrome c oxidase as a theory of the mechanism of the increase of ATP production in mitochondria by laser therapy. SPIE BiOS, 2014. International Society for Optics and Photonics, 893204-893204-6.

ZOROV, D. B., JUHASZOVA, M. & SOLLOTT, S. J. 2014. Mitochondrial reactive oxygen species (ROS) and ROS-induced ROS release. *Physiological Reviews,* 94**,** 909-950.

Appendices

Appendix I Published studies using low energy 630 nm light for therapeutic purposes

Model	Device	Energy density	Treatment period	Duration of irradiation	Frequency of irradiation	Power density	Results	Reference
Tympanic membrane perforation Guinea Pig	630 Diode laser	1.8 J/cm^2	10 days	1 minute	Daily	30 mW/cm^2	Reduction in tympanic membrane thickness Reduction in the number of inflammatory cells infiltrating the tympanic membrane	[1]
Mandibular advancement Rabbit (Albino)	630 low level laser	1.8 J/cm^2	3 weeks	3 minutes	Daily	10 mW/cm^2	Increase in bone formation in the condylar region of the mandible	[2]
Cultured pancreatic islet cells	630 Ga-As low level laser	1, 3 or 5 J/cm^2	Single treatment	8, 25 or 42 seconds	Single treatment	40 mW/cm^2	A significant increase in insulin secretion, but only with 1 J/cm^2	[3]
Genetically diabetic mice	Argon dye laser	5 J/cm^2	4 days	250 seconds	Daily Starting 6 hours after wounding	20 mW/cm^2	A significant increase in percentage wound closure at both 10 and 20 days after wounding	[4]
Injured cartilage 5 mm Ear punch hole Rabbit	630 laser	1.8 J/cm^2	20 days	1 minute	Daily 3-5 days after punch hole Every other day thereafter until day 20	30 mW/cm^2	A decrease in punch hole diameter at 7 14 and 21 days, however not significant. Increased pericondrial cell growth, increased longitudinal cartilage	[5]
Wound healing Rat	630 nm LED		5 days	10 minutes	Daily	50 mW/cm2	No significant effect of 630 nm light on wound area but a significant effect of blue light of on wound size	[6]

References

1. Maleki, S., et al., Effect of local irradiation with 630 and 860 nm low-level lasers on tympanic membrane perforation repair in guinea pigs. The Journal of Laryngology & Otology, 2013. 127(3): p. 260-264.

2. Abtahi, M., et al., The effect of low level laser on condylar growth during mandibular advancement in rabbits. *Head & Face Medicine*, 2012. 8(1): p. 4.

3. Irani, S., et al. Effect of low-level laser irradiation on in vitro function of pancreatic islets. in Transplantation proceedings. 2009. *Elsevier.*

4. Yu, W., J.O. Naim, and R.J. Lanzafame, Effects of photostimulation on wound healing in diabetic mice. *Lasers in Surgery and Medicine*, 1997. 20(1): p. 56-63.

5. Kamrava, S.K., et al., The histological and clinical effects of 630 nanometer and 860 nanometer low-level laser on rabbits' ear punch holes. *Lasers in Medical Science*, 2009. 24(6): p. 949-954.

6. Adamskaya, N., et al., Light therapy by blue LED improves wound healing in an excision model in rats. *Injury*, 2011. 42(9): p. 917-921.

Appendix II Published *in vitro* studies using low energy 670 nm light on neuronal cells for therapeutic purposes

Cell Type	Radiant exposure	Treatment period	Duration of irradiation	Frequency of irradiation	Irradiance	Results	Reference
Retinal cells	5 J/cm^2	4 days	200 seconds	Twice Daily	25 mW/cm^2	Prevents increased superoxide production, expression of inflammatory biomarkers and cell death induced associated with exposure to 30 mM Glucose	[1]
PC 12 cells	0.45 mJ/cm^2	4 days	20 seconds	Daily	3 mW/cm^2	Extention of NGF stimulated neurite out growth Prevents H_20_2 induced decrease in MMP Has a positive effet on cell viability	[2]
PC 12 cells	0.45 mJ/cm^2	4 days	15 minutes	Daily	3 mW/cm^2	Prevents H_20_2 induced decrease in MMP No effect on cell viability	[2]
Primary Visual cortical neurons	4 J/cm^2	5 days	80 seconds	Twice Daily	50 mW/cm^2	Reversal of the detrimental effects of low levels of KCN on COX activity and partially reversed the effects or NaN_3	[3]

Pretreated	4 J/cm^2	3 days prior to toxin exposure In addition to above treatment	80 seconds	Daily	50 mW/cm^2	A greater increase in COX activity	[3]
Primary Visual cortical neurons	30 J/cm^2	Single pretreatment	10 mins	Single exposure	50 mW/cm^2	Significant reduction in the number of apoptotic cells and the KCN induced increase in ROS	[4]
Primary occipital cortical and striatal neurons	4 J/cm^2	3 or 5 days	80 seconds	Twice daily	50 mW/cm^2	Rescued cells from the toxic effects of MPP^+ Rotenone and KCN. Increase in COX activity, ATP production, a reduction in apoptosis, ROS and RNS	[5]
Primary rat cortical neurons	4 J/cm^2	5 days	80 seconds	Daily	50 mW/cm^2	Reversion of the down-regulation of COX activity by TTX to control levels	[6]
Primary rat striatal and cortical neurons	4 J/cm^2	2 days	80 seconds	Twice daily	50 mW/cm^2	LED treatment prior and during MPP^+ and Rotenone exposure had more profound protective effects against neurotoxicity compared to LED treatment alone during toxin exposure	[7]
Rat neonatal myocytes and cardiac muscle cell line Hypoxia and reoxygenation induced cardiomyocyte injury	1.5, 7.5 and 15 J/cm^2	Single treatment	5 minutes	Single treatment	5, 25 and 50 mW/cm^2	7.5 J/cm^2 was optimal dose in reducing cell membrane injury, decreasing caspase 3 activity and preventing cytochrome c release from the mitochondria, reversing the NO induced inhibition of oxygen consumption, increases ATP production	[8]

References

1. Tang, J., et al., Low-Intensity Far-Red Light Inhibits Early Lesions That Contribute to Diabetic Retinopathy: In Vivo and In VitroFar-Red Light Inhibits DR. *Investigative Ophthalmology & Visual Science*, 2013. 54(5): p. 3681-3690.

2. Giuliani, A., et al., Low infrared laser light irradiation on cultured neural cells: effects on mitochondria and cell viability after oxidative stress. *BMC Complementary and Alternative Medicine*, 2009. 9(1): p. 8.

3. Wong-Riley, M.T., et al., Photobiomodulation directly benefits primary neurons functionally inactivated by toxins role of cytochrome c oxidase. *Journal of Biological Chemistry*, 2005. 280(6): p. 4761-4771.

4. Liang, H.L., et al., Photobiomodulation partially rescues visual cortical neurons from cyanide-induced apoptosis. *Neuroscience*, 2006. 139(2): p. 639-649.

5. Liang, H.L., et al., Near-infrared light via light-emitting diode treatment is therapeutic against rotenone-and 1-methyl-4-phenylpyridinium ion-induced neurotoxicity. *Neuroscience*, 2008. 153(4): p. 963-974.

6. Wong-Riley, M.T., et al., Light-emitting diode treatment reverses the effect of TTX on cytochrome oxidase in neurons. *Neuroreport*, 2001. 12(14): p. 3033-3037.

7. Ying, R., et al., Pretreatment with near-infrared light via light-emitting diode provides added benefit against rotenone-and MPP^+-induced neurotoxicity. *Brain Research*, 2008. 1243: p. 167-173.

8. Zhang, R., et al., Near infrared light protects cardiomyocytes from hypoxia and reoxygenation injury by a nitric oxide dependent mechanism. *Journal of Molecular and Cellular Cardiology*, 2009. 46(1): p. 4-14.

Appendix III Published *in vivo* studies using low energy 670 nm light in models of neurodegeneration

Animal models	Tissue treated	Fluence per treatment	Duration of total treatment period	Frequency of irradiation	Power intensity	Distance of light source from animal	General effect with light treatment	Molecular effects With light treatment	Ref.	Additional information
EAE Mice C57BL/6	Spinal cord	5 J/cm^2	7 days on 7 days off 7 days on	Daily	28 mW/cm^2	2 cm	Protection against apoptosis in the CNS Reduced clinical EAE in wt but not in iNOS knockout mice Reduced apoptosis at all stages of EAE	Down requlation of NO and iNOS Upregulation of antiapoptotic protein Bcl-2 No difference in pro apoptotic protein Bax	[1]	
Diabetic retinopathy induced rats Lewis	Retina	6 J/cm^2	10 weeks	Daily	25 mW/cm^2	1 inch Above head	Inhibition of RGC death 50% improvem-ent in reduced ERG amplitude	Inhibition of diabetes induced superoxide production Correction of the diabetes induced decrease in MnSOD Prevention of diabetes induced increase in leukostasis and expression of ICAM-1	[2]	Animals not forced or encouraged to look at light
Induced wound Mice SKH1-hr (Albino)	Skin	3.6 J/cm^2 was total fluence for high medium and low flux delivery of light	5 days	Daily	40 mW/cm^2 8 mW/cm^2 1.6 mW/cm^2	2-3 cm from wound	Percentage of wounds healed greater than control at 1 week after injury but not significant after 2 weeks and effect was greater than at lower fluxes	No difference in inflammation from control No difference in cell proliferation between the light treated groups and control 3 days after injury	[3]	Cage equipped with LEDs with LEDs Mice were 2 weeks younger in the lower flux group

Diabetic mice	Skin	4 J/cm^2	14 days	Daily	28 mW/cm^2	N/A	Reduction in wound area Upregulation of tissue regenerating genes		[4]	
MTPT induced Parkinsons mice BALB/c (Albino)	Brain	2 J/cm^2	30 hours	4 treatments Evenly spaced over 30 hours	40 mW/cm^2 5.3 mW/cm^2 reaching brain (10%)	1 cm above head	Reduction MTPT induced cell loss in SNc but no effect on cells in ZI-Hyp		[5]	Animals euthanized 6 days after last treatment
Light induced retinal degeneration rat Sprague–Dawley (Albino)	Retina	9 J/cm^2	5 days prior to light induced damage	Daily	60 mW/cm^2	2.5 cm from eyes	1 week post induction of light damage: reduced photoreceptor death and preserved structural integrity of muller cells	Upregulation of genes involved in neuroprotection Maintains muller cell ability to recycle neurotoxic glutamate Reduction in the upregulation nof TNFα	[6]	
Light induced model of atrophic AMD Rat Sprague–Dawley (albino)	Retina	9 J/cm^2	pre-treatment 5 days	Daily	60 mW/cm^2	2.5 cm from eyes	Prevention of the reduction in ONL thickness associated with light damage	Reduced expression of complement genes Reduced immunoreactivity for oxidative damage marker Reduuction in the recruitment of C3 expressing microglia/macrophages in the retina	[7]	

Photoreceptor degeneration rat (albino)	Retina	9 J/cm^2	Pre con: 5 days (Prior light damage) Mid con: During light damage Post con: 5 days (post light damage)	3 minutes daily	60 mW/cm2	2.5 cm form eyes	Positive results in pre-treated but not post treated animals Prevents photoreceptor cell loss and structural changes to the outer retina Loss in retinal function was reduced	The number of TUNEL+ cells was lowest in the Pre con group Reduction in the expression of outer segment cone protein was prevented in pre and mid con groups only	[8]	
Macular degeneration mice	Retina		35 hours	5 exposures over 35 hours	40 mW/cm^2	1 cm above the head	Increased membrane potential Reduction in macrophage number, TNFα and inflammatory biomarkers		[9]	
Macular degeneration mice	Retina		14 days	Twice daily For 6 minutes	Between 6 and 19 mW/cm^2	Between 0.4-13 cm from mouse (LED on both sides of cage)	Increased COX expression by 50?% Reduction in inflammatory and retinal stress markers	Number of Iba+ cells was reduced with 670 nm treatment however not significantly Cell bodies of macrophages were reduced in size while there processes extended The inflammatory marker was reduced on Bruchs membrane and photoreceptor outer segments	[10]	The animals cage was equipped with 670 nm LEDs which emitted 20 mW/cm^2 The lights were set to come on at 6 am and 6pm for 6 minutes

Optic nerve secondary degeneration Rats PVG	ON		7 days	Daily 30 minutes	60 mW/cm^2 at source	3 cm above head (WARP 10)	Prevention of changes in mitochondrial structure associated with secondary degeneration	Reduced number of mitochondrial autophagic profiles Aconitase which is inhibited by ROS is increased Citrate synthase (marker of mitochondrial content) was increased in dorsal ON while decreased in the ventral ON	[11]	
Photoreceptor degeneration-light damage model Rat (albino) Sprague–Dawley	Retina	5 J/cm^2	Various (2, 5, 7 and 10 days)	Daily 3 minutes	28 mW/cm^2	1-2 cm above head (WARP 75)	Reduced photoreceptor death Protection of photoreceptors increases with longer treatment periods	GFAP expression on Müller cells (upregulates with various stresses) is reduced	[12]	Device placed over animals head while in cage, mild restraint used
TBI model Sprague–Dawley Rat	Brain	15 J/cm^2	72 hours (biochemical) effects) 10 days behavioural effects)	Twice daily	50 mW/cm^2	0.5 cm	An improvement in nose poke behaviour	Significant decrease in the proapoptotic protein Bax and an increase antiapoptotic protein Bcl-2 Reduced glutathione levels	[13]	
Type 1 diabeties model rat		9 J/cm^2	18 days(acute) or 14 weeks (chronic) (treatment not given on weekend days)	Daily	30 mW/cm^2		Increase in antioxidant enzyme activity as measured after 18 day treatment but not after 14 week treatment		[14]	

Light induced photoreceptor damage Rat	Retina	90 J/cm^2	48 hours	3 hours before and 0, 24 and 48 hours after light damage	50 mW/cm^2	1 inch above head	Decrease in retinal degeneration Protected against damage induced reduction in retinal function		[15]	
Optic nerve secondary degeneration Rats	ON	5 J/cm^2 Per 88 second dose	3 months (6 days/ week)	Daily	60 mW/cm^2	3 cm above head	Prevents the RGC loss resulting from retinal injury and the associated loss in visual function		[16]	
Optic nerve secondary degeneration Rats	ON	5 J/cm^2 Per 88 second dose	Single treatment	Single treatment	60 mW/cm^2	3 cm above head	Increase in cytochrome c oxidase activity Reduction in ROS and RNS		[16]	
Oxygen induced retinopathy C57BL/6J mice or Sprague-Dawley albino rats	Retina	Retina	9 J/cm^2	Daily 18 days	50 mW/cm^2		Decrease in severity of vascular pathology Reduced cell death in all retinal layers		[17]	
Light induced retinal degeneration Rat	ON	3.4 J/cm2	5 days pre-treatment	Daily 3 mins	18.8 mW/cm^2	2.5 cm from eye	Reduction in the number of TUNEL+ cells		[18]	
TBI Rat	SC	28.4 J/cm2	7 days	Daily 30 mins	15 mW/cm^2	3 cm above animal	No significant improvements in motor or sensory function		[18]	
Partial optic nerve injury Rats	ON	28.4 J/cm2	7 days	Daily	28.4 J/cm^2	2.5 cm from eye	Increase in the number of visual responses Reduced ROS		[19]	

MPTP mice	Brain	4 J/cm2	4 days	Daily	50 mW/cm^2	Protocol 1. Directly to head Protocol 2. Directly to body-head foil covered	Significant rescue of tyrosine hydroxylase-positive cells in the substantia nigra pars compacta Protocol 2 less effective that protocol 1		[20]	
Rodent model of retinal toxicity	Retina	4 J/cm2	50 hours	3X 2 mins 24 sec exposures 5, 25 and 50 hrs after induced toxucity	28 mW/cm^2	1 inch	Significant recovery of rod- and M-cone-mediated retinal function and a significant recovery of UV-cone-mediated function Protection from methanol-induced histopathology		[21]	
Hyperoxia-induced retinopathy mouse	Retina	9 J/cm2	Pre-treatment 5 days	daily	60 mW/cm^2	2.5 cm from eyes	Slowed, but did not prevent photoreceptor loss	Reduced expression of markers of oxidative stress, acrolein and Hmox-1 stress, and reduced expression of complement component 3	[22]	
12 month old C57/BL mice	Retina and brain		84 hours	7X 90 s exposures spaced evenly over 84 hrs	40 mW/cm^2	15 cm from source	Increase in ATP Upregulation of COX un outer retina	Acrolein expression reduced in outer retina	[23]	
MPTP model of PD	Brain		6 days	Exposure was continuous for 6 days	0.16 mW/cm^2	Delivered intracranially	No significant protection against cell death in SNc with pulsed or continuous protocol but fewer TH+ cells in MPTP		[24]	An optical fiber linked to an LED or laser device was surgically implanted into

				or 90 sec per day for 4 days			group compared to MPTP-NIR groups			the lateral ventricle of the rats
MPTP model of PD C57/BL6 or albino Balb/c mice	Brain	0.5 J/cm^2 per treatment	6 days	4X 90 s treatments over 6 days		1-2 cm above head	TH+ cells significantly higher in MPTP-NIR group compared to MPTP group- 30% higher in Balb/c compared to 20% in C57BL/6 Locomotor activity values significantly higher with 670 nm light in Balb/c mice but did not reach significance in C57/BL6		[25]	Treatment with 670 nm light had different effects on different strains of mice

References

1. Muili, K.A., et al., Photobiomodulation induced by 670 nm light ameliorates MOG35-55 induced EAE in female C57BL/6 mice: a role for remediation of nitrosative stress. *PloS one*, 2013. 8(6): p. e67358.

2. Tang, J., et al., Low-Intensity Far-Red Light Inhibits Early Lesions That Contribute to Diabetic Retinopathy: In Vivo and In VitroFar-Red Light Inhibits DR. *Investigative Ophthalmology & Visual Science*, 2013. 54(5): p. 3681-3690.

3. Erdle, B.J., et al., Effects of continuous-wave (670-nm) red light on wound healing. *Dermatologic Surgery*, 2008. 34(3): p. 320-325.

4. Whelan, H.T., et al., Effect of NASA light-emitting diode irradiation on molecular changes for wound healing in diabetic mice. *Journal of Clinical Laser Medicine & Surgery, 2003*. 21(2): p. 67-74.

5. Shaw, V.E., et al., Neuroprotection of midbrain dopaminergic cells in MPTP-treated mice after near-infrared light treatment. *Journal of Comparative Neurology*, 2010. 518(1): p. 25-40.

6. Albarracin, R.S. and K. Valter, Treatment with 670-nm light protects the cone photoreceptors from white light-induced degeneration, in Retinal degenerative diseases. 2012, *Springer*. p. 121-128.

7. Rutar, M., et al., 670-nm light treatment reduces complement propagation following retinal degeneration. *Journal of Neuroinflammation*, 2012. 9(1): p. 257.

8. Albarracin, R. and K. Valter, 670 nm red light preconditioning supports Müller cell function: evidence from the white light-induced damage model in the rat retina. *Photochemistry and Photobiology*, 2012. 88(6): p. 1418-1427.

9. Kokkinopoulos, I., et al., Age-related retinal inflammation is reduced by 670 nm light via increased mitochondrial membrane potential. *Neurobiology of Aging*, 2013. 34(2): p. 602-609.

10. Begum, R., et al., Treatment with 670 nm light up regulates cytochrome C oxidase expression and reduces inflammation in an age-related macular degeneration model. *PloS one*, 2013. 8(2): p. e57828.

11. Cummins, N., et al., Changes to mitochondrial ultrastructure in optic nerve vulnerable to secondary degeneration in vivo are limited by irradiation at 670 nm. *BMC Neuroscience*, 2013. 14(1): p. 98.

12. Marco, F.D., et al., The time course of action of two neuroprotectants, dietary saffron and photobiomodulation, assessed in the rat retina. *American Journal of Neurodegenerative Disease*, 2013. 2(3): p. 208-220.

13. Quirk, B.J., et al., Near-infrared photobiomodulation in an animal model of traumatic brain injury: improvements at the behavioral and biochemical levels. *Photomedicine and Laser Surgery*, 2012. 30(9): p. 523-529.

14. Lim, J., et al., Effects of low-level light therapy on hepatic antioxidant defense in acute and chronic diabetic rats. *Journal of Biochemical and Molecular Toxicology*, 2009. 23(1): p. 1-8.

15. Qu, C., et al., Near-infrared light protect the photoreceptor from light-induced damage in rats, in Retinal Degenerative Diseases. 2010, *Springer*. p. 365-374.

16. Szymanski, C.R., et al., Paranode abnormalities and oxidative stress in optic nerve vulnerable to secondary degeneration: modulation by 670 nm light treatment. *PLoS one*, 2013. 8(6): p. e66448.

17. Natoli, R., et al., 670nm Photobiomodulation as a Novel Protection against Retinopathy of Prematurity: Evidence from Oxygen Induced Retinopathy Models. *PLoS one, 2013*. 8(8): p. e72135.

18. Giacci, M.K., et al., Differential Effects of 670 and 830 nm Red near Infrared Irradiation Therapy: A Comparative Study of Optic Nerve Injury, Retinal Degeneration, Traumatic Brain and Spinal Cord Injury. *PLoS one*, 2014. 9(8): p. e104565.

19. Ashworth, B.E., et al., Comparative assessment of phototherapy protocols for reduction of oxidative stress in partially transected spinal cord slices undergoing secondary degeneration*. BMC Neuroscience*, 2016. 17(1): p. 21.

20. Johnstone, D.M., et al., Indirect application of near infrared light induces neuroprotection in a mouse model of parkinsonism – An abscopal neuroprotective effect. *Neuroscience*, 2014. 274(Supplement C): p. 93-101.

21. Eells, J.T., et al., Therapeutic photobiomodulation for methanol-induced retinal toxicity. *Proceedings of National Academy of Sciences*, 2003. 100.

22. Albarracin, R., et al., 670 nm light mitigates oxygen-induced degeneration in C57BL/6J mouse retina. *BMC Neuroscience*, 2013. 14(1): p. 125.

23. Gkotsi, D., et al., Recharging mitochondrial batteries in old eyes. Near infra-red increases ATP. *Experimental Eye Research*, 2014. 122: p. 50-53.

24. Moro, C., et al., Photobiomodulation inside the brain: a novel method of applying near-infrared light intracranially and its impact on dopaminergic cell survival in MPTP-treated mice. *Journal of Neurosurgery*, 2014. 120(3): p. 670-683.

25. Moro, C., et al., Photobiomodulation preserves behaviour and midbrain dopaminergic cells from MPTP toxicity: evidence from two mouse strains. *BMC Neuroscience*, 2013. 14(1): p. 40.

Appendix IV Published studies using low energy 810 nm light in animal models of neurodegeneration

Model	Device	Radiant exposure	Treatment period	Duration of irradiation	Frequency of irradiation	Irradiance	Result	Reference
TBI mice	Ga-Al-As diode laser 10 Hz pulsed wave or CW	36 J/cm^2	Single treatment 4 hours post TBI	12 minutes	Single treatment	50 mW/cm^2 3-7.5 mW/cm^2 reaching brain	28 days post TBI: Reduced lesion volume Improvement in NSS Antidepressant effect Increased effectiveness at 10-Hz pulse frequency than at CW and 100-Hz 4 hours post TBI: No significant increase in ATP content	[1]
Familial amyotrophic lateral sclerosis mice		12 J/cm^2	5 months (51 days old until death)	120 seconds	Daily	140 mW/cm^2	No significant difference in motor neuron survival No significant improvement in motor function	[2]
Murine bone marrow derived dendritic cells	Laser (HOYA Conbio, Fremont, CA)	30, 3, 0.3 J/cm^2	Single treatment	5 minutes	Single treatment	100, 10, 0.1 mW/cm^2	Increased cell viability Reduced IL-12 secretion stimulated by LPS Reduced NF-kB activation in cells stimulated with CpG No observed dose response	[3]
Glutamate toxicity model Murine primary cortical neurons	Diode laser (Photothera, Inc., Carlsbad, CA),	3 J/cm^2	single	2 minutes	single	25 mW/cm^2	A significant yet modest decrease in cell death Highly significant increase on ATP production and MMP. Highly significant reduction in intracellular $Ca2^+$, oxidative stress and NO.	[4]
Oxidative stress model Murine primary cortical neurons	Diode laser (Photothera, Inc., Carlsbad, CA),	3 J/cm^2	single	150 seconds	single	20 mW/cm^2	Increased MMP, reduced ROS in stressed cells and increased ROS in control cells Reduction in cell death in stressed cells	[5]

Dermal abrasion model		4 J/cm2	7 days	6.6 minutes	Daily	10 mW/cm^2	Reduction in wound area Increased collagen accumulation	[6]
Diabetic mice	Diode laser	2 J/cm^2	7 days	40 seconds	Daily	50 mW/cm^2	Blood plasma fructosamine levels were lower in mice irradiated on left inguinal region compared to non-irradiated	[7]
Oxygen-glucose deprived primary cortical neurons	Diode laser	3 J/cm^2	single	2 minutes	Single	25 mW/cm^2	Reduction in cell death Increased mitochondrial reductive capacity Restoration of MMP and ATP production	[8]
Primary Cortical neurons	Diode laser	30, 10, 3, 0.3, 0.03 J/cm2	single	various	single	25 m W/cm2	Biphasic dose response was observed ATP and MMP and Ca22 increased at low radiant exposure and decreased at higher. ROS and NO increased at low radiant exposure, decreased at mid-range radiant exposure and had the largest increase at higher radiant exposures	[9]
Spinal cord injury Rat	continuous wave 810 nm diode laser with a delivery optical fibre	1,589 J/cm2	14 days	2,997 seconds	Daily	150 mW	Greater axon regrowth length and higher total axon number in following hemisection and contusion injuries with 810 nm light	[10]
Rat model of chronic mild stress	laser	120 J/cm2	3 weeks	2 minute	3 times per week	350 mW peak power	Less stress-induced immobility with 810 nm light	[11]
Spinal cord injury Rat	808-nm diode laser CW and pulsed	1,500 J/cm^2	3 weeks	50 minutes	daily	0.5 W/cm^2	Significantly higher total axon number in with both pulsed and CW No significant difference between pulsed and CW	[12]

							Significantly greater length of axonal regeneration with pulsed and CW but significantly greater in pulsed that CW	
	10-Hz pulsed wave laser 810 nm and 630 nm	1.2 J/cm-2 per treatment 14.4 J/cm ^{2} total	3 weeks		4 times per week	562 mw/cm^2	Mice had significantly reduced immobility and increased swim time with 810 nm laser but not 630 nm laser Cortisol levels were reduced with 630 nm but not 810 nm laser and blood glucose levels were reduced with both wavelengths	[13]

References

1. Ando, T., et al., Comparison of therapeutic effects between pulsed and continuous wave 810-nm wavelength laser irradiation for traumatic brain injury in mice. *PLoS one*, 2011. 6(10): p. e26212.

2. Moges, H., et al., Light therapy and supplementary Riboflavin in the SOD1 transgenic mouse model of familial amyotrophic lateral sclerosis (FALS). *Lasers in Surgery and Medicine*, 2009. 41(1): p. 52-59.

3. Chen, A.C.-H., et al., Effects of 810-nm laser on murine bone-marrow-derived dendritic cells. *Photomedicine and Laser Surgery*, 2011. 29(6): p. 383-389.

4. Huang, Y.Y., K. Nagata, and C.E. Tedford, Low-level laser therapy (810 nm) protects primary cortical neurons against excitotoxicity in vitro. *Journal of Biophotonics*, 2014. 7(8): p. 656-664.

5. Huang, Y.Y., et al., Low-level laser therapy (LLLT) reduces oxidative stress in primary cortical neurons in vitro. *Journal of Biophotonics*, 2013. 6(10): p. 829-838.

6. Gupta, A., T. Dai, and M.R. Hamblin, Effect of red and near-infrared wavelengths on low-level laser (light) therapy-induced healing of partial-thickness dermal abrasion in mice. *Lasers in Medical Science*, 2014. 29(1): p. 257-265.

7. Peplow, P.V. and G.D. Baxter, Testing infrared laser phototherapy (810 nm) to ameliorate diabetes: irradiation on body parts of diabetic mice*. Lasers in Surgery and Medicine, 2013.* 45(4): p. 240-245.

8. Yu, Z., et al., Near infrared radiation rescues mitochondrial dysfunction in cortical neurons after oxygen-glucose deprivation. *Metabolic Brain Disease*, 2015. 30(2): p. 491-496.

9. Sharma, S.K., et al., Dose response effects of 810 nm laser light on mouse primary cortical neurons. *Lasers in Surgery and Medicine*, 2011. 43(8): p. 851-859.

10. Wu, X., et al., 810 nm Wavelength light: an effective therapy for transected or contused rat spinal cord. *Lasers in Surgery and Medicine*, 2009. 41(1): p. 36-41.

11. Wu, X., et al., Pulsed light irradiation improves behavioral outcome in a rat model of chronic mild stress. *Lasers in Surgery and Medicine*, 2012. 44(3): p. 227-232.

12. Wu, X., et al., Comparison of the effects of pulsed and continuous wave light on axonal regeneration in a rat model of spinal cord injury. *Lasers in Medical Science*, 2012. 27(2): p. 525-528.

13. Salehpour, F., et al., Therapeutic effects of 10-HzPulsed wave lasers in rat depression model: A comparison between near-infrared and red wavelengths. *Lasers in Surgery and Medicine*, 2016. 48(7): p. 695-705.